Molecular Regulation of Satellite Cell Maintenance and Differentiation during Adult Myogenesis

Andrew E. D. Jones

Thesis submitted to the
Faculty of Graduate and Postdoctoral Studies
in partial fulfillment of the requirements
for a doctoral degree in Cellular and Molecular Medicine

Department of Cellular and Molecular Medicine
Faculty of Medicine
University of Ottawa

Reproduction Authorizations

Permission to reproduce content within General Introduction:

Transcriptional networks that regulate muscle stem cell function.
Punch VG, Jones AE, Rudnicki MA. Wiley Interdiscip Rev Syst Biol Med. 2009 Jul-Aug;1(1):128-40.

License Details

This is a License Agreement between Andrew E Jones ("You") and John Wiley and Sons ("John Wiley and Sons"). The license consists of your order details, the terms and conditions provided by John Wiley and Sons, and the payment terms and conditions.

Get the printable license.

License Number	3138590570236
License date	Apr 30, 2013
Licensed content publisher	John Wiley and Sons
Licensed content publication	Wiley Interdisciplinary Reviews: Systems Biology and Medicine
Licensed content title	Transcriptional networks that regulate muscle stem cell function
Licensed copyright line	Copyright © 2009 John Wiley & Sons, Inc.
Licensed content author	Vincent G. Punch,Andrew E. Jones,Michael A. Rudnicki
Licensed content date	May 4, 2009
Start page	128
End page	140
Type of use	Dissertation/Thesis
Requestor type	Author of this Wiley article
Format	Print and electronic
Portion	Full article
Will you be translating?	No
Total	**0.00 USD**

Permission to reproduce manuscript in Appendix B:

Transcriptional Dominance of Pax7 in Adult Myogenesis Is Due to High-Affinity Recognition of Homeodomain Motifs.
Soleimani VD, Punch VG, Kawabe YI, Jones AE, Palidwor GA, Porter CJ, Cross JW, Carvajal JJ, Kockx CE, van Ijcken WF, Perkins TJ, Rigby PW, Grosveld F, Rudnicki MA.
Dev Cell. 2012 Jun 12;22(6):1208-20.

License Details

This is a License Agreement between Andrew E Jones ("You") and Elsevier ("Elsevier"). The license consists of your order details, the terms and conditions provided by Elsevier, and the payment terms and conditions.

Get the printable license.

License Number	3137780126256
License date	Apr 28, 2013
Licensed content publisher	Elsevier
Licensed content publication	Developmental Cell
Licensed content title	Transcriptional Dominance of Pax7 in Adult Myogenesis Is Due to High-Affinity Recognition of Homeodomain Motifs
Licensed content author	Vahab D. Soleimani,Vincent G. Punch,Yoh-ichi Kawabe,Andrew E. Jones,Gareth A. Palidwor,Christopher J. Porter,Joe W. Cross,Jaime J. Carvajal,Christel E.M. Kockx,Wilfred F.J. van IJcken,Theodore J. Perkins,Peter W.J. Rigby,Frank Grosveld,Michael A. Rudnicki
Licensed content date	12 June 2012
Licensed content volume number	22
Licensed content issue number	6
Number of pages	13
Type of Use	reuse in a thesis/dissertation
Portion	full article
Format	both print and electronic
Are you the author of this Elsevier article?	Yes
Will you be translating?	No
Order reference number	None
Title of your thesis/dissertation	Molecular regulation of satellite cell maintenance and differentiation during adult myogenesis.
Expected completion date	Apr 2013
Estimated size (number of pages)	175
Elsevier VAT number	GB 494 6272 12
Permissions price	0.00 USD
VAT/Local Sales Tax	0.00 USD
Total	**0.00 USD**

Permission to reproduce manuscript in Appendix C:

Wnt7a activates the planar cell polarity pathway to drive the symmetric expansion of satellite stem cells.
Le Grand F, Jones AE, Seale V, Scimè A, Rudnicki MA. Cell Stem Cell. 2009 Jun 5;4(6):535-47.

License Details

This is a License Agreement between Andrew E Jones ("You") and Elsevier ("Elsevier"). The license consists of your order details, the terms and conditions provided by Elsevier, and the payment terms and conditions.

Get the printable license.

License Number	3138590472487
License date	Apr 30, 2013
Licensed content publisher	Elsevier
Licensed content publication	Cell Stem Cell
Licensed content title	Wnt7a Activates the Planar Cell Polarity Pathway to Drive the Symmetric Expansion of Satellite Stem Cells
Licensed content author	Fabien Le Grand,Andrew E. Jones,Vanessa Seale,Anthony Scimè,Michael A. Rudnicki
Licensed content date	5 June 2009
Licensed content volume number	4
Licensed content issue number	6
Number of pages	13
Type of Use	reuse in a thesis/dissertation
Portion	full article
Format	both print and electronic
Are you the author of this Elsevier article?	Yes
Will you be translating?	No
Order reference number	None
Title of your thesis/dissertation	Molecular regulation of satellite cell maintenance and differentiation during adult myogenesis.
Expected completion date	Apr 2013
Estimated size (number of pages)	175
Elsevier VAT number	GB 494 6272 12
Permissions price	0.00 USD
VAT/Local Sales Tax	0.00 USD
Total	**0.00 USD**

Abstract

The post-natal regenerative capacity of skeletal muscle is attributed to myogenic satellite cells, which function as lineage-committed precursors to replace terminally differentiated muscle. The development and differentiation of the satellite cell lineage is regulated by Pax7 and the myogenic regulatory factors. While the expression of Pax7 is vital to the function of the satellite cell compartment, the paired domain alternative splicing events that regulate its DNA binding potential remain elusive. Interestingly, the generation of Pax7 splice variants differentially regulate Myf5 expression. We performed a global analysis of two Pax7 isoforms, which differ by a glycine-leucine dipeptide, to determine how paired domain splicing events modify the ability of Pax7 to regulate target genes. To this end, we observe that although the homeodomain is important for Pax7 binding, these isoform differences in the paired domain can regulate Pax7 targets during myogenesis.

In addition to further examining the role of Pax7 during satellite cell proliferation and maintenance, it remains important to understand their downstream differentiation potential. Since activation of the canonical Wnt signalling pathway results in reduced regenerative efficiency *in vivo*, we undertook a global analysis of satellite cell derived myoblasts to examine their ability to respond to canonical Wnt signalling. We demonstrate that Wnt/β-Catenin signalling drives myogenic differentiation, via the myogenin-dependent control of follistatin expression, further fine-tuning the myogenic differentiation process. The effects of canonical Wnt signalling on myogenic differentiation complement our observations regarding Pax7 alternative splicing during myoblast proliferation and provide a greater comprehensive understanding of the molecular regulation of satellite cell development and differentiation during adult myogenesis.

Acknowledgements

First, I would like to thank my PhD supervisor, Dr. Michael Rudnicki, for providing me the opportunity to undertake this research project and for instilling the support and guidance to succeed. In addition, I would like to thank my fellow Rudnicki lab members and friends for providing a constructive and supportive environment through discussions, technical assistance or merely social support. I would like to thank my advisory committee, Dr. David Picketts, Dr. Jeffrey Dilworth, and Dr. John Bell, for their guidance and support throughout this degree. Finally, to Anna, my dearing wife whose unconditional love and support has provided the foundation to my success and has encouraged me to take chances.

Contributions of Co-Authors

All technical work and preparations of the thesis and manuscripts were carried out by the thesis author except as otherwise specified. I have been very fortunate to collaborate with the following people. Solexa sequencing and microarray analysis of RNA samples was carried out by the Stem Core Laboratories at the Ottawa Hospital Research Institute. Christopher Porter carried out initial bioinformatics analyses on RNA-Seq data and provided the corresponding figures used in Figure 5 of Chapter 2. Gareth Palidwor conducted RMA on microarray raw data and provided Figure 1 in Chapter 3. Jeff Ishibashi contributed to Western blots performed in Figure 1 of Chapter 2. Feodor Price and Fabien Le Grand carried out the differentiation fusion assays performed in Figure 2 of Chapter 3. Finally, unpublished ChIP-Seq data for Myogenin and Snail was provided by Vahab Soleimani for use in Chapter 3. I sincerely appreciate the help my collaborators provided to these projects. The author carried out experiments and provided data for all *in vitro* work within Appendix A, Figure 3C and 3D for Appendix B, and various aspects of the *in vitro* experiments throughout Appendix C.

Contents

List of Tables

Chapter 2 - Alternative splicing within the Pax7 paired-box DNA binding domain produces differential activation of myogenic target genes

Chapter 3 - Wnt/β-Catenin Controls Follistatin Signalling to Regulate Satellite Cell Myogenic Potential

List of Figures

List of Abbreviations

APC	adenomatous polyposis coli
bFGF	basic fibroblast growth factor
bHLH	basic helix-loop-helix
BIO	(2'Z,3'E)-6-Bromoindirubin-3'-oxime
Bmp	bone morphogenic protein
bp	base pair
BSA	bovine serum albumin
cDNA	complementary DNA
ChIP	chromatin immunoprecipitation
ChIP-Seq	high throughput ChIP sequencing
CTX	cardiotoxin
DAPI	4',6-diamidino-2-phenylindole
Dkk	dickkopf
DMEM	Dulbecco's modified Eagle's medium
DML	dorsomedial lip
DMSO	dimethyl sulfoxide
DNA	deoxyribonucleic acid
dpc	days post-coitum
DVL	dorsoventral lip
ECL	enhanced chemiluminescence
ECR	evolutionary conserved region
EDL	extensor digitalis longus
EMSA	electrophoretic mobility shift assay
EMT	epithelial to mesenchymal transition
FBS	fetal bovine serum
FDR	false discovery rate
FGF	fibroblast growth factor
FKHR	FoxO1
Fzd	frizzled
GAPDH	glyceraldyde-3-phosphate dehydrogenase
GDF8	growth and differentiation factor 8
GL	glycine-leucine
GO	gene ontology
GSK3β	glycogen synthase kinase 3 beta
H3K4	histone 3 lysine 4
HD	homeodomain
HDAC	histone deacetylase
HGF	hepatocyte growth factor
HMT	histone methyltransferase
HPLC	high-performance liquid chromatography
HTH	helix-turn-helix
Id	inhibitor of differentiation

IgG	Immunoglobulin G
kb	kilobase
Ki-67	proliferation-related Ki-67 antigen
Lbx1	ladybird
LRP	lipoprotein receptor-related protein
MAPK	mitogen-activated protein kinase
mdx	Duchenne muscular dystrophy
MEF	myocyte enhancer factor
MRF	myogenic regulatory factor
mRNA	messenger RNA
Myf5	myogenic factor 5
Myh2	myosin heavy chain
NO/NOS	nitric oxide/nitric oxide synthetase
Pax	paired-box transcription factor
PBS	phosphate-buffered saline
PCP	planar cell polarity
PCR	polymerase chain reaction
PD	paired domain
PDHD	paired domain and homeodomain
PEI	polyethylenimine
PFA	paraformaldehyde
PI3K	phosphoinositide 3-kinase
puro	puromycin
Q	glutamine
RIPA	radioimmunoprecipitation assay
RMA	robust multi-array average
RMS	rhabdomyosarcoma (alveolar, ARMS; embryonal, ERMS)
RNA	ribonucleic acid
RT	reverse transcription
S6RP	S6 Ribosomal Protein
SAM	significance analysis of microarrays
SDF	stromal derived factor
SDS-PAGE	sodium dodecyl sulfate-polyacrylamide gel electrophoresis
SEM	standard error of the mean
Shh	sonic hedgehog
TA	tibialis anterior
TBE	tris borate EDTA
TCF	T-cell factor
TF	transcription factor
TSS	transcription start site
VLL	ventrolateral lip
Wnt	wingless-related
wt	wild-type

Chapter 1 - General Introduction

1.1. Skeletal Muscle: An Overview

Muscle is classified as either smooth or striated skeletal and cardiac. In particular, the striated skeletal muscle comprises nearly 40% of the body's mass and is primarily responsible for skeletal movement. Skeletal muscle is composed of post-mitotic multinucleated muscle fibres that contain contractile elements, encircled by a layer of connective tissue and assembled into bundles (Charge and Rudnicki, 2004). These fibres are generated during development following the fusion of individual muscle progenitor cells.

The basic unit of the skeletal muscle is the myofibre; a syncytial cell packed with myofibrils, containing the sarcomeres that generate force by contraction. The fundamental mechanism of muscle contraction consists of a sliding mechanism of myosin-rich thick filaments over the actin-rich thin filaments following neuronal stimulation; known as the sliding filament model. These muscles are highly vascularized and are innervated by motor neurons. Stimulated by neural impulses from the central nervous system at neuromuscular junctions, calcium ions (Ca^{2+}) influx from the sarcoplasmic reticulum through voltage-gated Ca^{2+} channels. This Ca^{2+} binds to troponin C, causing an allosteric modulation of troponin T, and results in unblocking of myosin binding sites on actin filaments. This power stroke results in a release of adenosine diphosphate and shortening of the sarcomeres, resulting in muscle contraction. In addition, these muscles are anchored to the skeletal system through collagen fibres known as tendons.

While stable under physiological conditions, mammalian skeletal muscle has the remarkable ability to regenerate. Following injury, skeletal muscle undergoes a highly orchestrated degenerative and regenerative process, comprising changes at the tissue,

cellular and molecular levels. It is this ability for post-natal growth and repair that allows for continued muscle function throughout the lifespan of an organism.

1.2. Embryonic Myogenic Development

The segmentation of pre-somitic paraxial mesoderm, a derivative of the primitive streak, is one of the earliest occurrences of segmentation in the vertebrate embryo following gastrulation (Hollway and Currie, 2005). This highly coordinated anterior-posterior segmentation results in transient condensation of the paraxial mesoderm, which produces distinct units known as somites. These epithelial structures are arranged in pairs on either side of the neural tube and notochord and are produced under strict temporal and spatial control. These somites, which are patterned by signals from surrounding tissue, differentiate along the dorsal-ventral axis to give rise to the dorsally located epithelial dermomyotome and the ventrally located mesenchymal sclerotome by 8.0 days post-coitum (dpc) (Kaufman, 1992). The epaxial dermomyotome, located adjacent to the neural tube and notochord, will ultimately give rise to the deep back muscles, whereas the hypaxial dermomyotome will give rise to the remaining musculature of the body and limbs (Figure 1).

During somite maturation, myogenesis is initiated following delamination of cells from the epaxial and hypaxial lips of the dermomyotome. These cells translocate under the dermomyotome and subsequently differentiate into the skeletal muscle of the myotome. The epaxial myotome is formed following migration of progenitor cells of the dorsomedial lip (DML) beneath the dermomyotome by 8.5 dpc, where they withdraw from the cell cycle and terminally differentiate (Christ and Ordahl, 1995; Williams and Ordahl, 1997). Consistently,

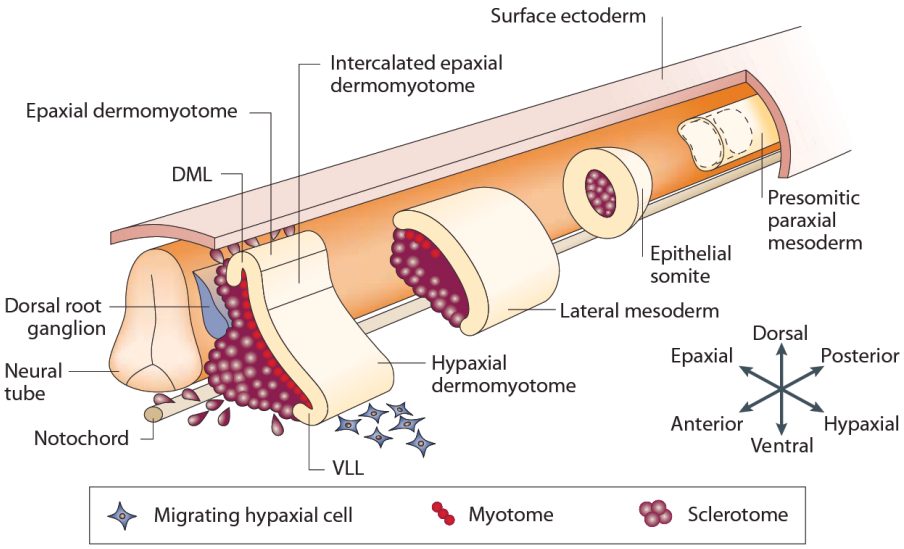

Figure 1. The embryonic origin of skeletal muscle
Segmentation of the presomitic paraxial mesoderm generates ball-like structures known as epithelial somites on either side of the neural tube, which ultimately give rise to muscle progenitor cells, amongst other tissues. Cells originating from the dorsomedial and ventrolateral regions of the dermomyotome translocate under the dermomyotome and form epaxial and hypaxial components of the myotome, respectively. Hypaxial cells from the VLL undergo an epithelial-to-mesenchymal transition, delaminate and migrate ventrally, while epaxial cells migrate from the DML and form deep back muscles. Adapted from (Parker et al., 2003).

a similar pattern of events occurs at the ventrolateral lip (VLL) of the dermomyotome by 9.5 dpc, establishing the ventral non-migrating hypaxial myotome (Kaufman, 1992). Further, cells from the VLL undergo an epithelial-to-mesenchymal transition (EMT), delaminate from the dermomyotome, and migrate ventrally, where they activate the myogenic program and form limb muscles, ventral body wall, diaphragm, and the tongue (Buckingham et al., 2003).

1.3. Myogenic Regulatory Factors

The development and differentiation of the myogenic lineage is regulated by the family of basic helix-loop-helix (bHLH) myogenic regulatory factors (MRFs) - MyoD, Myf5, myogenin and MRF4. The MRFs share a homologous bHLH domain that is required for DNA binding and dimerization with the E-protein family of transcription factors, including E12, E47 and HEB (Hu et al., 1992; Murre et al., 1989). MRF-E protein dimers bind the consensus E-box sequence CANNTG found in the promoters of many muscle-specific genes (Rudnicki and Jaenisch, 1995). Despite their similarities, MRFs share limited functional redundancy owing to sequence divergence in their amino- and carboxyl-termini (Braun et al., 1990; Weintraub et al., 1991).

In myogenic progenitor cells, the myogenic determination factors Myf5 and MyoD are responsible for establishing myogenic lineage commitment and specification. While a partial redundancy exists between Myf5 and MyoD (Braun et al., 1992; Rudnicki et al., 1992), the combined knock-out of both genes results in a complete absence of skeletal muscle (Rudnicki et al., 1993). In addition, muscle progenitors in $MyoD^{-/-}$;$Myf5^{-/-}$ mice acquire non-myogenic cell fates, indicative that either MyoD or Myf5 protein is required for

muscle specification. In MyoD$^{-/-}$ mice, myogenic cells compensate by upregulating Myf5 resulting in delayed differentiation, suggesting that Myf5 is initially insufficient for myogenic progression (Kablar et al., 1997). In contrast, while otherwise normal, Myf5$^{-/-}$ mice display delayed myotome formation until MyoD activation (Braun et al., 1994). Genetic lineage tracing studies using Myf5nLacZ reporter mice demonstrate that Myf5 is expressed in all embryonic muscles (Tajbakhsh et al., 1996), and LacZ-positive cells were found in the ribs of Myf5-deficient mice, indicating an essential role for Myf5 in myogenic specification.

Myogenin and MRF4 follow MyoD and Myf5 expression, and are required for myoblast fusion and terminal differentiation (Rudnicki and Jaenisch, 1995). While myogenin$^{-/-}$ mice initiate myogenesis, they possess a perinatal lethal defect in terminal differentiation while retaining a normal number of undifferentiated mononuclear myoblasts (Hasty et al., 1993; Nabeshima et al., 1993). While expressing higher levels of myogenin, MRF4$^{-/-}$ mice develop normal muscle suggesting a functional overlap (Zhang et al., 1995). This is further evident in MyoD$^{-/-}$;MRF4$^{-/-}$ mice, which display normal myogenin expression but phenocopy myogenin-null mice (Rawls et al., 1998). However, MRF4 may have a significant role in embryonic myogenesis with deficient mice exhibiting a range of phenotypes consistent with commitment, differentiation and maintenance (Braun and Arnold, 1995; Kassar-Duchossoy et al., 2004; Patapoutian et al., 1995).

In addition to the MRFs, the myocyte enhancer factor 2 (Mef2) family of MADS-box transcription factors act as cofactors to synergistically activate muscle specific genes (Molkentin and Olson, 1996). Mef2 proteins stimulate gene expression by binding AT-rich domains within the promoters of muscle specific genes. Myogenin and MRF4 both require

Mef2 binding in addition to MyoD or Myf5 for transcriptional activation (Black et al., 1995; Buchberger et al., 1994). In addition to the MRFs, several other molecular networks are important in regulating embryonic myogenesis.

1.4. Molecular Networks during Embryonic Myogenesis

Delamination and migration of skeletal progenitors from the hypaxial dermomyotome is dependent on the expression of c-Met, a receptor tyrosine kinase, and its ligand hepatocyte growth factor (HGF)/scatter factor. HGF signalling induces an EMT in the dermomyotome by inducing Snail transcription factors and PI3K/Akt signalling (Chang et al., 2011; Leroy and Mostov, 2007). HGF, which is required for long-range migration, is produced by non-somitic mesodermal cells and delineates the progenitor cell migratory routes (Dietrich et al., 1999). Mice lacking either c-Met or HGF lack limb musculature (Bladt et al., 1995), and the transcription of c-Met has been shown to be directly regulated by the paired-box transcription factor Pax3 (Epstein et al., 1996). Pax3 mutant mice lack limb and diaphragm muscles, owing to a deficit of c-Met expression, defective lateral migration and reduced proliferation in the dermomyotome (Bober et al., 1994; Daston et al., 1996; Tremblay et al., 1998).

In addition, Pax3 is required for the expression of the homeobox-containing transcription factor ladybird (Lbx1), which is expressed in migrating progenitors (Mennerich et al., 1998). Progenitor cells in Lbx1-deficient mice fail to properly migrate, and results in an extensive loss of limb musculature (Brohmann et al., 2000; Gross et al., 2000). While these progenitors delaminate, aberrant migration suggests that Lbx1 may function in interpreting signals along migratory routes and regulate an EMT switch (Yu et al., 2009).

Additional studies have identified an additional regulator of myogenic progenitor migration; the secreted cytokine stromal cell-derived factor and its receptor chemokine (C-X-C motif) receptor 4 (CXCR4). Mice deficient for CXCR4 exhibit migratory defects, in addition to genetic interaction with GRB2-associated binding protein, a c-Met signal transducer. These observations suggest an interaction between HGF-mediate signal transduction and chemokine activation by stromal derived factor (SDF) within myogenic progenitor cell migration (Vasyutina et al., 2005; Yusuf et al., 2006).

Pax3 is critical for the survival of the hypaxial dermomyotome through its role in the activation of MyoD expression (Borycki et al., 1999; Tajbakhsh et al., 1997); as well as ectopic Pax3 expression induces Myf5 and myogenin (Maroto et al., 1997). Transcriptional control of Pax3 expression is regulated by the sine oculis homeobox (Six) and eyes absent homologue (Eya) protein families, as Pax3 expression in the hypaxial dermomyotome is ablated and limb myogenesis is compromised in $Six1^{-/-}$;$Six4^{-/-}$ and $Eya1^{-/-}$;$Eya2^{-/-}$ double mutants (Grifone et al., 2007; Grifone et al., 2005). Six proteins also directly bind regulatory sequences upstream of Myf5 and myogenin (Giordani et al., 2007; Grifone et al., 2007; Spitz et al., 1998), suggesting a parallel function with Pax proteins during embryonic myogenesis. Six proteins have also demonstrated a role in epaxial myogenesis, through regulating the expression of MyoD and MRF4, while not affecting epaxial expression of Myf5 (Grifone et al., 2005). While embryonic muscle development is an intricate process regulating the spatial and temporal control of myogenic progenitors, skeletal muscle retains the eloquent ability to maintain a stable structure throughout adult stages following growth, injury and disease.

1.5. Myogenic Stem Cells – The Satellite Cell

The post-natal regenerative capacity of skeletal muscle is largely attributed to the satellite cell compartment. Satellite cells were first observed in a 1961 electron micrograph of frog skeletal muscle, where they were associated with the peripheral regions of the skeletal muscle fibres (Mauro, 1961). Having a low nuclear-to-cytoplasmic ratio and few organelles, satellite cells exhibited a nuclear morphology and were difficult to distinguish from peripheral myonuclei. However, electron microscopy identified a characteristic "wedged' appearance of the satellite cell position between the plasma membrane of the muscle fibre and the basement membrane. This morphology is consistent with the notion that satellite cells are mitotically quiescent (in G_0 phase), transcriptionally inactive, and can be characterized by an increased degree of heterochromatin (Schultz, 1976). Within perinatal mice, satellite cells comprise approximately 30-35% of sublaminar muscle nuclei, however, this population is reduced to approximately 2-7% in the adult following post-natal growth and development (Bischoff and Heintz, 1994). In response to stimuli following injury or exercise, satellite cells are activated, re-enter the cell cycle, and proliferate extensively to form a population of daughter myoblasts that will ultimately differentiate and fuse to repair damaged myofibres.

Satellite cells originate from the central region of the somitic dermomyotome during embryogenesis (Armand et al., 1983), and more recent reports have confirmed that these cells are responsible for both maintaining muscle growth during late embryonic development as well as contributing to a significant proportion of the satellite cell population (Gros et al., 2005; Relaix et al., 2005). By utilizing cell-labeling strategies, a population of cells originating from the hitherto unappreciated central domain of the

dermomyotome migrated to the myotome and continued to proliferate, while not expressing markers of myogenic differentiation. These cells were observed to be Pax3/Pax7 positive, persisted throughout the later stages of development and gave rise to skeletal muscle (Horst et al., 2006).

More recent generation of knock-in reporter alleles have permitted tracing of Pax3/Pax7 myogenic progenitors during muscle development and demonstrated their contributions to the satellite cell population (Lepper and Fan, 2010; Schienda et al., 2006). Further, Pax7+ cells gave rise to the dorsal trunk muscles, dorsal dermis, diaphragm and brown adipose tissues by 9.5 dpc, but not the ventral body wall or limb muscles. By 12.5 dpc, Pax7+ progenitors are muscle restricted, appear localized on fibres, establish the satellite cell position by 16.5 dpc and contribute to muscle regeneration (Lepper and Fan, 2010; Relaix et al., 2005). These populations of satellite cells are observed in close proximity to blood vessels and perisynaptic regions, and are located with greater density near the ends of myofibres, where longitudinal growth of skeletal muscle occurs (Allouh et al., 2008; Christov et al., 2007; Kelly, 1978).

1.6. Satellite Cell Self-Renewal and Commitment

The remarkable ability of satellite cells to sustain continued muscle regeneration is dependent on their ability to self-renew. This requirement was confirmed following cell transplantations, where single myofibre engraftments could undergo a 10-fold expansion of the satellite cell pool (Collins et al., 2005). Following activation, the proliferation of daughter myoblasts is accompanied by the rapid expression of MyoD and Myf5 (Cooper et al., 1999; Cornelison and Wold, 1997) (Figure 2), followed by the downregulation of Pax7

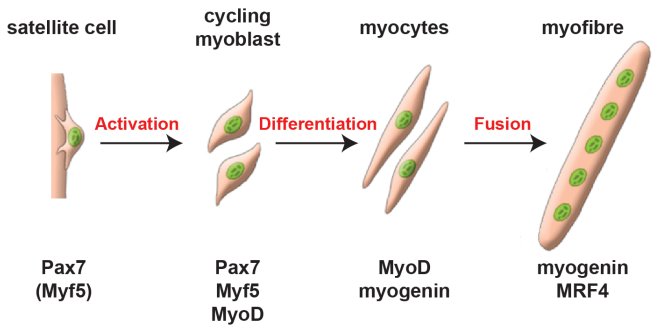

Figure 2. Schematic representation of adult myogenesis
Quiescent satellite cells are located along muscle fibres and persist as a heterogeneous population of satellite stem cells (Pax7+;Myf5-) and committed satellite myogenic cells (Pax7+;Myf5+). Following activation, these committed satellite myogenic cells further upregulate MyoD and form a population of rapidly proliferating myoblasts. Upon receiving signals to differentiate, these myoblasts upregulate myogenin expression and withdraw from the cell cycle. Differentiating myocytes will then align and fuse to form multinucleated, terminally differentiated myofibres.

expression. A small subset of cells will maintain Pax7 expression and repopulate the satellite cell compartment by returning to a quiescent state (Olguin and Olwin, 2004; Zammit et al., 2006). This ability to replenish the satellite cell pool is dependent on the capacity of satellite cells to self-renew.

One model for the self-renewal of the satellite cell compartment involves the return of active progenitor cells to the quiescent state through differential activation of the MRFs. It has been observed that Myf5+;MyoD- activated myoblasts exhibit increased proliferative capacity, but fail to initiate differentiation. This is consistent with the notion that these cells may represent an intermediate stage between a quiescent satellite cell and an activated myoblast (Megeney et al., 1996; Sabourin et al., 1999). Following the induction of differentiation, a population of undifferentiated Myf5+;MyoD- satellite cells persist, which retain the capacity to self-renew and to give raise to differentiation-competent progeny (Baroffio et al., 1996; Yoshida et al., 1998).

Within the satellite cell population, Cre/Lox lineage-tracing experiments revealed that while the majority of cells have expressed Myf5 during their developmental history, a minority, representing 10% of the sublaminar Pax7+ cells, never expressed Myf5 and thus are developmentally upstream of the main population (Kuang et al., 2007). Asymmetric divisions of Pax7+;Myf5- cells occurring in the apical-basal plane gave rise to both satellite stem cells (Pax7+;Myf5-) and committed satellite myogenic daughter cells (Pax7+;Myf5+). Further, planar cell divisions occurred for both populations and gave rise to two identical daughter cells through symmetric divisions. Transplantation experiments demonstrated that Pax7+;Myf5- satellite cells were able to efficiently repopulate the quiescent satellite cell

pool via symmetric expansion, and give rise to a population of committed myoblasts by asymmetric division.

1.7. The Paired-box (Pax) Transcription Factors

The paired-box (Pax) transcription factors, defined by the presence of a 128 amino acid DNA binding paired domain and named after the prototypical Drosophila paired gene, function as master regulatory genes in many aspects of embryonic patterning and organogenesis (Chi and Epstein, 2002). In mammals, nine Pax genes have been identified and characterized into four classes, and these genes primarily function through binding enhancer DNA sequences and modifying the transcriptional activity of downstream genes. The paired domain consists of independent amino- and carboxyl-terminal subdomains, each containing three α-helices arranged in a helix-turn-helix (HTH) unit, which bind to the major groove of DNA. These two subdomains are connected by an extended linker sequence, which binds the minor groove making numerous DNA contacts (Xu et al., 1999). A subset of Pax genes, including Pax7 and the closely related Pax3, contain an additional 60 amino acid DNA binding domain, the homeodomain, located carboxyl-terminal to the paired domain (Gehring et al., 1994). The homeodomain contains three α-helices connected by short loops, and an extended amino-terminal arm that is disordered in the absence of DNA. Upon binding with DNA, this arm inserts into the minor groove making sequence-specific contacts, whereas the recognition helix α3 fits into the major groove and interacts with bases on both strands of the DNA (Birrane et al., 2009). In addition, a conserved octapeptide motif is located in the intervening region between the two DNA binding domains. While both domains elicit the ability to bind DNA, reports suggest a functional interdependence of the

paired and homeodomain for Pax protein DNA binding (Jun and Desplan, 1996; Miskiewicz et al., 1996).

The sequence of Pax7 is highly homologous to the closely related Pax3, sharing 85% amino acid conservation overall and 94% identity within their DNA binding domains. Total Pax7 expression in satellite cells is a mixture of four isoforms generated by alternative splicing between exons 2 & 3 or exons 3 & 4 (Ziman and Kay, 1998) following alternative 3' splice site recognition at the exon boundary (Figure 3A). While both of these splice sites occur within the highly conserved paired domain, the exon 2/3 splicing event produces an inclusion or exclusion of a single glutamine residue (Q+/-), while the exon 3/4 change results in the presence or absence of a glycine-leucine dipeptide (GL+/-) (Ziman and Kay, 1998) (Figure 3B). Pax3 undergoes the same alternative splicing event for the Q+/- change (Vogan et al., 1996), however, Pax3 is only present lacking the GL dipeptide (GL-) (Du et al., 2005). In addition to splicing within the paired domain, several splice variants have been described for Pax3 and Pax7 following differential mRNA cleavage-polyadenylation within the carboxyl-terminal transactivation domain and resulting in the generation of products with diverse transactivational properties (Barber et al., 1999; Barr et al., 1999; Pritchard et al., 2003; Vorobyov and Horst, 2004). Similarly, alternative splicing has been described for other Pax proteins including Pax6, which results in a 14 amino acid insertion within the paired domain (Puschel et al., 1992). In contrast to other paired domains, which bind DNA predominantly by their amino termini, the extended Pax6 paired domain interacts with DNA exclusively through its carboxyl terminus (Epstein et al., 1994).

A

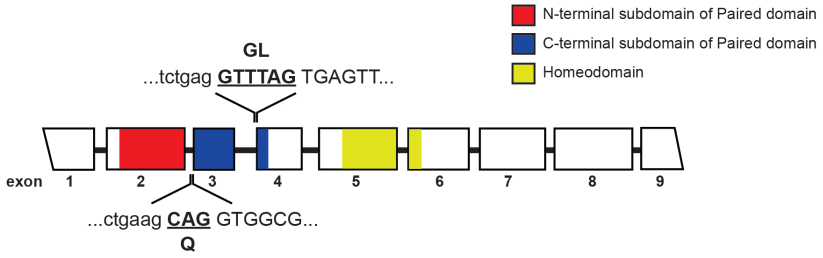

B

Isoform	Q (exon 2/3)	GL (exon 3/4
A	-	+
B	+	+
C	-	-
D	+	-

Figure 3. Schematic representation of Pax7 alternative splicing
(A) Alternative splicing events within the highly conserved Pax7 paired domain result in the inclusion or exclusion of a glutamine (Q+/-) residue or glycine-leucine (GL+/-) dipeptide. These splicing events are the result of alternative 3' splice site recognition at the exon 2/3 or 3/4 boundary, respectively.
(B) Summary of Pax7 alternative splicing events within the paired domain, which produces four isoforms known as Pax7a, Pax7b, Pax7c and Pax7d.

1.8 The Role and Function of Pax7 during Adult Myogenesis

During myogenic development, the absence of Pax7 results in adult skeletal muscles that are nearly devoid of satellite cells and the regenerative capacity of the muscle is extensively ablated (Kuang et al., 2006; Relaix et al., 2006; Seale et al., 2000). Analysis of Pax7-deficient mice has demonstrated the progressive loss of the satellite cell lineage, while remaining cells that survive in the satellite cell position arrest and die upon entering mitosis. Within Pax7-deficient muscles, myofibres contain approximately 50% the normal number of nuclei and fibre diameters are significantly reduced (Kuang et al., 2006).

In adult skeletal muscle, Pax3 is restricted to a subset of satellite cells, marking cells of the diaphragm and ventral trunk muscles (Relaix et al., 2005). Pax7-null mice retain Pax3 expression, but this does not compensate for the loss of Pax7 (Kuang et al., 2006; Relaix et al., 2005). Pax7 is involved in lineage survival through promoting satellite cell expansion and inhibiting apoptosis (Relaix et al., 2006; Zammit et al., 2004). Developing myoblasts undergo apoptosis within Pax3-null mice, a defect that can be rescued by ectopic Pax3 expression (Borycki et al., 1999). In addition, Pax3-null related neural tube defects can be rescued by the concurrent loss of p53 expression (Pani et al., 2002). In contrast, Pax3 does not play a critical role in adult muscle regeneration as its expression is absent from most satellite cells. However, Pax3 and Pax7 have some functional redundancy in the embryo; Pax7 can substitute for Pax3 in somite development and activation of myogenesis, but cannot compensate for Pax3 in regulating migration or efficient activation of c-Met (Relaix et al., 2004).

While more examination is required, the requirement for Pax7 in satellite cells has been suggested to be limited to a critical juvenile period when satellite cells are transitioning

to a quiescent state (Lepper et al., 2009). By employing tamoxifen inducible Pax7 conditional knockout mice, it was observed that deletion of Pax7 in the adult does not impact the function or survival of satellite cells. However, as further discussed in Appendix A, these observations are attributed to inefficient and incomplete Pax7 recombination following tamoxifen induction. Further, while non-myogenic derived cells have been shown to possess myogenic potential, the ablation of Pax7 expressing satellite cells by diphtheria toxin in adult muscle demonstrates that no other cell type is able to replenish the satellite cell pool (Lepper et al., 2011; Sambasivan et al., 2011).

Pax7 was observed to preferentially bind homeodomain binding motifs relative to Pax3, further suggesting mechanistic insight into the non-redundancy of these Pax proteins during muscle development and regeneration (Soleimani et al., 2012). Through binding to DNA, Pax7 recruits the Wdr5/Ash2L/MLL2 histone methyltransferase (HMT) complex resulting in Histone 3 Lysine 4 trimethylation (H3K4me3) (Kawabe et al., 2012; McKinnell et al., 2008). As a result, the recruitment of Pax7 functions to establish transcriptionally active chromatin domains, through epigenitic modifications, surrounding proximal promoters. Carm1, an arginine methyltransferase, interacts with Pax7 and mediates the recruitment of the HMT complex following Pax7 methylation, and functions as a molecular switch controlling the epigenetic induction of Myf5 during asymmetric divisions of satellite stem cells and entry into the myogenic program (Kawabe et al., 2012). In addition, since its activity is associated with remodeling of chromatin, it has been suggested that Pax7 may function as a pioneer transcription factor and possess the ability to navigate through condensed chromatin and promote a transcriptionally permissive environment (Budry et al., 2012).

Mutations within Pax3 lead to the development of the human Waardenburg syndrome. While characterized by hearing loss and changes in pigmentation of the hair, skin and eyes, interestingly, there is no observed muscle impairment (Wang et al., 2008). In contrast, both Pax3 and Pax7 are associated with the development of alveolar rhabdomyosarcomas (ARMS), a pediatric soft tissue cancer originating from muscle. This cancer arises from chromosomal translocations that fuses the carboxyl-terminal transactivation domain of the FoxO1 (FKHR) transcription factor to the amino-terminal DNA binding domains of either Pax3 or Pax7 (Wexler and Helman, 1994). In addition, Pax7 expression is associated with the embryonal subtype of RMS (eRMS) (Tiffin et al., 2003). Of interest, these fusion proteins act as aberrant transcription factors and regulate the expression of numerous genes, including the myogenic regulatory factors (Bennicelli et al., 1996). The resulting tumors contain poorly differentiated tissue, while displaying elements of a partial muscle phenotype. Specifically, it has been observed that these fusion proteins suppress the transcriptional activation of MyoD target genes, resulting in inhibition of myogenic differentiation (Calhabeu et al., 2013; Olguin et al., 2011).

1.9. Extrinsic Signalling Pathways during Adult Myogenesis

Satellite cells remain mitotically quiescent under normal physiological conditions; however, they undergo activation in response to muscle injury or growth. The ligand HGF has been identified as playing a crucial role in the cellular activation, and its receptor c-Met is found within the basal lamina of skeletal muscle fibres (Jennische et al., 1993; Tatsumi et al., 1998). In addition, nitric oxide (NO) production by nitric oxide synthase (NOS) triggers the release of HGF from the extracellular matrix and rapidly associates with its receptor

(Anderson, 2000; Tatsumi et al., 2002). NOS activity is also required for the maintenance of quiescence in satellite cells, suggesting a dual role of NO (Wozniak and Anderson, 2007). The fibroblast growth factor 2 (FGF2) may function as an alternative stimulus (Cornelison et al., 2001; Flanagan-Steet et al., 2000; Yablonka-Reuveni et al., 1999), and it should be noted that syndecans 3/4 are heparin sulphate proteoglycans that contribute to HGF and FGF signalling (Cornelison et al., 2001). HGF and FGF can stimulate the p38 mitogen-activated protein kinase (MAPK) signalling pathway. While initial studies demonstrated that p38α/β promotes myogenic differentiation (Wu et al., 2000; Zetser et al., 1999), additional studies have suggested that p38α/β MAPK is required for satellite cell proliferation (Jones et al., 2005). Further, p38γ signalling positively regulates myoblast expansion during muscle growth and regeneration (Gillespie et al., 2009).

Notch Signalling

The Notch signalling pathway mediates communication between Notch-expressing cells and cells expressing Notch-activating ligands such as Delta1. This pathway is activated by the interaction of the Notch receptor with its ligand leading to internal cleavage of the Notch intracellular domain (NICD). This leads to its subsequent translocation to the nucleus where it associates with other co-activators of transcription (Artavanis-Tsakonas et al., 1999). Notch1 signalling is responsible for maintaining the expansion of satellite cells, and its expression is lost during differentiation (Conboy and Rando, 2002; Gnocchi et al., 2009). Notch3 is upregulated in quiescent cells (Fukada et al., 2007), in addition to the satellite stem cell compartment (Pax7+;Myf5-), while Delta1 is increased in committed satellite cells (Pax7+;Myf5+) and interferes with MyoD expression (Kuang et al., 2007).

The Wnt Signalling Pathway

First discovered as the Drosophila wingless and mouse int-1 genes, Wnt proteins constitute a large family of cysteine-rich secreted glycoproteins that play a critical role during development. In mammals, the Wnt family consists of 19 members that, while sharing similarities in their amino acid sequence, have fundamentally distinct signalling properties (Nusse, 2012). Wnt proteins bind Frizzled (Fzd) receptors, seven-transmembrane proteins containing a large extracellular cysteine-rich domain, and low-density lipoprotein receptor-related protein (LRP5/6) pairs, resulting in an intracellular response. Classically, this signalling cascade can function via the canonical Wnt/β-catenin pathway (Clevers, 2006; Simons and Mlodzik, 2008) or may occur through non-canonical Wnt pathways; the Wnt/planar cell polarity (PCP) pathway (Simons and Mlodzik, 2008) or the Wnt/Ca^{2+} pathway (Saneyoshi et al., 2002) (Figure 4).

The canonical Wnt signalling pathway is regulated by the stabilization and subcellular localization of β-Catenin. In the absence of Wnt signal, intracellular β-Catenin is associated with Axin and adenomatous polyposis coli (APC) leading to proteasomal degradation following glycogen synthase kinase 3-β (GSK3β) dependent phosphorylation by casein kinase I (CK1) (Logan and Nusse, 2004). In the presence of Wnt proteins binding to the Fzd and LRP5/6 receptors, heterotrimeric G proteins and Disheveled (Dvl) become activated, leading to the recruitment of Axin to the LRP5/6 receptor (Grumolato et al., 2010). This results in inhibition of the GSK3β mediated phosphorylation, resulting in nuclear translocation of β-Catenin. Once localized to the nucleus, β-Catenin binds with members of the T-cell factor (TCF)/lymphoid-enhancer factor (Lef) family of transcription factors and modulate target gene expression (MacDonald et al., 2009).

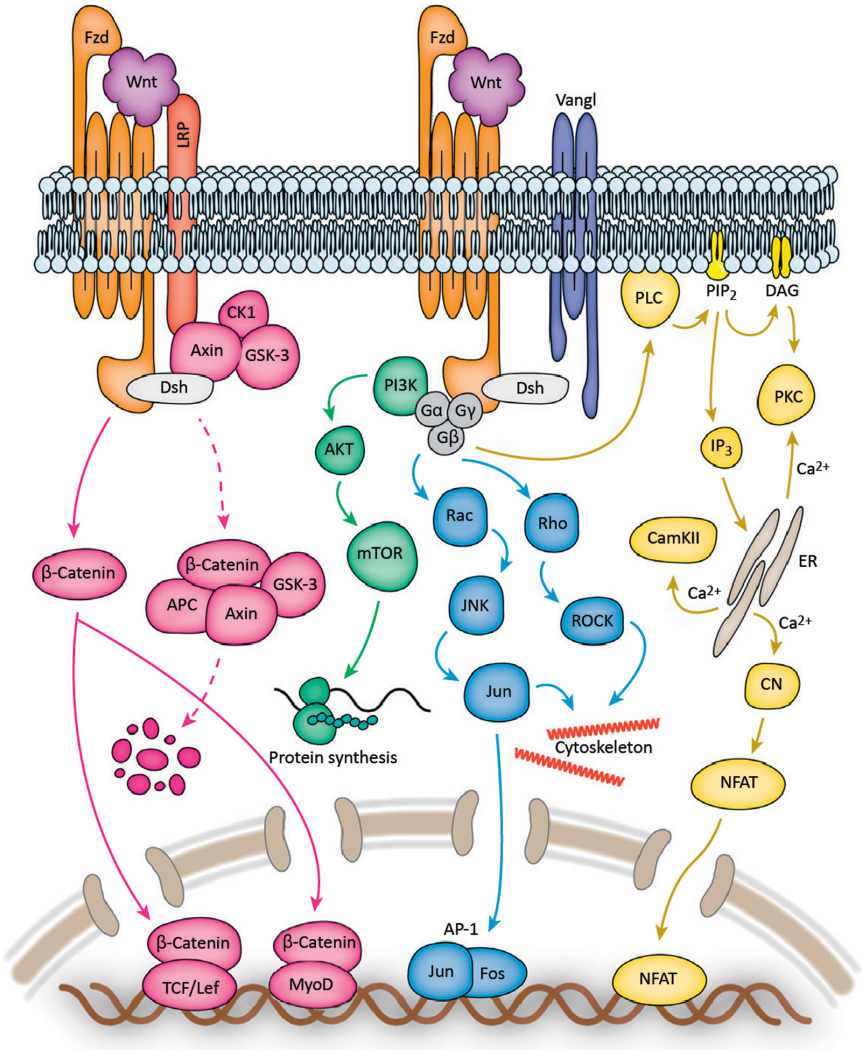

Figure 4. Summary of Wnt signalling pathways
Wnt signals occur through the canonical pathway (pink) or various non-canonical pathways (for example Wnt/PCP, Wnt/Akt/mTOR, or Wnt/Ca^{2+}). Specifically, the canonical Wnt signalling pathway functions through the intracellular protein β-Catenin. In the absence of Wnt signal, β-Catenin undergoes proteasomal degradation following phosphorylation by GSK3β. In the presence of Wnt ligand bound to the Fzd receptors, the destruction complex is localized to the membrane by Dvl, allowing for nuclear translocation of β-Catenin. Once in the nucleus, β-Catenin can complex with TCF/Lef proteins or other transcription factors such as MyoD, and alter the modulation of gene transcription. Adapted from (von Maltzahn et al., 2012).

Wnt signalling has been implicated in various stages of the satellite cell lineage. Exposure to Wnt7a induces satellite stem cells to undergo symmetric expansion through Fzd7 and the Wnt/PCP pathway, resulting in expanding the satellite stem cell population (Le Grand et al., 2009). In addition, Wnt7a-deficient mice exhibit reduced numbers of satellite cells following regeneration. In the early stages following injury, Wnt5a, Wnt5b and Wnt7a are upregulated, while Wnt3a and Wnt7b are expressed in the later stages of regeneration (Brack et al., 2008; Polesskaya et al., 2003). In addition, the canonical Wnt signalling pathway is involved in satellite cell-mediated regeneration. While Wnt signalling has been implicated in promoting the proliferation of satellite cells (Otto et al., 2008), another report has demonstrated that Wnt/β-Catenin signalling promotes terminal differentiation by limiting Notch signalling (Brack et al., 2008). During muscle regeneration, Notch signalling is activated and stimulates the proliferation of satellite cells leading to the expansion of proliferating myoblasts (Conboy and Rando, 2002). During differentiation, Wnt/β-Catenin signalling antagonizes the effects of Notch signalling, and through reduced GSK3β levels, allows progression of myogenic commitment and differentiation (Brack et al., 2008). In addition, canonical Wnt signalling is involved in the development of muscle fibrosis during aging. Canonical Wnt signals are increased in aged mice, and the exposure to Wnt3a leads to increased deposition of connective tissue following fibrogenic transdifferentiation of satellite cells (Brack et al., 2007). While additional studies are required, these observations further implicate canonical and non-canonical Wnt signalling within the satellite cell population.

TGF-β Signalling

In addition to Wnt signals, transforming growth factor-β (TGF-β) family members are important cytokines that regulate cell growth. Through binding membrane receptors, TGF-β activates phosphorylation of Smad proteins, resulting in their nuclear translocation and activation of target genes (Chen et al., 2002). Myostatin/growth and differentiation factor-8 (GDF-8) is a TGF-β family member that binds the activin receptor type II (ActRII) and acts as a negative regulator of skeletal muscle mass. Myostatin-null mice display hypertrophic and hyperplastic muscle (McPherron et al., 1997), and during development, myostatin expression limits the rate of muscle growth without impairing the establishment of myogenic structures (Amthor et al., 2002). Following exposure to myostatin, activin receptor-like kinases are phosphorylated by ActRII, leading to the phosphorylation of TGF-β specific Smad2 and Smad3, which complex with Smad4. Together, the Smad2/3/4 complex is translocated to the nucleus to mediate target gene expression, including Pax3, Pax7, Myf5 and MyoD (Amthor et al., 2002; Langley et al., 2002; Lee and McPherron, 2001; McFarlane et al., 2008).

Myostatin-null mice have a greater number of proliferating satellite cells, possibly due to increased self-renewal potential and delayed expression of myogenin (McCroskery et al., 2003; McCroskery et al., 2005). Inactivation of myostatin signalling enhances muscle regeneration and promotes satellite cell self-renewal through a Pax7-dependent mechanism (McFarlane et al., 2008). In contrast, a more recent report suggests that the hypertrophy observed in the absence of myostatin is independent from satellite cells, and hypertrophic muscle generated by myostatin blockage was achieved with no contribution from the satellite cell population (Amthor et al., 2009).

Follistatin is a secreted glycoprotein that antagonizes various members of the TGF-β superfamily, including myostatin (Hemmati-Brivanlou et al., 1994; Iemura et al., 1998). Originally identified in porcine ovarian follicular fluid, follistatin was suggested to promote muscle fibre hypertrophy by inhibiting the myostatin repressive effects on myogenic progenitor differentiation and muscle fibre growth (Lee and McPherron, 2001; Nakamura et al., 1990). Through antagonizing myostatin and activin A activity, follistatin overexpression leads to a more dramatic muscle phenotype than the myostatin-null mouse (Lee et al., 2005). Strikingly, follistatin regulation remains functional in myostatin-null mice, suggesting a myostatin-independent function (Lee, 2007; Lee et al., 2010). Recent observations suggest that follistatin promotes muscle hypertrophy through suppressing the phosphorylation of Smad3, resulting in potentiation of mTOR/S6 protein kinase (S6K)/S6 ribosomal protein (S6RP) signalling and inhibition of GSK3β (Ruvinsky et al., 2009; Winbanks et al., 2012). The mTOR dependent phosphorylation of S6RP leads to increased protein synthesis and cell size from enhanced protein translation initiation and elongation (Glass, 2005).

Another important TGF-β family member is bone morphogenic protein (BMP), which initiates signalling by binding to transmembrane type 1 and type 2 BMP receptors (BMPRs). On BMP binding, these receptors complex on the cell surface, and lead to phosphorylation of the R-Smads (Smad1/5/8), which translocate to the nucleus to regulate transcription of target genes (Feng and Derynck, 2005). These targets include the inhibitor of differentiation/DNA-binding (Id) proteins, which bind E-proteins to form inactive heterodimers, thus preventing association with MyoD and myogenin (Jen et al., 1992). In addition, activated satellite cells express BMPR1A, and exogenous BMP4 stimulation

results in enhanced satellite cell division while inhibiting cell cycle exit and myogenic differentiation (Friedrichs et al., 2011; Ono et al., 2011).

The endpoint of differentiation requires a substantial phenotypic shift from a proliferating mononucleated myoblast to a contractile, multinucleated muscle fibre. The induction of this terminal differentiation is aided by the MyoD-dependent activation of downstream target genes, including myogenin, M-cadherin, myosin heavy and light chains, and muscle creatine kinase (Berkes and Tapscott, 2005). MyoD expression peaks at the differentiation checkpoint in G_1 of the cell cycle, while Myf5 expression is high in S/G_2 (Kitzmann et al., 1998). This induction of differentiation follows the activation of the cell cycle arrest protein p21 and permanent exit from the cell cycle (Smith et al., 1994). Ultimately, these mononucleated myogenic cells undergo fusion to existing muscle fibres or to each other to form multinucleated syncytia, which then mature by synthesizing and organizing proteins necessary to function as contracting units within the post-natal muscle compartment (Charge and Rudnicki, 2004).

1.10. Rationale and Hypothesis

Given the functional importance of Pax7 during adult myogenesis, which is attributed to its ability to directly bind DNA, we rationalized that modifications within the DNA binding paired domain would effect the role of Pax7. In addition, mutational analyses of Pax3 have indicated that loss of DNA binding activity by one domain invariably leads to the loss of DNA binding by the other, suggesting that the paired domain and homeodomain functionally interact. While these splice variants of the Pax7 paired domain are believed to exhibit distinct tertiary structures, a specific function for these alternative splicing events has

not been described. We hypothesize that while Pax7 DNA binding domains play distinct functional roles during myogenesis, alternative splicing events of the paired domain generates four functionally important isoforms that evoke the potential to differentially activate target genes. The identification of unique roles for the Pax7 isoforms will complement functional data for the importance of Pax7 expression, and aims to provide a mechanistic explanation of binding properties of the paired domain splice variants.

In addition to further examining the role of Pax7 during satellite cell growth and maintenance, it remains important to obtain a greater understanding of the downstream differentiation effects of satellite cell derived myoblasts. Previous research has demonstrated that stimulation by Wnt3a results in the activation of the canonical Wnt signalling pathway in myogenic cells. Further, expression of Wnt3a in muscle results in an increase in the number of myofibres, which exhibit a dramatic reduction in the cross-sectional area and reduced regenerative efficiency (Appendix C). Given these findings, we hypothesize that canonical Wnt signalling induces premature myogenic differentiation of satellite cell derived myoblasts. Through mechanistically understanding the role of canonical Wnt signalling during myogenesis, we aim to obtain a better understanding of the myogenic function of β-Catenin signalling. The effects of canonical Wnt-signalling on myogenic differentiation will complement our observations regarding Pax7 alternative splicing during myoblast proliferation. These observations will provide a greater comprehensive understanding of the molecular regulation of satellite cell development and differentiation during adult myogenesis.

Chapter 2 - Alternative splicing within the Pax7 paired-box DNA binding domain produces differential activation of myogenic target genes

Alternative splicing within the Pax7 paired-box DNA binding domain produces differential activation of myogenic target genes

Andrew E. Jones[1,2], Jeff Ishibashi[1,2] and Michael A. Rudnicki[1,2]

1. Regenerative Medicine Program,
   Ottawa Hospital Research Institute,
   501 Smyth Road, Ottawa, ON K1H 8L6
   Canada

2. Department of Cellular and Molecular Medicine,
   Faculty of Medicine, University of Ottawa,
   451 Smyth Road, Ottawa, ON K1H 8M5
   Canada

SUMMARY

The transcription factor Pax7 is essential for the survival and function of satellite cells that repair skeletal muscle following damage. Alternative splicing acceptors at exons 3 and 4 allow for the variable inclusion of a Q residue or GL dipeptide within the highly conserved DNA binding domain, resulting in the expression of four distinct Pax7 isoforms (Pax7a, Pax7b, Pax7c, Pax7d). Of the four isoforms, we found that Pax7d (Q+GL-) was the most predominantly expressed isoform in myoblasts followed by Pax7b (Q+GL+). Given their abundant expression, we performed global transcriptome RNA sequencing analysis of both isoforms to identify if they differentially regulate Pax7 target genes. Interestingly, although we found that while both isoforms were able to activate and/or repress common target genes, Pax7d was a stronger gene activator and resulted in greater changes in gene expression, particularly in the expression of growth and proliferation genes. These results suggest that while the majority of Pax7 binding occurs via the homeodomain, the subtle differences in the paired domain of individual isoforms can provide an additional level of target gene regulation during myogenesis. Hence, we demonstrate that the essential role of Pax7 during myogenesis is mediated primarily through the action of the Pax7d splice variant.

INTRODUCTION

The post-natal regenerative capacity of skeletal muscle is attributed to a distinct population of myogenic stem cells, satellite cells, which function as lineage-committed precursors to replace terminally differentiated muscle fibres. Normally quiescent in the adult, satellite cells reside between the basal lamina and sarcolemma of the muscle fibre (Mauro, 1961; Montarras et al., 2005; Schultz et al., 1978). During muscle regeneration, this satellite cell pool is activated, proliferates as a population of daughter myoblasts and ultimately differentiates and fuses into new or existing myofibres.

Skeletal muscle has a remarkable ability to regenerate following injury through a highly orchestrated process contingent upon the proper expression of the paired-box transcription factor Pax7, and the basic helix-loop-helix (bHLH) myogenic regulatory factors (MRFs); Myf5, MyoD, myogenin and MRF4 (Perry and Rudnicki, 2000). In the adult, Myf5 and MyoD provide myogenic identity to proliferating myoblasts, while myogenin and MRF4 are expressed through differentiation (Sabourin and Rudnicki, 2000). Pax genes, defined by the presence of a 128 amino acid DNA binding paired domain, function as master regulatory genes in many aspects of embryonic patterning and organogenesis (Chi and Epstein, 2002). A subset of Pax genes, including Pax7 and the closely related Pax3, contain an additional 60 amino acid DNA binding domain located carboxyl-terminal to the paired domain, the homeodomain, which is also implicated in embryogenesis and development (Gehring et al., 1994). While both domains have the ability to bind DNA, reports suggest a functional interdependence of these two domains for Pax DNA binding (Jun and Desplan, 1996; Miskiewicz et al., 1996). During myogenic development, the absence of Pax7 results in adult skeletal muscles that are nearly devoid of

satellite cells and the regenerative capacity of the muscle is extensively ablated (Kuang et al., 2006; Relaix et al., 2006; Seale et al., 2000). Analysis of Pax7-null mice has demonstrated the progressive loss of the satellite cell lineage, while remaining cells that survive in the satellite cell position arrest and die upon entering mitosis. Within Pax7-deficient muscles, myofibres contain approximately half the normal number of nuclei and fibre diameters are significantly reduced (Kuang et al., 2006). However, while more examination is required, this requirement for Pax7 in satellite cells has been suggested to be limited to a critical juvenile period when satellite cells are transitioning to a quiescent state (Lepper et al., 2009).

The satellite cell compartment consists of a heterogeneous population of myogenic committed satellite cells (Pax7+;Myf5+) and a subpopulation of satellite stem cells (Pax7+;Myf5-), discriminated following asymmetric cell divisions based on Myf5 expression (Kuang et al., 2007). Through these asymmetric divisions, satellite stem cells possess the ability to self-renew, and it is this characteristic that allows adult skeletal muscle to undergo regeneration throughout the lifetime of an organism (Collins et al., 2005; Kuang et al., 2007; Zammit et al., 2004).

A recent analysis employed chromatin immunoprecipitation of Pax7 bound DNA motifs coupled with high-throughput massive parallel sequencing (ChIP-Seq) to identify active genes involved in specifying myogenic identity, promoting proliferation and inhibiting differentiation (Soleimani et al., 2012). In particular, Pax7 was observed to preferentially bind homeodomain binding motifs relative to Pax3, further suggesting mechanistic insight into the non-redundancy of these Pax proteins during muscle development and regeneration. Through binding to DNA, Pax7 protein recruits the

Wdr5/Ash2L/MLL2 histone methyltransferase (HMT) complex resulting in Histone 3 Lysine 4 trimethylation (H3K4me3) and subsequent gene activation (Kawabe et al., 2012; McKinnell et al., 2008). In addition, since its activity is associated with remodeling of chromatin, Pax7 may function as a pioneer transcription factor and possess the ability to navigate through condensed chromatin promoting a more transcriptionally permissive environment (Budry et al., 2012). Taken together, these data support an essential role for Pax7 in regulating the myogenic potential of satellite cells.

Total Pax7 expression in satellite cells is a mixture of four isoforms generated by alternative splicing events between exons 2 & 3 or exons 3 & 4 (Ziman and Kay, 1998) following alternative 3' splice site recognition at the exon boundary. The exon 2/3 splicing event produces an inclusion or exclusion of a single glutamine residue (Q+/- at position #138); the exon 3/4 change results in the presence or absence of a glycine-leucine dipeptide (GL+/- at position #180 or #181) (Ziman and Kay, 1998). The structure of Pax7 is highly homologous to the closely related Pax3, sharing 85% amino acid conservation overall, and of particular interest, 94% identity within the DNA binding domains. Pax3 undergoes the same alternative splicing event for the Q+/- change (Vogan et al., 1996), which occurs within the linker region between the two paired-box subdomains. However, unlike Pax7, Pax3 is only present as a GL- form (Du et al., 2005), an event that is located within the carboxyl-terminal paired-box subdomain. Given the Q+/- and GL+/- changes occur within the highly conserved paired-box DNA binding domain, this would suggest that they could modulate the DNA binding site recognition or affinity of the splice variants. While splicing-dependent modifications for DNA binding affinity have been previously confirmed for the

Q+/- change in Pax3 (Vogan et al., 1996), a specific function for the Pax7 GL+/- alternative splicing event has not been described.

To further investigate the function of Pax7 alternative splicing events in adult myogenesis, we ectopically expressed the Pax7 isoforms in myoblasts and fibroblasts. Strikingly, while Pax7 is able to increase Myf5 expression in myogenic cells, only the GL- isoforms Pax7c and Pax7d can initiate Myf5 expression in non-myogenic cells. Further, we identified that Pax7d (Q+GL-) is the predominant expressed Pax7 isoform, and undertook a global transcriptome analysis to identify Pax7b (Q+GL+) and Pax7d (Q+GL-) targets. Interestingly, we observed that while both isoforms are able to activate or repress Pax7d targets, this observed regulation was stronger for the Pax7d isoform. To this end, we observe that while the majority of Pax7 binding occurs via the homeodomain, these subtle isoform changes in the paired domain can provide an additional level of Pax7 target gene regulation during myogenesis. Therefore, we demonstrate that the essential role of Pax7 during satellite cell derived myogenesis is primarily due to the Pax7d splice variants mode of action.

METHODS

Cell Culture and Viral Infection

Primary myoblasts were isolated from the hind limbs of 4-6 week old wild type C57Bl/6 mice as previously described (Megeney et al., 1996), and propagated on collagen-coated culture dishes in Ham's F10 media supplemented with 20% fetal bovine serum (FBS), 1% penicillin/streptomycin and 2.5 ng/ml human recombinant bFGF. Myogenic differentiation was induced by shifting to differentiation media (DMEM supplemented with 5% horse serum). C2C12 myoblasts and C3H10T1/2 fibroblasts were cultured in DMEM media supplemented with 10% FBS and 1% penicillin/streptomycin. Expression plasmids (Pax7a-, Pax7b-, Pax7c- or Pax7d-FLAG, and empty vector) were constructed in a modified pHAN backbone containing a SV40-driven puromycin resistance element by fusing mouse Pax7 in-frame with a carboxyl-terminal 3xFLAG tag (McKinnell et al., 2008). Retrovirus was produced in 293FT cells by transient transfection of expression constructs using Lipofectamine 2000 reagent (Invitrogen). Virus-containing supernatant was used to infect C2C12, 10T1/2 or low-passage primary myoblasts supplemented with DMEM or Ham's complete medium; respectively, and 8 μg/ml polybrene (Sigma). Transgenic cells were obtained by antibiotic selection and maintained in DMEM or Ham's complete medium containing 1.0 μg/ml puromycin (Sigma).

Gene Expression Analyses

Global gene expression was assessed in retroviral Pax7bFLAG and Pax7dFLAG low-passage primary myoblasts relative to an empty vector control (puro). Total RNA was isolated and subjected to on-column DNase digestion using an RNeasy Kit as per the

manufacturer's instructions (Qiagen), and submitted to Stem Core Laboratories (Ottawa, ON) for whole transcriptome analysis (RNA-Seq) as per manufacturer's recommendations (Illumina). Reads from RNA-Seq samples were mapped to the mm9 (NCBI build 37) mouse genome assembly by Tophat (Trapnell et al., 2009). Gene expression values were calculated by Cufflinks with default parameters (Trapnell et al., 2010). Differentially expressed genes between Pax7bFLAG, Pax7dFLAG and control samples (puro) were called by Cuffdiff (Roberts et al., 2011a; Roberts et al., 2011b; Trapnell et al., 2010). Gene ontology of expression data was performed using the functional annotation module of DAVID 6.7 (Huang et al., 2009a, b).

Real-Time PCR

Total RNA was isolated using the RNeasy Kit and subjected to on-column DNase digestion as per manufacturer's instructions (Qiagen). cDNA synthesis was performed using the Superscript III reverse transcriptase with random hexamer primers (Invitrogen). SYBR Green Real-Time PCR was carried out as previously described (Holterman et al., 2007). Transcript levels were normalized to GAPDH transcript levels and relative fold change in expression was calculated using the ΔΔCT method (CT values < 30). PCR primers were designed using the online Primer3 software (http://primer3.wi.mit.edu) (Rozen and Skaletsky, 2000). Primer sequences are listed in Table S1.

^{32}P End-Labeled RT-PCR

Pax7 exon 2 forward primers were end-labeled with γ-[^{32}P]-ATP (Amersham Biosciences) by T4 kinase (Invitrogen) in a final reaction volume of 20 µl, as previously described (Huh

et al., 2004). Pax7 RT-PCR was performed under standard conditions using 0.4 µl of end-labeled primer in each 10 µl PCR reaction. 20 ng cDNA was used as a starting template in each PCR reaction. Radiolabeled PCR products were resolved on a 7% denaturing polyacrylamide gel and exposed to film. Band densities were quantified using ImageJ analysis software (Schneider et al., 2012).

Western Blot

Total protein was harvested in RIPA lysis buffer fortified with protease inhibitors (Complete-Mini; Roche-Boehringer), and protein concentration was determined by Bradford assay (BioRad). Samples (20 µg) were subjected to SDS-PAGE and electroblotted onto Immobilon-P membrane (Millipore). Membranes were blocked in 5% non-fat milk in PBST prior to sequential probing with primary antibody and HRP-conjugated secondary antibody in blocking solution. ECL (Amersham-Pharmacia) with BioMax XAR film (Kodak) was used to detect target proteins. Primary antibodies used for detection are as follows: α-Myf5 (Santa Cruz), α-MyoD (Sigma), α-Pax7 (Developmental Studies Hybridoma Bank), α-Tubulin (Sigma) and α-FLAG (Sigma). Secondary antibodies were HRP-conjugated anti-mouse and anti-rabbit (BioRad).

Electrophoretic Mobility Shift Assays (EMSA)

All probes were synthesized as full-length oligonucleotides and purified by HPLC (Integrated DNA Technologies). EMSA experiments were carried out as previously described (Soleimani et al., 2012). In brief, single stranded probes (+) were radiolabeled by incubation with T4 Kinase (Invitrogen) in the presence of γ-[^{32}P]-ATP for 1 hour at 37°C.

Double stranded probes were generated by hybridizing with opposite strand probe (-), boiling for 2 minutes, and slowly cooling to room temperature over 2 hours. Pax7b and Pax7d proteins were synthesized *in vitro* using TNT Coupled Reticulocyte Lysate System (Promega) following manufacturer's recommendation. Pax7b and Pax7d proteins were incubated with cold non-specific probe (ΔPD/ΔHD) for 20 min to reduce the internal background and then incubated with radiolabeled probe for 30 min at room temperature. DNA-protein complexes were separated on 5% non-denaturing polyacrylamide gel (0.5× TBE), dried onto 3 mm Whatman paper, and exposed to BioMax MS film (Kodak). Probe sequences are listed in Supplementary Table S1.

Luciferase Reporter Assays

Luciferase reporter vectors were constructed as follows. For the paired domain (PD) and homeodomain (HD) reporters, three copies of 30 bp sequences covering the PD or HD motifs were directionally concatamerized and cloned upstream of a minimal Myf5 promoter driving the *luc* gene of pGL4.10 (Promega), as previously described (Soleimani et al., 2012). A 70 bp sequence covering the entire Myf5 ECR111 regulatory element, including both the PD and HD regions was also concatamerized and cloned as above to generate the PDHD reporter. Reporter vectors were cotransfected with a *renilla* vector standard and either empty vector (FKHR), Pax7bFKHR or Pax7dFKHR for 16 hours into Cos7 cells using linear polyethylenimine (PEI; Sigma). Luciferase assays were carried out using the Dual-Reporter Luciferase Assay System (Promega) and analyzed on a Lumistar Optima (BMG Labtech) fluorescent plate reader.

ChIP Analysis

Protein-DNA complexes were cross-linked with 1% formaldehyde (Sigma) and sheared by sonication. Processing of samples was performed, as previously described (Soleimani et al., 2012); 2000 μg of protein-DNA complexes were immunoprecipitated with M2-Agarose (Sigma) for 2 hours, followed by wash conditions and DNA elution performed according to the ChIP Assay Kit (Upstate). The immunoprecipitated DNA was subjected to Real-Time PCR, and results were normalized using control locus representing DNA fragments that were non-specifically immunoprecipitated.

Statistical Analysis

Three or more replicates were analyzed for each experiment presented. Data is shown as standard error of the mean (SEM) and results were assessed for statistical significance by a Student's T-Test. Differences were considered statistically significant at the $p < 0.05$ level.

RESULTS

Alternative splicing of Pax7 differentially activates Myf5 expression

Previously, we observed that Pax7d was capable of upregulating Myf5 expression in C2C12 myoblasts and satellite cell derived myoblasts (McKinnell et al., 2008; Soleimani et al., 2012). Given these observations, we examined whether this function was common to all four Pax7 isoforms. To test this, each of the four isoforms were stably expressed in C2C12 myoblasts following infection with drug-selectable retrovirus. Western blots of total protein from each of these populations demonstrate that Myf5 protein was increased by Pax7a, Pax7b, Pax7c and Pax7d, compared to the empty vector (puro) control (Figure 1A), while MyoD levels were unaffected. We observed similar results when examining Myf5 transcript levels following overexpression of each Pax7 isoform (Figure 1B), further confirming Pax7's role in regulating Myf5 expression during myogenesis. In addition to myogenic cells, we examined whether Pax7 was capable of regulating Myf5 expression in a non-myogenic cell type such as fibroblasts. While expression of Pax7 in 10T1/2 fibroblasts produced no overt signs of myogenic conversion, extended exposure of our Western blots and RT-PCR analysis revealed that Pax7c and Pax7d (both GL-) induced Myf5 expression, a capacity not observed by Pax7a or Pax7b (both GL+) (Figure 1C,D). While the level of Myf5 induced in 10T1/2 fibroblasts was low compared to the endogenous expression in proliferating C2C12 myoblasts, it is very intriguing that the Myf5 induction potential is limited to Pax7c and Pax7d in non-myogenic cells.

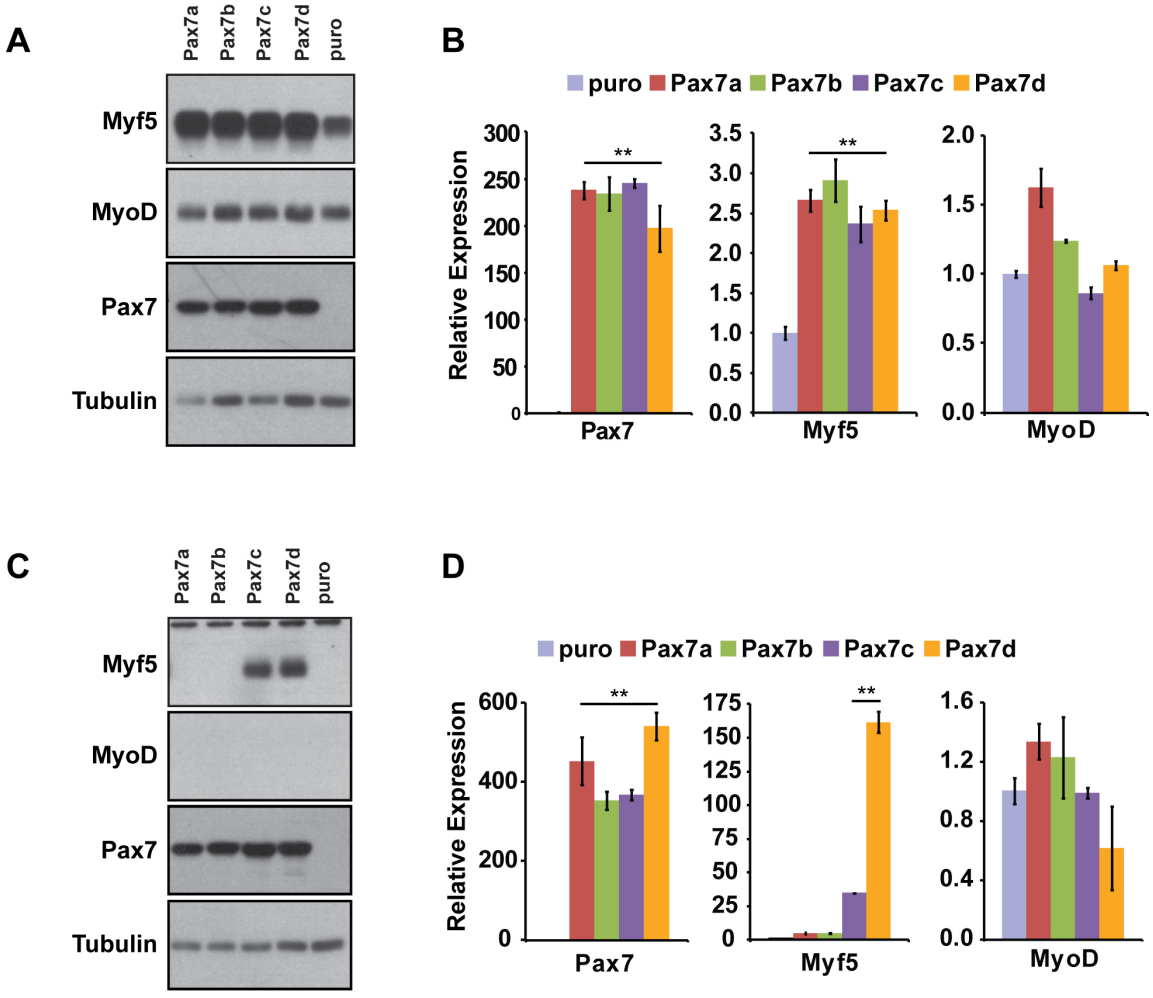

Figure 1. Exclusion of Pax7 GL-dipeptide promotes myogenic expression
(A) Western blot analysis of ectopic Pax7 isoform expression in C2C12 myoblasts. All four Pax7 isoforms can further upregulate Myf5 protein, while MyoD expression remains unchanged.
(B) Real-Time RT-PCR analysis of Pax7, Myf5 and MyoD expression following ectopic Pax7 isoform expression in C2C12 myoblasts. Interestingly, all Pax7 isoforms are able to induce Myf5 expression, while MyoD levels remain unchanged. Data are presented as the mean ± SEM (n=3, ** $p < 0.01$), normalized to GAPDH, and shown relative to puro control.
(C) Western blot analysis of ectopic Pax7 isoform expression in 10T1/2 fibroblasts. Compared to myoblasts, only Pax7 isoforms excluding the GL-dipeptide (Pax7c and Pax7d) are able to activate Myf5 expression. Note that Myf5 Western blot is exposed 30x longer for fibroblasts compared to myoblasts (A). MyoD expression is not induced.
(D) Real-Time RT-PCR analysis of Pax7, Myf5 and MyoD expression following ectopic Pax7 isoform expression in 10T1/2 fibroblasts. Strikingly, Pax7c and Pax7d increase Myf5 expression levels, while Pax7a and Pax7b have no effect on Myf5. Similar to C2C12 myoblasts, Pax7 expression has no affect on MyoD expression levels. Data are presented as the mean ± SEM (n=3, ** $p < 0.01$), normalized to GAPDH, and shown relative to puro control.

Pax7 splice variants display consistent expression levels

Given the differential abilities to activate Myf5 expression, we set out to examine the relative abundance of the Pax7 splice variants. Previous studies have employed a labour-intensive PCR-cloning-sequencing strategy to examine the relative Pax7 isoform expression levels between different mouse strains with mixed results (Ziman and Kay, 1998). Hence, we set out to optimize an efficient ^{32}P end-labeled RT-PCR-based approach to quantitate the relative Pax7 isoform ratios. We applied our system to a set of known samples (10T1/2 fibroblasts ectopically expressing Pax7 isoforms) and tested its ability to estimate the relative abundance of the Pax7 isoforms in a 1:1:1:1 mixture of cDNA from all four isoform sources (Figure 2B). Following confirmation of unbiased PCR amplification, we next examined the relative isoform ratios in proliferating primary myoblasts, where Pax7 expression is maximally observed. Following PCR band density quantification, we observed that Pax7d (56.5%) is the predominant isoform expressed in myoblasts, followed by Pax7b (25.1%), Pax7c (13.7%) and at a much lower level, Pax7a (4.7%) (Figure 2C). These results follow a similar splice frequency previously described (Ziman and Kay, 1998), however, enabled us to further examine Pax7 splicing at various stages of myogenesis.

While Pax7 expression is high in proliferating myoblasts, its transcription diminishes rapidly during myogenic differentiation, while the expression of differentiation markers (such as Myosin Heavy Chain, Myh2) become elevated (Figure 2A). We observed that Myf5 expression follows a similar expression pattern as Pax7 during differentiation, while myogenin expression is rapidly increased early during myogenic differentiation. A primary myoblast differentiation time-course was used to examine whether Pax7 isoform distributions were altered during myogenic differentiation. Within the total pool of Pax7

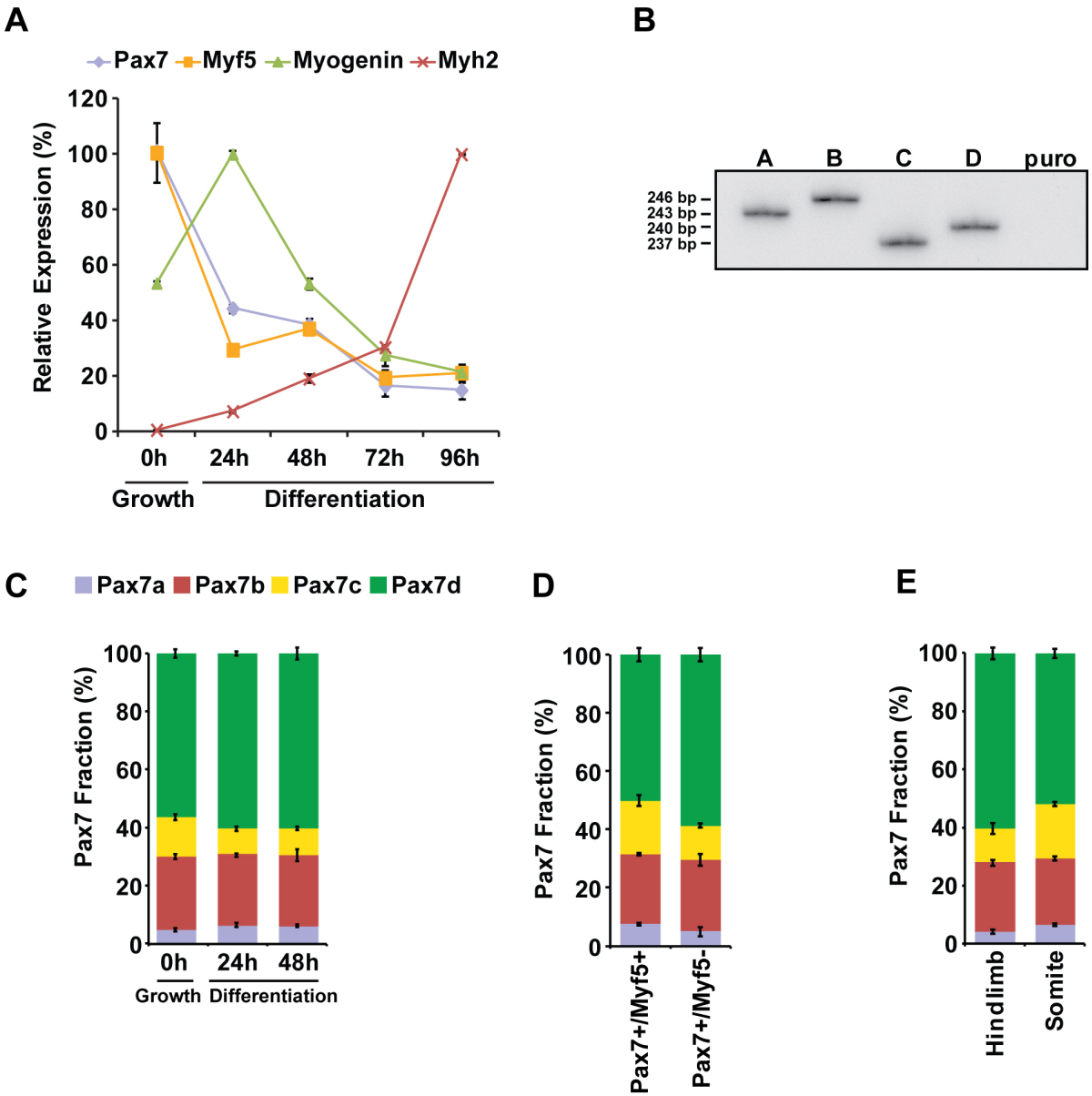
A
Pax7
Myf5
Myogenin
Myh2
Relative Expression (%)
120
100
80
60
40
20
0
0h
24h
48h
72h
96h
Growth
Differentiation
B
A
B
C
D
puro
246 bp
243 bp
240 bp
237 bp
C
Pax7a
Pax7b
Pax7c
Pax7d
Pax7 Fraction (%)
100
80
60
40
20
0
0h
24h
48h
Growth
Differentiation
D
Pax7 Fraction (%)
100
80
60
40
20
0
Pax7+/Myf5+
Pax7+/Myf5-
E
Pax7 Fraction (%)
100
80
60
40
20
0
Hindlimb
Somite

Figure 2. Pax7d is the predominant isoform following alternative splicing
(A) Real-Time RT-PCR analysis of total Pax7, Myf5, myogenin and myosin heavy chain (Myh2) expression levels during growth and early differentiation of primary myoblasts. While Pax7 and Myf5 are reduced following induction of differentiation, myogenin expression increases within 24 hours of differentiation, while myosin heavy chain is a late marker for myogenic differentiation. Data are presented as the mean ± SEM (n=3), normalized to GAPDH.
(B) RT-PCR analysis of ectopic Pax7 isoform expression in 10T1/2 fibroblasts. Amplified PCR products can be separated on 7% denaturing acrylamide gel and relative band intensities quantified by ImageJ software.
(C) RT-PCR analysis of Pax7 isoform expression ratios during growth and early differentiation. While total quantity of Pax7 expression dramatically drops in the first 48 hours of differentiation (A), the proportion of the four Pax7 isoforms remain constant over the same period. Relative band intensities quantified by ImageJ software. Data are presented as the mean ± SEM (n=3).
(D) RT-PCR analysis of Pax7 isoform expression ratios in quiescent and activated satellite cells. Both populations display a similar Pax7 expression ratio as adult proliferating myoblasts. Relative band intensities quantified by ImageJ software. Data are presented as the mean ± SEM (n=3).
(E) RT-PCR analysis of embryonic Pax7 isoform expression ratios in 11.5 dpc myogenic development. Pax7+ progenitors originating from the somite migrate to the limb buds by 11.5 dpc, and display a similar Pax7 expression ratio as adult satellite cell derived myoblasts. Amniotic sac is included as negative control. Relative band intensities quantified by ImageJ software. Data are presented as the mean ± SEM (n=3).

transcripts, we observed that the relative proportions of Pax7 isoforms remain effectively unchanged (Figure 2C), suggesting that while total Pax7 levels rapidly decrease, alternative splicing machinery does not alter the proportions of Pax7 splice variants during myogenic differentiation.

In addition to cycling myoblasts, Pax7 expression is critical for establishing the satellite cell lineage (Kuang et al., 2006; Seale et al., 2000). We examined the relative Pax7 isoform proportions in freshly isolated Pax7+;Myf5+ committed progenitors and Pax7+;Myf5- satellite stem cells. Similar to proliferating myoblasts, we observed that Pax7d is the predominately expressed splice isoform, followed by Pax7b (Figure 2D). These results suggest that the heterogeneous Myf5 expression observed within these populations of satellite cells, both of which express Pax7, is not attributed to differential expression patterns of Pax7 splice variants.

Finally, to ascertain if developmental stages differentially regulate Pax7 splicing, we examined tissue from newly developing hindlimb musculature and the somites of 11.5 dpc embryos, a developmental time point when Pax7+ myogenic progenitors migrate from the somite and arrive in the limb buds. Similar to our previous findings, we observe that Pax7d is the predominantly expressed splice variant (Figure 2E). These results suggest that Pax7d is the dominant isoform throughout myogenic development, and hence is primarily responsible for the function of Pax7.

The Pax7 homeodomain mediates DNA binding

We henceforth focused our studies on Pax7b (Q+GL+) and Pax7d (Q+GL-) since these two Pax7 isoforms show the highest expression levels (Figure 2) and differ in their

ability to induce Myf5 expression in fibroblasts (GL+/-) (Figure 1). In addition, changes in the Q+/- residue between Pax7c (Q-GL-) and Pax7d (Q+GL-) did not affect their ability to induce Myf5 expression (Figure 1). To test the ability of Pax7b and Pax7d to bind DNA motifs, we performed an electromobility shift assay (EMSA) using short oligonucleotides derived from a recently characterized Pax7 binding site (Myf5 ECR111) responsible for driving Myf5 expression in the satellite cell (Soleimani et al., 2012). This element contains both a paired domain (PD) and a homeodomain (HD) motif separated by a 29 nt sequence. EMSA analysis confirmed that both Pax7b and Pax7d proteins are capable of binding this Myf5 regulatory element (Figure 3A), as observed by a robust shift following the incubation of equal amounts of *in vitro* synthesized Pax7b or Pax7d proteins with the probe (Figure S1). Two species of shifted probe were identified, likely representing monomer and dimer binding, consistent with a previous report suggesting that the homeodomain motif repeats facilitate protein dimerization (Birrane et al., 2009). To confirm the potential of Pax7 isoforms to form dimers, we performed coimmunoprecipitations of FLAG-tagged Pax7b or Pax7d with HA-tagged Pax7d. We observe that both splice variants were able to immunoprecipitate with the predominantly expressed Pax7d isoform (Figure 3B). These results suggest that alternative splicing, in the paired domain, does not negatively affect the ability of Pax7 to form homodimers via the homeodomain. In fact, the ability of Pax7 isoforms to form heterodimers may potentially provide an additional level of target gene regulation.

Many previous studies have examined the ability of Pax proteins to bind DNA elements containing either paired motifs, homeodomain motifs, or both separated by short intervening sequences. To confirm the mode of Pax7 DNA binding to the recently identified

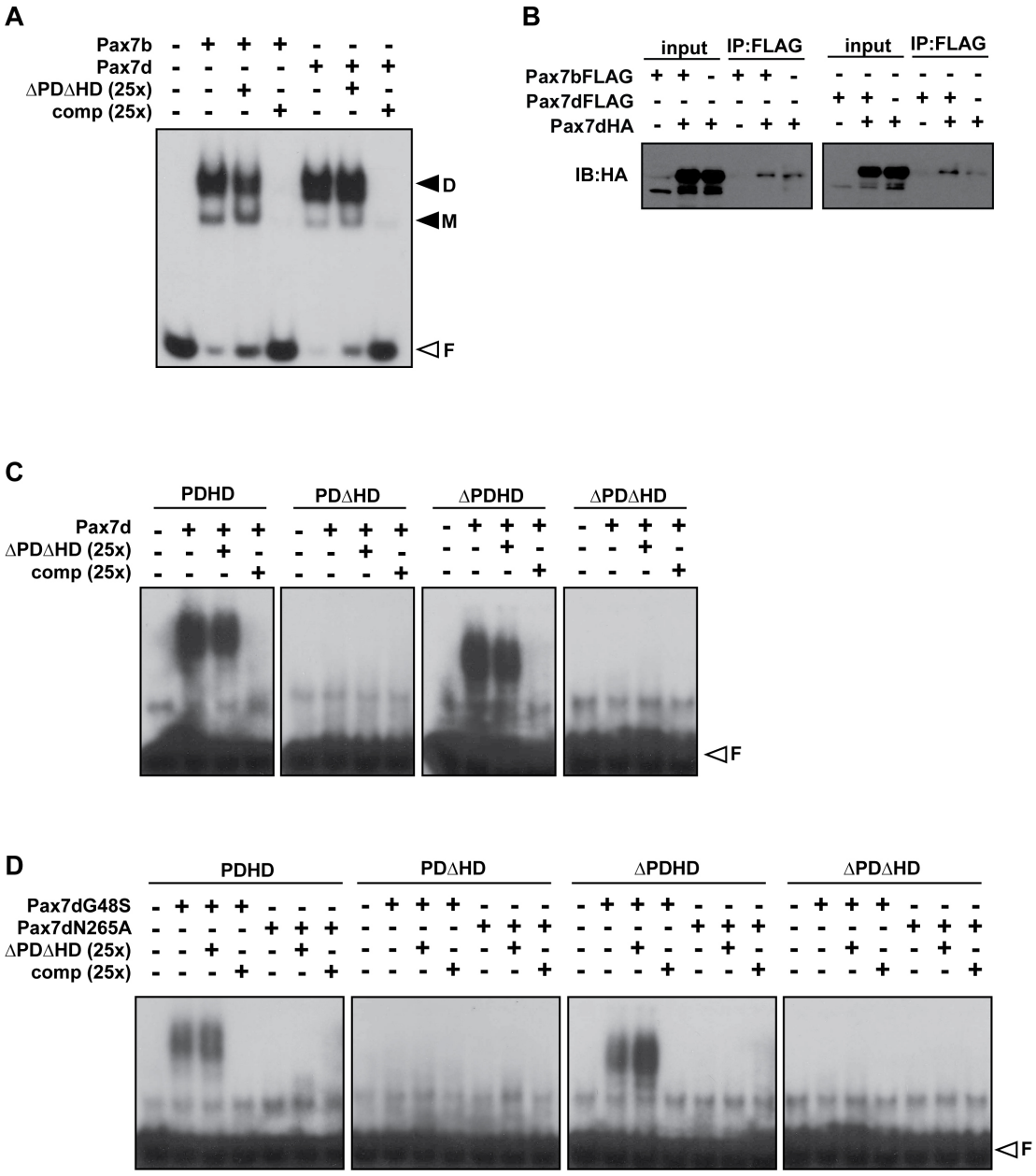
A
Pax7b
Pax7d
ΔPDΔHD (25x)
comp (25x)
D
M
F
B
input
IP:FLAG
input
IP:FLAG
Pax7bFLAG
Pax7dFLAG
Pax7dHA
IB:HA
C
PDHD
PDΔHD
ΔPDHD
ΔPDΔHD
Pax7d
ΔPDΔHD (25x)
comp (25x)
F
D
PDHD
PDΔHD
ΔPDHD
ΔPDΔHD
Pax7dG48S
Pax7dN265A
ΔPDΔHD (25x)
comp (25x)
F

Figure 3. Pax7 DNA binding occurs predominantly via the homeodomain
(A) Electrophoretic mobility shift assay (EMSA) on synthesized oligomers designed around the Myf5 ECR111 locus examining Pax7b and Pax7d DNA binding. Both isoforms are able to bind DNA, and are present as a monomer (M) and dimer (D). Free probe is identified by open arrowhead (F).
(B) Coimmunoprecipitation of Pax7 isoforms following ectopic expression. Interactions between HA-tagged Pax7d and FLAG-tagged Pax7b or Pax7d are detectable by HA immunoblotting following FLAG immunoprecipitation.
(C) Binding assay examining Pax7 bound DNA motifs. When examining the Myf5 ECR111, Pax7 binding occurs through the HD element, as mutation in this DNA motif (PDΔHD or ΔPDΔHD) prevented a shift in probe by full length Pax7d. Free probe is identified by open arrowhead (F).
(D) Binding assay examining the role of the Pax7 paired domain and homeodomain during DNA binding to the Myf5 ECR111. Interestingly, a mutation in the homeodomain (Pax7dN265A) prevented binding to DNA, while a mutation in the paired domain (Pax7dG48S) did not affect DNA binding. As observed in (C), mutation in the HD element of the DNA motif (PDΔHD or ΔPDΔHD) prevented DNA binding. Free probe is identified by open arrowhead (F).

Myf5 ECR111 regulatory element, which is bound by Pax7 under myogenic conditions, we performed EMSA analysis using oligonucleotides containing mutations in either the PD or HD motif. We observed a robust shift following a selective mutation of the PD motif (ΔPDHD), however, this shift was completely abolished when the HD motif was mutated (PDΔHD and ΔPDΔHD) (Figure 3C). These results further show that Pax7d primarily binds the Myf5 ECR111 element via its homeodomain, a functional role this protein domain shares with the ability to form dimers (Wilson et al., 1993). While EMSA analysis focused primarily on the Pax7d protein, we confirmed similar binding specificities with Pax7b (data not shown). The DNA binding requirement of the homeodomain was further confirmed when we introduced single point mutations into either the paired domain (G48S) or homeodomain (N265A) of the Pax7 protein, mutations that have been previously characterized as inhibiting the function of the respective domains in Pax3 (Fortin et al., 1997; Kappen et al., 1993; Lam et al., 1999). Within the paired domain, there are two subdomains separated by a β-sheet linker (Xu et al., 1999). Glycine-48 is located in the amino-terminal subdomain, and has direct contact with the DNA in its minor groove. Within the three α-helices of the homeodomain, Asparagine-265 is located in the third α-helical region and has direct contact with the major groove of the bound DNA (Wilson et al., 1995). We observed a shift in the full length Myf5 ECR111 (PDHD) and PD mutant (ΔPDHD) probe in the presence of Pax7dG48S, which retains a functional homeodomain (Figure 3D). However, when a point mutation was introduced into the Pax7 homeodomain (Pax7dN265A), the ability of Pax7 to shift the Myf5 ECR111 probe was abolished (PDHD, ΔPDHD, PDΔHD, ΔPDΔHD) (Figure 3D). Collectively, these observations further confirm

that the Pax7 homeodomain is responsible for binding to Myf5 regulatory elements, which suggests that the paired domain may be responsible for fine-tuning binding site recognition.

The paired and homeodomain have synergistic transactivation potential

In addition to examining the mode of Pax7 DNA binding by EMSA, we performed luciferase reporter assays on a set of reporter plasmids containing different permutations of the Myf5 ECR111 element. Reporter constructs were designed to contain concatamerized (3x) copies of either the PD motif, the HD motif, or the full length binding motif (PDHD) upstream of the Myf5 minimal promoter (Figure 4A). Reporter plasmids were cotransfected with plasmids expressing Pax7bFKHR, Pax7dFKHR or empty vector (FKHR) into Cos7 cells. Initial experiments found that Pax7 is a weak transactivator, while FKHR fused in-frame carboxyl-terminal of the gene has been shown to be a more potent transactivator of Pax7 target genes (Figure S2) (Bennicelli et al., 1999; Bennicelli et al., 1996). Both Pax7bFKHR and Pax7dFKHR were weak inducers from the PD motif alone, while increased reporter gene expression was observed from the HD motif alone (Figure 4B). Strikingly, the presence of the juxtaposed PD and HD motif (PDHD) has a synergistic effect on reporter gene expression (Figure 4C), with greatest activation observed with Pax7dFKHR. This enhanced effect is drastically reduced when the paired or homeodomain of Pax7 is mutated (Pax7dG48S/FKHR or Pax7dN265A/FKHR), and is completely abolished when both domains are mutated (Pax7dG48S+N265A/FKHR) (Figure 4D). These results suggest that while Pax7 DNA binding may occur primarily via the HD, both domains are required for the full binding of Pax7 and its transactivation potential on the Myf5 regulatory element.

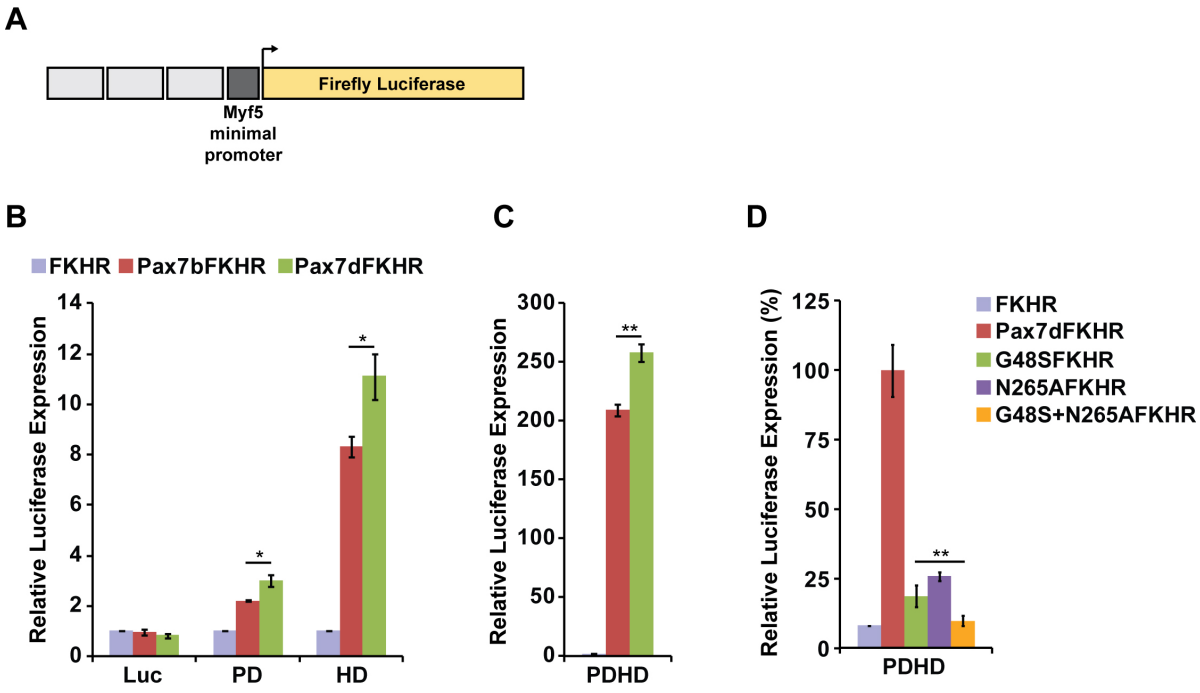

Figure 4. Pax7 gene activation is dependent on paired and homeodomain motif
(A) Schematic of multimerized (3x) oligonucleotide containing Myf5 ECR111 element directionally cloned into a pGL4.10 reporter vector driven by a Myf5 minimal promoter. In addition to full length ECR111 element, the PD and the HD were individually multimerized and directionally cloned.
(B) Relative luciferase activity following Cos7 transfection of paired domain (PD) or homeodomain (HD) containing luciferase reporter with Pax7b or Pax7d fused in-frame with FKHR (a strong transactivator) at the carboxyl-terminal. Expression of luciferase was measured and normalized to renilla expression and a control (FKHR) reporter construct. Data are presented as the mean ± SEM (n=3, * $p < 0.05$).
(C) Relative luciferase activity following Cos7 transfection of a paired- and homeodomain (PDHD) with Pax7bFKHR, Pax7dFKHR or FKHR control. The presence of both domains synergistically enhances luciferase transcriptional output, however, Pax7dFKHR retains enhanced activation. Data are presented as the mean ± SEM (n=3, * $p < 0.05$, ** $p < 0.01$).
(D) Relative luciferase activity following Cos7 transfection of the PDHD element with Pax7dFKHR constructs containing point mutations in the paired domain (G48S), the homeodomain (N265A), or both (G48S+N265A). Mutations in the paired or homeodomain greatly reduce luciferase transcriptional output, while a mutation in both domains completely ablates expression. Data are presented as the mean ± SEM (n=3, ** $p < 0.01$).

Global transcriptome analysis of Pax7 splice variants

Our recent observations show that while Pax7 binding occurs primarily through the homeodomain, changes in the paired domain (GL+/-) affect its ability to induce Myf5 expression in non-myogenic cells where both DNA binding domains were required to obtain full transactivation potential. Given these findings, we set out to understand the role of alternative splicing within the Pax7 paired domain. To gain a better understanding of the biological differences between Pax7 isoforms, we performed whole transcriptome analysis (RNA-Seq) to identify global targets of Pax7b (GL+) and Pax7d (GL-) in proliferating myoblasts. Carboxyl-terminal FLAG-tagged Pax7b and Pax7d were stably expressed in low-passage primary myoblasts using drug-selectable retrovirus. Relatively equal expression of Pax7bFLAG and Pax7dFLAG were confirmed by RT-PCR (Figure 5A) and Western blot (Figure 5B) relative to empty vector control virus (puro). In addition, the induction of Myf5 protein was examined to confirm functional Pax7 protein expression (Figure 5B). An increased proliferation rate was observed following ectopic expression of either Pax7bFLAG or Pax7dFLAG (Figure 5C), consistent with previous reports of Pax7 expression affecting myoblast proliferation genes (Collins et al., 2009; Soleimani et al., 2012) with no noticeable affects on cell morphology (data not shown).

Expression of Pax7bFLAG or Pax7dFLAG resulted in significant expression changes of 951 and 1053 genes, respectively, relative to puro control (fold change > 2, q-value < 0.05). We confirmed RNA-Seq read quality and the distribution of reads prior to further gene analysis. Genes were divided into upregulated, downregulated and unchanged groups based on their expression patterns between Pax7 expression and puro control. In addition, genes have been categorized based on significant fold changes in expression

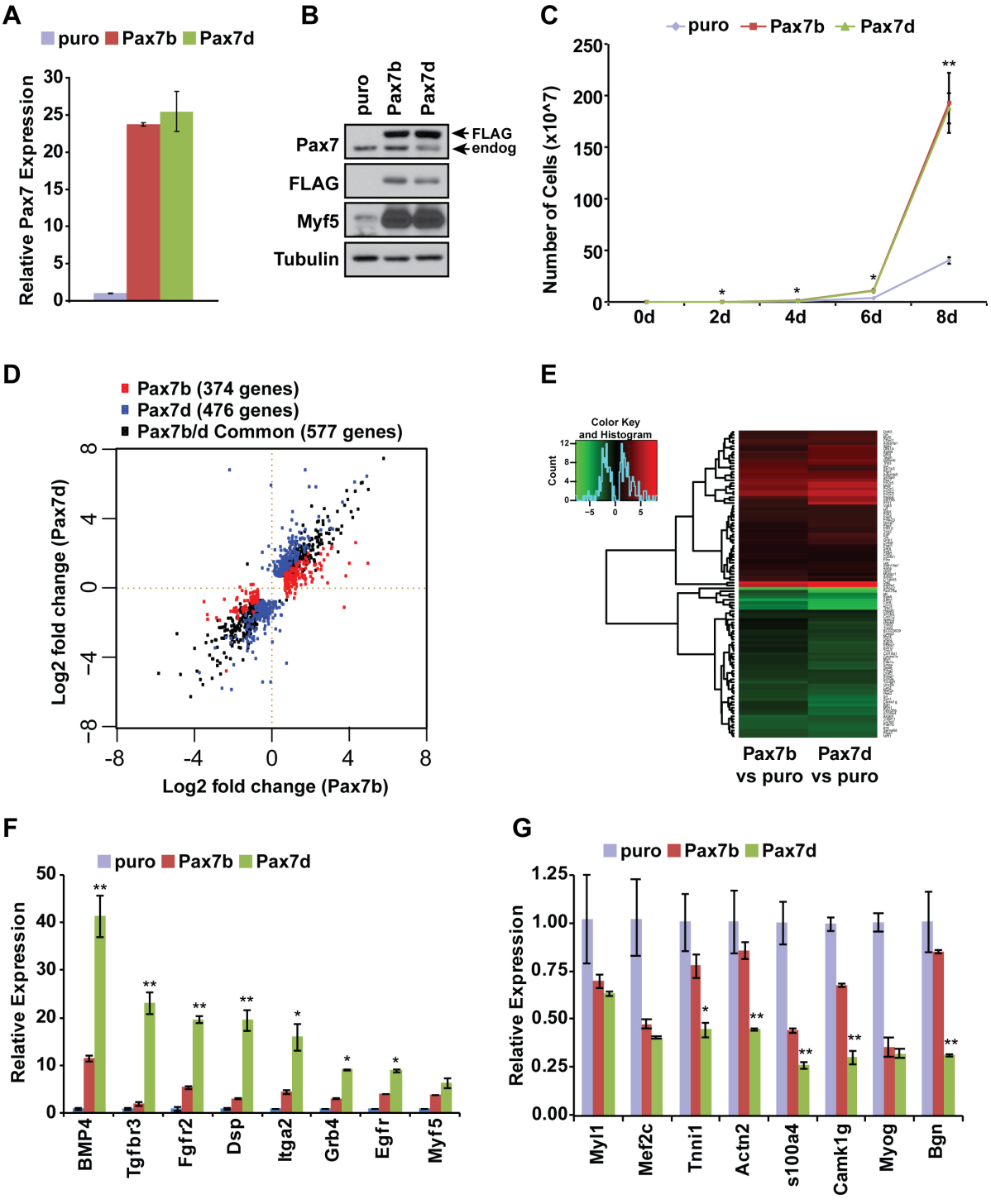
A
puro Pax7b Pax7d
Relative Pax7 Expression
30
25
20
15
10
5
0
B
puro
Pax7b
Pax7d
Pax7
FLAG
endog
FLAG
Myf5
Tubulin
C
puro Pax7b Pax7d
Number of Cells (x10^7)
250
200
150
100
50
0
0d
2d
4d
6d
8d
D
Pax7b (374 genes)
Pax7d (476 genes)
Pax7b/d Common (577 genes)
Log2 fold change (Pax7d)
Log2 fold change (Pax7b)
8
4
0
−4
−8
E
Color Key and Histogram
Count
Pax7b vs puro
Pax7d vs puro
F
puro Pax7b Pax7d
Relative Expression
50
40
30
20
10
0
BMP4
Tgfbr3
Fgfr2
Dsp
Itga2
Grb4
Egfr
Myf5
G
puro Pax7b Pax7d
Relative Expression
1.25
1.00
0.75
0.50
0.25
0.00
Myl1
Mef2c
Tnni1
Actn2
s100a4
Camk1g
Myog
Bgn

Figure 5. Global analysis of Pax7b and Pax7d gene regulation
(A) Real-Time RT-PCR analysis of ectopic Pax7 isoform expression in primary myoblasts following retroviral infection of FLAG-tagged virus encoding Pax7b or Pax7d. Empty vector (puro) virus is used as control. Data are presented as the mean ± SEM (n=3), normalized to GAPDH, and shown relative to puro control.
(B) Western blot analysis of ectopic Pax7 isoform expression in primary myoblasts following retroviral infection. FLAG-tagged Pax7b and Pax7d have no effect on endogenous Pax7 expression levels, and both isoforms are able to induce Myf5 protein levels, relative to puro control.
(C) Proliferation assay of primary myoblasts following ectopic Pax7 isoform expression. Expression of Pax7b or Pax7d results in a dramatic increase in myoblast proliferation, relative to puro control. Data are presented as the mean ± SEM (n=3, * $p < 0.05$, ** $p < 0.01$).
(D) Scatterplot of significantly regulated genes in Pax7b or Pax7d expressing primary myoblasts. RNA-Seq analysis was performed on purified mRNA. Black squares represent significantly regulated (fold change > 2, q-value < 0.05) genes common between Pax7b and Pax7d expressing myoblasts, red squares represent genes that are significantly regulated by Pax7b, and blue squares represent genes that are significantly regulated by Pax7d. Values are plotted relative to puro control.
(E) A heat map based on hierarchical clustering showing the fold change pattern of most significantly regulated genes (q-value < 10^{-10}) following RNA-Seq analysis of Pax7b or Pax7d expressing primary myoblasts. Green represents genes downregulated, whereas red represents genes upregulated following Pax7 expression. Fold change shown relative to puro control.
(F) Real-Time RT-PCR validation of a subset of genes upregulated following ectopic Pax7 expression relative to puro control. Interestingly, many genes are more strongly regulated by Pax7d relative to Pax7b. Data are presented as the mean ± SEM (n=3, * $p < 0.05$, ** $p < 0.01$), normalized to GAPDH, and shown relative to puro control.
(G) Real-Time RT-PCR validation of a subset of genes downregulated following ectopic Pax7 expression relative to puro control. As observed in (F), many genes are more strongly regulated by Pax7d relative to Pax7b. Data are presented as the mean ± SEM (n=3, * $p < 0.05$, ** $p < 0.01$), normalized to GAPDH, and shown relative to puro control.

patterns unique to Pax7bFLAG (373 genes), Pax7dFLAG (476 genes) or common to both isoforms (577 genes) (Figure 5D). Heat maps were generated to examine expression values for Pax7bFLAG or Pax7dFLAG vs puro control by plotting fold change values for the top 108 genes (q-value < 10^{-10}) relative to control myoblasts (Figure 5E). We observed that gene expression values are regulated consistently between Pax7b and Pax7d, and observed no genes oppositely regulated (for example, upregulated by Pax7dFLAG while downregulated by Pax7bFLAG). These results suggest that while Pax7 isoforms do not have opposing effects, their ability to regulate common targets may vary. Further, when examining unique genes that were significantly regulated relative to control myoblasts, many genes were found to be not significantly changed by the opposing isoform.

Pax7d possesses greater myogenic transcriptional regulation

To investigate the global transcriptional effects of Pax7 isoforms, we conducted an unbiased DAVID analysis of our RNA-Seq data. Functional annotation clustering of related gene ontology (GO) terms revealed that both Pax7b and Pax7d regulated the expression of many genes involved in regulating cell proliferation, cell adhesion and cell signaling (Table S2-S4). However, Pax7d induced the expression of many additional genes involved in growth and proliferation and repressed a large set of genes involved in muscle cell differentiation, a finding that was not significantly regulated by Pax7b (Table S5-S7).

We validated a subset of regulated genes by Real-Time RT-PCR, and observed that many genes associated with growth and proliferation, such as Bmp4, Fgfr2 and Egfr were significantly upregulated by Pax7b and Pax7d relative to puro control (Figure 5F). Strikingly, while expression of many genes was effected by either isoform, Pax7d was a

stronger gene activator and resulted in greater changes in gene expression. Differentiation-specific genes, such as Myl1, Mef2c, Myogenin, and Actn2, were significantly repressed by both Pax7b and Pax7d (Figure 5G), however, we observed that Pax7d was able to modulate target genes with greater potential (Figure 5F).

In addition to observing differential changes in Pax7b and Pax7d target genes, we wanted to examine whether these differences were directly attributed to the ability of Pax7 to bind DNA. A recently published data set comprising Pax7d ChIP-Seq allowed us to examine potential Pax7 binding sites that may regulate target gene activation (Soleimani et al., 2012). In particular, we focused on the strongly activated Bmp4 and the Myf5 regulatory element previously examined in this study. Bmp4 is well characterized for its ability to block myogenic differentiation through inhibiting the upregulation of differentiation-associated genes (Dahlqvist et al., 2003; Ono et al., 2011). It is upregulated by both Pax7bFLAG and Pax7dFLAG, with greater activation attributed to Pax7dFLAG. By ChIP-PCR, we observed a significant increase in enrichment of the Myf5 ECR111 element and a potential binding site 116 kb upstream of Bmp4 in Pax7dFLAG cells relative to Pax7bFLAG or puro controls (Figure 6, S3). Both of these elements contain a PD motif and a HD motif, suggesting Pax7 protein binding is modulated by both domains. While we have previously identified the homeodomain predominantly responsible for Pax7 binding, these observations suggest that modulation of the paired domain of Pax7 may further regulate target gene activation or repression, and further exemplify the dominant role of the GL-Pax7d splice variant during myogenesis.

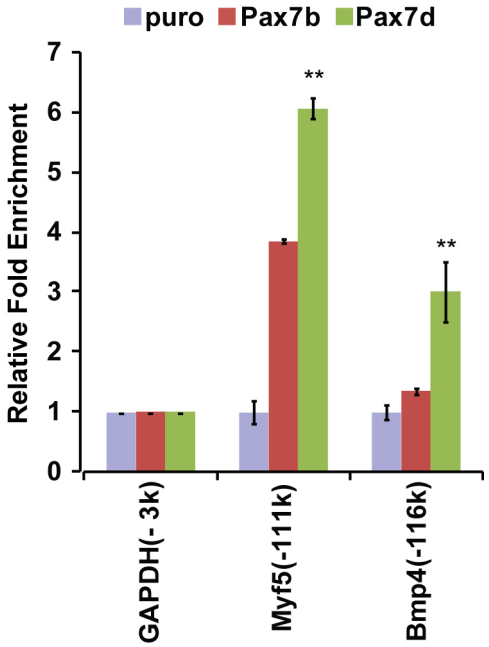

Figure 6. Pax7 isoforms exhibit differential gene regulation potential
(A) Real-Time PCR analysis of locus enrichment in chromatin immunoprecipitated (ChIP) with α-FLAG antibody from Pax7 isoform expressing myoblasts. Fold enrichment is normalized to GAPDH(-3kb) locus and shown relative to FLAG (puro) control. Interestingly, two independent Pax7-bound loci display greater enrichment for Pax7d relative to Pax7b. Data are presented as the mean ± SEM (n=3, ** $p < 0.01$).

DISCUSSION

The paired-box transcription factor Pax7 is a critical regulator of skeletal myogenesis and is essential for maintenance and self-renewal of the satellite cell compartment and proper muscle regeneration (Kuang et al., 2006; Seale et al., 2000). Genetically upstream of the myogenic regulatory factors Myf5 and MyoD, Pax7 regulates satellite cell commitment to the myogenic lineage. Our results demonstrate that Pax7 alternative splice variants possess consistent expression patterns in set ratios throughout myogenic development, while exhibiting differential abilities to regulate downstream target gene activation. In addition, splicing of the Pax7 transcript to produce variant paired-box DNA binding domains remains evolutionarily conserved and partially shared with the closely related Pax3.

Alternative splicing of pre-mRNA is an important regulatory mechanism, resulting in control of gene expression and generating diverse protein species (Black, 2003; Lopez, 1998). The intron/exon boundaries are defined by short and degenerate classical splice sites, and alternative splicing can occur through altering the position of the splice donor or acceptor sites, know as alternative 5' or 3' splice site recognition, and affecting the recognition and interaction with the basal splicing machinery (Mercatante and Kole, 2000). When specifically examining the common Q+/- splicing event between Pax3 and Pax7, a previous report examined the widespread occurrence of the NAGNAG 3' acceptor splice site motif, resulting in isoforms which differ by a 3 nt sequence (Hiller et al., 2004). This study suggested that the NAGNAG motif is present in 30% of genes, and results in a functional insertion/deletion in at least 5% of the genes, including amongst Pax3 the insulin-like growth factor IGF1R (Condorelli et al., 1994) and the neurodegenerative disorder DRPLA (Tadokoro et al., 2005).

In addition to the Q+/- splicing event, Pax7 undergoes a second splice variation affecting a hexanucleotide sequence (GL+/-). While evolutionarily conserved, we observed divergent abilities in Pax7 isoforms to activate the myogenic regulatory factor Myf5 following splicing of the GL dipeptide at the exon 3/4 boundary. This GL+/- splicing occurs in the same manner as the Q+/- splicing, resulting from the presence of a GAGGTTTAG 3' acceptor splice site motif, distinguishing Pax7a and Pax7b from Pax7c and Pax7d. This GL+/- splicing event does not occur in Pax3 due to sequence differences at the exon 3/4 boundary, rendering Pax3 with a GL- status. *In silico* analysis predicts that the Q+/- splicing event in the linker region would not alter the secondary structure of the paired domain (Ziman and Kay, 1998), however, the GL+/- dipeptide was predicted to change the protein conformation by altering the secondary structure of the third α-helix of the carboxyl-terminal subdomain (Xu et al., 1999). This α-helix structure makes direct contact with the DNA, thus the GL+/- variations are proposed to directly affect Pax DNA binding (Jaworski et al., 1997). While the Q+/- splice variant is suggested to not alter secondary structure, splicing in Pax3 has shown differential DNA binding, through varied proximity of the two paired subdomains following the inclusion or exclusion of the Q residue (Underhill and Gros, 1997; Vogan et al., 1996). These results suggest that both alternative splice sites may impart functional relevance to Pax7 proteins ability to bind DNA, and ultimately regulate target gene expression.

While paired domain alternative splicing is highly conserved, these events remain restricted to vertebrates as the Amphioxus Pax3/7 lacks the intron and splicing that generates the Q+/- variant (Holland et al., 1999). Given the common feature of Q+/- between Pax3 and Pax7, this splicing event evolved after the divergence of vertebrates, but prior to the

duplication of the ancestral Pax3/7 gene (Noll, 1993). While the GL+/- splice variation is only present in Pax7, the intron containing the alternative 3' splice site sequence shows high conservation between Amphioxus Pax3/7 and vertebrate Pax3 and Pax7 (Holland et al., 1999). These high levels of conservation suggest that evolutionary retention of these splice variants should impart functional relevance to the ability of Pax7 to bind DNA.

While our results suggest that the majority of Pax7 DNA binding occurs via the homeodomain, our luciferase reporter assays further confirm the necessity of both Pax7 DNA binding domains for full activation potential (Figure 4C). This cooperative interaction between the paired and homeodomain potentially expands their target gene recognition repertoire (Jun and Desplan, 1996; Miskiewicz et al., 1996). These findings coincide with our observations that both Pax7 isoforms are able to bind DNA sequences (Figure 3A), however, gene expression analysis points to a more dominant role for Pax7d (GL-) relative to Pax7b (GL+) during myogenesis (Figure 5). In addition, structural changes of the paired domain can affect the binding properties of the homeodomain (Underhill and Gros, 1997), which implies a functional interaction of these domains during DNA binding (Corry et al., 2010; Jun and Desplan, 1996; Miskiewicz et al., 1996).

Recent studies have highlighted Pax7 proteins function through binding to DNA sequences and eliciting the recruitment of the HMT complex (Kawabe et al., 2012; McKinnell et al., 2008). Through conservation of multiple splice variants and the ability to form homo- and heterodimers, Pax7 has maintained the potential to activate a larger repertoire of genes. While we were able to examine the relative abundance of the four splice variants, we were unable to ascertain which species of Pax7 isoforms were bound to DNA under native myogenic conditions due to subtle sequence changes attributed to the splice

variants. Currently, reagents are not available to distinguish between Pax7 splice variant protein species or selectively modulate transcripts through siRNA mediated gene silencing. However, our data suggests that Pax7d (GL-) maintains an enhanced ability to regulate many genes related to promoting satellite cell identity and blocking the progression of terminal differentiation. While 577 genes were common between Pax7b and Pax7d, many of these genes remained more responsive to Pax7d expression. These genes are involved in diverse biological functions including proliferation, cell signalling, cell adhesion and myogenic differentiation.

The ability of Pax7 to induce genes such as Myf5, Bmp4 and Fgfr2, among others (Table S5-S7), suggests a functional role for Pax7 in the expansion of the satellite cell population. Bone morphogenic proteins (Bmp) form a subgroup of the transforming growth factor (TGF)-β super family. Specifically, Bmp4 has been shown to block myogenic differentiation (Dahlqvist et al., 2003; Ono et al., 2011), resulting in increased numbers of myogenic progenitors and satellite cells (Wang et al., 2010). Indeed, Pax7-induced expression of Bmp4 correlates with the strong repression of myogenic differentiation genes such as Myh1, Mef2c and myogenin. In addition to enhancing proliferation, Pax7 expression may function in maintaining stem cell populations. Angiopoietin 1 (Ang1), and its tyrosine kinase Tie2 receptor, have been established to inhibit satellite cell proliferation and differentiation, thus promoting a return to cellular quiescence (Abou-Khalil et al., 2009). Interestingly, we observed strong inhibition of Ang1 following expression of either Pax7b or Pax7d (Table S5-S7), which may further be attributed to the enhanced proliferative capacity we observed for both populations (Figure 5C).

Pax7 and Pax3 are also expressed in the developing central nervous system and neural crest. However, Pax7-null mice do not show any adverse phenotype in either lineage, further suggesting a functional overlap between Pax3 and Pax7 within the developing neural tube and neural crest (Mansouri et al., 1996). While we observed consistent expression of Pax7 isoforms during neural development (Figure S4), our GO analysis displayed an enrichment of terms associated with neuron development, neural projection and differentiation (Table S2-S4) specifically associated with Pax7b. While this requires further examination, there remains the potential for Pax7 splice variants to differentially regulate gene expression within different tissues and developing stages that are dependent on Pax7.

Through chromatin remodeling, the potential for Pax7 to function through pioneer transcription factor activity has recently been described in pituitary cells (Budry et al., 2012). Likewise, the observation that only GL- isoforms were able to induce Myf5 expression in non-myogenic cells further suggests that the potential of this pioneer factor may vary within splice variants of the paired domain. These data suggest that the absence of the GL dipeptide maintains an enhanced ability to access and bind transcriptionally inactive heterochromatin present around the Myf5 locus in non-myogenic fibroblasts. While Myf5 induction was not strong enough to induce myogenic conversion, this binding activation potential was not observed for GL+ isoforms.

While Q+ splice variants were most abundantly expressed (> 80% of total Pax7), the Q- Pax7 isoforms have not been functionally characterized. As previously discussed, the Q+/- splicing event affects the ability of Pax3 to bind DNA sequences (Underhill and Gros, 1997; Vogan et al., 1996). However, given their low abundance and no overt affect on Myf5 expression in fibroblasts (Pax7c compared to Pax7d), characterization of a potential role of

the Q+/- splice variants remains elusive. Specifically, there remains a possibility that Pax7a (Q-GL+) is an alternative splicing mis-splice given its very low transcript abundance (4.7%). It has been estimated that approximately 2% of transcripts from the average gene are mis-spliced (Pickrell et al., 2010) resulting in stochastic 'noise' of non-functional products (Baek and Green, 2005; Melamud and Moult, 2009). Whether Pax7a (Q-GL+) and Pax7c (Q-GL-) are products of Q+/- mis-splicing of Pax7b (Q+GL+) and Pax7d (Q+GL-), or functionally important splice variants naturally occurring in lower abundance remains to be further characterized.

Together, our data suggest that while the binding of Pax7 to DNA may occur predominantly through the homeodomain, this interaction is dependent on the paired domain. Subtle changes arising from alternative splicing events within the paired domain, coupled with the ability to form dimers amongst splice variants, can modulate the regulation of Pax7 target genes, thereby increasing the biological complexity of this transcription factor. Further understanding of the molecular controls underlying satellite cell function will provide greater understanding of the molecular regulation present during myogenesis and muscle regeneration.

ACKNOWLEDGEMENTS

M.A.R. holds the Canada Research Chair in Molecular Genetics and is an International Research Scholar of the Howard Hughes Medical Institute. This work was supported by grants to M.A.R. from the Canadian Institutes of Health Research, Muscular Dystrophy Association, the National Institutes of Health, the Howard Hughes Medical Institute, the Canadian Stem Cell Network, and the Canada Research Chair Program. A.E.J. was supported by scholarships from the Natural Sciences and Engineering Research Council of Canada. The authors declare no conflict of interest.

REFERENCES

Abou-Khalil, R., Le Grand, F., Pallafacchina, G., Valable, S., Authier, F.J., Rudnicki, M.A., Gherardi, R.K., Germain, S., Chretien, F., Sotiropoulos, A.*, et al.* (2009). Autocrine and paracrine angiopoietin 1/Tie-2 signaling promotes muscle satellite cell self-renewal. Cell Stem Cell *5*, 298-309.

Baek, D., and Green, P. (2005). Sequence conservation, relative isoform frequencies, and nonsense-mediated decay in evolutionarily conserved alternative splicing. Proc Natl Acad Sci U S A *102*, 12813-12818.

Bennicelli, J.L., Advani, S., Schafer, B.W., and Barr, F.G. (1999). PAX3 and PAX7 exhibit conserved cis-acting transcription repression domains and utilize a common gain of function mechanism in alveolar rhabdomyosarcoma. Oncogene *18*, 4348-4356.

Bennicelli, J.L., Edwards, R.H., and Barr, F.G. (1996). Mechanism for transcriptional gain of function resulting from chromosomal translocation in alveolar rhabdomyosarcoma. Proc Natl Acad Sci U S A *93*, 5455-5459.

Birrane, G., Soni, A., and Ladias, J.A. (2009). Structural basis for DNA recognition by the human PAX3 homeodomain. Biochemistry *48*, 1148-1155.

Black, D.L. (2003). Mechanisms of alternative pre-messenger RNA splicing. Annu Rev Biochem *72*, 291-336.

Budry, L., Balsalobre, A., Gauthier, Y., Khetchoumian, K., L'Honore, A., Vallette, S., Brue, T., Figarella-Branger, D., Meij, B., and Drouin, J. (2012). The selector gene Pax7 dictates alternate pituitary cell fates through its pioneer action on chromatin remodeling. Genes Dev *26*, 2299-2310.

Chi, N., and Epstein, J.A. (2002). Getting your Pax straight: Pax proteins in development and disease. Trends Genet *18*, 41-47.

Collins, C.A., Gnocchi, V.F., White, R.B., Boldrin, L., Perez-Ruiz, A., Relaix, F., Morgan, J.E., and Zammit, P.S. (2009). Integrated functions of Pax3 and Pax7 in the regulation of proliferation, cell size and myogenic differentiation. PLoS One *4*, e4475.

Collins, C.A., Olsen, I., Zammit, P.S., Heslop, L., Petrie, A., Partridge, T.A., and Morgan, J.E. (2005). Stem cell function, self-renewal, and behavioral heterogeneity of cells from the adult muscle satellite cell niche. Cell *122*, 289-301.

Condorelli, G., Bueno, R., and Smith, R.J. (1994). Two alternatively spliced forms of the human insulin-like growth factor I receptor have distinct biological activities and internalization kinetics. J Biol Chem *269*, 8510-8516.

Corry, G.N., Raghuram, N., Missiaen, K.K., Hu, N., Hendzel, M.J., and Underhill, D.A. (2010). The PAX3 paired domain and homeodomain function as a single binding module in vivo to regulate subnuclear localization and mobility by a mechanism that requires base-specific recognition. J Mol Biol *402*, 178-193.

Dahlqvist, C., Blokzijl, A., Chapman, G., Falk, A., Dannaeus, K., Ibanez, C.F., and Lendahl, U. (2003). Functional Notch signaling is required for BMP4-induced inhibition of myogenic differentiation. Development *130*, 6089-6099.

Du, S., Lawrence, E.J., Strzelecki, D., Rajput, P., Xia, S.J., Gottesman, D.M., and Barr, F.G. (2005). Co-expression of alternatively spliced forms of PAX3, PAX7, PAX3-FKHR and PAX7-FKHR with distinct DNA binding and transactivation properties in rhabdomyosarcoma. Int J Cancer *115*, 85-92.

Fortin, A.S., Underhill, D.A., and Gros, P. (1997). Reciprocal effect of Waardenburg syndrome mutations on DNA binding by the Pax-3 paired domain and homeodomain. Hum Mol Genet *6*, 1781-1790.

Gehring, W.J., Affolter, M., and Burglin, T. (1994). Homeodomain proteins. Annu Rev Biochem *63*, 487-526.

Hiller, M., Huse, K., Szafranski, K., Jahn, N., Hampe, J., Schreiber, S., Backofen, R., and Platzer, M. (2004). Widespread occurrence of alternative splicing at NAGNAG acceptors contributes to proteome plasticity. Nat Genet *36*, 1255-1257.

Holland, L.Z., Schubert, M., Kozmik, Z., and Holland, N.D. (1999). AmphiPax3/7, an amphioxus paired box gene: insights into chordate myogenesis, neurogenesis, and the possible evolutionary precursor of definitive vertebrate neural crest. Evol Dev *1*, 153-165.

Holterman, C.E., Le Grand, F., Kuang, S., Seale, P., and Rudnicki, M.A. (2007). Megf10 regulates the progression of the satellite cell myogenic program. J Cell Biol *179*, 911-922.

Huang, D.W., Sherman, B.T., and Lempicki, R.A. (2009a). Bioinformatics enrichment tools: paths toward the comprehensive functional analysis of large gene lists. Nucleic Acids Res *37*, 1-13.

Huang, D.W., Sherman, B.T., and Lempicki, R.A. (2009b). Systematic and integrative analysis of large gene lists using DAVID bioinformatics resources. Nat Protoc *4*, 44-57.

Huh, M.S., Parker, M.H., Scime, A., Parks, R., and Rudnicki, M.A. (2004). Rb is required for progression through myogenic differentiation but not maintenance of terminal differentiation. J Cell Biol *166*, 865-876.

Jaworski, C., Sperbeck, S., Graham, C., and Wistow, G. (1997). Alternative splicing of Pax6 in bovine eye and evolutionary conservation of intron sequences. Biochem Biophys Res Commun *240*, 196-202.

Jun, S., and Desplan, C. (1996). Cooperative interactions between paired domain and homeodomain. Development *122*, 2639-2650.

Kappen, C., Schughart, K., and Ruddle, F.H. (1993). Early evolutionary origin of major homeodomain sequence classes. Genomics *18*, 54-70.

Kawabe, Y., Wang, Y.X., McKinnell, I.W., Bedford, M.T., and Rudnicki, M.A. (2012). Carm1 regulates Pax7 transcriptional activity through MLL1/2 recruitment during asymmetric satellite stem cell divisions. Cell Stem Cell *11*, 333-345.

Kuang, S., Charge, S.B., Seale, P., Huh, M., and Rudnicki, M.A. (2006). Distinct roles for Pax7 and Pax3 in adult regenerative myogenesis. J Cell Biol *172*, 103-113.

Kuang, S., Kuroda, K., Le Grand, F., and Rudnicki, M.A. (2007). Asymmetric self-renewal and commitment of satellite stem cells in muscle. Cell *129*, 999-1010.

Lam, P.Y., Sublett, J.E., Hollenbach, A.D., and Roussel, M.F. (1999). The oncogenic potential of the Pax3-FKHR fusion protein requires the Pax3 homeodomain recognition helix but not the Pax3 paired-box DNA binding domain. Mol Cell Biol *19*, 594-601.

Lepper, C., Conway, S.J., and Fan, C.M. (2009). Adult satellite cells and embryonic muscle progenitors have distinct genetic requirements. Nature *460*, 627-631.

Lopez, A.J. (1998). Alternative splicing of pre-mRNA: developmental consequences and mechanisms of regulation. Annu Rev Genet *32*, 279-305.

Mansouri, A., Stoykova, A., Torres, M., and Gruss, P. (1996). Dysgenesis of cephalic neural crest derivatives in Pax7-/- mutant mice. Development *122*, 831-838.

Mauro, A. (1961). Satellite cell of skeletal muscle fibers. J Biophys Biochem Cytol *9*, 493-495.

McKinnell, I.W., Ishibashi, J., Le Grand, F., Punch, V.G., Addicks, G.C., Greenblatt, J.F., Dilworth, F.J., and Rudnicki, M.A. (2008). Pax7 activates myogenic genes by recruitment of a histone methyltransferase complex. Nat Cell Biol *10*, 77-84.

Megeney, L.A., Kablar, B., Garrett, K., Anderson, J.E., and Rudnicki, M.A. (1996). MyoD is required for myogenic stem cell function in adult skeletal muscle. Genes Dev *10*, 1173-1183.

Melamud, E., and Moult, J. (2009). Stochastic noise in splicing machinery. Nucleic Acids Res *37*, 4873-4886.

Mercatante, D., and Kole, R. (2000). Modification of alternative splicing pathways as a potential approach to chemotherapy. Pharmacol Ther *85*, 237-243.

Miskiewicz, P., Morrissey, D., Lan, Y., Raj, L., Kessler, S., Fujioka, M., Goto, T., and Weir, M. (1996). Both the paired domain and homeodomain are required for in vivo function of Drosophila Paired. Development *122*, 2709-2718.

Montarras, D., Morgan, J., Collins, C., Relaix, F., Zaffran, S., Cumano, A., Partridge, T., and Buckingham, M. (2005). Direct isolation of satellite cells for skeletal muscle regeneration. Science *309*, 2064-2067.

Noll, M. (1993). Evolution and role of Pax genes. Curr Opin Genet Dev *3*, 595-605.

Ono, Y., Calhabeu, F., Morgan, J.E., Katagiri, T., Amthor, H., and Zammit, P.S. (2011). BMP signalling permits population expansion by preventing premature myogenic differentiation in muscle satellite cells. Cell Death Differ *18*, 222-234.

Perry, R.L., and Rudnicki, M.A. (2000). Molecular mechanisms regulating myogenic determination and differentiation. Front Biosci, D750-D767.

Pickrell, J.K., Pai, A.A., Gilad, Y., and Pritchard, J.K. (2010). Noisy splicing drives mRNA isoform diversity in human cells. PLoS Genet *6*, e1001236.

Relaix, F., Montarras, D., Zaffran, S., Gayraud-Morel, B., Rocancourt, D., Tajbakhsh, S., Mansouri, A., Cumano, A., and Buckingham, M. (2006). Pax3 and Pax7 have distinct and overlapping functions in adult muscle progenitor cells. J Cell Biol *172*, 91-102.

Roberts, A., Pimentel, H., Trapnell, C., and Pachter, L. (2011a). Identification of novel transcripts in annotated genomes using RNA-Seq. Bioinformatics *27*, 2325-2329.

Roberts, A., Trapnell, C., Donaghey, J., Rinn, J.L., and Pachter, L. (2011b). Improving RNA-Seq expression estimates by correcting for fragment bias. Genome Biol *12*, R22.

Rozen, S., and Skaletsky, H. (2000). Primer3 on the WWW for general users and for biologist programmers. Methods Mol Biol *132*, 365-386.

Sabourin, L.A., and Rudnicki, M.A. (2000). The molecular regulation of myogenesis. Clin Genet *57*, 16-25.

Schneider, C.A., Rasband, W.S., and Eliceiri, K.W. (2012). NIH Image to ImageJ: 25 years of image analysis. Nat Methods *9*, 671-675.

Schultz, E., Gibson, M.C., and Champion, T. (1978). Satellite cells are mitotically quiescent in mature mouse muscle: an EM and radioautographic study. J Exp Zool *206*, 451-456.

Seale, P., Sabourin, L.A., Girgis-Gabardo, A., Mansouri, A., Gruss, P., and Rudnicki, M.A. (2000). Pax7 is required for the specification of myogenic satellite cells. Cell *102*, 777-786.

Soleimani, V.D., Punch, V.G., Kawabe, Y., Jones, A.E., Palidwor, G.A., Porter, C.J., Cross, J.W., Carvajal, J.J., Kockx, C.E., van, I.W.F.*, et al.* (2012). Transcriptional dominance of Pax7 in adult myogenesis is due to high-affinity recognition of homeodomain motifs. Dev Cell *22*, 1208-1220.

Tadokoro, K., Yamazaki-Inoue, M., Tachibana, M., Fujishiro, M., Nagao, K., Toyoda, M., Ozaki, M., Ono, M., Miki, N., Miyashita, T.*, et al.* (2005). Frequent occurrence of protein isoforms with or without a single amino acid residue by subtle alternative splicing: the case of Gln in DRPLA affects subcellular localization of the products. J Hum Genet *50*, 382-394.

Trapnell, C., Pachter, L., and Salzberg, S.L. (2009). TopHat: discovering splice junctions with RNA-Seq. Bioinformatics *25*, 1105-1111.

Trapnell, C., Williams, B.A., Pertea, G., Mortazavi, A., Kwan, G., van Baren, M.J., Salzberg, S.L., Wold, B.J., and Pachter, L. (2010). Transcript assembly and quantification by RNA-Seq reveals unannotated transcripts and isoform switching during cell differentiation. Nat Biotechnol *28*, 511-515.

Underhill, D.A., and Gros, P. (1997). The paired-domain regulates DNA binding by the homeodomain within the intact Pax-3 protein. J Biol Chem *272*, 14175-14182.

Vogan, K.J., Underhill, D.A., and Gros, P. (1996). An alternative splicing event in the Pax-3 paired domain identifies the linker region as a key determinant of paired domain DNA-binding activity. Mol Cell Biol *16*, 6677-6686.

Wang, H., Noulet, F., Edom-Vovard, F., Tozer, S., Le Grand, F., and Duprez, D. (2010). Bmp signaling at the tips of skeletal muscles regulates the number of fetal muscle progenitors and satellite cells during development. Dev Cell *18*, 643-654.

Wilson, D., Sheng, G., Lecuit, T., Dostatni, N., and Desplan, C. (1993). Cooperative dimerization of paired class homeo domains on DNA. Genes Dev *7*, 2120-2134.

Wilson, D.S., Guenther, B., Desplan, C., and Kuriyan, J. (1995). High resolution crystal structure of a paired (Pax) class cooperative homeodomain dimer on DNA. Cell *82*, 709-719.

Xu, H.E., Rould, M.A., Xu, W., Epstein, J.A., Maas, R.L., and Pabo, C.O. (1999). Crystal structure of the human Pax6 paired domain-DNA complex reveals specific roles for the linker region and carboxy-terminal subdomain in DNA binding. Genes Dev *13*, 1263-1275.

Zammit, P.S., Golding, J.P., Nagata, Y., Hudon, V., Partridge, T.A., and Beauchamp, J.R. (2004). Muscle satellite cells adopt divergent fates: a mechanism for self-renewal? J Cell Biol *166*, 347-357.

Ziman, M.R., and Kay, P.H. (1998). Differential expression of four alternate Pax7 paired box transcripts is influenced by organ- and strain-specific factors in adult mice. Gene *217*, 77-81.

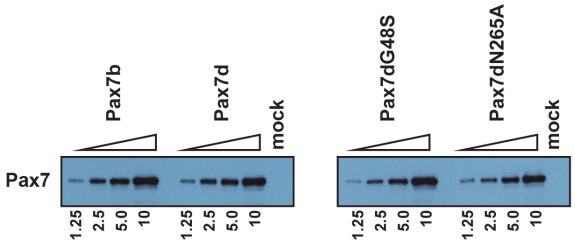

Figure S1. Validation of *in vitro* synthesized Pax7 protein
Pax7b, Pax7d, Pax7dG48S and Pax7dN265A proteins were synthesized *in vitro* using TNT Coupled Reticulocyte Lysate System (Promega) following manufacturer's recommendations. Western blot analysis using 1.25 µl, 2.5 µl, 5.0 µl and 10 µl of *in vitro* synthesized proteins confirming equal protein production prior to EMSA experiments.

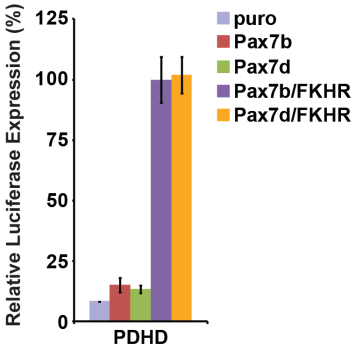

Figure S2. Pax7 is a weak transactivator
Relative luciferase activity following Cos7 transfection of a paired- and homeodomain (PDHD) with Pax7b, Pax7d, Pax7bFKHR, Pax7dFKHR or control. Relative to FKHR fusion proteins, Pax7b and Pax7d exhibit weak luciferase transcriptional output. Data are presented as the mean ± SEM (n=3).

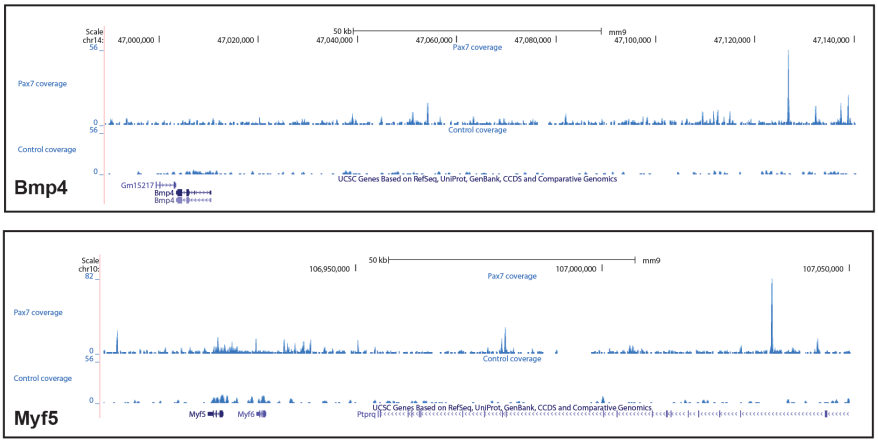

Figure S3. Pax7 binding sites upstream of myogenic genes
Pax7 peaks mapped to the UCSC genome browser, with scale set to automatic. Shown are bound motifs 116 kb upstream of Bmp4 and the previously characterized 111 kb element upstream of Myf5. Data available from (Soleimani et al., 2012).

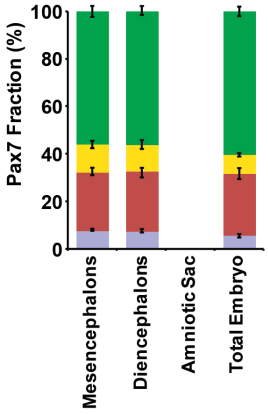

Figure S4. Pax7d is the predominant isoform within embryonic neural development
RT-PCR analysis of embryonic Pax7 isoform expression ratios in 11.5 dpc neural development. Pax7+ cells located within the developing mesencephalons and diencephalons at 11.5 dpc display a similar Pax7 expression ratio as adult satellite cell derived myoblasts. Amniotic sac is included as negative control. Relative band intensities quantified by ImageJ software. Data are presented as the mean ± SEM (n=3).

Table S1. Primer and Probe Sequences

Real-Time RT-PCR	
Pax7_F	CTGGATGAGGGCTCAGATGT
Pax7_R	GGTTAGCTCCTGCCTGCTTA
Myf5_F	TGAGGGAACAGGTGGAGAAC
Myf5_R	AGCTGGACACGGAGCTTTTA
MyoD_F	TACCCAAGGTGGAGATCCTG
MyoD_R	CATCATGCCATCAGAGCAGT
Myogenin_F	GAAGTGAATGAGGCCTTCG
Myogenin_R	ACGATGGACGTAAGGGAGTG
Myh2_F	CAGAACAGAGACGGCTTCAT
Myh2_R	AGTTTCTCCCCAAACATCGT
Bmp4_F	ATCTTTACCGGCTCCAGTCT
Bmp4_R	CTGCTGAGGTTGAAGAGGAA
Tgfbr3_F	TCCTAAACCTCCGCAGTACA
Tgfbr3_R	GGAGTTGAGCAGGAACACAA
Fgfr2_F	GCATCGCATTGGAGGCTATA
Fgfr2_R	GGTAGGTGTGGTTGATGGAC
Dsp_F	AACCGAGAGCTGGATGAGTA
Dsp_R	TGTAAAGGGCTCGCATTTGT
Itga2_F	CTGGCGTATAATGTTGGCCT
Itga2_R	CACAGGGCACTTGTACACAT
Grb14_F	CAGGGCCAATTCAAGGAAGA
Grb14_R	TCAACAGCTGGCAAACATCT
Egfr_F	ACTGGGCACTTTTGAAGACC
Egfr_R	GATTCTCTCCACGGTGTTGA
Myl1_F	CGAATCGAGGCTCAGAACAA
Myl1_R	CGTACTTGGGAGGGTTCATG
Mef2c_F	GCCAGCACTGACATGGATAA
Mef2c_R	GTGGGGTGAGTGCATAAGAG
Tnni1_F	CAAGGAGTGTTGGGAGCAG
Tnni1_R	TCCTCATCCACCACCTCTAC
Actn2_F	CGAGGAGGATTTCAGGAACG
Actn2_R	ACTCCCTTGCTGGCTATGTA
s100a4_F	GGAGGCCCTGGATGTAATTG
s100a4_R	TTGCTGTCCAAGTTGCTCAT
Camk1g_F	TGAAGCAAAGAGTGACTGGG
Camk1g_R	TAGTAGTGGGTGGTGCTCTC
Bgn_F	AGATCTCACCTGACACCACA
Bgn_R	TTGTTTACCAAGACCAGGGC
GAPDH_F	TGTCCGTCGTGGATCTGAC
GAPDH_R	GGTCCTCAGTGTAGCCCAAG
RT-PCR	
Pax7_2_F	GTGCCGATATCAGGAGACTG
Pax7_4_R	TCCTCTTTCTTCCCGAACTT
Luciferase	
Myf5ECR111 PD_F	GATCTTCATTTCCTGATTGTCATGCTTCTATCCTTGCACAG
Myf5ECR111 PD_R	GATCCTGTGCAAGGATAGAAGCATGACAATCAGGAAATGAA
Myf5ECR111 HD_F	GATCTCTGGTTTTCACAATAATGCATTTTCTGTAACTAACG
Myf5ECR111 HD_R	GATCCGTTAGTTACAGAAAATGCATTATTGTGAAAACCAGA
Myf5ECR111 PDHD_F	GATCCTGTGCAAGGATAGAAGCATGACAATCAGGAAATGATGGT

	TGTTAGTTACAGAAAATGCATTATTGTGAAAACCAGA
	GATCTCTGGTTTTCACAATAATGCATTTTCTGTAACTAACAACCAT
Myf5ECR111 PDHD_R	CATTTCCTGATTGTCATGCTTCTATCCTTGCACAG
EMSA	
	TTCACAATAATGCATTTTCTGTAACTAACAACCATCATTTCCTGAT
Myf5ECR111 PDHD	TGTCATGCTTCTAT
	TTCACAATAATGCATTTTCTGTAACTAACAACCATCATTTCCTGAT
Myf5ECR111 dPDHD	CTCAGCTACCCTAT
	TTCACAACGGCTAGCCCTCTTCGGACGGAAACCATCATTTCCTG
Myf5ECR111 PDdHD	ATTGTCATGCTTCTAT
	TTCACAACGGCTAGCCCTCTTCGGACGGAAACCATCATTTCCTG
Myf5ECR111 dPDdHD	ATCTCAGCTACCCTAT
ChIP	
GAPDH(-3k)_F	TCCAGTGAGGACGGTATGAT
GAPDH(-3k)_R	CATAAAGATGGGGCAAAATG
Myf5(-111k)_F	CATCCCACATAATCCAATCAC
Myf5(-111k)_R	ACACAGATGGATGGGAAAGA
Bmp4(-116k)_F	TCACATTTCTGGTGAATGGA
Bmp4(-116k)_F	GGGGGTGATCTTTCTTTCAG

Table S2. Enriched GO Terms Among Pax7B/D Common Genes

Term	Count	P-value	Fold Enrich	Benjamini
GO:0044449~contractile fiber part	17	3.81E-09	6.644	1.03E-06
GO:0043292~contractile fiber	17	1.70E-08	6.015	2.31E-06
GO:0030016~myofibril	16	6.46E-08	5.910	5.84E-06
GO:0030017~sarcomere	15	8.18E-08	6.302	5.54E-06
GO:0003012~muscle system process	13	1.02E-06	6.146	2.07E-03
GO:0006936~muscle contraction	12	2.27E-06	6.335	2.30E-03
GO:0005576~extracellular region	83	2.37E-06	1.661	1.29E-04
GO:0003779~actin binding	26	2.80E-06	2.940	1.71E-03
GO:0001501~skeletal system development	26	3.83E-06	2.890	2.58E-03
GO:0008092~cytoskeletal protein binding	31	1.14E-05	2.439	3.47E-03
GO:0007155~cell adhesion	38	1.79E-05	2.145	9.05E-03
GO:0022610~biological adhesion	38	1.84E-05	2.142	7.41E-03
GO:0060348~bone development	15	2.01E-05	4.026	6.78E-03
GO:0044421~extracellular region part	45	2.35E-05	1.954	1.06E-03
GO:0008083~growth factor activity	16	2.74E-05	3.696	5.56E-03
GO:0030029~actin filament-based process	18	4.11E-05	3.239	1.18E-02
GO:0001944~vasculature development	22	4.34E-05	2.787	1.09E-02
GO:0009069~serine family amino acid metabolic process	7	4.58E-05	10.078	1.03E-02
GO:0005788~endoplasmic reticulum lumen	11	4.88E-05	5.135	1.89E-03
GO:0001568~blood vessel development	21	9.21E-05	2.726	1.85E-02
GO:0005615~extracellular space	32	1.26E-04	2.105	4.27E-03
GO:0015629~actin cytoskeleton	18	1.30E-04	2.951	3.91E-03
GO:0048514~blood vessel morphogenesis	18	1.77E-04	2.879	3.21E-02
GO:0014706~striated muscle tissue development	14	1.83E-04	3.492	3.04E-02
GO:0042470~melanosome	11	2.02E-04	4.350	5.47E-03
GO:0048770~pigment granule	11	2.02E-04	4.350	5.47E-03
GO:0030036~actin cytoskeleton organization	16	2.27E-04	3.071	3.47E-02
GO:0005509~calcium ion binding	45	3.31E-04	1.745	4.93E-02
GO:0060537~muscle tissue development	14	3.60E-04	3.261	5.09E-02
GO:0030018~Z disc	8	3.77E-04	5.846	9.25E-03
GO:0008652~cellular amino acid biosynthetic process	8	4.09E-04	5.759	5.38E-02
GO:0016459~myosin complex	9	4.15E-04	4.959	9.33E-03
GO:0032559~adenyl ribonucleotide binding	68	4.44E-04	1.517	5.27E-02
GO:0007517~muscle organ development	16	4.55E-04	2.879	5.60E-02
GO:0005886~plasma membrane	115	4.68E-04	1.330	9.72E-03
GO:0031668~cellular response to extracellular stimulus	8	4.72E-04	5.631	5.47E-02
GO:0001503~ossification	12	5.03E-04	3.586	5.51E-02
GO:0006418~tRNA aminoacylation for protein translation	8	5.42E-04	5.508	5.62E-02
GO:0043039~tRNA aminoacylation	8	5.42E-04	5.508	5.62E-02
GO:0043038~amino acid activation	8	5.42E-04	5.508	5.62E-02
GO:0005524~ATP binding	67	5.43E-04	1.512	5.37E-02
GO:0016875~ligase activity, forming carbon-oxygen bonds	8	5.98E-04	5.428	5.08E-02
GO:0016876~ligase activity, forming aminoacyl-tRNA and related compounds	8	5.98E-04	5.428	5.08E-02
GO:0004812~aminoacyl-tRNA ligase activity	8	5.98E-04	5.428	5.08E-02
GO:0030554~adenyl nucleotide binding	70	6.36E-04	1.485	4.74E-02

Table S3. Enriched GO Terms Among Pax7B Unique Genes

Term	Count	P-Value	Fold Enrich	Benjamini
GO:0007010~cytoskeleton organization	13	6.80E-05	4.136	6.82E-02
GO:0007167~enzyme linked receptor protein signaling pathway	10	1.24E-03	3.799	4.75E-01
GO:0008092~cytoskeletal protein binding	12	2.62E-03	2.918	5.69E-01
GO:0007017~microtubule-based process	8	4.16E-03	3.933	7.64E-01
GO:0000226~microtubule cytoskeleton organization	6	4.24E-03	5.607	6.68E-01
GO:0030017~sarcomere	5	5.54E-03	6.978	6.77E-01
GO:0044449~contractile fiber part	5	7.15E-03	6.491	5.17E-01
GO:0030016~myofibril	5	8.70E-03	6.134	4.46E-01
GO:0051789~response to protein stimulus	5	9.66E-03	5.961	8.67E-01
GO:0005856~cytoskeleton	19	9.71E-03	1.891	3.90E-01
GO:0043292~contractile fiber	5	1.01E-02	5.876	3.37E-01
GO:0031674~I band	4	1.16E-02	8.426	3.25E-01
GO:0030534~adult behavior	5	1.21E-02	5.577	8.79E-01
GO:0042127~regulation of cell proliferation	12	1.41E-02	2.314	8.79E-01
GO:0006323~DNA packaging	5	1.60E-02	5.135	8.77E-01
GO:0043228~non-membrane-bounded organelle	27	1.61E-02	1.571	3.75E-01
GO:0043232~intracellular non-membrane-bounded organelle	27	1.61E-02	1.571	3.75E-01
GO:0031175~neuron projection development	7	1.84E-02	3.331	8.82E-01
GO:0045893~positive regulation of transcription, DNA-dependent	10	1.85E-02	2.493	8.56E-01
GO:0009066~aspartate family amino acid metabolic process	3	1.85E-02	14.144	8.29E-01
GO:0051254~positive regulation of RNA metabolic process	10	1.92E-02	2.476	8.14E-01
GO:0032989~cellular component morphogenesis	9	1.95E-02	2.660	7.93E-01
GO:0010858~calcium-dependent protein kinase regulator activity	2	1.96E-02	100.667	9.58E-01
GO:0019887~protein kinase regulator activity	4	2.04E-02	6.825	8.90E-01
GO:0030036~actin cytoskeleton organization	6	2.11E-02	3.772	7.95E-01
GO:0008344~adult locomotory behavior	4	2.15E-02	6.692	7.78E-01
GO:0045944~positive regulation of transcription from RNA polymerase II promoter	9	2.17E-02	2.608	7.59E-01
GO:0048666~neuron development	8	2.22E-02	2.842	7.46E-01
GO:0003779~actin binding	8	2.39E-02	2.796	8.57E-01
GO:0042592~homeostatic process	12	2.43E-02	2.131	7.59E-01
GO:0045935~positive regulation of nucleobase, nucleoside, nucleotide and nucleic acid metabolic process	11	2.45E-02	2.237	7.43E-01
GO:0043112~receptor metabolic process	3	2.54E-02	11.968	7.37E-01

Table S4. Enriched GO Terms Among Pax7D Unique Genes

Term	Count	P-value	Fold Enrich	Benjamini
GO:0030016~myofibril	16	1.46E-09	7.824	3.81E-07
GO:0016529~sarcoplasmic reticulum	11	2.20E-09	14.396	2.86E-07
GO:0030017~sarcomere	15	2.32E-09	8.343	2.01E-07
GO:0043292~contractile fiber	16	2.72E-09	7.494	1.77E-07
GO:0016528~sarcoplasm	11	4.11E-09	13.597	2.14E-07
GO:0044449~contractile fiber part	15	6.18E-09	7.761	2.68E-07
GO:0031674~I band	10	2.33E-06	8.396	8.64E-05
GO:0030018~Z disc	9	7.13E-06	8.706	2.32E-04
GO:0044421~extracellular region part	38	9.74E-06	2.185	2.81E-04
GO:0001568~blood vessel development	19	2.01E-05	3.286	3.31E-02
GO:0007155~cell adhesion	31	2.60E-05	2.332	2.15E-02
GO:0022610~biological adhesion	31	2.72E-05	2.328	1.50E-02
GO:0001944~vasculature development	19	2.79E-05	3.207	1.16E-02
GO:0019838~growth factor binding	10	5.59E-05	5.732	2.61E-02
GO:0015629~actin cytoskeleton	16	5.85E-05	3.473	1.52E-03
GO:0005539~glycosaminoglycan binding	12	9.68E-05	4.344	2.26E-02
GO:0044459~plasma membrane part	60	1.11E-04	1.635	2.62E-03
GO:0005578~proteinaceous extracellular matrix	19	1.27E-04	2.847	2.75E-03
GO:0005509~calcium ion binding	39	1.37E-04	1.916	2.14E-02
GO:0008201~heparin binding	10	1.71E-04	4.972	2.00E-02
GO:0031012~extracellular matrix	19	2.06E-04	2.736	4.11E-03
GO:0001871~pattern binding	12	2.71E-04	3.869	2.53E-02
GO:0030247~polysaccharide binding	12	2.71E-04	3.869	2.53E-02
GO:0016323~basolateral plasma membrane	12	3.27E-04	3.787	6.05E-03
GO:0046872~metal ion binding	122	4.05E-04	1.308	3.14E-02
GO:0016459~myosin complex	8	4.06E-04	5.836	7.02E-03
GO:0009986~cell surface	18	5.18E-04	2.626	8.39E-03
GO:0005886~plasma membrane	90	5.82E-04	1.378	8.87E-03
GO:0043169~cation binding	122	5.95E-04	1.296	3.93E-02
GO:0005856~cytoskeleton	43	6.28E-04	1.705	9.03E-03
GO:0043167~ion binding	123	6.65E-04	1.290	3.85E-02
GO:0030246~carbohydrate binding	19	7.12E-04	2.473	3.66E-02
GO:0007507~heart development	15	8.58E-04	2.838	2.49E-01
GO:0048514~blood vessel morphogenesis	14	8.63E-04	2.984	2.14E-01
GO:0008092~cytoskeletal protein binding	22	1.13E-03	2.193	5.20E-02
GO:0006928~cell motion	20	1.19E-03	2.300	2.47E-01
GO:0034329~cell junction assembly	5	1.33E-03	10.047	2.43E-01
GO:0005996~monosaccharide metabolic process	13	1.96E-03	2.872	3.06E-01
GO:0019318~hexose metabolic process	12	2.27E-03	2.996	3.16E-01
GO:0006937~regulation of muscle contraction	6	2.66E-03	6.175	3.33E-01
GO:0043062~extracellular structure organization	11	2.84E-03	3.115	3.27E-01
GO:0008047~enzyme activator activity	15	3.00E-03	2.486	1.21E-01
GO:0007517~muscle organ development	12	3.11E-03	2.877	3.30E-01
GO:0007044~cell-substrate junction assembly	4	3.92E-03	12.057	3.74E-01
GO:0003012~muscle system process	7	4.94E-03	4.409	4.24E-01
GO:0060537~muscle tissue development	10	4.98E-03	3.103	4.07E-01

Table S5. Pax7B/D Common Regulated Changes in Gene Expression

Gene ID	Gene Symbol	Fold Change (log2) Pax7b	Fold Change (log2) Pax7d	q-value (Pax7b)	q-value (Pax7d)
ENSMUSG00000054889	Dsp	6.649	8.106	3.04E-07	2.86E-12
ENSMUSG00000037685	Atp8a1	5.795	7.486	4.93E-06	1.47E-11
ENSMUSG00000079092	Prl2c2	4.698	6.101	0.00E+00	0.00E+00
ENSMUSG00000056457	Prl2c3	4.637	6.063	0.00E+00	0.00E+00
ENSMUSG00000022548	Apod	5.006	5.694	3.40E-02	3.39E-03
ENSMUSG00000063011	Msln	3.888	5.627	0.00E+00	0.00E+00
ENSMUSG00000055360	Prl2c5	4.330	5.594	0.00E+00	0.00E+00
ENSMUSG00000062551	Prl2c1	3.945	5.122	8.42E-08	1.80E-13
ENSMUSG00000034613	Ppm1h	3.782	4.785	2.45E-02	1.79E-03
ENSMUSG00000031351	Zfp185	2.075	4.738	6.14E-04	0.00E+00
ENSMUSG00000028370	Pappa	2.728	4.593	5.49E-09	0.00E+00
ENSMUSG00000057722	Lepr	4.476	4.558	3.47E-07	1.40E-07
ENSMUSG00000090837	Gm7233	3.409	4.428	1.64E-02	5.01E-04
ENSMUSG00000028736	Pax7	4.117	4.411	0.00E+00	0.00E+00
ENSMUSG00000058656	Samd12	2.910	4.128	1.52E-02	2.83E-05
ENSMUSG00000038094	Atp13a4	4.201	4.077	3.18E-03	5.63E-03
ENSMUSG00000029816	Gpnmb	2.661	3.881	0.00E+00	0.00E+00
ENSMUSG00000033717	Adra2a	2.432	3.870	1.59E-03	7.41E-09
ENSMUSG00000040329	Il7	2.373	3.820	4.97E-04	4.13E-09
ENSMUSG00000024810	Il33	2.670	3.685	3.35E-04	8.51E-09
ENSMUSG00000015533	Itga2	1.629	3.632	6.99E-05	0.00E+00
ENSMUSG00000028542	Slc6a9	3.636	3.581	0.00E+00	0.00E+00
ENSMUSG00000032715	Trib3	3.004	3.402	0.00E+00	0.00E+00
ENSMUSG00000022894	Adamts5	3.368	3.381	0.00E+00	1.31E-10
ENSMUSG00000031995	St14	3.454	3.380	5.59E-03	3.13E-03
ENSMUSG00000032085	Tagln	2.556	3.364	0.00E+00	0.00E+00
ENSMUSG00000039982	Dtx4	2.295	3.353	4.18E-08	7.33E-12
ENSMUSG00000038295	Atg9b	2.390	3.272	5.54E-12	0.00E+00
ENSMUSG00000029314	Agpat9	1.718	3.269	1.88E-03	4.14E-08
ENSMUSG00000026888	Grb14	1.534	3.180	1.82E-03	0.00E+00
ENSMUSG00000005125	Ndrg1	2.843	3.178	7.37E-04	1.00E-04
ENSMUSG00000053141	Ptprt	3.586	3.172	0.00E+00	1.94E-08
ENSMUSG00000018507	Trpv2	2.977	3.150	4.44E-02	3.09E-02
ENSMUSG00000054136	Adm2	2.558	3.102	2.84E-02	4.55E-03
ENSMUSG00000041624	Gucy1a2	2.461	3.085	4.37E-03	5.08E-05
ENSMUSG00000074785	Plxnc1	2.456	2.954	2.28E-06	1.49E-06
ENSMUSG00000063873	Slc24a3	2.334	2.941	1.83E-03	3.45E-05
ENSMUSG00000020019	Ntn4	2.290	2.902	7.76E-05	8.30E-07
ENSMUSG00000024924	Vldlr	2.069	2.870	2.25E-03	2.26E-06
ENSMUSG00000033022	Cdo1	3.195	2.846	9.78E-03	3.90E-02
ENSMUSG00000000435	Myf5	2.100	2.831	0.00E+00	0.00E+00
ENSMUSG00000033542	Arhgef5	1.990	2.776	3.20E-04	7.12E-06
ENSMUSG00000037035	Inhbb	2.576	2.772	5.19E-10	1.63E-07
ENSMUSG00000043259	Fam13c	2.400	2.742	5.86E-07	3.11E-07
ENSMUSG00000020122	Egfr	1.300	2.691	2.57E-06	0.00E+00
ENSMUSG00000040133	Gpr176	2.368	2.688	2.30E-07	2.11E-06
ENSMUSG00000021186	Fbln5	2.984	2.634	4.01E-09	1.00E-04
ENSMUSG00000039518	Cdsn	2.465	2.593	6.19E-06	1.45E-04
ENSMUSG00000027313	Chac1	2.619	2.571	0.00E+00	1.64E-09
ENSMUSG00000030623	1700019G06Rik	1.675	2.552	4.59E-04	1.25E-06
ENSMUSG00000028364	Tnc	1.257	2.551	0.00E+00	0.00E+00

ENSMUSG00000022893	Adamts1	2.494	2.526	1.44E-12	3.45E-08
ENSMUSG00000024907	Gal	3.123	2.522	6.90E-14	1.20E-05
ENSMUSG00000020589	Fam49a	1.689	2.509	1.48E-03	9.54E-06
ENSMUSG00000026956	Uap1l1	2.147	2.507	1.92E-08	3.01E-10
ENSMUSG00000028179	Cth	1.958	2.505	2.70E-12	0.00E+00
ENSMUSG00000048720	Tbc1d12	1.924	2.487	8.82E-03	1.26E-04
ENSMUSG00000029084	Cd38	1.501	2.425	4.33E-02	9.57E-04
ENSMUSG00000025408	Ddit3	2.115	2.416	8.95E-13	7.28E-12
ENSMUSG00000038587	Akap12	1.458	2.395	6.39E-04	3.99E-07
ENSMUSG00000091002	Tcerg1l	2.397	2.388	2.55E-03	4.44E-03
ENSMUSG00000043289	Mei4	1.640	2.364	3.02E-02	2.54E-04
ENSMUSG00000030022	Adamts9	1.936	2.348	3.03E-04	5.11E-05
ENSMUSG00000038602	Slc35f1	1.243	2.307	3.71E-03	3.35E-07
ENSMUSG00000020598	Nrcam	0.943	2.303	3.52E-02	3.92E-08
ENSMUSG00000027500	Stmn2	1.760	2.299	3.27E-06	6.19E-07
ENSMUSG00000034813	Grip1	1.565	2.274	4.11E-06	2.10E-11
ENSMUSG00000022865	Cxadr	1.368	2.241	1.29E-07	6.21E-14
ENSMUSG00000020256	Aldh1l2	1.583	2.229	7.90E-05	3.48E-09
ENSMUSG00000030499	Kctd15	2.150	2.221	1.13E-02	3.72E-03
ENSMUSG00000078853	Igtp	2.038	2.186	7.33E-03	1.46E-02
ENSMUSG00000039405	Prss23	1.747	2.160	3.93E-11	4.95E-11
ENSMUSG00000029126	Nsg1	1.641	2.151	1.30E-02	3.47E-03
ENSMUSG00000020303	Stc2	1.620	2.147	2.69E-02	1.38E-03
ENSMUSG00000002688	Prkd1	1.506	2.113	2.08E-03	1.66E-04
ENSMUSG00000031297	Slc7a3	3.441	2.093	1.91E-11	2.81E-03
ENSMUSG00000010307	Tmem86a	1.753	2.052	8.66E-04	1.62E-03
ENSMUSG00000033295	Ptprf	1.089	2.045	2.23E-07	0.00E+00
ENSMUSG00000030717	Nupr1	1.813	2.042	1.96E-07	1.52E-06
ENSMUSG00000039697	Ncoa7	1.281	2.019	3.55E-08	0.00E+00
ENSMUSG00000030669	Calca	2.428	2.009	7.15E-05	8.58E-03
ENSMUSG00000021365	Nedd9	1.733	1.989	1.00E-04	5.64E-04
ENSMUSG00000031202	Rab39b	1.648	1.982	1.74E-04	2.88E-04
ENSMUSG00000038508	Gdf15	1.814	1.980	8.80E-04	5.24E-03
ENSMUSG00000028680	Plk3	1.273	1.970	4.46E-04	7.76E-08
ENSMUSG00000027692	Tnik	2.301	1.959	6.75E-04	7.90E-03
ENSMUSG00000031714	Gab1	1.467	1.957	1.30E-03	3.02E-04
ENSMUSG00000033722	BC034090	1.901	1.950	1.33E-07	4.37E-05
ENSMUSG00000091243	Vgll3	1.828	1.943	3.09E-12	6.01E-09
ENSMUSG00000027506	Tpd52	1.228	1.892	1.40E-03	3.48E-08
ENSMUSG00000040296	Ddx58	1.848	1.890	3.55E-02	1.21E-02
ENSMUSG00000024055	Cyp4f13	2.011	1.879	1.25E-05	1.40E-04
ENSMUSG00000024014	Pim1	1.762	1.847	6.59E-03	2.65E-02
ENSMUSG00000015568	Lpl	1.757	1.839	8.47E-12	2.14E-08
ENSMUSG00000024063	Lbh	1.204	1.836	2.32E-06	3.99E-10
ENSMUSG00000040618	Pck2	1.626	1.831	6.90E-14	6.18E-12
ENSMUSG00000028133	Rwdd3	1.871	1.825	3.39E-02	3.95E-02
ENSMUSG00000075122	Cd80	0.912	1.812	5.46E-03	3.94E-09
ENSMUSG00000027805	Pfn2	1.482	1.811	9.47E-07	1.39E-06
ENSMUSG00000032368	Zic1	1.320	1.809	1.33E-02	9.05E-04
ENSMUSG00000045954	Sdpr	1.889	1.804	1.99E-13	4.23E-08
ENSMUSG00000029446	Psph	1.625	1.798	0.00E+00	0.00E+00
ENSMUSG00000039934	Pion	1.215	1.754	2.29E-02	3.40E-03
ENSMUSG00000042246	Tmc7	2.053	1.751	9.05E-03	2.19E-02
ENSMUSG00000028893	Sesn2	1.421	1.748	4.26E-06	5.25E-06

ENSMUSG00000020432	Tcn2	1.056	1.731	1.46E-07	6.21E-14
ENSMUSG00000021203	Otub2	1.740	1.726	5.47E-04	2.94E-03
ENSMUSG00000062991	Nrg1	1.511	1.713	6.18E-03	8.17E-03
ENSMUSG00000024778	Fas	1.529	1.710	2.84E-02	4.55E-02
ENSMUSG00000072294	Klf12	1.661	1.700	1.06E-02	4.69E-02
ENSMUSG00000029814	Igf2bp3	1.052	1.689	3.50E-02	1.62E-03
ENSMUSG00000024521	Pmaip1	1.188	1.685	1.27E-03	9.56E-05
ENSMUSG00000048040	Arxes2	1.329	1.674	4.58E-02	3.04E-02
ENSMUSG00000068196	Col8a1	1.127	1.672	1.46E-03	4.22E-05
ENSMUSG00000039450	Dcxr	1.191	1.671	3.03E-04	5.25E-07
ENSMUSG00000026471	Mr1	1.172	1.669	2.30E-02	4.36E-03
ENSMUSG00000031239	Itm2a	1.623	1.669	1.64E-09	1.41E-06
ENSMUSG00000023883	Phf10	1.324	1.668	0.00E+00	0.00E+00
ENSMUSG00000028015	Ctso	1.385	1.654	7.93E-03	5.49E-03
ENSMUSG00000027220	Syt13	1.734	1.635	5.79E-05	6.85E-03
ENSMUSG00000035783	Acta2	2.203	1.634	0.00E+00	3.08E-06
ENSMUSG00000000278	Scpep1	0.949	1.613	2.54E-04	2.19E-07
ENSMUSG00000022575	Gsdmd	1.931	1.601	2.51E-04	4.28E-02
ENSMUSG00000024339	Tap2	2.215	1.599	1.68E-04	2.76E-02
ENSMUSG00000018800	Abca5	0.878	1.599	2.25E-02	1.99E-05
ENSMUSG00000042156	Dzip1	1.232	1.598	8.17E-07	1.10E-07
ENSMUSG00000019850	Tnfaip3	1.171	1.596	4.42E-02	2.01E-03
ENSMUSG00000032298	Neil1	1.378	1.585	6.20E-03	5.44E-03
ENSMUSG00000066152	Slc31a2	1.464	1.531	1.42E-02	3.13E-02
ENSMUSG00000010660	Plcd1	1.117	1.531	3.44E-02	1.21E-02
ENSMUSG00000028020	Glrb	1.958	1.530	6.26E-05	2.57E-02
ENSMUSG00000032271	Nnmt	1.693	1.528	3.95E-04	7.05E-03
ENSMUSG00000031700	Gpt2	1.696	1.518	0.00E+00	2.19E-08
ENSMUSG00000025420	Katnal2	2.235	1.512	3.52E-05	4.30E-02
ENSMUSG00000043336	Filip1l	1.017	1.504	1.64E-03	6.79E-05
ENSMUSG00000025104	Hdgfrp3	1.077	1.485	2.14E-02	5.63E-03
ENSMUSG00000037321	Tap1	1.086	1.480	3.47E-02	3.72E-03
ENSMUSG00000045312	Lhfpl2	1.390	1.465	8.57E-06	3.68E-06
ENSMUSG00000034795	Ccdc122	1.153	1.459	1.32E-02	1.85E-03
ENSMUSG00000034647	Ankrd12	1.148	1.458	3.23E-02	4.15E-03
ENSMUSG00000034731	Dgkh	1.100	1.448	4.71E-02	3.33E-02
ENSMUSG00000031490	Eif4ebp1	1.009	1.413	1.15E-03	1.08E-04
ENSMUSG00000029470	P2rx4	1.250	1.406	8.26E-03	1.75E-03
ENSMUSG00000025007	Aldh18a1	1.347	1.400	5.01E-12	1.29E-09
ENSMUSG00000023092	Fhl1	-1.246	1.394	5.98E-03	2.71E-05
ENSMUSG00000032826	Ank2	1.087	1.391	2.20E-04	7.14E-05
ENSMUSG00000026786	Apbb1ip	0.928	1.386	2.93E-02	3.27E-03
ENSMUSG00000046312	AI464131	1.812	1.384	2.44E-08	4.72E-03
ENSMUSG00000023809	Rps6ka2	0.953	1.379	4.08E-03	1.51E-04
ENSMUSG00000054863	Fam19a5	-1.368	-1.630	3.16E-10	5.27E-09
ENSMUSG00000090850	Orai2-ps	-1.327	-1.643	1.33E-04	2.80E-04
ENSMUSG00000039747	Orai2	-1.412	-1.652	0.00E+00	0.00E+00
ENSMUSG00000044337	Cxcr7	-0.980	-1.655	9.00E-03	5.65E-05
ENSMUSG00000021549	Rasa1	-1.487	-1.674	0.00E+00	0.00E+00
ENSMUSG00000026414	Tnnt2	-0.363	-1.675	2.78E-02	0.00E+00
ENSMUSG00000039270	Megf9	-0.977	-1.682	3.90E-03	3.27E-05
ENSMUSG00000041911	Dlx1	-1.085	-1.704	4.65E-04	8.94E-07
ENSMUSG00000061086	Myl4	-0.670	-1.707	3.27E-06	0.00E+00
ENSMUSG00000075316	Scn9a	-1.787	-1.708	0.00E+00	2.52E-11

ENSMUSG00000026043	Col3a1	-0.850	-1.716	3.55E-03	2.93E-08
ENSMUSG00000050737	Ptges	-2.100	-1.726	2.84E-05	7.62E-03
ENSMUSG00000044951	Mylk4	-0.628	-1.728	2.48E-02	3.85E-09
ENSMUSG00000027800	Tm4sf1	-2.231	-1.734	1.99E-13	3.20E-06
ENSMUSG00000029378	Areg	-1.752	-1.738	3.86E-05	2.61E-03
ENSMUSG00000052085	Dock8	-1.606	-1.764	4.64E-08	3.68E-06
ENSMUSG00000022297	Fzd6	-1.249	-1.786	2.19E-02	9.14E-03
ENSMUSG00000079243	Xirp1	-0.862	-1.797	3.41E-02	1.23E-04
ENSMUSG00000022512	Cldn1	-1.529	-1.803	1.34E-02	2.38E-02
ENSMUSG00000029683	Lmod2	-1.304	-1.811	6.57E-04	2.65E-04
ENSMUSG00000032014	Oaf	-1.347	-1.813	2.02E-04	1.19E-04
ENSMUSG00000042751	Nmnat2	-2.021	-1.831	3.09E-07	5.13E-04
ENSMUSG00000033685	Ucp2	-0.849	-1.840	3.34E-04	5.17E-11
ENSMUSG00000025854	Fam20c	-1.166	-1.847	1.04E-06	7.92E-10
ENSMUSG00000038210	Hoxa11	-1.313	-1.853	6.27E-06	1.73E-07
ENSMUSG00000016494	Cd34	-2.775	-1.856	3.25E-08	8.65E-04
ENSMUSG00000086427	Hoxa11as	-1.315	-1.885	2.39E-04	1.87E-05
ENSMUSG00000061462	Obscn	-1.192	-1.888	4.55E-07	5.41E-09
ENSMUSG00000001435	Col18a1	-1.354	-1.899	7.89E-13	0.00E+00
ENSMUSG00000032735	Ablim3	-1.301	-1.904	4.81E-04	9.05E-04
ENSMUSG00000024486	Hbegf	-2.002	-1.906	8.25E-10	8.03E-06
ENSMUSG00000031740	Mmp2	-0.849	-1.911	1.68E-02	1.79E-06
ENSMUSG00000033350	Chst2	-1.469	-1.931	2.79E-07	1.06E-07
ENSMUSG00000036867	Smad6	-1.639	-1.939	8.46E-04	4.76E-03
ENSMUSG00000061816	Myl1	-1.146	-1.970	0.00E+00	0.00E+00
ENSMUSG00000004791	Pgf	-1.337	-1.980	1.13E-03	2.09E-04
ENSMUSG00000028369	Svep1	-1.266	-2.001	1.06E-03	4.66E-05
ENSMUSG00000026407	Cacna1s	-1.019	-2.015	8.76E-05	4.05E-11
ENSMUSG00000031520	Vegfc	-1.686	-2.038	1.42E-06	7.24E-06
ENSMUSG00000017300	Tnnc2	-0.977	-2.060	8.91E-03	5.96E-06
ENSMUSG00000029153	Ociad2	-0.793	-2.066	4.49E-02	3.20E-06
ENSMUSG00000028348	Murc	-0.934	-2.067	3.88E-03	2.94E-08
ENSMUSG00000064246	Chi3l1	-2.371	-2.080	1.13E-02	2.70E-02
ENSMUSG00000026418	Tnni1	-0.786	-2.083	0.00E+00	0.00E+00
ENSMUSG00000052374	Actn2	-0.751	-2.087	1.02E-03	0.00E+00
ENSMUSG00000028773	Fabp3	-1.338	-2.090	3.85E-02	7.14E-03
ENSMUSG00000008658	Rbfox1	-0.850	-2.108	6.57E-07	0.00E+00
ENSMUSG00000028864	Hgf	-1.940	-2.111	4.35E-08	6.89E-06
ENSMUSG00000035105	Egln3	-1.575	-2.163	9.86E-09	4.84E-10
ENSMUSG00000041633	Kctd12b	-1.148	-2.176	1.33E-02	1.54E-04
ENSMUSG00000037605	Lphn3	-2.067	-2.177	4.91E-02	3.97E-02
ENSMUSG00000018500	Adora2b	-1.745	-2.181	6.35E-05	1.52E-04
ENSMUSG00000020099	Unc5b	-1.778	-2.191	5.10E-12	9.07E-12
ENSMUSG00000075307	Kbtbd10	-1.071	-2.206	7.05E-04	8.66E-09
ENSMUSG00000030470	Csrp3	-1.162	-2.210	3.29E-03	1.11E-05
ENSMUSG00000022015	Tnfsf11	-2.413	-2.217	0.00E+00	0.00E+00
ENSMUSG00000054013	Tmem179	-2.405	-2.223	2.14E-02	3.61E-02
ENSMUSG00000092569	Gm20544	-2.522	-2.249	2.80E-05	2.99E-03
ENSMUSG00000066026	Dhrs3	-1.907	-2.250	1.51E-02	5.94E-03
ENSMUSG00000079588	Tmem182	-1.141	-2.253	1.55E-03	9.51E-07
ENSMUSG00000029307	Dmp1	-1.891	-2.257	5.29E-05	2.47E-04
ENSMUSG00000033849	B3galt2	-1.378	-2.259	7.58E-03	4.36E-04
ENSMUSG00000051048	P4ha3	-2.601	-2.273	3.60E-02	1.42E-02
ENSMUSG00000022602	Arc	-1.796	-2.273	2.52E-02	1.45E-02

ENSMUSG00000022636	Alcam	-2.697	-2.273	0.00E+00	0.00E+00
ENSMUSG00000004347	Pde1c	-1.088	-2.277	1.02E-05	1.06E-11
ENSMUSG00000057003	Myh4	-0.908	-2.296	2.14E-02	9.92E-07
ENSMUSG00000029869	Ephb6	-1.170	-2.325	1.12E-03	4.23E-08
ENSMUSG00000041731	Pgm5	-0.784	-2.325	8.00E-03	4.97E-11
ENSMUSG00000027559	Car3	-1.667	-2.329	1.41E-10	2.36E-13
ENSMUSG00000041476	Smpx	-1.247	-2.332	4.10E-10	0.00E+00
ENSMUSG00000024049	Myom1	-1.157	-2.355	6.25E-04	3.92E-07
ENSMUSG00000033196	Myh2	-1.077	-2.359	7.49E-04	3.16E-09
ENSMUSG00000030306	Tmtc1	-1.245	-2.368	1.12E-03	1.78E-06
ENSMUSG00000005583	Mef2c	-1.820	-2.390	0.00E+00	0.00E+00
ENSMUSG00000054342	Kcnn4	-1.928	-2.397	2.87E-04	4.65E-04
ENSMUSG00000026580	Selp	-2.266	-2.402	2.06E-10	2.79E-10
ENSMUSG00000044734	Serpinb1a	-1.095	-2.409	3.43E-02	7.84E-05
ENSMUSG00000022123	Scel	-2.330	-2.410	1.19E-02	1.44E-02
ENSMUSG00000022367	Has2	-1.828	-2.414	5.70E-11	3.37E-11
ENSMUSG00000039891	Txlnb	-1.637	-2.422	2.53E-05	1.73E-06
ENSMUSG00000031451	Gas6	-1.241	-2.442	6.27E-06	6.21E-14
ENSMUSG00000071847	Apcdd1	-2.043	-2.446	3.44E-07	3.20E-06
ENSMUSG00000031778	Cx3cl1	-2.415	-2.453	0.00E+00	1.77E-09
ENSMUSG00000037010	Apln	-1.863	-2.462	4.55E-06	5.86E-06
ENSMUSG00000039114	Nrn1	-2.104	-2.508	0.00E+00	0.00E+00
ENSMUSG00000047250	Ptgs1	-2.008	-2.536	0.00E+00	0.00E+00
ENSMUSG00000001768	Rin2	-2.061	-2.551	7.58E-07	5.41E-08
ENSMUSG00000039621	Prex1	-1.265	-2.566	2.14E-02	1.66E-03
ENSMUSG00000035095	Fam167a	-1.450	-2.595	8.99E-04	1.43E-06
ENSMUSG00000053093	Myh7	-1.075	-2.616	9.32E-03	5.45E-09
ENSMUSG00000026673	Sh2d1b1	-4.885	-2.626	2.13E-02	2.27E-02
ENSMUSG00000051985	Igfn1	-1.431	-2.657	9.44E-04	4.11E-06
ENSMUSG00000002289	Angptl4	-2.053	-2.667	1.90E-03	1.20E-05
ENSMUSG00000070469	Adamtsl3	-1.315	-2.703	3.43E-03	3.26E-05
ENSMUSG00000080741	Gm11398	-3.298	-2.707	8.94E-03	3.56E-02
ENSMUSG00000014453	Blk	-1.868	-2.726	8.11E-03	1.53E-03
ENSMUSG00000004939	Itgb1bp3	-1.420	-2.751	3.22E-03	6.88E-06
ENSMUSG00000057604	Lmcd1	-2.327	-2.752	5.61E-03	5.17E-03
ENSMUSG00000007877	Tcap	-1.442	-2.754	2.67E-03	6.79E-06
ENSMUSG00000027200	Sema6d	-2.107	-2.768	0.00E+00	0.00E+00
ENSMUSG00000019990	Pde7b	-2.393	-2.768	1.23E-12	9.28E-06
ENSMUSG00000056328	Myh1	-1.372	-2.772	0.00E+00	0.00E+00
ENSMUSG00000051339	2900026A02Rik	-1.372	-2.816	5.29E-04	9.80E-08
ENSMUSG00000038530	Rgs4	-1.962	-2.833	1.57E-07	1.09E-07
ENSMUSG00000022265	Ank	-2.570	-2.880	0.00E+00	0.00E+00
ENSMUSG00000030000	Add2	-2.468	-2.893	4.74E-08	6.17E-07
ENSMUSG00000085479	9430073C21Rik	-1.779	-2.955	4.03E-02	1.35E-02
ENSMUSG00000031785	Gpr56	-2.032	-2.969	1.61E-07	2.14E-08
ENSMUSG00000041482	Fam38b	-1.502	-2.975	7.89E-13	0.00E+00
ENSMUSG00000003665	Has1	-2.901	-2.982	2.72E-02	2.72E-02
ENSMUSG00000007122	Casq1	-1.539	-2.986	1.06E-03	1.03E-07
ENSMUSG00000026639	Lamb3	-2.860	-2.990	5.40E-10	1.05E-07
ENSMUSG00000001020	S100a4	-1.599	-2.991	0.00E+00	0.00E+00
ENSMUSG00000042793	Lgr6	-3.086	-3.069	1.48E-04	1.05E-04
ENSMUSG00000016179	Camk1g	-1.235	-3.075	4.28E-09	0.00E+00
ENSMUSG00000038580	Sct	-1.922	-3.099	0.00E+00	0.00E+00
ENSMUSG00000032968	Inha	-1.705	-3.107	4.14E-02	4.85E-03

ENSMUSG00000071540	3425401B19Rik	-3.385	-3.143	7.33E-04	1.09E-03
ENSMUSG00000041836	Ptpre	-1.199	-3.205	2.84E-02	1.36E-06
ENSMUSG00000006221	Hspb7	-2.101	-3.216	1.85E-06	7.66E-08
ENSMUSG00000030218	Mgp	-1.192	-3.226	1.92E-02	2.72E-07
ENSMUSG00000004655	Aqp1	-2.027	-3.270	2.38E-06	2.69E-08
ENSMUSG00000037217	Syn1	-2.036	-3.335	0.00E+00	3.16E-12
ENSMUSG00000025582	Nptx1	-2.796	-3.409	9.36E-09	8.16E-08
ENSMUSG00000022296	Baalc	-1.677	-3.418	9.01E-03	3.97E-08
ENSMUSG00000031375	Bgn	-1.213	-3.440	8.09E-10	0.00E+00
ENSMUSG00000021622	Ckmt2	-2.915	-3.442	4.35E-08	2.59E-07
ENSMUSG00000002020	Ltbp2	-1.597	-3.447	1.37E-03	1.90E-04
ENSMUSG00000004371	Il11	-3.974	-3.473	1.12E-07	3.45E-08
ENSMUSG00000018893	Mb	-2.445	-3.730	0.00E+00	0.00E+00
ENSMUSG00000027794	Sohlh2	-3.197	-3.862	9.93E-03	1.06E-02
ENSMUSG00000060284	Sp7	-2.337	-3.988	1.10E-02	2.26E-05
ENSMUSG00000051159	Cited1	-2.122	-4.068	1.29E-04	8.30E-07
ENSMUSG00000026678	Rgs5	-3.052	-4.077	0.00E+00	0.00E+00
ENSMUSG00000024471	Myot	-3.022	-4.078	2.89E-07	5.15E-06
ENSMUSG00000020123	Avpr1a	-1.472	-4.137	3.74E-02	2.56E-04
ENSMUSG00000043165	Lor	-2.792	-4.195	3.51E-03	3.77E-03
ENSMUSG00000001494	Sost	-2.651	-4.317	2.52E-03	2.57E-03
ENSMUSG00000078202	Nrarp	-2.800	-4.465	1.06E-03	1.53E-03
ENSMUSG00000076490	Trbc1	-3.852	-4.786	7.61E-10	2.39E-09
ENSMUSG00000022076	Klhl1	-5.834	-4.915	2.55E-03	2.52E-04
ENSMUSG00000027368	Dusp2	-2.630	-4.954	1.03E-08	7.31E-09
ENSMUSG00000042379	Esm1	-4.703	-4.977	0.00E+00	0.00E+00
ENSMUSG00000041261	Car8	-3.068	-5.198	0.00E+00	0.00E+00
ENSMUSG00000036295	Lrrn3	-3.672	-5.274	0.00E+00	1.22E-13
ENSMUSG00000076498	Trbc2	-3.547	-5.567	0.00E+00	0.00E+00
ENSMUSG00000056270	Prr9	-4.177	-6.257	4.84E-06	9.25E-04
ENSMUSG00000023886	Smoc2	-6.195	-7.733	0.00E+00	3.43E-12
ENSMUSG00000042045	Sln	-15.000	-15.000	2.80E-03	1.72E-02

Table S6. Pax7B Regulated Changes in Gene Expression

Gene ID	Gene Symbol	Fold Change (log2) Pax7b	Fold Change (log2) Pax7d	q-value (Pax7b)	q-value (Pax7d)
ENSMUSG00000028358	Zfp618	4.982	1.441	9.61E-03	8.55E-02
ENSMUSG00000013415	Igf2bp1	4.349	2.629	6.56E-07	1.00E+00
ENSMUSG00000085410	2010110K18Rik	4.024	1.440	1.39E-02	1.00E+00
ENSMUSG00000018387	Shroom1	3.844	0.711	4.41E-04	1.00E+00
ENSMUSG00000025432	Avil	3.758	-1.105	3.92E-02	1.00E+00
ENSMUSG00000028644	Ermap	3.131	2.413	8.91E-03	5.29E-02
ENSMUSG00000028167	Bdh2	3.092	2.298	1.12E-02	1.44E-01
ENSMUSG00000023032	Slc4a8	2.902	1.935	1.10E-02	5.09E-01
ENSMUSG00000031340	Gabre	2.901	0.308	4.73E-02	1.00E+00
ENSMUSG00000032698	Lmo2	2.713	1.626	9.64E-03	4.33E-01
ENSMUSG00000047735	Samd9l	2.678	2.283	2.83E-02	1.38E-01
ENSMUSG00000021200	Asb2	2.619	0.648	3.27E-03	1.00E+00
ENSMUSG00000047115	D330028D13Rik	2.579	1.286	1.04E-02	4.01E-01
ENSMUSG00000002980	Bcam	2.560	1.071	1.85E-03	6.38E-01
ENSMUSG00000022935	Grik1	2.547	1.980	6.16E-03	8.18E-02
ENSMUSG00000056552	Zfp953	2.490	1.430	6.30E-04	1.25E-01
ENSMUSG00000039070	Cpa4	2.388	1.115	1.01E-02	1.00E+00
ENSMUSG00000030827	Fgf21	2.285	1.378	9.00E-07	1.03E-01
ENSMUSG00000025993	Slc40a1	2.218	1.327	4.92E-06	1.42E-01
ENSMUSG00000087142	Gm12454	2.134	0.538	2.30E-02	9.07E-01
ENSMUSG00000027562	Car2	2.089	0.366	2.82E-04	9.40E-01
ENSMUSG00000017969	Ptgis	2.062	0.899	3.94E-06	4.53E-01
ENSMUSG00000082160	Gm11578	2.024	0.673	3.04E-02	8.63E-01
ENSMUSG00000021182	Ccdc88c	1.968	0.928	1.46E-05	1.00E+00
ENSMUSG00000024663	Rab3il1	1.902	1.457	4.48E-03	1.06E-01
ENSMUSG00000080058	Gm11175	1.900	1.996	2.84E-02	5.65E-02
ENSMUSG00000037341	Slc9a7	1.884	1.546	1.28E-03	5.81E-02
ENSMUSG00000032425	Zfp949	1.816	1.465	4.84E-02	1.71E-01
ENSMUSG00000028445	Enho	1.767	1.157	4.89E-06	8.10E-02
ENSMUSG00000028328	Tmod1	1.762	0.553	1.12E-03	7.81E-01
ENSMUSG00000069874	Irgm2	1.761	1.742	1.36E-02	6.35E-02
ENSMUSG00000035934	Pknox2	1.758	0.244	1.12E-07	9.17E-01
ENSMUSG00000029757	Dync1i1	1.744	0.464	1.81E-05	8.54E-01
ENSMUSG00000028497	Ptplad2	1.712	0.736	1.64E-02	7.10E-01
ENSMUSG00000027371	Fahd2a	1.686	1.395	9.64E-03	6.16E-02
ENSMUSG00000001802	Lrp3	1.672	1.538	2.42E-02	5.21E-02
ENSMUSG00000068742	Cry2	1.655	1.414	1.66E-02	7.96E-02
ENSMUSG00000055435	Maf	1.653	0.592	7.15E-05	6.49E-01
ENSMUSG00000026814	Eng	1.584	0.775	2.78E-03	4.96E-01
ENSMUSG00000032579	Hemk1	1.575	1.099	1.65E-03	1.01E-01
ENSMUSG00000042766	Trim46	1.571	0.814	3.33E-02	3.61E-01
ENSMUSG00000038463	Olfml2b	1.570	0.648	1.04E-05	5.04E-01
ENSMUSG00000057751	Megf6	1.529	0.192	4.96E-02	9.75E-01
ENSMUSG00000002109	Ddb2	1.495	1.122	2.25E-02	2.08E-01
ENSMUSG00000029380	Cxcl1	1.476	1.530	3.55E-02	1.00E-01
ENSMUSG00000056698	Elmod3	1.436	0.573	2.29E-02	7.44E-01
ENSMUSG00000005357	Slc1a6	1.398	0.834	1.10E-02	5.22E-01
ENSMUSG00000044548	Dact1	1.391	0.745	4.63E-03	5.62E-01
ENSMUSG00000020653	Klf11	1.381	1.379	1.02E-02	6.49E-02
ENSMUSG00000035266	Helq	1.379	0.958	3.93E-03	1.01E-01
ENSMUSG00000022358	Fbxo32	1.323	0.773	4.56E-06	1.30E-01

ENSMUSG00000001053	N4bp3	1.316	1.173	7.89E-03	9.53E-02
ENSMUSG00000039485	Tspyl4	1.313	1.292	1.30E-02	8.95E-02
ENSMUSG00000007682	Dio2	1.293	0.088	3.68E-06	9.77E-01
ENSMUSG00000047786	Lix1	1.286	0.240	5.58E-06	9.03E-01
ENSMUSG00000091592	Gm17460	1.283	0.948	2.25E-02	3.63E-01
ENSMUSG00000045211	Nudt18	1.270	1.138	3.52E-02	2.31E-01
ENSMUSG00000090053	Palm2	1.267	1.380	3.38E-02	6.12E-02
ENSMUSG00000032348	Gsta4	1.262	0.225	4.56E-05	9.23E-01
ENSMUSG00000068015	Lrch1	1.257	0.465	6.02E-04	6.76E-01
ENSMUSG00000032507	Fbxl2	1.246	0.492	5.13E-03	6.69E-01
ENSMUSG00000062040	Zfp27	1.245	0.634	4.89E-04	2.49E-01
ENSMUSG00000028019	Pdgfc	1.243	0.795	1.65E-06	5.81E-02
ENSMUSG00000044456	Rin3	1.236	-0.043	2.65E-03	9.97E-01
ENSMUSG00000022206	Npr3	1.235	0.562	3.94E-06	3.44E-01
ENSMUSG00000017897	Eya2	1.221	-0.308	2.10E-02	9.13E-01
ENSMUSG00000021094	Dhrs7	1.220	1.115	8.91E-03	1.14E-01
ENSMUSG00000003812	Dnase2a	1.214	0.570	5.22E-03	4.62E-01
ENSMUSG00000028654	Mycl1	1.211	0.429	1.42E-05	6.33E-01
ENSMUSG00000021226	Acot2	1.201	0.991	1.57E-02	2.38E-01
ENSMUSG00000022244	Amacr	1.197	0.650	3.67E-03	5.26E-01
ENSMUSG00000020182	Ddc	1.183	0.353	3.43E-02	9.05E-01
ENSMUSG00000035172	Plekhh3	1.181	1.079	2.35E-02	9.70E-02
ENSMUSG00000056091	St3gal5	1.177	0.228	5.41E-04	9.31E-01
ENSMUSG00000045404	Kcnk13	1.176	-0.573	3.63E-02	8.14E-01
ENSMUSG00000022661	Cd200	1.164	0.288	3.87E-08	6.52E-01
ENSMUSG00000024978	Gpam	1.147	0.490	3.68E-08	3.19E-01
ENSMUSG00000075297	H60b	1.147	0.561	1.90E-02	7.13E-01
ENSMUSG00000047443	Fam132b	1.135	0.559	2.90E-02	7.44E-01
ENSMUSG00000021373	Cap2	1.128	0.524	5.16E-10	1.36E-01
ENSMUSG00000031023	D930014E17Rik	1.127	1.143	2.85E-02	6.70E-02
ENSMUSG00000019944	Rhobtb1	1.120	0.192	4.78E-04	9.35E-01
ENSMUSG00000022090	Pdlim2	1.098	0.740	3.03E-04	1.31E-01
ENSMUSG00000039232	Stx11	1.088	0.998	1.13E-02	1.04E-01
ENSMUSG00000039985	Fam60a	1.087	0.487	3.67E-02	6.57E-01
ENSMUSG00000043415	Otud1	1.080	0.668	1.29E-02	4.98E-01
ENSMUSG00000037060	Prkcdbp	1.078	1.069	3.42E-02	1.49E-01
ENSMUSG00000031792	AA960436	1.054	0.745	1.51E-03	1.75E-01
ENSMUSG00000031133	Arhgef6	1.053	0.452	5.08E-03	6.66E-01
ENSMUSG00000016128	Stard13	1.047	0.338	2.13E-03	7.68E-01
ENSMUSG00000051855	Mest	1.044	0.090	2.14E-09	9.57E-01
ENSMUSG00000021271	Zfp839	1.044	0.979	4.96E-02	2.21E-01
ENSMUSG00000044033	Ccdc141	1.039	0.433	2.30E-05	4.78E-01
ENSMUSG00000030157	Clec2d	1.036	1.151	4.03E-02	8.91E-02
ENSMUSG00000037306	Man1c1	1.035	0.544	7.15E-05	2.58E-01
ENSMUSG00000038132	Rbm24	1.033	0.093	4.97E-04	9.75E-01
ENSMUSG00000036820	Amdhd2	1.033	0.533	3.91E-02	6.27E-01
ENSMUSG00000004896	Rrnad1	1.027	0.568	6.44E-03	3.47E-01
ENSMUSG00000042997	Nhlrc3	1.018	0.966	2.36E-02	1.14E-01
ENSMUSG00000021759	Ppap2a	1.011	0.584	1.72E-04	2.66E-01
ENSMUSG00000026004	1110028C15Rik	0.988	0.507	4.55E-07	1.61E-01
ENSMUSG00000021806	Nid2	0.986	-0.268	2.36E-03	8.95E-01
ENSMUSG00000028399	Ptprd	0.980	0.707	9.34E-03	1.56E-01
ENSMUSG00000039883	Lrrc17	0.978	0.518	1.84E-03	4.67E-01
ENSMUSG00000041120	Nbl1	0.977	0.722	5.76E-05	5.96E-02

ENSMUSG00000002043	Trappc6a	0.974	0.717	3.44E-02	3.06E-01
ENSMUSG00000019841	Rev3l	0.974	0.618	1.89E-02	3.19E-01
ENSMUSG00000057147	Atpbd4	0.958	0.529	6.20E-04	1.88E-01
ENSMUSG00000031431	Tsc22d3	0.957	0.619	1.06E-06	5.03E-02
ENSMUSG00000033763	Mtss1l	0.954	0.488	3.45E-04	3.34E-01
ENSMUSG00000026594	Ralgps2	0.948	-0.049	1.39E-02	9.93E-01
ENSMUSG00000025920	Stau2	0.948	0.742	6.85E-03	9.48E-02
ENSMUSG00000001334	Fndc5	0.945	-0.261	9.32E-03	9.16E-01
ENSMUSG00000030203	Dusp16	0.943	0.839	2.62E-02	7.60E-02
ENSMUSG00000032503	Arpp21	0.940	-0.172	5.66E-05	9.16E-01
ENSMUSG00000040859	Bsdc1	0.932	0.748	4.24E-02	2.29E-01
ENSMUSG00000026459	Myog	0.926	-0.222	2.38E-03	9.03E-01
ENSMUSG00000038305	Spats2l	0.918	0.151	3.91E-02	9.71E-01
ENSMUSG00000014773	Dll1	0.918	0.121	7.52E-04	9.64E-01
ENSMUSG00000029676	Pot1a	0.914	0.618	6.75E-03	2.04E-01
ENSMUSG00000026463	Atp2b4	0.913	0.108	9.37E-04	9.64E-01
ENSMUSG00000046743	Fat4	0.912	0.900	1.92E-02	1.05E-01
ENSMUSG00000038046	Rnmtl1	0.900	0.055	3.60E-02	9.93E-01
ENSMUSG00000021235	Coq6	0.890	0.235	1.81E-02	9.03E-01
ENSMUSG00000031770	Herpud1	0.887	0.585	7.24E-06	5.83E-02
ENSMUSG00000022708	Zbtb20	0.884	0.646	2.29E-02	2.19E-01
ENSMUSG00000015202	Cnksr3	0.884	0.674	3.04E-02	3.70E-01
ENSMUSG00000043671	Dpy19l3	0.879	0.600	1.92E-02	3.12E-01
ENSMUSG00000013997	Nit1	0.871	0.406	5.01E-03	5.97E-01
ENSMUSG00000034858	BC031353	0.864	0.656	2.78E-03	1.95E-01
ENSMUSG00000020647	Ncoa1	0.860	0.062	1.47E-03	9.81E-01
ENSMUSG00000045414	1190002N15Rik	0.859	-0.027	3.68E-03	9.97E-01
ENSMUSG00000023904	Hcfc1r1	0.857	0.639	1.77E-02	3.24E-01
ENSMUSG00000026142	Rhbdd1	0.850	0.910	1.51E-02	5.19E-02
ENSMUSG00000052139	Bre	0.846	0.594	3.93E-03	1.89E-01
ENSMUSG00000029469	Ift81	0.845	0.685	8.94E-03	1.82E-01
ENSMUSG00000058756	Thra	0.837	0.798	3.81E-02	1.01E-01
ENSMUSG00000024420	Zfp521	0.823	0.286	6.90E-03	8.24E-01
ENSMUSG00000061436	Hipk2	0.821	0.712	6.59E-03	6.10E-02
ENSMUSG00000060429	Sntb1	0.821	-0.469	2.84E-02	6.69E-01
ENSMUSG00000044646	Zbtb7c	0.818	0.631	2.64E-02	3.64E-01
ENSMUSG00000032436	Cmtm7	0.805	0.665	2.62E-02	2.60E-01
ENSMUSG00000003824	Syce2	0.804	0.180	3.03E-02	9.48E-01
ENSMUSG00000022591	Gm9747	0.804	0.749	3.40E-02	1.83E-01
ENSMUSG00000030681	Mvp	0.792	0.688	4.42E-02	3.61E-01
ENSMUSG00000032380	Dapk2	0.784	-0.294	1.98E-03	7.62E-01
ENSMUSG00000050315	Synpo2	0.782	0.056	4.60E-03	9.86E-01
ENSMUSG00000032531	Amotl2	0.776	0.369	6.56E-07	2.12E-01
ENSMUSG00000071477	Zfp777	0.774	0.625	4.30E-02	2.43E-01
ENSMUSG00000007867	1700019E19Rik	0.771	0.737	1.62E-02	9.83E-02
ENSMUSG00000074221	Zfp568	0.534	-0.074	1.78E-02	9.71E-01
ENSMUSG00000063275	Ptpla	0.528	0.099	3.52E-02	9.64E-01
ENSMUSG00000025485	Ric8	0.523	0.455	2.61E-02	1.90E-01
ENSMUSG00000041028	Ghitm	0.517	0.497	8.82E-03	6.77E-02
ENSMUSG00000090262	Mpv17	0.514	0.507	2.19E-02	6.01E-02
ENSMUSG00000043384	Gprasp1	0.509	0.491	1.33E-02	1.29E-01
ENSMUSG00000034354	Mtmr3	0.501	0.362	4.83E-03	1.74E-01
ENSMUSG00000026253	Chrng	0.486	-0.248	2.22E-02	6.95E-01
ENSMUSG00000058056	Palld	0.484	0.153	1.42E-02	8.68E-01

ENSMUSG00000027253	Lrp4	0.477	-0.181	3.05E-02	8.67E-01
ENSMUSG00000051747	Ttn	0.476	0.011	2.03E-02	9.99E-01
ENSMUSG00000020078	Vps26a	0.466	0.432	3.40E-02	1.72E-01
ENSMUSG00000040785	Ttc3	0.464	0.248	1.71E-03	4.01E-01
ENSMUSG00000046062	Ppp1r15b	0.455	0.355	2.40E-02	3.68E-01
ENSMUSG00000022191	Drosha	0.439	0.197	1.87E-02	6.63E-01
ENSMUSG00000032366	Tpm1	0.401	-0.072	3.27E-06	8.92E-01
ENSMUSG00000025283	Sat1	0.399	0.292	1.32E-02	2.94E-01
ENSMUSG00000018567	Gabarap	0.389	0.436	4.94E-02	9.09E-02
ENSMUSG00000026150	Mff	0.377	0.316	2.36E-02	2.20E-01
ENSMUSG00000022952	Runx1	0.338	0.107	1.05E-02	8.55E-01
ENSMUSG00000021910	Nisch	0.246	0.073	3.04E-02	9.13E-01
ENSMUSG00000054808	Actn4	-0.284	-0.183	2.51E-02	4.62E-01
ENSMUSG00000006498	Ptbp1	-0.314	0.080	4.66E-02	9.28E-01
ENSMUSG00000028693	Nasp	-0.314	-0.350	4.73E-02	9.32E-02
ENSMUSG00000078812	Eif5a	-0.324	-0.197	1.02E-02	4.36E-01
ENSMUSG00000021585	Cast	-0.335	0.095	1.22E-02	9.03E-01
ENSMUSG00000066551	Hmgb1	-0.366	-0.259	2.14E-02	3.35E-01
ENSMUSG00000020330	Hmmr	-0.387	-0.378	4.71E-02	1.69E-01
ENSMUSG00000059495	Arhgef12	-0.390	-0.358	3.63E-02	1.85E-01
ENSMUSG00000028410	Dnaja1	-0.410	-0.332	3.19E-02	2.56E-01
ENSMUSG00000018339	Gpx3	-0.454	-0.071	4.71E-02	9.71E-01
ENSMUSG00000018362	Kpna2	-0.455	-0.284	3.39E-03	3.32E-01
ENSMUSG00000022673	Mcm4	-0.459	-0.410	2.25E-02	1.67E-01
ENSMUSG00000025130	P4hb	-0.460	-0.248	3.91E-02	6.38E-01
ENSMUSG00000045962	Wnk1	-0.468	-0.397	1.22E-02	1.23E-01
ENSMUSG00000029177	Cenpa	-0.490	-0.397	7.02E-03	1.42E-01
ENSMUSG00000067367	Lyar	-0.491	-0.132	2.36E-02	9.13E-01
ENSMUSG00000039231	Suv39h1	-0.523	-0.472	1.51E-02	9.44E-02
ENSMUSG00000024953	Prdx5	-0.524	-0.524	1.10E-02	8.43E-02
ENSMUSG00000020534	Shmt1	-0.535	-0.363	4.11E-02	4.52E-01
ENSMUSG00000047534	Mis18bp1	-0.545	-0.435	4.73E-02	2.83E-01
ENSMUSG00000024659	Anxa1	-0.550	0.096	1.48E-03	9.40E-01
ENSMUSG00000015217	Hmgb3	-0.556	-0.619	3.88E-02	7.66E-02
ENSMUSG00000021782	Dlg5	-0.561	-0.376	2.02E-03	2.01E-01
ENSMUSG00000026683	Nuf2	-0.571	-0.639	3.44E-02	6.31E-02
ENSMUSG00000059981	Taok2	-0.582	-0.420	4.96E-02	5.24E-01
ENSMUSG00000028044	Cks1b	-0.585	-0.323	4.10E-02	6.63E-01
ENSMUSG00000027889	Ampd2	-0.589	-0.532	2.51E-02	1.60E-01
ENSMUSG00000028207	Asph	-0.590	-0.436	1.45E-04	6.66E-02
ENSMUSG00000027422	Rrbp1	-0.599	-0.267	1.42E-03	5.59E-01
ENSMUSG00000042489	Clspn	-0.600	-0.464	4.94E-02	3.50E-01
ENSMUSG00000017724	Etv4	-0.600	-0.128	3.61E-02	9.33E-01
ENSMUSG00000023106	Denr	-0.604	-0.306	2.14E-02	6.61E-01
ENSMUSG00000032254	Kif23	-0.611	-0.550	4.64E-03	7.69E-02
ENSMUSG00000005514	Por	-0.618	-0.477	2.14E-02	2.52E-01
ENSMUSG00000042626	Shc1	-0.623	-0.460	8.87E-04	9.32E-02
ENSMUSG00000036093	Arl5a	-0.626	-0.512	4.96E-02	3.69E-01
ENSMUSG00000032193	Ldlr	-0.638	-0.699	3.45E-02	1.67E-01
ENSMUSG00000025747	Tyms	-0.650	-0.656	1.64E-02	8.32E-02
ENSMUSG00000056737	Capg	-0.651	-0.153	2.72E-03	9.00E-01
ENSMUSG00000015053	Gata2	-0.655	-0.500	6.95E-03	1.84E-01
ENSMUSG00000041936	Agrn	-0.675	-0.569	2.69E-03	9.08E-02
ENSMUSG00000027469	Tpx2	-0.679	-0.124	1.64E-03	9.38E-01

ENSMUSG00000025823	Pdia4	-0.681	-0.750	4.94E-02	9.38E-02
ENSMUSG00000039202	Abhd2	-0.690	-0.618	3.45E-02	2.13E-01
ENSMUSG00000022797	Tfrc	-0.691	-1.174	2.95E-02	1.39E-01
ENSMUSG00000021360	Gcnt2	-0.693	-0.445	3.44E-02	5.01E-01
ENSMUSG00000016756	Cmah	-0.696	-0.407	1.30E-02	6.27E-01
ENSMUSG00000002900	Lamb1	-0.697	-0.419	4.49E-04	2.19E-01
ENSMUSG00000009418	Nav1	-0.704	-0.459	7.65E-04	1.19E-01
ENSMUSG00000027306	Nusap1	-0.708	-0.650	4.64E-02	2.27E-01
ENSMUSG00000030208	Emp1	-0.712	-0.294	3.44E-02	8.01E-01
ENSMUSG00000046711	Hmga1	-0.712	-0.127	7.27E-05	9.17E-01
ENSMUSG00000033487	Fndc3a	-0.715	-0.317	1.23E-03	5.41E-01
ENSMUSG00000035107	Dcbld2	-0.716	-0.261	1.92E-02	8.11E-01
ENSMUSG00000025511	Tspan4	-0.718	-0.590	1.95E-03	9.12E-02
ENSMUSG00000084274	Gm12504	-0.720	-0.620	3.86E-02	2.52E-01
ENSMUSG00000024691	Fam111a	-0.720	-0.083	2.15E-02	9.75E-01
ENSMUSG00000047414	Flrt2	-0.728	-0.318	5.13E-03	6.22E-01
ENSMUSG00000001517	Foxm1	-0.734	-0.721	1.51E-02	5.38E-02
ENSMUSG00000018547	Pip4k2b	-0.736	-0.443	3.71E-02	5.80E-01
ENSMUSG00000072082	Ccnf	-0.740	-0.544	1.09E-02	3.11E-01
ENSMUSG00000046668	Cxxc5	-0.742	-0.835	3.07E-02	6.12E-02
ENSMUSG00000001482	Def8	-0.755	-0.267	2.68E-02	8.49E-01
ENSMUSG00000026204	Ptprn	-0.777	-0.440	3.00E-03	4.27E-01
ENSMUSG00000034612	Chst11	-0.801	-0.695	1.88E-02	1.81E-01
ENSMUSG00000028412	Slc44a1	-0.815	-0.715	2.36E-02	2.02E-01
ENSMUSG00000039942	Ptger4	-0.832	-0.561	3.74E-04	2.12E-01
ENSMUSG00000020042	Btbd11	-0.839	-0.722	1.31E-02	6.49E-02
ENSMUSG00000001507	Itga3	-0.845	-0.472	6.11E-03	3.73E-01
ENSMUSG00000030748	Il4ra	-0.854	-0.796	5.24E-03	6.98E-02
ENSMUSG00000032643	Fhl3	-0.865	-0.714	8.42E-03	1.29E-01
ENSMUSG00000078249	Hmga1-rs1	-0.868	-0.200	1.42E-02	9.27E-01
ENSMUSG00000001985	Grik3	-0.909	-0.678	1.84E-05	8.66E-02
ENSMUSG00000040752	Myh6	-0.914	-1.368	4.89E-02	2.57E-01
ENSMUSG00000046447	Camk2n1	-0.929	-0.850	3.31E-02	1.96E-01
ENSMUSG00000022157	Mcpt8	-0.937	-0.449	4.52E-03	5.91E-01
ENSMUSG00000053702	Nebl	-0.942	0.212	1.72E-02	9.14E-01
ENSMUSG00000038648	Creb3l2	-0.942	-0.648	4.20E-03	2.49E-01
ENSMUSG00000032012	Pvrl1	-0.954	-0.636	3.10E-02	4.56E-01
ENSMUSG00000070348	Ccnd1	-0.955	-0.582	6.19E-06	8.66E-02
ENSMUSG00000026827	Gpd2	-0.971	-0.244	4.14E-02	9.17E-01
ENSMUSG00000044447	Dock5	-0.974	-0.732	4.51E-03	1.89E-01
ENSMUSG00000040189	Ccdc114	-0.990	-0.701	2.63E-02	2.85E-01
ENSMUSG00000051341	Zfp52	-0.993	-0.750	3.14E-03	1.65E-01
ENSMUSG00000021065	Fut8	-0.996	-0.852	8.84E-04	7.18E-02
ENSMUSG00000031827	Cotl1	-1.002	-0.876	1.03E-02	1.35E-01
ENSMUSG00000001131	Timp1	-1.003	-0.509	5.30E-09	5.08E-02
ENSMUSG00000024952	Rps6ka4	-1.012	-0.632	1.76E-06	2.00E-01
ENSMUSG00000052397	Ezr	-1.017	-0.795	4.98E-04	7.48E-02
ENSMUSG00000001542	Ell2	-1.043	-0.788	4.80E-04	8.43E-02
ENSMUSG00000074934	Grem1	-1.063	0.209	4.66E-03	9.29E-01
ENSMUSG00000005397	Nid1	-1.072	-0.527	3.51E-04	4.07E-01
ENSMUSG00000041912	Tdrkh	-1.074	-0.712	1.38E-02	4.99E-01
ENSMUSG00000046733	Gprc5a	-1.091	-0.291	1.45E-03	8.59E-01
ENSMUSG00000031561	Odz3	-1.236	-0.709	2.44E-02	3.80E-01
ENSMUSG00000048450	Msx1	-1.263	-1.253	4.85E-02	1.69E-01

ENSMUSG00000010751	Tnfrsf22	-1.317	-0.303	3.34E-02	9.11E-01
ENSMUSG00000050069	Grem2	-1.318	-1.017	3.18E-03	1.43E-01
ENSMUSG00000029377	Ereg	-1.319	-0.193	1.81E-03	9.51E-01
ENSMUSG00000029804	Herc3	-1.372	-1.215	3.50E-02	8.13E-02
ENSMUSG00000023243	Kcnk5	-1.390	-0.723	2.42E-02	6.27E-01
ENSMUSG00000026235	Epha4	-1.449	-1.138	1.57E-02	2.20E-01
ENSMUSG00000045027	Prss22	-1.454	-1.128	1.82E-02	2.53E-01
ENSMUSG00000022382	Wnt7b	-1.460	-1.377	2.83E-03	6.65E-02
ENSMUSG00000031927	1700012B09Rik	-1.506	-1.188	6.15E-04	6.70E-02
ENSMUSG00000085183	Gm12603	-1.519	-0.131	2.05E-03	9.75E-01
ENSMUSG00000027419	Pcsk2	-1.629	0.055	7.90E-05	9.92E-01
ENSMUSG00000028289	Epha7	-1.729	-1.586	3.68E-02	1.27E-01
ENSMUSG00000079514	Gm16309	-1.746	-1.763	4.28E-02	1.10E-01
ENSMUSG00000024654	Asrgl1	-1.759	-1.282	4.86E-03	3.45E-01
ENSMUSG00000036192	Rorb	-1.770	-1.367	7.92E-04	5.08E-02
ENSMUSG00000039997	Ifi203	-1.775	-0.550	6.11E-03	5.99E-01
ENSMUSG00000029097	2310079F23Rik	-1.810	-0.666	9.34E-03	7.38E-01
ENSMUSG00000050505	Pcdh20	-1.834	-1.126	1.28E-03	2.38E-01
ENSMUSG00000045103	Dmd	-1.873	-1.369	3.05E-02	8.55E-02
ENSMUSG00000007035	Msh5	-1.914	-1.164	2.61E-02	5.60E-01
ENSMUSG00000022231	Sema5a	-1.921	-1.201	3.82E-03	1.78E-01
ENSMUSG00000083012	2810453I06Rik	-1.936	-1.193	6.93E-03	2.33E-01
ENSMUSG00000026826	Nr4a2	-1.939	-1.272	6.40E-05	5.42E-02
ENSMUSG00000090222	Gm16340	-1.955	-1.340	2.47E-03	1.71E-01
ENSMUSG00000090272	Mndal	-2.104	-1.326	2.72E-05	7.84E-02
ENSMUSG00000041771	Slc24a4	-2.335	-4.775	4.32E-02	1.29E-01
ENSMUSG00000022054	Nefm	-2.438	-0.640	1.70E-03	7.47E-01
ENSMUSG00000021750	Fam107a	-2.676	-1.847	3.39E-03	7.02E-01
ENSMUSG00000032281	Acsbg1	-2.842	-1.711	3.25E-04	8.14E-01
ENSMUSG00000058252	1700008I05Rik	-3.300	-1.796	6.81E-03	9.40E-02
ENSMUSG00000019590	Cyb561	-3.316	-1.522	6.80E-03	1.67E-01
ENSMUSG00000036661	Dennd3	-3.488	-0.773	8.33E-03	9.39E-01
ENSMUSG00000041193	Pla2g5	-5.046	-15.000	1.82E-03	1.90E-01

Table S7. Pax7D Regulated Changes in Gene Expression

Gene ID	Gene Symbol	Fold Change (log2) Pax7b	Fold Change (log2) Pax7d	q-value (Pax7b)	q-value (Pax7d)
ENSMUSG00000001240	Ramp2	22.000	22.000	1.00E+00	2.47E-02
ENSMUSG00000010797	Wnt2	22.000	22.000	1.00E+00	1.61E-04
ENSMUSG00000021348	Prl7d1	22.000	22.000	1.43E-01	3.85E-04
ENSMUSG00000028871	Rspo1	22.000	22.000	2.56E-01	3.23E-02
ENSMUSG00000029287	Tgfbr3	22.000	22.000	1.00E+00	1.46E-02
ENSMUSG00000034427	Myo15b	22.000	22.000	1.16E-01	9.43E-04
ENSMUSG00000046159	Chrm3	22.000	22.000	1.00E+00	6.62E-03
ENSMUSG00000054204	Fam150b	0.000	22.000	1.00E+00	8.27E-03
ENSMUSG00000056870	Gulp1	22.000	22.000	7.68E-02	3.11E-03
ENSMUSG00000079269	Gm3676	22.000	22.000	1.00E+00	1.90E-02
ENSMUSG00000084128	Esrp2	22.000	22.000	1.00E+00	3.29E-02
ENSMUSG00000085862	Gm13483	22.000	22.000	1.00E+00	2.88E-02
ENSMUSG00000093629	Gm19357	0.000	22.000	1.00E+00	2.65E-02
ENSMUSG00000039963	Ccdc40	1.742	6.827	1.00E+00	1.08E-03
ENSMUSG00000005089	Slc1a2	-2.168	6.826	1.00E+00	4.20E-04
ENSMUSG00000072568	Fam84b	4.927	6.463	1.00E+00	4.96E-04
ENSMUSG00000036596	Cpz	4.295	6.128	1.00E+00	3.01E-03
ENSMUSG00000041608	Entpd3	-0.027	5.945	1.00E+00	2.18E-03
ENSMUSG00000026069	Il1rl1	1.948	5.858	4.46E-01	1.35E-11
ENSMUSG00000019851	Perp	2.295	5.847	1.00E+00	2.65E-03
ENSMUSG00000048078	Odz4	3.670	4.965	1.00E+00	2.31E-05
ENSMUSG00000000627	Sema4f	1.091	4.418	1.00E+00	1.24E-02
ENSMUSG00000021835	Bmp4	2.445	4.130	4.28E-01	1.01E-02
ENSMUSG00000020399	Havcr2	1.053	3.942	1.00E+00	8.96E-03
ENSMUSG00000014602	Kif1a	2.978	3.893	1.00E+00	7.93E-06
ENSMUSG00000074788	5830416P10Rik	1.296	3.710	2.76E-01	2.29E-08
ENSMUSG00000063767	S100a7a	0.558	3.477	1.00E+00	2.93E-02
ENSMUSG00000028270	Gbp2	3.062	3.461	1.00E+00	3.29E-02
ENSMUSG00000037990	Sh3rf3	3.163	3.414	1.00E+00	1.22E-02
ENSMUSG00000062393	Dgkk	1.748	3.391	1.00E+00	1.96E-09
ENSMUSG00000030790	Adm	2.558	3.366	1.96E-01	3.91E-02
ENSMUSG00000023043	Krt18	0.973	3.352	1.00E+00	4.03E-02
ENSMUSG00000030518	Fam189a1	1.441	3.231	3.52E-01	1.29E-06
ENSMUSG00000020963	Tshr	1.089	3.008	1.00E+00	5.93E-04
ENSMUSG00000028444	Cntfr	1.887	2.976	2.46E-01	1.11E-02
ENSMUSG00000049191	Rgag4	1.268	2.939	1.00E+00	2.09E-03
ENSMUSG00000017754	Pltp	1.605	2.895	9.80E-02	4.47E-05
ENSMUSG00000030849	Fgfr2	0.891	2.887	5.39E-01	8.41E-06
ENSMUSG00000015702	Anxa9	1.966	2.880	3.98E-01	4.30E-02
ENSMUSG00000021696	Elovl7	1.069	2.880	1.00E+00	1.07E-04
ENSMUSG00000030020	Prickle2	1.480	2.870	1.00E+00	1.02E-06
ENSMUSG00000054994	AV320801	1.941	2.853	1.00E+00	2.03E-02
ENSMUSG00000028033	Kcnq5	1.707	2.852	3.58E-01	1.08E-02
ENSMUSG00000034855	Cxcl10	1.492	2.821	1.41E-01	8.12E-05
ENSMUSG00000039145	Camk1d	1.243	2.709	1.00E+00	4.62E-03
ENSMUSG00000034818	Celf5	1.050	2.694	6.45E-01	1.44E-02
ENSMUSG00000020121	Srgap1	1.156	2.679	5.60E-02	8.15E-08
ENSMUSG00000048764	Tmprss11f	0.931	2.677	1.00E+00	1.64E-04
ENSMUSG00000034205	Loxl2	0.997	2.610	1.02E-01	1.03E-08
ENSMUSG00000020120	Plek	1.309	2.597	1.00E+00	3.39E-03
ENSMUSG00000079018	Ly6c1	1.079	2.531	6.09E-01	1.42E-02

ENSMUSG00000026873	Phf19	1.429	2.474	1.00E+00	7.14E-03
ENSMUSG00000041112	Elmo1	1.786	2.455	1.00E+00	9.82E-03
ENSMUSG00000050711	Scg2	-0.142	2.421	1.00E+00	1.48E-03
ENSMUSG00000022055	Nefl	0.978	2.412	1.00E+00	2.86E-03
ENSMUSG00000007655	Cav1	1.222	2.405	3.15E-01	1.22E-03
ENSMUSG00000020689	Itgb3	0.461	2.398	1.00E+00	1.90E-04
ENSMUSG00000047497	Adamts12	1.719	2.371	2.09E-01	2.66E-02
ENSMUSG00000074796	Slc4a11	1.671	2.348	3.24E-01	4.51E-02
ENSMUSG00000032470	Mras	1.708	2.320	1.55E-01	1.31E-02
ENSMUSG00000084141	Olfr1372-ps1	1.892	2.319	1.40E-01	4.55E-02
ENSMUSG00000031709	Tbc1d9	1.162	2.258	2.36E-01	5.01E-04
ENSMUSG00000085128	Gm2115	0.679	2.228	4.04E-01	9.33E-06
ENSMUSG00000041324	Inhba	0.177	2.218	1.00E+00	2.80E-02
ENSMUSG00000060487	Samd5	0.973	2.214	1.00E+00	3.43E-02
ENSMUSG00000053007	Creb5	0.687	2.196	1.00E+00	3.37E-03
ENSMUSG00000038296	Galntl4	0.496	2.186	7.44E-01	4.06E-04
ENSMUSG00000052942	Glis3	0.961	2.184	4.43E-01	1.08E-04
ENSMUSG00000049281	Scn3b	0.773	2.152	2.53E-01	5.24E-08
ENSMUSG00000025185	Loxl4	1.703	2.147	1.00E+00	4.33E-02
ENSMUSG00000079057	Cyp4v3	1.117	2.136	1.96E-01	3.39E-03
ENSMUSG00000001313	Rnd2	1.230	2.129	7.87E-02	6.35E-04
ENSMUSG00000026831	1700007K13Rik	1.714	2.088	1.13E-01	2.41E-02
ENSMUSG00000063727	Tnfrsf11b	-0.474	2.073	1.00E+00	9.33E-03
ENSMUSG00000019894	Slc6a15	0.858	2.050	1.00E+00	1.44E-02
ENSMUSG00000018012	Rac3	1.341	2.041	1.83E-01	1.12E-02
ENSMUSG00000019734	Tmc4	1.362	1.989	3.81E-01	3.83E-02
ENSMUSG00000087494	Gm16728	1.405	1.985	9.59E-02	1.89E-02
ENSMUSG00000018774	Cd68	1.022	1.975	5.73E-01	3.83E-02
ENSMUSG00000020325	Fstl3	1.000	1.953	1.81E-01	1.25E-03
ENSMUSG00000045658	Pid1	0.968	1.950	6.74E-01	1.45E-02
ENSMUSG00000029406	Pitpnm2	0.769	1.920	6.13E-01	1.56E-02
ENSMUSG00000021127	Zfp36l1	1.217	1.910	1.17E-01	8.99E-03
ENSMUSG00000019997	Ctgf	0.468	1.869	7.18E-01	1.83E-03
ENSMUSG00000027217	Tspan18	0.709	1.855	7.86E-01	3.82E-02
ENSMUSG00000028354	Fmn2	1.167	1.821	1.00E+00	7.41E-03
ENSMUSG00000039633	Lonrf1	1.198	1.821	7.08E-02	8.44E-03
ENSMUSG00000027611	Procr	0.911	1.818	4.61E-01	7.68E-03
ENSMUSG00000043969	Emx2	0.640	1.808	7.39E-01	2.36E-02
ENSMUSG00000091586	Cyp4f17	1.335	1.785	6.61E-02	2.63E-02
ENSMUSG00000022361	Zhx1	0.787	1.785	4.06E-01	1.89E-03
ENSMUSG00000042659	Arrdc4	0.551	1.780	8.37E-01	2.76E-02
ENSMUSG00000043391	2510009E07Rik	1.013	1.776	5.84E-02	9.86E-04
ENSMUSG00000028487	Bnc2	0.984	1.768	6.33E-01	3.98E-02
ENSMUSG00000092274	Neat1	0.933	1.766	3.56E-01	1.34E-02
ENSMUSG00000085092	Gm16867	0.815	1.751	5.21E-01	1.53E-02
ENSMUSG00000070327	Rnf213	0.665	1.732	1.33E-01	5.25E-07
ENSMUSG00000045672	Col27a1	0.889	1.721	4.22E-01	5.75E-03
ENSMUSG00000040483	Xaf1	1.226	1.714	2.32E-01	3.29E-02
ENSMUSG00000030554	Synm	0.624	1.702	1.00E+00	1.47E-02
ENSMUSG00000001986	Gria3	1.040	1.692	3.87E-01	2.72E-02
ENSMUSG00000026730	Pter	0.548	1.651	6.71E-01	2.30E-03
ENSMUSG00000031523	Dlc1	0.565	1.632	6.41E-01	1.60E-02
ENSMUSG00000055044	Pdlim1	0.689	1.618	2.12E-01	3.89E-04
ENSMUSG00000038831	Ralgps1	0.803	1.606	1.00E+00	2.80E-02

ENSMUSG00000033577	Myo6	1.341	1.580	1.04E-01	4.48E-02
ENSMUSG00000042810	Krba1	0.593	1.549	7.22E-01	1.89E-02
ENSMUSG00000037999	Arap2	0.393	1.547	8.74E-01	1.15E-02
ENSMUSG00000023868	Pde10a	0.299	1.544	9.04E-01	1.11E-02
ENSMUSG00000005686	Ampd3	0.704	1.529	1.25E-01	5.05E-05
ENSMUSG00000031342	Gpm6b	0.535	1.526	4.07E-01	7.20E-05
ENSMUSG00000032118	Fez1	0.111	1.521	9.74E-01	9.34E-04
ENSMUSG00000046449	C77370	0.808	1.518	1.00E+00	1.42E-02
ENSMUSG00000034910	Pygo1	1.233	1.517	1.00E+00	4.78E-02
ENSMUSG00000040717	Il17rd	1.021	1.455	5.44E-02	1.30E-02
ENSMUSG00000073411	H2-D1	0.624	1.445	4.47E-01	1.70E-03
ENSMUSG00000075118	Gpr137b-ps	0.511	1.438	6.66E-01	3.23E-02
ENSMUSG00000070056	Mfhas1	0.585	1.433	4.08E-01	1.63E-03
ENSMUSG00000058420	Syt17	0.914	1.429	1.76E-01	3.78E-02
ENSMUSG00000040701	Ap1g2	0.429	1.410	8.89E-01	4.64E-02
ENSMUSG00000038301	Snx10	0.611	1.409	3.58E-01	9.06E-04
ENSMUSG00000029119	Man2b2	0.790	1.407	2.14E-01	2.83E-02
ENSMUSG00000028439	2310028H24Rik	1.294	1.406	6.25E-02	4.26E-02
ENSMUSG00000026819	Slc25a25	0.867	1.403	4.53E-01	2.24E-02
ENSMUSG00000035969	Rusc2	0.460	1.382	7.16E-01	2.67E-03
ENSMUSG00000022620	Arsa	0.992	1.376	8.27E-02	1.82E-02
ENSMUSG00000049409	Prokr1	0.589	1.374	4.97E-01	2.24E-02
ENSMUSG00000031387	Renbp	0.953	1.373	1.23E-01	9.33E-03
ENSMUSG00000034744	Nagk	0.803	1.346	5.65E-02	1.44E-04
ENSMUSG00000036461	Elf1	0.542	1.343	1.66E-01	2.36E-04
ENSMUSG00000087141	Plcxd2	0.186	1.335	9.11E-01	3.85E-03
ENSMUSG00000015094	Npdc1	0.527	1.333	2.71E-01	1.12E-05
ENSMUSG00000010358	Ifi35	0.895	1.331	1.23E-01	1.68E-02
ENSMUSG00000073821	8030451A03Rik	-0.095	1.327	9.79E-01	4.22E-02
ENSMUSG00000026104	Stat1	0.721	1.322	3.17E-01	3.77E-02
ENSMUSG00000054855	Rnd1	0.699	1.303	2.68E-01	5.44E-03
ENSMUSG00000027580	BC006779	0.464	1.297	5.32E-01	7.05E-03
ENSMUSG00000002983	Relb	0.867	1.287	6.57E-02	5.19E-03
ENSMUSG00000025277	Abhd6	0.842	1.285	8.36E-02	5.81E-03
ENSMUSG00000034551	Hdx	0.459	1.281	6.65E-01	1.70E-02
ENSMUSG00000018417	Myo1b	0.738	1.277	1.29E-01	7.07E-04
ENSMUSG00000058254	Tspan7	0.788	1.271	1.37E-01	1.97E-02
ENSMUSG00000022306	Zfpm2	0.563	1.270	1.42E-01	1.59E-04
ENSMUSG00000025314	Ptprj	0.626	1.265	3.72E-01	1.92E-02
ENSMUSG00000034040	Wbscr17	0.751	1.251	2.16E-01	1.56E-02
ENSMUSG00000041180	Hectd2	0.271	1.248	8.86E-01	4.20E-02
ENSMUSG00000019889	Ptprk	0.209	1.240	7.85E-01	2.63E-05
ENSMUSG00000031072	Oraov1	0.654	1.237	4.88E-01	4.33E-02
ENSMUSG00000029161	Cgref1	0.675	1.233	2.86E-01	3.06E-02
ENSMUSG00000030287	Itpr2	0.257	1.222	9.14E-01	2.50E-02
ENSMUSG00000006457	Actn3	0.228	-1.029	8.10E-01	1.38E-02
ENSMUSG00000031791	Tmem38a	0.040	-1.029	9.85E-01	3.77E-02
ENSMUSG00000034648	Lrrn1	-0.025	-1.031	9.94E-01	7.75E-03
ENSMUSG00000024754	Tmem2	-0.579	-1.038	1.03E-01	3.53E-03
ENSMUSG00000023942	Slc29a1	-0.024	-1.051	9.78E-01	1.69E-10
ENSMUSG00000040663	Clcf1	-0.570	-1.054	2.17E-01	1.19E-02
ENSMUSG00000001911	Nfix	-0.823	-1.056	1.68E-01	1.28E-02
ENSMUSG00000025092	Hspa12a	-0.402	-1.059	5.78E-01	4.54E-02
ENSMUSG00000067071	Hes6	0.000	-1.076	1.00E+00	4.13E-05

ENSMUSG00000035357	Pdzrn3	-0.834	-1.078	6.34E-02	1.84E-02
ENSMUSG00000031310	Zmym3	-0.509	-1.080	4.32E-01	7.62E-03
ENSMUSG00000030257	Srgap3	-0.524	-1.084	7.38E-02	7.86E-04
ENSMUSG00000039824	Myl6b	0.038	-1.088	9.85E-01	2.67E-02
ENSMUSG00000028121	Bcar3	-0.415	-1.090	5.17E-01	2.12E-02
ENSMUSG00000042734	Ttc9	-0.603	-1.112	1.74E-01	1.42E-02
ENSMUSG00000025321	Itgb8	0.412	-1.114	5.29E-01	3.06E-02
ENSMUSG00000025789	St8sia2	-0.020	-1.116	9.96E-01	4.37E-03
ENSMUSG00000030592	Ryr1	-0.297	-1.116	6.89E-01	5.37E-03
ENSMUSG00000057280	Musk	-0.243	-1.117	4.61E-01	5.43E-07
ENSMUSG00000074607	Tox2	-0.311	-1.135	6.09E-01	2.75E-03
ENSMUSG00000048583	Igf2	0.267	-1.143	4.39E-01	3.92E-08
ENSMUSG00000062077	Trim54	0.087	-1.157	9.55E-01	3.93E-03
ENSMUSG00000026141	Col19a1	-0.616	-1.168	3.12E-01	2.80E-02
ENSMUSG00000021636	Marveld2	-0.119	-1.172	9.45E-01	1.53E-02
ENSMUSG00000027797	Dclk1	-0.527	-1.175	1.41E-01	5.14E-04
ENSMUSG00000021798	Ldb3	-0.340	-1.178	2.43E-01	6.56E-06
ENSMUSG00000038623	Tm6sf1	-0.182	-1.179	8.75E-01	3.25E-03
ENSMUSG00000031461	Myom2	-0.134	-1.185	9.50E-01	1.61E-02
ENSMUSG00000027333	Smox	0.001	-1.187	1.00E+00	1.22E-03
ENSMUSG00000020393	Kremen1	-0.145	-1.192	9.08E-01	6.34E-04
ENSMUSG00000059810	Rgs3	-0.662	-1.202	1.77E-01	8.52E-03
ENSMUSG00000029163	Emilin1	-0.455	-1.202	4.28E-01	5.63E-03
ENSMUSG00000061143	Maml3	-0.606	-1.208	8.90E-02	1.55E-03
ENSMUSG00000026042	Col5a2	-0.456	-1.213	6.02E-02	2.92E-07
ENSMUSG00000040797	Iqsec3	-0.054	-1.222	9.49E-01	3.15E-12
ENSMUSG00000006360	Crip1	-0.180	-1.224	9.09E-01	2.93E-02
ENSMUSG00000018796	Acsl1	0.032	-1.232	9.95E-01	2.83E-02
ENSMUSG00000030352	Tspan9	-0.363	-1.239	4.36E-01	1.70E-05
ENSMUSG00000030672	Mylpf	-0.244	-1.253	4.56E-01	1.23E-08
ENSMUSG00000032024	9030425E11Rik	-0.782	-1.270	1.02E-01	8.34E-03
ENSMUSG00000038871	Bpgm	-0.640	-1.274	1.38E-01	1.71E-03
ENSMUSG00000055322	Tns1	-0.021	-1.279	9.96E-01	2.36E-03
ENSMUSG00000014846	Tppp3	-0.233	-1.287	6.38E-01	8.86E-06
ENSMUSG00000062646	Ganc	-0.635	-1.288	4.76E-01	2.60E-02
ENSMUSG00000026640	Plxna2	-0.413	-1.300	3.94E-01	1.74E-04
ENSMUSG00000019787	Trdn	-0.407	-1.313	6.01E-01	1.41E-02
ENSMUSG00000026208	Des	-0.426	-1.322	6.33E-02	2.30E-10
ENSMUSG00000026185	Igfbp5	-0.502	-1.330	1.24E-01	3.31E-06
ENSMUSG00000033060	Lmo7	-0.599	-1.336	1.21E-01	3.02E-04
ENSMUSG00000073591	Pcdhb22	-0.536	-1.350	5.22E-01	4.15E-02
ENSMUSG00000064043	Trerf1	-0.960	-1.350	6.23E-02	3.52E-02
ENSMUSG00000020475	Pgam2	0.039	-1.363	9.87E-01	1.57E-02
ENSMUSG00000036256	Igfbp7	-0.516	-1.367	2.73E-01	8.35E-04
ENSMUSG00000034898	Filip1	-0.310	-1.370	8.30E-01	2.74E-02
ENSMUSG00000020067	Mypn	-0.232	-1.382	8.75E-01	1.31E-02
ENSMUSG00000009633	G0s2	-0.595	-1.394	3.01E-01	1.01E-02
ENSMUSG00000035296	Sgcg	-0.121	-1.397	9.54E-01	2.02E-02
ENSMUSG00000030930	Chst15	-0.417	-1.415	5.81E-01	7.28E-04
ENSMUSG00000006435	Neurl1a	-0.540	-1.428	2.97E-01	3.13E-03
ENSMUSG00000029093	Sorcs2	-0.168	-1.435	9.06E-01	8.37E-04
ENSMUSG00000091898	Tnnc1	-0.291	-1.440	7.09E-01	1.54E-04
ENSMUSG00000027009	Itga4	-0.070	-1.471	9.78E-01	1.55E-02
ENSMUSG00000033906	Zdhhc15	-0.295	-1.477	8.50E-01	3.36E-02

ENSMUSG00000031097	Tnni2	-0.254	-1.480	8.52E-01	4.76E-03
ENSMUSG00000031312	Itgb1bp2	-0.468	-1.524	5.52E-01	7.78E-03
ENSMUSG00000038403	Hfe2	-0.269	-1.526	8.27E-01	4.94E-03
ENSMUSG00000044086	Lmod3	-0.287	-1.527	7.27E-01	2.54E-04
ENSMUSG00000018983	E2f2	0.491	-1.540	7.81E-01	1.30E-02
ENSMUSG00000027276	Jag1	-0.754	-1.541	3.01E-01	1.92E-02
ENSMUSG00000042834	D0H4S114	-0.546	-1.547	2.02E-01	2.98E-07
ENSMUSG00000063296	Tmem117	-0.899	-1.550	2.08E-01	4.48E-02
ENSMUSG00000019577	Pdk4	-0.687	-1.550	1.15E-01	1.00E-04
ENSMUSG00000037206	Islr	0.189	-1.554	7.47E-01	3.37E-05
ENSMUSG00000019278	Dpep1	0.514	-1.556	5.71E-01	4.05E-02
ENSMUSG00000057123	Gja5	-1.331	-1.559	5.38E-01	1.39E-02
ENSMUSG00000025229	Pitx3	-0.438	-1.561	6.07E-01	2.38E-03
ENSMUSG00000020941	Map3k14	-0.623	-1.563	2.98E-01	1.83E-03
ENSMUSG00000042451	Mybph	-0.546	-1.563	1.88E-01	1.20E-05
ENSMUSG00000021909	Tnnc1	-0.495	-1.593	2.73E-01	1.07E-05
ENSMUSG00000020722	Cacng1	-0.154	-1.599	9.23E-01	1.90E-03
ENSMUSG00000086454	4930500J02Rik	-0.883	-1.606	3.35E-01	3.38E-02
ENSMUSG00000007097	Atp1a2	-0.399	-1.611	6.98E-01	2.66E-03
ENSMUSG00000074794	Arrdc3	-0.388	-1.634	6.94E-01	1.91E-04
ENSMUSG00000055775	Myh8	-0.664	-1.649	5.35E-02	4.89E-07
ENSMUSG00000020695	Mrc2	-0.739	-1.649	9.45E-02	3.44E-04
ENSMUSG00000042826	Fgf11	-0.153	-1.649	8.87E-01	1.08E-05
ENSMUSG00000044022	Pcdhb21	-0.628	-1.660	4.54E-01	1.74E-02
ENSMUSG00000038239	Hrc	-0.167	-1.688	8.71E-01	8.22E-05
ENSMUSG00000042828	Trim72	-0.568	-1.695	2.40E-01	8.76E-05
ENSMUSG00000061723	Tnnt3	-0.211	-1.710	4.99E-01	0.00E+00
ENSMUSG00000002007	Srpk3	0.077	-1.719	9.82E-01	1.30E-02
ENSMUSG00000037139	Myom3	-0.149	-1.730	8.80E-01	2.11E-08
ENSMUSG00000022309	Angpt1	-0.961	-1.750	9.56E-02	7.90E-03
ENSMUSG00000001510	Dlx3	-1.176	-1.780	1.19E-01	4.07E-02
ENSMUSG00000049303	Syt12	-0.768	-1.803	3.15E-01	4.95E-03
ENSMUSG00000075330	A930003A15Rik	-0.595	-1.833	6.59E-01	4.53E-02
ENSMUSG00000008318	Relt	-1.146	-1.849	7.63E-02	8.42E-03
ENSMUSG00000087090	Nctc1	-1.326	-1.875	5.19E-02	2.03E-02
ENSMUSG00000039031	Arhgap18	-0.374	-1.882	8.96E-01	4.50E-02
ENSMUSG00000040694	Apobec2	-0.174	-1.889	9.23E-01	1.69E-03
ENSMUSG00000036411	9530077C05Rik	-1.075	-1.896	5.42E-01	4.15E-02
ENSMUSG00000041548	Hspb8	-0.403	-1.900	2.17E-01	8.99E-12
ENSMUSG00000030513	Pcsk6	-1.370	-1.910	1.10E-01	1.53E-02
ENSMUSG00000047180	Neurl3	-1.020	-1.915	2.66E-01	3.79E-02
ENSMUSG00000084946	Dlx1as	-1.075	-1.915	2.93E-01	4.48E-02
ENSMUSG00000073236	2500004C02Rik	-0.148	-2.065	9.69E-01	1.92E-02
ENSMUSG00000025213	Kazald1	-1.197	-2.107	1.66E-01	2.70E-02
ENSMUSG00000032717	Mdfi	-0.327	-2.181	8.75E-01	1.30E-02
ENSMUSG00000028116	Myoz2	-1.151	-2.192	3.20E-01	4.37E-02
ENSMUSG00000020656	Grhl1	-1.237	-2.224	1.18E-01	5.53E-03
ENSMUSG00000020577	Tspan13	-0.989	-2.247	1.66E-01	1.33E-02
ENSMUSG00000026971	Itgb6	0.218	-2.351	9.75E-01	5.44E-03
ENSMUSG00000092491	Nrap	-0.361	-2.359	4.99E-01	5.52E-07
ENSMUSG00000056271	Lman1l	-0.810	-2.365	4.54E-01	7.78E-03
ENSMUSG00000060470	Gpr97	-1.295	-2.376	6.74E-02	3.20E-03
ENSMUSG00000032322	Pstpip1	0.439	-2.454	8.96E-01	3.32E-02
ENSMUSG00000029570	Lfng	-0.861	-2.459	1.33E-01	5.12E-05

ENSMUSG00000043867	Foxl1	-1.135	-2.538	2.35E-01	1.56E-02
ENSMUSG00000054675	Tmem119	-0.331	-2.619	7.00E-01	3.85E-07
ENSMUSG00000029778	Adcyap1r1	-1.171	-2.731	1.17E-01	1.35E-04
ENSMUSG00000038987	1700019L03Rik	-1.842	-2.805	7.73E-01	2.57E-02
ENSMUSG00000030433	Sbk2	-0.920	-2.808	4.41E-01	1.61E-02
ENSMUSG00000087591	Gm14635	-1.086	-2.813	1.41E-01	7.11E-05
ENSMUSG00000025497	Cdhr5	-1.270	-2.822	1.33E-01	1.65E-02
ENSMUSG00000019874	Fabp7	-2.349	-2.844	5.75E-02	4.11E-02
ENSMUSG00000022525	Hrasls	-2.095	-2.889	2.56E-01	9.04E-03
ENSMUSG00000056366	Fabp3-ps1	-1.296	-2.891	1.88E-01	3.40E-02
ENSMUSG00000025129	Ppp1r27	-0.986	-2.915	3.28E-01	3.63E-03
ENSMUSG00000029158	Yipf7	-0.719	-2.915	6.47E-01	3.34E-02
ENSMUSG00000023328	Ache	-0.912	-3.010	9.44E-01	3.56E-02
ENSMUSG00000031448	Adprhl1	-1.473	-3.017	6.31E-01	2.12E-02
ENSMUSG00000091826	Gm17504	-1.220	-3.067	1.28E-01	1.65E-03
ENSMUSG00000037868	Egr2	0.047	-3.100	1.00E+00	1.60E-02
ENSMUSG00000048572	E030010A14Rik	-1.054	-3.131	1.65E-01	1.68E-04
ENSMUSG00000020435	Osbp2	-2.105	-3.155	6.28E-02	6.23E-08
ENSMUSG00000040569	Slc26a7	-1.230	-3.355	7.87E-01	2.61E-02
ENSMUSG00000028197	Col24a1	-2.918	-3.444	5.75E-02	4.05E-04
ENSMUSG00000093765	RP24-386J17.2	-1.252	-3.611	4.53E-01	1.74E-02
ENSMUSG00000006362	Cbfa2t3	-0.969	-3.691	8.50E-01	2.22E-02
ENSMUSG00000054196	Cthrc1	-0.812	-4.056	1.97E-01	7.45E-05
ENSMUSG00000032744	Heyl	0.777	-4.326	8.86E-01	3.39E-03
ENSMUSG00000020723	Cacng4	-1.951	-4.421	6.28E-01	4.41E-03
ENSMUSG00000044041	Krt13	-3.728	-4.867	2.46E-01	1.22E-02
ENSMUSG00000038216	Pnmt	-0.459	-5.411	9.75E-01	4.06E-02
ENSMUSG00000030996	Art1	-0.042	-5.413	1.00E+00	7.38E-04
ENSMUSG00000086219	2410137F16Rik	-2.558	-5.774	5.85E-01	1.74E-02
ENSMUSG00000050592	Fam78a	-2.069	-5.846	1.51E-01	6.59E-11
ENSMUSG00000036169	Sostdc1	-4.027	-15.000	9.50E-02	1.72E-02
ENSMUSG00000036570	Fxyd1	-1.027	-15.000	8.53E-01	3.83E-02
ENSMUSG00000076494	Trbj2-3	-2.612	-15.000	6.51E-02	1.54E-02

Chapter 3 - Wnt/β-Catenin Controls Follistatin Signalling to Regulate Satellite Cell Myogenic Potential

Wnt/β-Catenin Controls Follistatin Signalling to Regulate Satellite Cell Myogenic Potential

Andrew E. Jones[1,2], Feodor D. Price[1,2], Fabien Le Grand[3] and Michael A. Rudnicki[1,2]

1. Regenerative Medicine Program,
   Ottawa Hospital Research Institute,
   501 Smyth Road, Ottawa, ON K1H 8L6
   Canada

2. Department of Cellular and Molecular Medicine,
   Faculty of Medicine, University of Ottawa,
   451 Smyth Road, Ottawa, ON K1H 8M5
   Canada

3. Institut Cochin, Université Paris Descartes, CNRS
   (UMR 8104), 24 Rue du Fg St Jacques, Paris,
   France

SUMMARY

Myogenesis is a complex and orchestrated biological process that leads to the progression of satellite cells through the myogenic pathway by generating a transient amplifying progenitor pool and subsequent fusion of these committed precursors into multinucleated myotubes. During regeneration, canonical Wnt signalling is activated, and has been implicated in regulating myogenic lineage progression (Brack et al., 2008). Here, we have undertaken a global analysis of committed satellite cell-derived myoblasts to examine their ability to respond to canonical Wnt/β-Catenin signalling. We demonstrate that Wnt/β-Catenin signalling drives myogenic differentiation via the myogenin-dependent control of follistatin expression by committed myogenic cells. Together, this data reveals that canonical Wnt signalling enhances the activation of follistatin expression, and the fine regulation of the myogenic differentiation process.

INTRODUCTION

The growth, maintenance and regeneration of skeletal muscle is attributed to the satellite cell; a mitotically quiescent cell that resides between the basal lamina and sarcolemma of the muscle fibre (Mauro, 1961; Montarras et al., 2005; Schultz et al., 1978). During muscle regeneration, satellite cells activate, proliferate and differentiate into new myofibres or fuse to existing myofibres. Skeletal muscle regeneration is a highly orchestrated process contingent upon the proper expression of the paired-box transcription factor Pax7, and the basic helix-loop-helix (bHLH) myogenic regulatory factors (MRFs); Myf5, MyoD, myogenin and MRF4 (Perry and Rudnicki 2000). Collectively, MRFs undergo heterodimerization with the ubiquitously expressed E-protein family of bHLH proteins that mediate the recognition of E-box consensus sequences (CANNTG) found in the promoters of many muscle specific genes (Berkes and Tapscott, 2005). In the adult, Myf5 and MyoD function genetically upstream of myogenin and MRF4 to specify myogenic identity in proliferating myoblasts. In contrast, myogenin and MRF4 are upregulated during the differentiation process and trigger the expression of myogenic differentiation specific genes (Bentzinger et al., 2012).

The initial expression of the MRFs is modulated by Pax7 and the closely related Pax3, both of which have been shown to directly regulate MyoD and Myf5 expression (Bajard et al., 2006; Hu et al., 2008; McKinnell et al., 2008). These Pax proteins are important in maintaining the proliferation of myogenic progenitors and preventing differentiation. In the absence of Pax7, adult skeletal muscles are nearly devoid of satellite cells and the regenerative capacity of the muscle is nearly entirely ablated (Kuang et al., 2006; Seale et al., 2000). The satellite cell compartment consists of a heterogeneous

population of myogenic committed satellite cells (Pax7+;Myf5+) and a subpopulation of satellite stem cells (Pax7+;Myf5-) which are discriminated following asymmetric cell divisions based on Myf5 expression (Kuang et al., 2007). Satellite stem cells possess the ability to self-renew, and it is this characteristic that allows adult skeletal muscle to undergo regeneration throughout the lifetime of an organism (Collins et al., 2005; Kuang et al., 2007; Zammit et al., 2004).

Skeletal muscle regeneration is a highly systematic process that is regulated through mechanisms involving cellular interactions and extracellular signalling pathways. The Wnt signalling pathway has been shown to play a critical role in regulating various developmental programs through embryonic development and in the regulation of stem cell function in adult tissues (Clevers, 2006). This pathway is activated following the binding of secreted Wnt glycoproteins with Frizzled (Fzd) receptors and lipoprotein receptor-related proteins 5/6 (LRP5/6) co-receptors (Nelson and Nusse, 2004). Fzd receptors are seven-transmembrane proteins, containing a large extracellular cysteine-rich domain, which interact with Dishevelled (Dvl) and heterotrimeric G proteins (Katoh, 2007). The canonical Wnt signalling pathway is regulated by the expression and subcellular localization of β-Catenin. In the absence of Wnt signal, intracellular β-Catenin is associated with Axin and adenomatous polyposis coli (APC) and undergoes proteasomal degradation following glycogen synthase kinase 3-β (GSK3β) dependent phosphorylation by casein kinase I (CK1) (Logan and Nusse, 2004). In the presence of Wnt proteins binding to the Fzd and LRP5/6 receptors, heterotrimeric G proteins and Dvl become activated, leading to the recruitment of Axin to the LRP5/6 receptor (Grumolato et al., 2010). This results in inhibition of the GSK3β mediated phosphorylation, resulting in nuclear translocation of β-Catenin. Once

localized to the nucleus, β-Catenin binds with members of the T-cell factor (TCF)/lymphoid-enhancer factor (Lef) family of transcription factors and activates target gene expression (MacDonald et al., 2009). In contrast to canonical Wnt signalling, the non-canonical Wnt signalling pathways function independently of β-Catenin through Fzd receptors either dependent or independent of LRP receptors (Nusse, 2012). Non-canonical Wnt signalling pathways include the planar cell polarity (PCP), Wnt/calcium (Ca^{2+}), and phosphatidylinositol 3-kinase (PI3K)/AKT/mammalian target of rapamycin (mTOR) signalling cascades.

During muscle regeneration, multiple Wnt signals are activated within the skeletal muscle tissue (von Maltzahn et al., 2012). We have previously shown that the symmetric expansion of satellite stem cells is controlled by the non-canonical Wnt/PCP-mediated orientation along the axis of stem cell division (Le Grand et al., 2009). Wnt7a-mediated polarization of α7-integrin and the PCP core-component molecule Vangl2, on opposite poles of the daughter cells, allows both cells to maintain contact with the basal lamina and thus preserve their orientation relative to the niche. However, there are paradoxical roles for the canonical Wnt/β-Catenin pathway during adult skeletal muscle regeneration. While canonical Wnt signalling has been implicated in promoting the proliferation of satellite cells, (Otto et al., 2008), another report has demonstrated that Wnt/β-Catenin signalling controls myogenic lineage progression and promotes terminal differentiation by limiting Notch signalling (Brack et al., 2008). During muscle regeneration, Notch signalling is activated and stimulates the proliferation of satellite cells leading to the expansion of myoblasts (Conboy and Rando, 2002). During differentiation, Wnt/β-Catenin signalling antagonizes the effects of Notch signalling, and through reduced GSK3β levels, allows progression of

myogenic commitment and differentiation (Brack et al., 2008). Among others, we have previously shown that myogenic cells stimulated with Wnt3a activate the canonical Wnt pathway leading to nuclear stabilization of activated β-Catenin. *In vivo*, overexpression of Wnt3a in the tibialis anterior (TA) muscle results in an increased number of myofibres, which exhibit a dramatic reduction in the cross-sectional area and reduced regenerative efficiency (Le Grand et al., 2009). *In vitro*, canonical Wnt treatment of satellite cell derived myoblasts inhibits cellular proliferation, a characteristic not observed by non-canonical Wnt treatment. In addition to modulating the satellite cell compartment, canonical Wnt signalling has been implicated in satellite cell-related transdifferentiation and increasing myogenic potential (Brack et al., 2007; Polesskaya et al., 2003).

In addition to Wnt signals, the transforming growth factor-β (TGF-β) family members are important cytokines that regulate cell growth. Through binding membrane receptors, TGF-β activates phosphorylation of Smad proteins, resulting in their nuclear translocation and activation of target genes (Chen et al., 2002). Myostatin/growth and differentiation factor-8 (GDF-8) is a TGF-β family member that binds the activin receptor type II (ActRII) and acts as a negative regulator of skeletal muscle mass. Myostatin-null mice display hypertrophic and hyperplastic muscle (McPherron et al., 1997). During development, myostatin expression limits the rate of muscle growth without impairing the establishment of myogenic structures (Amthor et al., 2002). Following exposure to myostatin, activin receptor-like kinases are phosphorylated by ActRII, leading to the phosphorylation of TGF-β specific Smad2 and Smad3, which complex with Smad4. Together, the Smad2/3/4 complex is translocated to the nucleus to mediate target gene

expression, including Pax3, Pax7, Myf5 and MyoD (Amthor et al., 2002; Langley et al., 2002; Lee and McPherron, 2001; McFarlane et al., 2008).

Follistatin is a secreted glycoprotein that antagonizes various members of the TGF-β superfamily, including myostatin (Hemmati-Brivanlou et al., 1994; Iemura et al., 1998). Originally identified in porcine ovarian follicular fluid, follistatin was suggested to promote muscle fibre hypertrophy by inhibiting the myostatin repressive effects on myogenic progenitor differentiation and muscle fibre growth (Lee and McPherron, 2001; Nakamura et al., 1990). Through antagonizing myostatin and activin A activity, follistatin overexpression leads to a more dramatic muscle phenotype than the myostatin-null mouse (Lee et al., 2005). Strikingly, follistatin regulation remains functional in myostatin-null mice, suggesting a myostatin-independent function (Lee, 2007; Lee et al., 2010). Recent observations suggest that follistatin promotes muscle hypertrophy through suppressing the phosphorylation of Smad3. This results in potentiation of mTOR/S6 protein kinase (S6K)/S6 ribosomal protein (S6RP) signalling and inhibition of GSK3β (Ruvinsky et al., 2009; Winbanks et al., 2012). The mTOR dependent phosphorylation of S6RP leads to increased protein synthesis and cell size from enhanced protein translation initiation and elongation (Glass, 2005).

To further investigate the role of canonical Wnt signalling in adult myogenesis, we analyzed the response of satellite cell derived myoblasts to Wnt/β-Catenin signalling. We show that canonical Wnt signalling is associated with committed satellite cell differentiation potential and control of follistatin expression. Investigation of the role for a Wnt-follistatin pathway lead us to demonstrate that Wnt3a/β-Catenin signalling controls the induction of myogenic differentiation via the MyoD-dependent activation of myogenin expression. These

findings suggest that Wnt/β-Catenin signalling controls multiple steps of adult myogenesis by promoting premature myogenic differentiation in a myogenin-dependent manner.

METHODS

Cell Culture and Transfection

Primary myoblasts were isolated from the hind limbs of 4-6 week old wild type C57Bl/6J mice, as previously described (Megeney et al., 1996), and propagated on collagen-coated culture dishes in Ham's F10 media supplemented with 20% fetal bovine serum (FBS), 1% penicillin/streptomycin and 2.5 ng/ml human recombinant bFGF. Myogenic differentiation was induced by shifting to differentiation media (DMEM supplemented with 5% horse serum). For cell stimulation, recombinant Wnt3a (20 ng/ml), Dkk1 (50 ng/ml), and follistatin (250 ng/ml) proteins were added in the culture medium (R&D Systems). siRNA transfections were performed in growth media using Lipofectamine 2000 Reagent (Invitrogen), as per manufacturer's instructions. siFollistatin and siMyogenin duplexes were from Ambion (ID s66250, s70334) and used at the final concentration of 2 nM each.

Animals

8 to 12 weeks old wild type C57Bl/6J mice were used in this study. All mice were maintained inside a barrier facility and experiments were performed following the University of Ottawa regulations for animal care and handling. The TA muscle was injured by injection of 50 µl cardiotoxin (10 µM, Sigma). (2'Z,3'E)-6-Bromoindirubin-3'-oxime (BIO) was reconstituted in DMSO at a concentration of 5 mM (B1686, Sigma) combined with saline as vehicle and injected directly into the TA muscle in a volume of 10 µl at a final concentration of 1 µM.

Gene Expression Analyses

Affymetrix MoGene 1.0 ST chipsets were RMA normalized (Irizarry et al., 2003) using the xps in Bioconductor R package (Gentleman et al., 2004) with the Affymetrix provided MoGene-1_0-st-v1.r4 chip layout and scheme files. The RMA normalized data was log2 transformed and analyzed using the Significance Analysis of Microarrays (SAM) (Tusher et al., 2001) method as implemented in the Bioconductor siggenes package (Schwender, 2009). Heat maps were generated by GenePattern (Reich et al., 2006). Gene ontology of expression data was performed using the functional annotation module of DAVID 6.7 (Huang et al., 2009a, b).

Real-Time PCR

Total RNA was isolated using the RNeasy Kits and subjected to on-column DNase digestion, as per manufacturer's instructions (Qiagen). cDNA synthesis was performed using the Superscript III reverse transcriptase with random hexamer primers (Invitrogen). SYBR Green Real-Time PCR was carried out as previously described (Holterman et al., 2007). Transcript levels were normalized to GAPDH transcript levels. Relative fold change in expression was calculated using the ΔΔCT method (CT values < 30). PCR primers were designed using the online Primer3 software (http://primer3.wi.mit.edu) (Rozen and Skaletsky, 2000). Primer sequences are listed in Table S1.

Western Blot

Total protein was harvested in RIPA lysis buffer fortified with protease inhibitors (Complete-Mini; Roche-Boehringer), and protein concentration was determined by Bradford

assay (BioRad). Samples (20 μg) were subjected to SDS-PAGE and electroblotted onto Immobilon-P membrane (Millipore). Membranes were blocked in 5% non-fat milk in PBST, prior to sequential probing with primary antibody and HRP-conjugated secondary antibody in blocking solution. ECL (Amersham-Pharmacia) with BioMax XAR film (Kodak) was used to detect target proteins. Primary antibodies used for detection are as follows: α-Pax7 (Developmental Studies Hybridoma Bank), α-myogenin (F5D; Developmental Studies Hybridoma Bank), α-Follistatin (Abcam) and α-Tubulin (Sigma). Secondary antibodies were HRP-conjugated anti-mouse and anti-rabbit (BioRad).

Immunocytochemistry

Adherent cell cultures were fixed with 4% PFA, permeabilized with 0.2% Triton-X in PBS, and incubated with primary antibodies: α-MyHC (Developmental Studies Hybridoma Bank) and α-Laminin (Sigma). Alexa-488 and Alexa-555 conjugated secondary antibodies, that matched the primary antibodies, were used at 1:1000 in PBS (Invitrogen). Nuclei were counterstained with DAPI (Sigma-Aldrich). Images were obtained using Axioplan2 microscope (Carl Zeiss), a 20× NA 0.75 plan Apochromat (ω/0.17; Carl Zeiss) objective, and a digital Axiocam camera (Carl Zeiss). Digital images were captured using Axiovision (Carl Zeiss) and were processed with Photoshop (Adobe).

ChIP Analysis

Protein-DNA complexes were cross-linked with 1% formaldehyde (Sigma) and sheared by sonication. Processing of samples was performed as previously described (Soleimani et al., 2012a); 2000 μg of protein-DNA complexes were immunoprecipitated with 4-5 μg of α-

myogenin (Santa Cruz) or control Rabbit IgG overnight, followed by wash conditions and DNA elution performed according to the ChIP Assay Kit (Upstate). The immunoprecipitated DNA was subjected to Real-Time PCR, and results were normalized using control locus representing DNA fragments that were non-specifically bound. Myogenin ChIP-Seq was performed by chromatin tandem affinity purification and data was analyzed as described previously (Soleimani et al., 2012b).

Statistical Analysis

Three or more replicates were analyzed for each experiment presented. Data is shown as standard error of the mean (SEM) and results were assessed for statistical significance by a Student's T-Test. Differences were considered statistically significant at the $p < 0.05$ level.

RESULTS

Canonical Wnt signalling induces follistatin expression in myoblasts

During muscle regeneration, multiple Wnt signals are activated within the skeletal muscle (von Maltzahn et al., 2012). To further investigate the role of canonical Wnt signalling in adult myogenesis, we analyzed the response of satellite cell derived myoblasts to Wnt/β-Catenin signalling by genome-wide microarray expression analysis. Low-passage primary myoblasts were treated with recombinant Wnt3a, which we previously demonstrated activates the canonical Wnt/β-Catenin pathway in satellite cells (Le Grand et al., 2009), or control BSA protein for 24 hours. Genes were divided into upregulated, downregulated and unchanged groups based on their expression patterns between Wnt3a and BSA treatments. Wnt3a stimulation resulted in significant expression changes in 401 genes relative to BSA control (fold change > 2, p-value < 0.05); 90 genes were upregulated, while 311 genes were downregulated. Heat maps were generated to examine expression values for Wnt3a vs BSA control by plotting fold changes for the top 20 regulated genes relative to BSA treated control myoblasts (Figure 1A). To investigate the global transcriptional effects of Wnt3a treatment, we conducted an unbiased DAVID analysis of our microarray data. Functional annotation clustering of related gene ontology (GO) terms revealed that Wnt3a stimulation strongly regulated cell cycle, cell division and the progression of mitosis (Figure S1). We validated a subset of regulated genes by Real-Time RT-PCR, and observed a decrease in Pax7 expression following Wnt3a stimulation, indicative of myogenic commitment, as well as genes associated with the progression of mitosis and cell proliferation (such as E2F1, Ki67 and cyclin E2) (Figure 1C, S1). Upregulation of the canonical Wnt-responsive gene Axin2 confirmed activation of canonical Wnt signalling, in

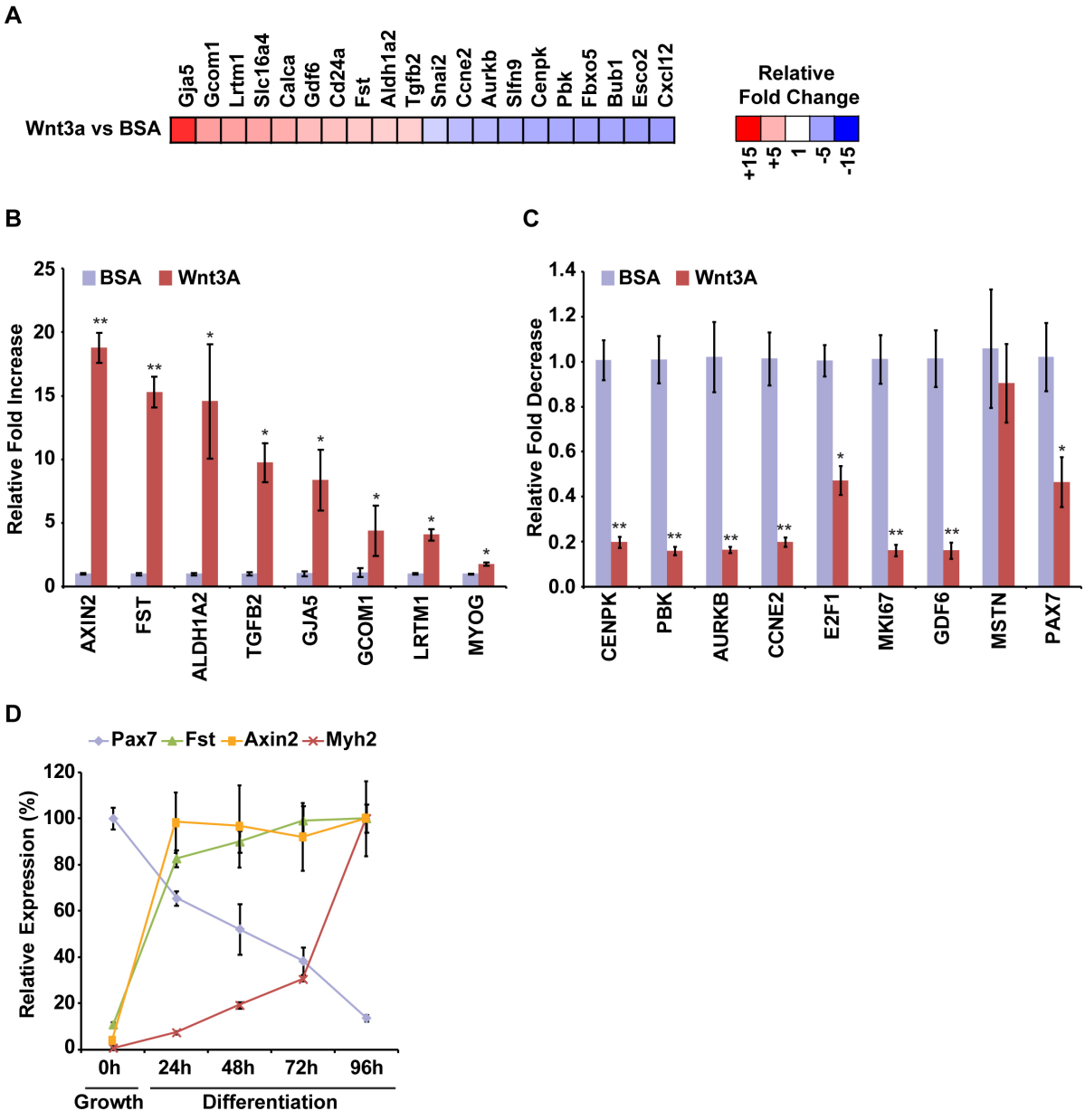
A
Gja5
Gcom1
Lrtm1
Slc16a4
Calca
Gdf6
Cd24a
Fst
Aldh1a2
Tgfb2
Snai2
Ccne2
Aurkb
Slfn9
Cenpk
Pbk
Fbxo5
Bub1
Esco2
Cxcl12
Wnt3a vs BSA
Relative Fold Change
+15
+5
1
-5
-15
B
BSA
Wnt3A
Relative Fold Increase
AXIN2
FST
ALDH1A2
TGFB2
GJA5
GCOM1
LRTM1
MYOG
C
BSA
Wnt3A
Relative Fold Decrease
CENPK
PBK
AURKB
CCNE2
E2F1
MKI67
GDF6
MSTN
PAX7
D
Pax7
Fst
Axin2
Myh2
Relative Expression (%)
0h
24h
48h
72h
96h
Growth
Differentiation

Figure 1. Follistatin expression is regulated by canonical Wnt/β-Catenin signalling
(A) Global heat map ratio representing the difference in gene expression patterns following treatment with recombinant Wnt3a or control BSA protein. Red represents genes that increase in expression relative to the BSA-treated control, while blue represents a decrease.
(B) Real-Time RT-PCR validation of a subset of genes upregulated following Wnt3a treatment relative to BSA control. Interestingly, the canonical Wnt target Axin2 and follistatin are strongly upregulated following Wnt3a treatment. Data are presented as the mean ± SEM (n=3, * $p < 0.05$, ** $p < 0.01$), normalized to GAPDH and shown relative to BSA control.
(C) Real-Time RT-PCR validation of a subset of genes downregulated following Wnt3a treatment relative to BSA control. Interestingly, many genes associated with cell-cycle progression are downregulated, while myostatin remains unchanged. Data are presented as the mean ± SEM (n=3, * $p < 0.05$, ** $p < 0.01$), normalized to GAPDH, and shown relative to BSA control.
(D) Real-Time RT-PCR analysis of Pax7, follistatin, Axin2 and Myh2 expression levels in a myoblast differentiation time-course. Pax7 expression is reduced while Myh2 expression increases during differentiation. Follistatin expression is upregulated during the first 24 hours of differentiation in a similar fashion as the Wnt target Axin2. Data are presented as the mean ± SEM (n=3), normalized to GAPDH.

addition to an observed increase in TGFβ2 and myogenin expression (Figure 1B). Strikingly, we observed that expression of follistatin, a secreted glycoprotein that antagonizes members of the TGF-β superfamily, was increased by 15.3-fold following Wnt3a stimulation (Figure 1B), independent of an effect on myostatin expression (Figure 1C). Following our global microarray analysis, we focused on follistatin, given its strong upregulation following Wnt treatment and its previously characterized role in promoting differentiation and muscle hypertrophy.

Since follistatin expression appeared to be linked to increased Wnt/β-Catenin signalling, we analyzed its relative expression during a myoblast differentiation time-course (Figure 1D). During myogenic differentiation, Pax7 transcription diminishes while the expression of differentiation markers (such as Myosin Heavy Chain, Myh2) become elevated. We observed that Axin2 expression was strongly increased within the first 24 hours of differentiation, consistent with an increase in Wnt/β-Catenin signalling, and this was concomitant with a 10-fold increase in follistatin expression.

Canonical Wnt signalling promotes myoblast fusion in a follistatin-dependent manner

Given follistatin expression is rapidly upregulated following the induction of differentiation, we next examined if the modulation of Wnt/β-Catenin signalling during myogenic differentiation resulted in further variation in follistatin expression. To this aim, we treated differentiating cells with recombinant Wnt3a protein, the canonical Wnt antagonist Dickkopf-related protein 1 (Dkk1), or BSA as a control. We observed that, while Wnt3a stimulation resulted in an increase in follistatin and Axin2 expression levels, their expression levels were reduced following Dkk1 mediated inhibition of Wnt/β-Catenin

activity (Figure 2A). These observations further confirm that the regulation of follistatin expression following Wnt3a treatment is dependent on the canonical Wnt signalling pathway.

To determine if the induction of follistatin expression by canonical Wnt signals was necessary for myogenic differentiation, we analyzed the impacts of gain- and loss-of-function of both signalling pathways. To that extent, we observed that either Wnt3a or follistatin treatment resulted in larger myotubes with an increased number of nuclei per myotube, while inhibition of Wnt/β-Catenin signalling via Dkk1 treatment and inhibition of follistatin signalling via siRNA mediated gene silencing limited myogenic fusion, and led to the formation of short myotubes (Figure 2B,C).

To validate that follistatin acts downstream of Wnt/β-Catenin signalling during myogenic differentiation, we first determined the optimal concentration of siRNA against follistatin for transfection in the presence of Wnt3a to reduce follistatin expression to control levels (transfected with non-silencing Scrambled siRNAs) (Figure 2D, top). Under this condition, we observed that in differentiating myoblasts the increase in fusion index induced by Wnt3a is dependent on the increase in follistatin expression (Figure 2D, bottom). Taken together, these observations implicate follistatin as a canonical Wnt signalling target whose expression promotes differentiation-induced myogenic fusion.

Canonical Wnt/β-Catenin signalling primes myoblasts for myogenic differentiation

A recent report demonstrated that myogenin expression represses genes involved in cell-cycle progression, and is sufficient to induce exit from the cell-cycle (Liu et al., 2012). Since we observed a major suppression of cell proliferation genes following Wnt3a

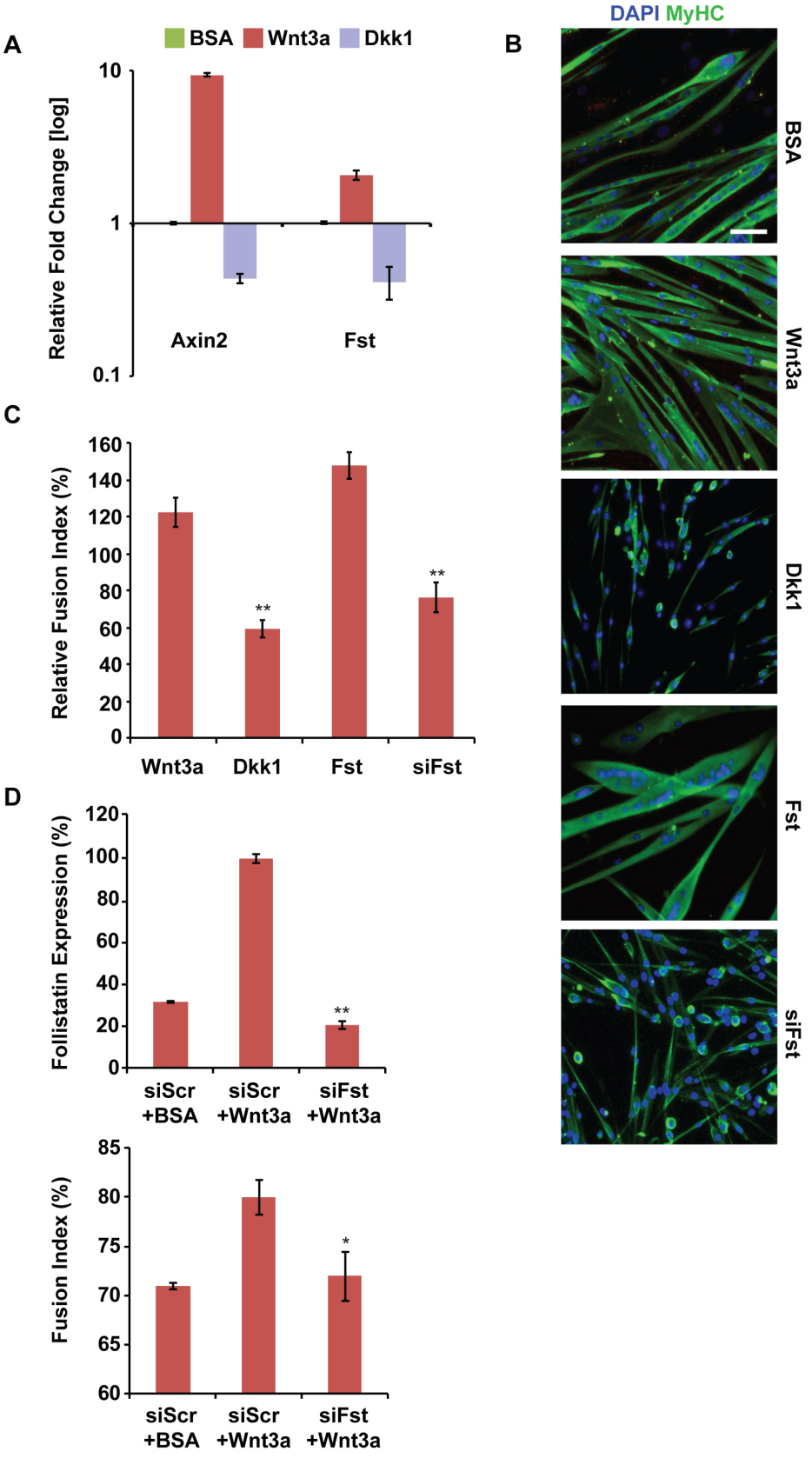
A
BSA
Wnt3a
Dkk1
Relative Fold Change [log]
10
1
0.1
Axin2
Fst
B
DAPI MyHC
BSA
Wnt3a
Dkk1
Fst
siFst
C
Relative Fusion Index (%)
160
140
120
100
80
60
40
20
0
**
**
Wnt3a
Dkk1
Fst
siFst
D
Follistatin Expression (%)
120
100
80
60
40
20
0
**
siScr +BSA
siScr +Wnt3a
siFst +Wnt3a
Fusion Index (%)
85
80
75
70
65
60
*
siScr +BSA
siScr +Wnt3a
siFst +Wnt3a

Figure 2. Canonical Wnt/β-Catenin signalling promotes myoblast fusion in a follistatin dependent manner
(A) Real-Time RT-PCR analysis of Axin2 and follistatin expression in myoblasts cultured in differentiation media for 24 hours, following recombinant Wnt3a, Dkk1 or control BSA protein treatments. Wnt3a stimulation increased follistatin and Axin2 expression levels. Data are presented as the mean ± SEM (n=3), normalized to GAPDH.
(B) Myoblasts were cultured in differentiation media for 3 days in the presence of recombinant Wnt3a, Dkk1, follistatin or control BSA proteins or transfected with siRNAs against follistatin and immunostained for Myh2 expression. Scale bar: 25 μM.
(C) Quantification of the fusion index in myogenic cultures. Changes are expressed as relative to the control (BSA treatment or siScr transfection). Effects of the modulation of canonical Wnt signalling or follistatin treatment during myogenic differentiation are similar. Data are presented as the mean ± SEM (n=3, ** $p < 0.01$).
(D) Real-Time RT-PCR analysis of follistatin expression (top) and quantification of the fusion index (bottom) of myoblasts cultured in differentiation media for 24 hours treated with siScr and BSA, siScr and Wnt3a or siFst and Wnt3a. siFst transfection decreases follistatin expression in Wnt3a-treated cells to a level similar as untreated cells. Data are presented as the mean ± SEM (n=3, * $p < 0.05$, ** $p < 0.01$), normalized to GAPDH.

stimulation (Figure 1C, S1), we sought to explore the possible involvement of myogenin through Wnt/β-Catenin signalling. We first quantified the relative expression levels of follistatin and myogenin in growth conditions, where expression levels are low relative to differentiation conditions (Figure 3A). In addition, we observed increased myogenin and follistatin expression in growth conditions following Wnt stimulation, compared to BSA control, at both the transcript and protein levels (Figure 3B,C), while Pax7 levels were decreased. While myogenin and follistatin expression are induced during differentiation, it was striking to observe that Wnt3a stimulation upregulated their expression in growth conditions.

A recent study has revealed that β-Catenin can directly interact with MyoD and enhance its transcriptional activity through binding to regulatory E-box elements necessary for muscle differentiation in a TCF/Lef-independent manner (Kim et al., 2008). In light of this observation that β-Catenin is able to synergistically enhance MyoD binding to the myogenin promoter, resulting in increased myogenin expression, led us to further examine TCF/Lef-independent β-Catenin signalling. By employing an unpublished data set comprising myogenin chromatin immunoprecipitation coupled with massive parallel high-throughput sequencing (ChIP-Seq) we examined potential myogenin bound regulatory elements upstream of follistatin during differentiation (Figure S2, *unpublished data*). We identified a conserved regulatory E-box element 30 kb upstream of the follistatin gene locus that is occupied by myogenin during early differentiation (Figure S1). Interestingly, this element is not occupied by myogenin in growth conditions. Rather, during proliferative conditions, this element is bound by the Snail-HDAC1/2 repressive complex inhibiting the MRF-dependent access to this E-box motif. Further, we analyzed the binding

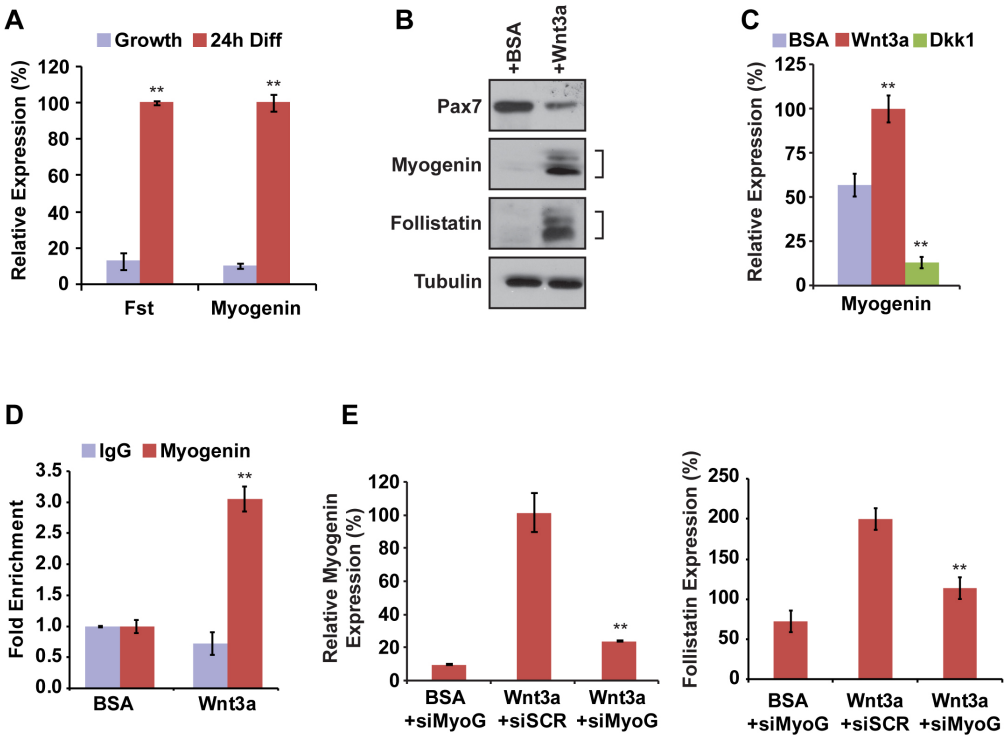

Figure 3. Wnt3a primes myoblasts for myogenic differentiation

(A) Real-Time RT-PCR analysis of follistatin and myogenin expression levels in proliferating and differentiating myoblasts. Follistatin and myogenin are rapidly upregulated early during myogenic differentiation. Data are presented as the mean ± SEM (n=3, ** $p < 0.01$), normalized to GAPDH.

(B) Western blot analysis of Pax7, myogenin and follistatin expression in proliferating myoblasts following recombinant Wnt3a or control BSA protein treatments. Canonical Wnt signalling increased myogenin and follistatin expression, and decreased Pax7 expression.

(C) Real-Time RT-PCR analysis of myogenin expression in proliferating myoblasts following recombinant Wnt3a, Dkk1 or control BSA protein treatments. Canonical Wnt signalling modulates the expression of myogenin. Data are presented as the mean ± SEM (n=3, ** $p < 0.01$), normalized to GAPDH.

(D) Real-Time PCR analysis of locus enrichment in chromatin immunoprecipitated with α-myogenin or control IgG antibodies from proliferating myoblasts following recombinant Wnt3a or control BSA protein treatments. Data are presented as the mean ± SEM (n=3, ** $p < 0.01$).

(E) Real-Time RT-PCR analysis of follistatin expression in myoblasts treated with siScr and BSA, siScr and Wnt3a or siMyog and Wnt3a. siMyog transfection decreases follistatin expression in Wnt3a-treated cells to a level similar to untreated cells. Data are presented as the mean ± SEM (n=3, ** $p < 0.01$), normalized to GAPDH.

of myogenin on this regulatory element in proliferating conditions following Wnt3a stimulation by ChIP-PCR. Our results demonstrate an enrichment of myogenin binding to this conserved element following Wnt3a stimulation (Figure 3D), which correlates to the observed increase of follistatin expression following Wnt3a treatment. Taken together, these observations along with the induction of follistatin expression via Wnt stimulation, directly link the extracellular canonical Wnt signals to the expression of follistatin in a myogenin-dependent manner.

Follistatin acts downstream of myogenin during differentiation

To demonstrate that follistatin acts downstream of myogenin expression, we first determined the optimal concentration of siRNA against myogenin for transfection in the presence of Wnt3a to reduce myogenin expression similar to control levels (BSA treatment transfected with siScrambled) (Figure 3E, left). Under this condition, we observed that the induction of follistatin expression by Wnt3a is dependent on myogenin expression in proliferating myoblasts (Figure 3E, right). Together, these results support the notion that, *in vitro*, canonical Wnt stimulation activates myogenin-dependent follistatin expression, leading to premature myogenic differentiation.

Canonical Wnt signalling promotes premature differentiation *in vivo*

To investigate the role of the Wnt-follistatin pathway in muscle regeneration *in vivo*, we stimulated canonical Wnt signalling by inhibiting GSK3β activity following muscle damage (Figure 4A). Previous studies demonstrate that Wnt proteins are secreted by the

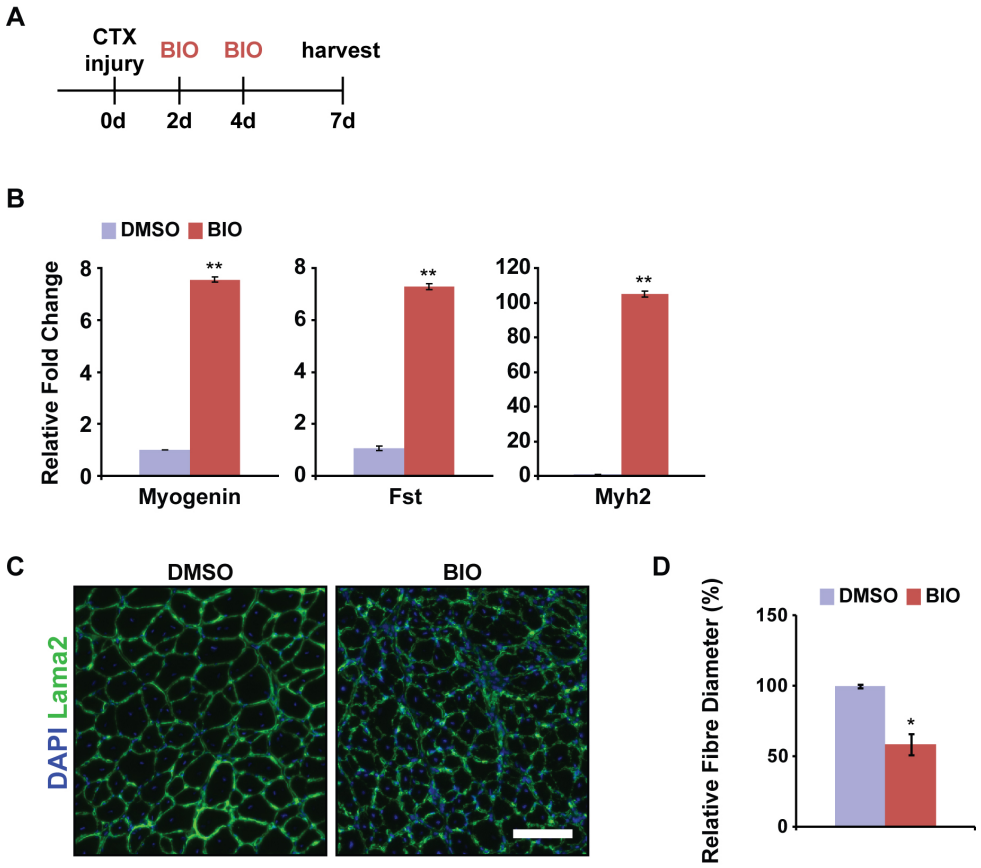

Figure 4. Canonical Wnt signalling promotes premature differentiation *in vivo*
(A) Experimental time-course for *in vivo* muscle injury. Mice undergo direct muscle injections of BIO following 2 and 4 days post-CTX injury.
(B) Real-Time RT-PCR analysis of myogenin, follistatin and Myh2 expression in TA muscle 7 days following CTX injury. Stimulation of β-Catenin signalling (BIO) results in increased myogenin and follistatin expression *in vivo*. Data are presented as the mean ± SEM (n=3, ** $p < 0.01$), normalized to GAPDH.
(C) Representative cryosections of TA muscle 7 days following CTX injury and treatment with GSK3-β inhibitor (BIO) or DMSO control. BIO treatment leads to altered muscle morphology relative to DMSO control. Scale bar: 50 μM
(D) Quantification of muscle fibre calibre in TA muscles 7 days following CTX injury and BIO treatment. BIO treatment leads to reduced fibre diameters relative to DMSO control. Data are presented as the mean ± SEM (n=3, * $p < 0.05$).

myofibre during muscle regeneration (Brack et al., 2008; Le Grand et al., 2009; Polesskaya et al., 2003). To further examine β-Catenin signalling during regeneration, we injected TA muscles with 10 µl of the small molecule (2'Z,3'E)-6-Bromoindirubin-3'-oxime (BIO), a pharmacological agent known to inhibit GSK3β activity (Polychronopoulos et al., 2004), or DMSO vehicle 2 and 4 days following cardiotoxin (CTX) injury. By inhibiting GSK3β, we effectively activate the canonical Wnt signalling pathway in muscle and satellite cells. Seven days following injury, we harvested RNA from total muscle tissue and examined gene expression profiles. Consistent with our *in vitro* data, we observed an overall increase in myogenin and follistatin expression, as well as an increase in Myh2 (Figure 4B). These results suggest that stimulation of β-Catenin activity promotes myogenic differentiation through regulating gene expression within muscle tissue.

Following the direct delivery of the Wnt agonist BIO we observed an altered muscle fibre morphology (Figure 4C), resulting in an increased number of fibres, as well as a dramatic reduction in cross sectional area (Figure 4D). These results corroborate previous experiments examining Wnt stimulation in regenerating muscle (Brack et al., 2008; Le Grand et al., 2009). Furthermore, these results substantiate our *in vitro* observations as treatment of regenerating skeletal muscle with a canonical Wnt signalling agonist reduces its regenerative potential through initiating premature myogenic differentiation. Taken together, these observations implicate the myogenin-dependent activation of follistatin expression following canonical Wnt stimulation in myogenic differentiation.

DISCUSSION

In response to muscle injury, quiescent satellite cells become activated, proliferate, and generate a pool of adult progenitor myoblasts necessary for the proper repair and maintenance. Within this progenitor population, Myf5 and MyoD expression is responsible for commitment to the myogenic lineage, while myogenin and MRF4 expression follows for myoblast fusion and terminal differentiation. The integration of this highly orchestrated transcriptional control of myogenesis and extrinsic signalling pathways allows for continued regenerative potential throughout the life of an organism.

Throughout embryogenesis, extrinsic Wnt signalling is important for proper myogenic development. Wnt1, Wnt3a and Wnt4 are expressed in the dorsal regions of the neural tube and induce somitic myogenesis (Munsterberg et al., 1995). Wnt/β-Catenin signalling is required for the proper formation of the dermomyotome and myotome from the somite, in addition to myogenic determination of limb muscle progenitors (Hutcheson et al., 2009). Within the adult, Wnt5a, Wnt5b and Wnt7a are expressed in resting skeletal muscle and are upregulated in the early phases of myogenic regeneration (von Maltzahn et al., 2012). R-spondins are secreted proteins that activate the canonical Wnt signalling pathway at the receptor level, leading to β-Catenin dependent gene activation (Han et al., 2011). This positive regulation of differentiation is shared with GSK3β inhibition, leading to enhanced myogenic differentiation (Rochat et al., 2004; van der Velden et al., 2006). While non-canonical Wnt signalling imparts regulation of satellite cell expansion (Le Grand et al., 2009), muscle differentiation is further orchestrated by the canonical Wnt/β-Catenin pathway.

Premature differentiation of progenitor cells occurs following the exogenous induction of canonical Wnt signalling during the early phases of regeneration, leading to a depletion of the satellite cell pool (Brack et al., 2008). Interestingly, we observed that Wnt3a promoted myoblast fusion following induction of myogenic differentiation (Figure 2B,C), an effect lost following Dkk1-mediated inhibition of endogenous Wnt signalling. Endogenous Wnt3a expression is induced in cultured myofibres, consistent with the observation that Wnt expression is low during the early phase of regeneration when progenitor expansion is occurring, then increasing to promote myogenic commitment and differentiation (Brack et al., 2008; Polesskaya et al., 2003; Zhao and Hoffman, 2004). These findings led us to further examine the canonical Wnt/β-Catenin signalling mode of action following Wnt3a stimulation of satellite cell derived myoblasts.

Among the genes upregulated following Wnt3a stimulation of proliferating myoblasts, the myogenic regulatory factor myogenin is well characterized to play a role during muscle differentiation. While expression is normally upregulated during differentiation, we observed a strong increase of myogenin protein following Wnt3a stimulation (Figure 3B), a feature not observed following non-canonical Wnt7a stimulation (data not shown). This upregulation of myogenin may serve as a node for the canonical Wnt induced switch to myogenic differentiation, regardless of the pro-proliferative culture conditions. We previously observed that canonical Wnt signalling reduced myoblast proliferation *in vitro* (Le Grand et al., 2009), and these results are further exemplified following activation of myogenin and the significant repression of genes involved in cell-cycle progression (Figure 1C, Table S2). Myogenic differentiation is a highly orchestrated process, with cell-cycle withdrawal occurring before the expression of contractile proteins or

cell fusion (Nadal-Ginard, 1978; Rosenthal, 1989; Weintraub, 1993). Myogenin expression leads to the downregulation of genes involved in cell-cycle progression, and is sufficient to induce cell-cycle withdrawal (Liu et al., 2012). This indirect cell-cycle repression occurs via the myogenin-dependent expression of miR-20a, a miRNA well characterized for its silencing of E2F1 and E2F3 (O'Donnell et al., 2005; Sylvestre et al., 2007). In addition, the induction of myogenin expression is dependent on tissue-specific expression of MyoD, co-operating with ubiquitously expressed Six, Mef2 and Pbx1 protein families and in concert with the epigenetic modifications of chromatin structure (Faralli and Dilworth, 2012). While Wnt3a treatment did not further induce MyoD expression, it should be noted that activated myoblasts already express strong levels of MyoD protein.

While its transcriptional activity is generally associated with TCF/Lef proteins, recent studies are establishing a potential TCF/Lef-independent function of β-Catenin. As discussed, MyoD is able to complex with β-Catenin independent of E-proteins (Kim et al., 2008), whose interaction preferentially binds muscle-specific E-box elements and promotes myogenic differentiation. In addition to MyoD, β-Catenin has been described in regulating TCF-independent transcription with Sox proteins (Kormish et al., 2010), FoxO proteins (Almeida et al., 2007), homeodomain proteins Prop1 (Olson et al., 2006) and PitX2 (Kioussi et al., 2002), hypoxia-inducible factor 1α (HIF1α) (Kaidi et al., 2007), and type I and type II nuclear receptors (Mulholland et al., 2005). These findings further suggest that, while the classical TCF/Lef-dependent β-Catenin transcriptional activation remains important, a TCF/Lef-independent role for β-Catenin provides a previously uncharacterized level of gene regulation.

In the absence of exogenous Wnt stimulation, myogenin is bound to the follistatin locus early during differentiation, and is presumably responsible for the rapid follistatin expression observed following 24 hours of myogenic differentiation (Figure 1D). In addition, a recent study observed that the Snail DNA-binding zinc finger transcriptional repressors bind the same DNA motif as the bHLH transcription factors MyoD and myogenin (Soleimani et al., 2012b). In proliferating myoblasts, Snail prevents MyoD occupancy on differentiation-specific regulatory elements, and the change from Snail to MyoD/myogenin binding often results in enhancer switching during differentiation and recruitment of histone acetylase activity on the myogenin promoter. Upon Wnt3a stimulation, we observe myogenin binding to an E-box element not occupied during proliferating conditions (Figure 3D, S1). This binding of myogenin upstream of follistatin, to a potential regulatory E-box element, suggests that myogenin is directly involved in regulating follistatin expression, both during differentiation and following the Wnt3a induced precocious differentiation.

Following injury-induced regeneration, we observed that treatment with a GSK3β antagonist further potentiated the differentiation effects of canonical Wnt signalling (Figure 4B,C). Specifically, further induction of myogenic genes and follistatin expression induced rapid differentiation of regenerating fibres, resulting in premature fusion and production of an increased number of smaller fibres (Figure 4C,D). The application of a pharmacological antagonist, which replicates observations from plasmid electroporation and protein injections, remains promising as it provides efficient delivery and dispersion within structured skeletal muscle. The Wnt pathway has been implicated as a key regulator of myogenic commitment and terminal differentiation (Anakwe et al., 2003; Brack et al., 2008), in addition to potentially regulating myogenic fate during cell aging (Brack et al.,

2007). While further analysis remains necessary, the differentiation potential of myogenic progenitors may undergo transcriptional regulation by extrinsically secreted Wnt molecules within the muscle fibre milieu, further providing the necessary control to regulate the highly orchestrated regenerative potential.

The equilibrium between follistatin and myostatin *in vivo* during muscle maturation has been extensively studied. During development, follistatin complexes with myostatin and antagonizes the myostatin-mediated inhibition of myogenesis (Amthor et al., 2004; Amthor et al., 2006). Initial studies suggested that follistatin promotes muscle hypertrophy by inhibiting the repressive effects of myostatin (Lee and McPherron, 2001; Nakamura et al., 1990), however, the muscle dependent effects of follistatin expression can be recapitulated in myostatin-null mice (Lee, 2007; Lee et al., 2010). As previously discussed, the ability of follistatin to potentiate the mTOR/S6K/S6RP-signalling cascade leads to muscle hypertrophy (Winbanks et al., 2012). In addition, the myostatin-dependent repressive effects on muscle growth attenuate Akt/mTOR signalling (Morissette et al., 2006; Ruvinsky et al., 2009), suggesting that myostatin inhibition may stimulate Akt/mTOR to promote muscle hypertrophy by a similar downstream mechanism as follistatin. Follistatin-null mice are perinatal lethal, displaying severe defects in growth and muscle development (Matzuk et al., 1995). However, follistatin overexpression leads to a greater myogenic potential, independent of myostatin expression, and enhanced myoblast engraftment (Benabdallah et al., 2009). Within this study, we observe that the pro-differentiation effects of follistatin occurred independent of changes in myostatin expression. These results further implicate the ability of follistatin to promote myogenic differentiation, further enhanced in the presence of canonical Wnt signalling.

In this report, we describe a role for canonical Wnt/β-Catenin signalling to regulate follistatin expression during myogenesis. Moreover, we observed this regulation functions in a myogenin-dependent manner following canonical Wnt stimulation, and the siRNA-mediated inhibition of myogenin expression led to a loss of follistatin activation. Thus, these results provide a mechanistic framework that helps explain how canonical Wnt/β-Catenin signalling can promote early myogenic differentiation. These observations are corroborated by our previous *in vivo* electroporation of a Wnt3a-expressing plasmid, and the injection of recombinant Wnt3a proteins that both resulted in a massive alteration in muscle fusion and regeneration kinetics (Brack et al., 2008; Le Grand et al., 2009). These studies will be of great importance to find new target genes or small molecule compounds that can regulate muscle homeostasis and growth. Knowledge gained from this research on satellite cell differentiation will be of great benefit for the design of experimental therapies to treat myogenic degenerative disorders.

ACKNOWLEDGEMENTS

M.A.R. holds the Canada Research Chair in Molecular Genetics and is an International Research Scholar of the Howard Hughes Medical Institute. This work was supported by grants to M.A.R. from the Canadian Institutes of Health Research, Muscular Dystrophy Association, the National Institutes of Health, the Howard Hughes Medical Institute, the Canadian Stem Cell Network, and the Canada Research Chair Program. A.E.J. was supported by scholarships from the Natural Sciences and Engineering Research Council of Canada. The authors declare no conflict of interest.

REFERENCES

Almeida, M., Han, L., Martin-Millan, M., O'Brien, C.A., and Manolagas, S.C. (2007). Oxidative stress antagonizes Wnt signaling in osteoblast precursors by diverting beta-catenin from T cell factor- to forkhead box O-mediated transcription. J Biol Chem *282*, 27298-27305.

Amthor, H., Huang, R., McKinnell, I., Christ, B., Kambadur, R., Sharma, M., and Patel, K. (2002). The regulation and action of myostatin as a negative regulator of muscle development during avian embryogenesis. Dev Biol *251*, 241-257.

Amthor, H., Nicholas, G., McKinnell, I., Kemp, C.F., Sharma, M., Kambadur, R., and Patel, K. (2004). Follistatin complexes Myostatin and antagonises Myostatin-mediated inhibition of myogenesis. Dev Biol *270*, 19-30.

Amthor, H., Otto, A., Macharia, R., McKinnell, I., and Patel, K. (2006). Myostatin imposes reversible quiescence on embryonic muscle precursors. Dev Dyn *235*, 672-680.

Anakwe, K., Robson, L., Hadley, J., Buxton, P., Church, V., Allen, S., Hartmann, C., Harfe, B., Nohno, T., Brown, A.M.*, et al.* (2003). Wnt signalling regulates myogenic differentiation in the developing avian wing. Development *130*, 3503-3514.

Bajard, L., Relaix, F., Lagha, M., Rocancourt, D., Daubas, P., and Buckingham, M.E. (2006). A novel genetic hierarchy functions during hypaxial myogenesis: Pax3 directly activates Myf5 in muscle progenitor cells in the limb. Genes Dev *20*, 2450-2464.

Benabdallah, B.F., Bouchentouf, M., Rousseau, J., and Tremblay, J.P. (2009). Overexpression of follistatin in human myoblasts increases their proliferation and differentiation, and improves the graft success in SCID mice. Cell Transplant *18*, 709-718.

Bentzinger, C.F., Wang, Y.X., and Rudnicki, M.A. (2012). Building muscle: molecular regulation of myogenesis. Cold Spring Harb Perspect Biol *4*.

Berkes, C.A., and Tapscott, S.J. (2005). MyoD and the transcriptional control of myogenesis. Semin Cell Dev Biol *16*, 585-595.

Brack, A.S., Conboy, I.M., Conboy, M.J., Shen, J., and Rando, T.A. (2008). A temporal switch from notch to Wnt signaling in muscle stem cells is necessary for normal adult myogenesis. Cell Stem Cell *2*, 50-59.

Brack, A.S., Conboy, M.J., Roy, S., Lee, M., Kuo, C.J., Keller, C., and Rando, T.A. (2007). Increased Wnt signaling during aging alters muscle stem cell fate and increases fibrosis. Science *317*, 807-810.

Chen, W., Fu, X., and Sheng, Z. (2002). Review of current progress in the structure and function of Smad proteins. Chin Med J (Engl) *115*, 446-450.

Clevers, H. (2006). Wnt/beta-catenin signaling in development and disease. Cell *127*, 469-480.

Collins, C.A., Olsen, I., Zammit, P.S., Heslop, L., Petrie, A., Partridge, T.A., and Morgan, J.E. (2005). Stem cell function, self-renewal, and behavioral heterogeneity of cells from the adult muscle satellite cell niche. Cell *122*, 289-301.

Conboy, I.M., and Rando, T.A. (2002). The regulation of Notch signaling controls satellite cell activation and cell fate determination in postnatal myogenesis. Dev Cell *3*, 397-409.

Faralli, H., and Dilworth, F.J. (2012). Turning on myogenin in muscle: a paradigm for understanding mechanisms of tissue-specific gene expression. Comp Funct Genomics *2012*, 836374.

Gentleman, R.C., Carey, V.J., Bates, D.M., Bolstad, B., Dettling, M., Dudoit, S., Ellis, B., Gautier, L., Ge, Y., Gentry, J.*, et al.* (2004). Bioconductor: open software development for computational biology and bioinformatics. Genome Biol *5*, R80.

Glass, D.J. (2005). Skeletal muscle hypertrophy and atrophy signaling pathways. Int J Biochem Cell Biol *37*, 1974-1984.

Grumolato, L., Liu, G., Mong, P., Mudbhary, R., Biswas, R., Arroyave, R., Vijayakumar, S., Economides, A.N., and Aaronson, S.A. (2010). Canonical and noncanonical Wnts use a common mechanism to activate completely unrelated coreceptors. Genes Dev *24*, 2517-2530.

Han, X.H., Jin, Y.R., Seto, M., and Yoon, J.K. (2011). A WNT/beta-catenin signaling activator, R-spondin, plays positive regulatory roles during skeletal myogenesis. J Biol Chem *286*, 10649-10659.

Hemmati-Brivanlou, A., Kelly, O.G., and Melton, D.A. (1994). Follistatin, an antagonist of activin, is expressed in the Spemann organizer and displays direct neuralizing activity. Cell *77*, 283-295.

Holterman, C.E., Le Grand, F., Kuang, S., Seale, P., and Rudnicki, M.A. (2007). Megf10 regulates the progression of the satellite cell myogenic program. J Cell Biol *179*, 911-922.

Hu, P., Geles, K.G., Paik, J.H., DePinho, R.A., and Tjian, R. (2008). Codependent activators direct myoblast-specific MyoD transcription. Dev Cell *15*, 534-546.

Huang, D.W., Sherman, B.T., and Lempicki, R.A. (2009a). Bioinformatics enrichment tools: paths toward the comprehensive functional analysis of large gene lists. Nucleic Acids Res *37*, 1-13.

Huang, D.W., Sherman, B.T., and Lempicki, R.A. (2009b). Systematic and integrative analysis of large gene lists using DAVID bioinformatics resources. Nat Protoc *4*, 44-57.

Hutcheson, D.A., Zhao, J., Merrell, A., Haldar, M., and Kardon, G. (2009). Embryonic and fetal limb myogenic cells are derived from developmentally distinct progenitors and have different requirements for beta-catenin. Genes Dev *23*, 997-1013.

Iemura, S., Yamamoto, T.S., Takagi, C., Uchiyama, H., Natsume, T., Shimasaki, S., Sugino, H., and Ueno, N. (1998). Direct binding of follistatin to a complex of bone-morphogenetic protein and its receptor inhibits ventral and epidermal cell fates in early Xenopus embryo. Proc Natl Acad Sci U S A *95*, 9337-9342.

Irizarry, R.A., Hobbs, B., Collin, F., Beazer-Barclay, Y.D., Antonellis, K.J., Scherf, U., and Speed, T.P. (2003). Exploration, normalization, and summaries of high density oligonucleotide array probe level data. Biostatistics *4*, 249-264.

Kaidi, A., Williams, A.C., and Paraskeva, C. (2007). Interaction between beta-catenin and HIF-1 promotes cellular adaptation to hypoxia. Nat Cell Biol *9*, 210-217.

Katoh, M. (2007). WNT signaling pathway and stem cell signaling network. Clin Cancer Res *13*, 4042-4045.

Kim, C.H., Neiswender, H., Baik, E.J., Xiong, W.C., and Mei, L. (2008). Beta-catenin interacts with MyoD and regulates its transcription activity. Mol Cell Biol *28*, 2941-2951.

Kioussi, C., Briata, P., Baek, S.H., Rose, D.W., Hamblet, N.S., Herman, T., Ohgi, K.A., Lin, C., Gleiberman, A., Wang, J.*, et al.* (2002). Identification of a Wnt/Dvl/beta-Catenin --> Pitx2 pathway mediating cell-type-specific proliferation during development. Cell *111*, 673-685.

Kormish, J.D., Sinner, D., and Zorn, A.M. (2010). Interactions between SOX factors and Wnt/beta-catenin signaling in development and disease. Dev Dyn *239*, 56-68.

Kuang, S., Charge, S.B., Seale, P., Huh, M., and Rudnicki, M.A. (2006). Distinct roles for Pax7 and Pax3 in adult regenerative myogenesis. J Cell Biol *172*, 103-113.

Kuang, S., Kuroda, K., Le Grand, F., and Rudnicki, M.A. (2007). Asymmetric self-renewal and commitment of satellite stem cells in muscle. Cell *129*, 999-1010.

Langley, B., Thomas, M., Bishop, A., Sharma, M., Gilmour, S., and Kambadur, R. (2002). Myostatin inhibits myoblast differentiation by down-regulating MyoD expression. J Biol Chem *277*, 49831-49840.

Le Grand, F., Jones, A.E., Seale, V., Scime, A., and Rudnicki, M.A. (2009). Wnt7a activates the planar cell polarity pathway to drive the symmetric expansion of satellite stem cells. Cell Stem Cell *4*, 535-547.

Lee, S.-J., and McPherron, A.C. (2001). Regulation of myostatin activity and muscle growth. Proceedings of the National Academy of Sciences *98*, 9306-9311.

Lee, S.J. (2007). Quadrupling muscle mass in mice by targeting TGF-beta signaling pathways. PLoS One *2*, e789.

Lee, S.J., Lee, Y.S., Zimmers, T.A., Soleimani, A., Matzuk, M.M., Tsuchida, K., Cohn, R.D., and Barton, E.R. (2010). Regulation of muscle mass by follistatin and activins. Mol Endocrinol *24*, 1998-2008.

Lee, S.J., Reed, L.A., Davies, M.V., Girgenrath, S., Goad, M.E., Tomkinson, K.N., Wright, J.F., Barker, C., Ehrmantraut, G., Holmstrom, J.*, et al.* (2005). Regulation of muscle growth by multiple ligands signaling through activin type II receptors. Proc Natl Acad Sci U S A *102*, 18117-18122.

Liu, Q.C., Zha, X.H., Faralli, H., Yin, H., Louis-Jeune, C., Perdiguero, E., Pranckeviciene, E., Munoz-Canoves, P., Rudnicki, M.A., Brand, M.*, et al.* (2012). Comparative expression profiling identifies differential roles for Myogenin and p38alpha MAPK signaling in myogenesis. J Mol Cell Biol *4*, 386-397.

Logan, C.Y., and Nusse, R. (2004). The Wnt signaling pathway in development and disease. Annu Rev Cell Dev Biol *20*, 781-810.

MacDonald, B.T., Tamai, K., and He, X. (2009). Wnt/beta-catenin signaling: components, mechanisms, and diseases. Dev Cell *17*, 9-26.

Matzuk, M.M., Lu, N., Vogel, H., Sellheyer, K., Roop, D.R., and Bradley, A. (1995). Multiple defects and perinatal death in mice deficient in follistatin. Nature *374*, 360-363.

Mauro, A. (1961). Satellite cell of skeletal muscle fibers. J Biophys Biochem Cytol *9*, 493-495.

McFarlane, C., Hennebry, A., Thomas, M., Plummer, E., Ling, N., Sharma, M., and Kambadur, R. (2008). Myostatin signals through Pax7 to regulate satellite cell self-renewal. Exp Cell Res *314*, 317-329.

McKinnell, I.W., Ishibashi, J., Le Grand, F., Punch, V.G., Addicks, G.C., Greenblatt, J.F., Dilworth, F.J., and Rudnicki, M.A. (2008). Pax7 activates myogenic genes by recruitment of a histone methyltransferase complex. Nat Cell Biol *10*, 77-84.

McPherron, A.C., Lawler, A.M., and Lee, S.J. (1997). Regulation of skeletal muscle mass in mice by a new TGF-beta superfamily member. Nature *387*, 83-90.

Megeney, L.A., Kablar, B., Garrett, K., Anderson, J.E., and Rudnicki, M.A. (1996). MyoD is required for myogenic stem cell function in adult skeletal muscle. Genes Dev *10*, 1173-1183.

Montarras, D., Morgan, J., Collins, C., Relaix, F., Zaffran, S., Cumano, A., Partridge, T., and Buckingham, M. (2005). Direct isolation of satellite cells for skeletal muscle regeneration. Science *309*, 2064-2067.

Morissette, M.R., Cook, S.A., Foo, S., McKoy, G., Ashida, N., Novikov, M., Scherrer-Crosbie, M., Li, L., Matsui, T., Brooks, G.*, et al.* (2006). Myostatin regulates cardiomyocyte growth through modulation of Akt signaling. Circ Res *99*, 15-24.

Mulholland, D.J., Dedhar, S., Coetzee, G.A., and Nelson, C.C. (2005). Interaction of nuclear receptors with the Wnt/beta-catenin/Tcf signaling axis: Wnt you like to know? Endocr Rev *26*, 898-915.

Munsterberg, A.E., Kitajewski, J., Bumcrot, D.A., McMahon, A.P., and Lassar, A.B. (1995). Combinatorial signaling by Sonic hedgehog and Wnt family members induces myogenic bHLH gene expression in the somite. Genes Dev *9*, 2911-2922.

Nadal-Ginard, B. (1978). Commitment, fusion and biochemical differentiation of a myogenic cell line in the absence of DNA synthesis. Cell *15*, 855-864.

Nakamura, T., Takio, K., Eto, Y., Shibai, H., Titani, K., and Sugino, H. (1990). Activin-binding protein from rat ovary is follistatin. Science *247*, 836-838.

Nelson, W.J., and Nusse, R. (2004). Convergence of Wnt, beta-catenin, and cadherin pathways. Science *303*, 1483-1487.

Nusse, R. (2012). Wnt signaling. Cold Spring Harb Perspect Biol *4*.

O'Donnell, K.A., Wentzel, E.A., Zeller, K.I., Dang, C.V., and Mendell, J.T. (2005). c-Myc-regulated microRNAs modulate E2F1 expression. Nature *435*, 839-843.

Olson, L.E., Tollkuhn, J., Scafoglio, C., Krones, A., Zhang, J., Ohgi, K.A., Wu, W., Taketo, M.M., Kemler, R., Grosschedl, R.*, et al.* (2006). Homeodomain-mediated beta-catenin-dependent switching events dictate cell-lineage determination. Cell *125*, 593-605.

Otto, A., Schmidt, C., Luke, G., Allen, S., Valasek, P., Muntoni, F., Lawrence-Watt, D., and Patel, K. (2008). Canonical Wnt signalling induces satellite-cell proliferation during adult skeletal muscle regeneration. J Cell Sci *121*, 2939-2950.

Polesskaya, A., Seale, P., and Rudnicki, M.A. (2003). Wnt signaling induces the myogenic specification of resident CD45+ adult stem cells during muscle regeneration. Cell *113*, 841-852.

Polychronopoulos, P., Magiatis, P., Skaltsounis, A.L., Myrianthopoulos, V., Mikros, E., Tarricone, A., Musacchio, A., Roe, S.M., Pearl, L., Leost, M.*, et al.* (2004). Structural basis for the synthesis of indirubins as potent and selective inhibitors of glycogen synthase kinase-3 and cyclin-dependent kinases. J Med Chem *47*, 935-946.

Reich, M., Liefeld, T., Gould, J., Lerner, J., Tamayo, P., and Mesirov, J.P. (2006). GenePattern 2.0. Nat Genet *38*, 500-501.

Rochat, A., Fernandez, A., Vandromme, M., Moles, J.P., Bouschet, T., Carnac, G., and Lamb, N.J. (2004). Insulin and wnt1 pathways cooperate to induce reserve cell activation in differentiation and myotube hypertrophy. Mol Biol Cell *15*, 4544-4555.

Rosenthal, N. (1989). Muscle cell differentiation. Curr Opin Cell Biol *1*, 1094-1101.

Rozen, S., and Skaletsky, H. (2000). Primer3 on the WWW for general users and for biologist programmers. Methods Mol Biol *132*, 365-386.

Ruvinsky, I., Katz, M., Dreazen, A., Gielchinsky, Y., Saada, A., Freedman, N., Mishani, E., Zimmerman, G., Kasir, J., and Meyuhas, O. (2009). Mice deficient in ribosomal protein S6 phosphorylation suffer from muscle weakness that reflects a growth defect and energy deficit. PLoS One *4*, e5618.

Schultz, E., Gibson, M.C., and Champion, T. (1978). Satellite cells are mitotically quiescent in mature mouse muscle: an EM and radioautographic study. J Exp Zool *206*, 451-456.

Schwender, H. (2009). siggenes: Multiple testing using SAM and Efron's empirical Bayes approaches. R package version 1200.

Seale, P., Sabourin, L.A., Girgis-Gabardo, A., Mansouri, A., Gruss, P., and Rudnicki, M.A. (2000). Pax7 is required for the specification of myogenic satellite cells. Cell *102*, 777-786.

Soleimani, V.D., Punch, V.G., Kawabe, Y., Jones, A.E., Palidwor, G.A., Porter, C.J., Cross, J.W., Carvajal, J.J., Kockx, C.E., van, I.W.F.*, et al.* (2012a). Transcriptional dominance of Pax7 in adult myogenesis is due to high-affinity recognition of homeodomain motifs. Dev Cell *22*, 1208-1220.

Soleimani, V.D., Yin, H., Jahani-Asl, A., Ming, H., Kockx, C.E., van Ijcken, W.F., Grosveld, F., and Rudnicki, M.A. (2012b). Snail regulates MyoD binding-site occupancy to direct enhancer switching and differentiation-specific transcription in myogenesis. Mol Cell *47*, 457-468.

Sylvestre, Y., De Guire, V., Querido, E., Mukhopadhyay, U.K., Bourdeau, V., Major, F., Ferbeyre, G., and Chartrand, P. (2007). An E2F/miR-20a autoregulatory feedback loop. J Biol Chem *282*, 2135-2143.

Tusher, V.G., Tibshirani, R., and Chu, G. (2001). Significance analysis of microarrays applied to the ionizing radiation response. Proc Natl Acad Sci U S A *98*, 5116-5121.

van der Velden, J.L., Langen, R.C., Kelders, M.C., Wouters, E.F., Janssen-Heininger, Y.M., and Schols, A.M. (2006). Inhibition of glycogen synthase kinase-3beta activity is sufficient to stimulate myogenic differentiation. Am J Physiol Cell Physiol *290*, C453-462.

von Maltzahn, J., Chang, N.C., Bentzinger, C.F., and Rudnicki, M.A. (2012). Wnt signaling in myogenesis. Trends Cell Biol *22*, 602-609.

Weintraub, H. (1993). The MyoD family and myogenesis: redundancy, networks, and thresholds. Cell *75*, 1241-1244.

Winbanks, C.E., Weeks, K.L., Thomson, R.E., Sepulveda, P.V., Beyer, C., Qian, H., Chen, J.L., Allen, J.M., Lancaster, G.I., Febbraio, M.A.*, et al.* (2012). Follistatin-mediated skeletal muscle hypertrophy is regulated by Smad3 and mTOR independently of myostatin. The Journal of Cell Biology *197*, 997-1008.

Zammit, P.S., Golding, J.P., Nagata, Y., Hudon, V., Partridge, T.A., and Beauchamp, J.R. (2004). Muscle satellite cells adopt divergent fates: a mechanism for self-renewal? J Cell Biol *166*, 347-357.

Zhao, P., and Hoffman, E.P. (2004). Embryonic myogenesis pathways in muscle regeneration. Dev Dyn *229*, 380-392.

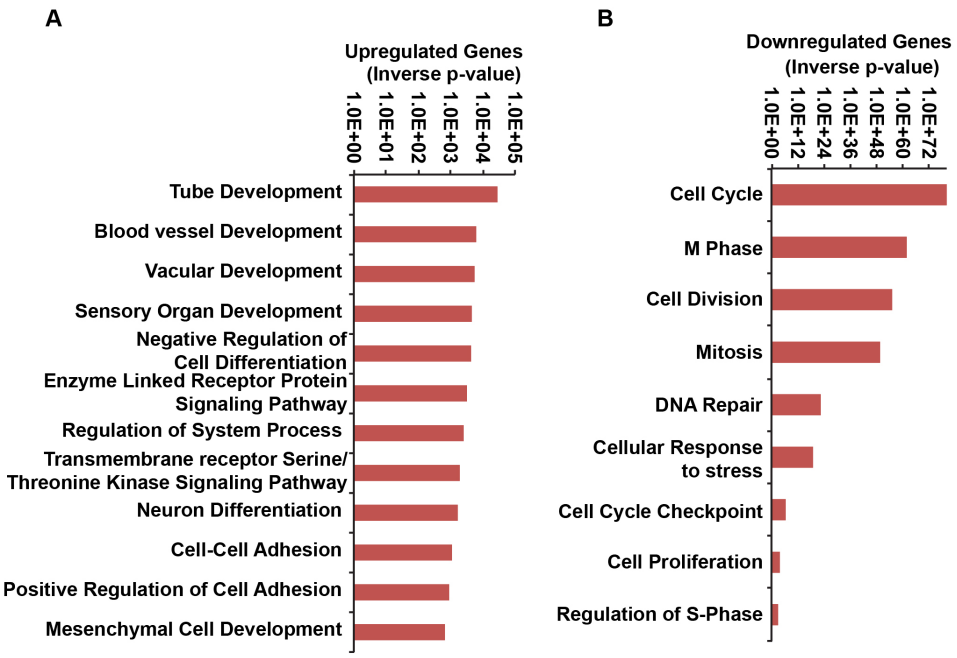

Figure S1. Enriched Gene Ontology terms following Wnt3a treatment
(A) Gene Ontology terms enriched among upregulated genes following Wnt3a stimulation for 24 hours relative to BSA control.
(B) Gene Ontology terms enriched among downregulated genes following Wnt3a stimulation for 24 hours relative to BSA control. Interestingly, many categories related to Cell Cycle, Cell Division, and Proliferation were enriched.

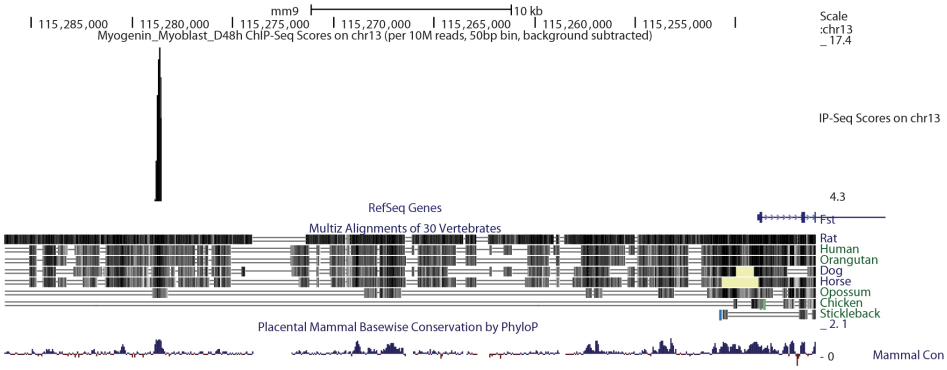

Figure S2. Myogenin binding site upstream of the follistatin locus
Myogenin peaks mapped to the UCSC genome brower, with scale set to automatic. Shown is bound motif 30 kb upstream of follistatin bound by myogenin following induction of 2 days differentiation (Rudnicki lab, *unpublished data*).

Table S1. Primer Sequences

Real Time RT-PCR	
Gja5_F	CAGAGCCTGAAGAAGCCAAC
Gja5_R	GCAACCAGGCTGAATGGTAT
Gcom_F	TTGTGGACGTGACTTTGGAA
Gcom_R	ATTGGCTTCTTGCGATGACT
Lrtm1_F	ACCCTTGGATTTGTGACTGC
Lrtm1_R	AGAACCAGGCTGCTGGACTA
Gdf6_F	CAATGCCAGCTTTTTCCAGT
Gdf6_R	CCCACCAGCTCTTCTTTGTC
Fst_F	GCTCCTGCTGCTGCTACTCT
Fst_R	CCCGTTGAAAATCATCCACT
Aldh1a2_F	CCATGACTTCCAGCGAGAT
Aldh1a2_R	CAGGGAACACTCTCCCACTC
Tgfb2_F	CCGGAGGTGATTTCCATCTA
Tgfb2_R	GCGGACGATTCTGAAGTAGG
Ccne2_F	GGCATGTTCACAGGAGGTTT
Ccne2_R	AATCCCAATGAGTTGAAGCA
E2F1_F	GACTCCTCGCAGATCGTCAT
E2F1_R	CAGCGAGGTACTGATGGTCA
Mki67_F	CAGACTTGCTCTGGCCTACC
Mki67_R	TGTCCACCAAAGGATACACG
Cenpk_F	CATTTTCCTCTGCCTGAAGC
Cenpk_R	TATGGTGGCCAAAAGGAATC
Pbk_F	GTGGAAGTCCTTTTCCAGCA
Pbk_R	TTCATCCAATGGCAGAGAGA
Aurkb_F	AGGTCTGCAGGGAGAACTGA
Aurkb_R	ACGTCTCACTGTGGCTAGGG
Axin2_F	CGACCTCAAGTGCAAACTCT
Axin2_R	CTGGATAACTCGCTGTCGTT
Myog_F	GAAGTGAATGAGGCCTTCG
Myog_R	ACGATGGACGTAAGGGAGTG
Mstn_F	GACAGCAGTGATGGCTCTTT
Mstn_R	TAGGAGTCTTGACGGGTCTG
Pax7_F	CTGGATGAGGGCTCAGATGT
Pax7_R	GGTTAGCTCCTGCCTGCTTA
Myh2_F	CAGAACAGAGACGGCTTCAT
Myh2_R	AGTTTCTCCCCAAACATCGT
GAPDH_F	TGTCCGTCGTGGATCTGAC
GAPDH_R	GGTCCTCAGTGTAGCCCAAG
ChIP	
GAPDH(-3kb)_F	TCCAGTGAGGACGGTATGAT
GAPDH(-3kb)_R	CATAAAGATGGGGCAAAATG
Fst(-30kb)_F	CTTTGTGCCCGTTTGAAAAT
Fst(-30kb)_R	GAAAGTGCCGCAAAGAAGAG

Table S2. Wnt3a Regulated Changes in Gene Expression

Gene Symbol	Ensembl ID	Fold Change	P-value
Gja5	ENSMUSG00000057123	12.5375	7.34E-42
Gcom1	ENSMUSG00000041361	6.2437	5.06E-28
Lrtm1	ENSMUSG00000045776	6.0716	5.92E-36
Slc16a4	ENSMUSG00000027896	5.8579	3.77E-33
Calca	ENSMUSG00000030669	5.4211	1.46E-32
Gdf6	ENSMUSG00000051279	4.5604	1.43E-38
Cd24a	ENSMUSG00000047139	4.3579	2.63E-25
Fst	ENSMUSG00000021765	3.8138	8.97E-44
Aldh1a2	ENSMUSG00000013584	3.5783	4.57E-09
Tgfb2	ENSMUSG00000039239	3.5448	0.00E+00
Bhlhe40	ENSMUSG00000030103	3.4108	1.52E-27
F5	ENSMUSG00000026579	3.1836	2.14E-09
Cadps	ENSMUSG00000054423	3.1473	1.14E-16
Stmn2	ENSMUSG00000027500	3.1203	5.27E-20
Prokr1	ENSMUSG00000049409	3.0486	4.90E-26
Clstn2	ENSMUSG00000032452	2.9915	5.85E-37
Odz4	ENSMUSG00000048078	2.9888	6.03E-26
H60b	ENSMUSG00000075297	2.8679	8.85E-11
Edn1	ENSMUSG00000021367	2.7636	5.30E-23
Inhbb	ENSMUSG00000037035	2.7634	4.98E-19
Pfn2	ENSMUSG00000027805	2.7620	3.84E-36
Sema3b	ENSMUSG00000057969	2.7464	0.00E+00
Slc16a2	ENSMUSG00000033965	2.7348	4.14E-24
Sp7	ENSMUSG00000060284	2.6793	7.61E-25
Padi2	ENSMUSG00000028927	2.6784	8.94E-34
Axin2	ENSMUSG00000000142	2.6729	8.47E-18
Mir206	ENSMUSG00000065559	2.6607	2.51E-35
Bmp2	ENSMUSG00000027358	2.6585	3.14E-17
Frmpd1	ENSMUSG00000035615	2.6449	0.00E+00
Col25a1	ENSMUSG00000058897	2.6381	1.59E-39
Syt13	ENSMUSG00000027220	2.6348	2.21E-34
Pla1a	ENSMUSG00000002847	2.6190	2.25E-26
Thy1	ENSMUSG00000032011	2.6052	5.27E-15
Gpm6b	ENSMUSG00000031342	2.5819	0.00E+00
Il33	ENSMUSG00000024810	2.5778	1.63E-26
Fam107a	ENSMUSG00000021750	2.5670	2.52E-26
Igfbp2	ENSMUSG00000039323	2.5480	1.70E-23
Tmem86a	ENSMUSG00000010307	2.5350	1.83E-28
Acsl3	ENSMUSG00000032883	2.5299	0.00E+00
Sema3d	ENSMUSG00000040254	2.5166	0.00E+00
Ifi205	ENSMUSG00000054203	2.4915	1.53E-14
Cyp1b1	ENSMUSG00000024087	2.4870	1.10E-13
Sema5a	ENSMUSG00000022231	2.4681	0.00E+00
Tnfrsf19	ENSMUSG00000060548	2.4339	0.00E+00
Cdc42ep2	ENSMUSG00000045664	2.4139	1.52E-30
Srgap1	ENSMUSG00000020121	2.4054	5.17E-27
Adamtsl2	ENSMUSG00000036040	2.3999	1.07E-23
Ch25h	ENSMUSG00000050370	2.3988	1.55E-16
Arl4a	ENSMUSG00000047446	2.3268	8.60E-35
Mir133b	ENSMUSG00000065480	2.3191	2.07E-36
Tmem123	ENSMUSG00000050912	2.2829	5.14E-45

Nrcam	ENSMUSG00000020598	2.2806	5.56E-32
Pcp4l1	ENSMUSG00000038370	2.2519	2.54E-11
Rasl11b	ENSMUSG00000049907	2.2502	7.85E-16
Stc2	ENSMUSG00000020303	2.2365	9.68E-26
Rxfp1	ENSMUSG00000034009	2.2284	0.00E+00
Col8a1	ENSMUSG00000068196	2.2132	2.79E-32
Fam198b	ENSMUSG00000027955	2.2092	1.08E-38
Cdk5r1	ENSMUSG00000048895	2.2071	1.99E-31
Frem2	ENSMUSG00000037016	2.2030	2.97E-38
Grik1	ENSMUSG00000022935	2.1871	4.65E-10
Baiap2l1	ENSMUSG00000038859	2.1769	0.00E+00
Tbc1d12	ENSMUSG00000048720	2.1705	4.69E-22
Gdnf	ENSMUSG00000022144	2.1651	1.30E-17
Tspan9	ENSMUSG00000030352	2.1586	2.56E-41
Gadd45b	ENSMUSG00000015312	2.1553	5.14E-30
Adamts5	ENSMUSG00000022894	2.1533	2.85E-34
Dll1	ENSMUSG00000014773	2.1360	7.68E-37
Ube2e2	ENSMUSG00000058317	2.1360	3.73E-36
2900062L11Rik	ENSMUSG00000048040	2.1217	6.25E-24
Nav3	ENSMUSG00000020181	2.1087	0.00E+00
Slc7a7	ENSMUSG00000000958	2.1046	1.11E-24
Tgm2	ENSMUSG00000037820	2.1044	2.56E-13
P4ha2	ENSMUSG00000018906	2.0864	4.44E-27
Itgb1bp3	ENSMUSG00000004939	2.0798	2.60E-32
Nkd1	ENSMUSG00000031661	2.0727	3.34E-19
Fgf9	ENSMUSG00000021974	2.0643	1.59E-33
AI464131	ENSMUSG00000046312	2.0608	3.48E-39
Scn5a	ENSMUSG00000032511	2.0582	9.14E-42
Ror1	ENSMUSG00000035305	2.0536	5.40E-16
5530400B01Rik	ENSMUSG00000043186	2.0516	8.36E-26
Gprc5c	ENSMUSG00000051043	2.0474	0.00E+00
Gadd45g	ENSMUSG00000021453	2.0467	7.13E-38
Ache	ENSMUSG00000023328	2.0366	1.07E-23
Epha3	ENSMUSG00000052504	2.0283	3.85E-17
Lmcd1	ENSMUSG00000057604	2.0279	7.66E-34
Pak3	ENSMUSG00000031284	2.0221	9.36E-38
Rab40b	ENSMUSG00000025170	2.0141	1.53E-23
Slc10a7	ENSMUSG00000031684	0.4996	3.81E-37
Gm5465	ENSMUSG00000075502	0.4994	4.84E-08
6720489N17Rik	ENSMUSG00000072066	0.4994	5.89E-09
Slc8a1	ENSMUSG00000054640	0.4962	1.01E-38
Gpr137b-ps	ENSMUSG00000075118	0.4961	9.46E-20
Snai2	ENSMUSG00000022676	0.4956	2.74E-40
Ska1	ENSMUSG00000036223	0.4956	3.73E-07
Vrk2	ENSMUSG00000064090	0.4952	5.63E-36
Bard1	ENSMUSG00000026196	0.4949	9.19E-10
Slc27a3	ENSMUSG00000027932	0.4941	2.09E-12
D330028D13Rik	ENSMUSG00000047115	0.4939	6.38E-11
Syce2	ENSMUSG00000003824	0.4935	2.75E-24
Mdc1	ENSMUSG00000061607	0.4921	3.32E-25
Avpr1a	ENSMUSG00000020123	0.4908	2.10E-14
Suv39h2	ENSMUSG00000026646	0.4893	5.28E-17
Hhip	ENSMUSG00000064325	0.4892	6.24E-14
Sh2d3c	ENSMUSG00000059013	0.4889	3.74E-15

E2f7	ENSMUSG00000020185	0.4888	2.42E-19
Zranb3	ENSMUSG00000036086	0.4876	2.00E-17
Prkcb	ENSMUSG00000052889	0.4875	1.56E-26
Pold1	ENSMUSG00000038644	0.4869	3.12E-17
Nid1	ENSMUSG00000005397	0.4861	1.48E-42
Syne2	ENSMUSG00000063450	0.4858	2.55E-11
Ndst3	ENSMUSG00000027977	0.4857	7.34E-16
Chaf1a	ENSMUSG00000002835	0.4846	1.35E-18
Efna5	ENSMUSG00000048915	0.4841	1.80E-27
Tmem48	ENSMUSG00000028614	0.4839	0.00E+00
Fads1	ENSMUSG00000010663	0.4836	4.67E-46
Cx3cl1	ENSMUSG00000031778	0.4836	8.50E-22
Apln	ENSMUSG00000037010	0.4832	5.31E-10
Topbp1	ENSMUSG00000032555	0.4829	1.68E-35
Rragb	ENSMUSG00000041658	0.4816	7.64E-13
4632419I22Rik	ENSMUSG00000085208	0.4791	1.26E-25
Rfc5	ENSMUSG00000029363	0.4751	1.70E-13
Vcam1	ENSMUSG00000027962	0.4750	0.00E+00
Msh2	ENSMUSG00000024151	0.4744	1.24E-28
Cyyr1	ENSMUSG00000041134	0.4722	8.64E-14
Prps2	ENSMUSG00000025742	0.4720	1.61E-41
Gm12181	ENSMUSG00000082250	0.4717	3.92E-18
Zfp125	ENSMUSG00000069755	0.4712	3.74E-45
Ckap2l	ENSMUSG00000048327	0.4710	8.67E-28
Dnajc9	ENSMUSG00000021811	0.4696	6.35E-27
Steap1	ENSMUSG00000015652	0.4686	5.44E-25
Fanca	ENSMUSG00000032815	0.4672	6.48E-20
Tmem171	ENSMUSG00000052485	0.4667	9.59E-13
Pla2g4a	ENSMUSG00000056220	0.4655	0.00E+00
Hn1l	ENSMUSG00000024165	0.4654	7.74E-29
BC048355	ENSMUSG00000040658	0.4650	2.72E-21
Bend6	ENSMUSG00000042182	0.4620	6.34E-31
1700007K13Rik	ENSMUSG00000026831	0.4610	7.80E-16
Dck	ENSMUSG00000029366	0.4607	1.28E-20
Myo1b	ENSMUSG00000018417	0.4606	8.41E-34
Mertk	ENSMUSG00000014361	0.4605	1.35E-21
9030425E11Rik	ENSMUSG00000032024	0.4599	2.99E-16
Cntln	ENSMUSG00000038070	0.4589	1.12E-28
Msh6	ENSMUSG00000005370	0.4569	5.17E-25
Polq	ENSMUSG00000034206	0.4561	2.42E-14
Cdc7	ENSMUSG00000029283	0.4553	2.74E-12
Usp1	ENSMUSG00000028560	0.4553	3.83E-19
Srd5a1	ENSMUSG00000021594	0.4539	4.84E-17
Gsg2	ENSMUSG00000050107	0.4536	4.24E-12
Blm	ENSMUSG00000030528	0.4528	5.95E-40
Cit	ENSMUSG00000029516	0.4525	1.26E-25
Haus6	ENSMUSG00000038047	0.4507	3.27E-38
Prrg4	ENSMUSG00000027171	0.4497	1.60E-32
Pask	ENSMUSG00000026274	0.4483	1.34E-16
Rpp25	ENSMUSG00000062309	0.4481	1.10E-05
4930534B04Rik	ENSMUSG00000061533	0.4467	3.74E-13
Ptgs1	ENSMUSG00000047250	0.4461	3.18E-32
Mme	ENSMUSG00000027820	0.4449	0.00E+00
Dnmt1	ENSMUSG00000004099	0.4435	0.00E+00

Etaa1	ENSMUSG00000016984	0.4422	2.54E-17
Sfxn1	ENSMUSG00000021474	0.4409	2.67E-34
Ccne1	ENSMUSG00000002068	0.4405	1.99E-42
Dscc1	ENSMUSG00000022422	0.4400	6.59E-07
Cenpm	ENSMUSG00000068101	0.4397	5.70E-14
Cdc45	ENSMUSG00000000028	0.4397	2.85E-27
Gfra1	ENSMUSG00000025089	0.4393	5.63E-25
Donson	ENSMUSG00000022960	0.4381	4.55E-19
Mcm2	ENSMUSG00000002870	0.4379	1.54E-36
Mcm8	ENSMUSG00000027353	0.4365	2.84E-28
Cenpp	ENSMUSG00000021391	0.4354	2.14E-15
Olfr1372-ps1	ENSMUSG00000084141	0.4351	1.92E-08
Eps8	ENSMUSG00000015766	0.4315	0.00E+00
Nmnat2	ENSMUSG00000042751	0.4311	9.30E-18
Dmp1	ENSMUSG00000029307	0.4301	6.53E-14
Fat4	ENSMUSG00000046743	0.4299	1.34E-18
Cenpl	ENSMUSG00000026708	0.4276	9.45E-16
Atad5	ENSMUSG00000017550	0.4274	7.09E-26
Ccdc34	ENSMUSG00000027160	0.4266	9.32E-26
Nsl1	ENSMUSG00000062510	0.4260	1.13E-11
Rfc4	ENSMUSG00000022881	0.4252	3.74E-44
Vav3	ENSMUSG00000033721	0.4248	2.77E-43
Gas7	ENSMUSG00000033066	0.4246	6.77E-14
Fam19a5	ENSMUSG00000054863	0.4217	1.04E-26
Smc4	ENSMUSG00000034349	0.4203	0.00E+00
Spc24	ENSMUSG00000074476	0.4184	1.54E-13
6720463M24Rik	ENSMUSG00000022070	0.4181	1.88E-21
Trim59	ENSMUSG00000034317	0.4172	1.05E-32
Cxcl13	ENSMUSG00000023078	0.4167	3.64E-12
Orc1	ENSMUSG00000028587	0.4146	4.76E-09
Fads2	ENSMUSG00000024665	0.4130	8.53E-31
4930422G04Rik	ENSMUSG00000051278	0.4129	1.79E-18
Wdr76	ENSMUSG00000027242	0.4125	3.14E-22
Lonrf3	ENSMUSG00000016239	0.4077	2.00E-10
Mcm7	ENSMUSG00000029730	0.4072	7.01E-24
Ces2g	ENSMUSG00000031877	0.4068	3.56E-09
Prim2	ENSMUSG00000026134	0.4063	1.01E-33
Mcm4	ENSMUSG00000022673	0.4063	2.02E-41
Wee1	ENSMUSG00000031016	0.4059	5.37E-34
2610021K21Rik	ENSMUSG00000021176	0.4059	7.24E-12
Sass6	ENSMUSG00000027959	0.4056	7.96E-39
Troap	ENSMUSG00000032783	0.4054	2.42E-18
Mybl2	ENSMUSG00000017861	0.4037	4.73E-10
Gtse1	ENSMUSG00000022385	0.4032	5.34E-33
Abcb1b	ENSMUSG00000028970	0.4019	3.15E-12
Tacc3	ENSMUSG00000037313	0.3993	1.27E-32
Cdc6	ENSMUSG00000017499	0.3983	6.43E-10
Ppil5	ENSMUSG00000034883	0.3978	2.70E-09
Arhgap11a	ENSMUSG00000041219	0.3933	4.53E-36
Cdk1	ENSMUSG00000019942	0.3933	6.80E-29
Tipin	ENSMUSG00000032397	0.3929	1.78E-35
Cd200	ENSMUSG00000022661	0.3914	4.76E-20
Rgs5	ENSMUSG00000026678	0.3875	4.67E-46
Dut	ENSMUSG00000027203	0.3866	5.17E-24

Iqgap3	ENSMUSG00000028068	0.3859	2.05E-17
Sema6d	ENSMUSG00000027200	0.3851	0.00E+00
Ncapd2	ENSMUSG00000038252	0.3840	6.06E-32
Lmnb1	ENSMUSG00000024590	0.3837	2.37E-26
Ccdc18	ENSMUSG00000056531	0.3836	8.69E-14
Adcyap1r1	ENSMUSG00000029778	0.3830	7.82E-30
Rbl1	ENSMUSG00000027641	0.3813	0.00E+00
Ngf	ENSMUSG00000027859	0.3806	2.31E-15
C3ar1	ENSMUSG00000040552	0.3790	6.68E-11
Pde3b	ENSMUSG00000030671	0.3790	6.74E-28
Fam54a	ENSMUSG00000019992	0.3789	1.58E-13
Hist1h1a	ENSMUSG00000049539	0.3781	4.59E-23
Dhfr	ENSMUSG00000021707	0.3776	1.35E-24
BC030867	ENSMUSG00000034773	0.3769	5.59E-12
Espl1	ENSMUSG00000058290	0.3753	3.02E-11
Eme1	ENSMUSG00000039055	0.3752	9.35E-14
Cdca3	ENSMUSG00000023505	0.3748	3.89E-19
Zdhhc2	ENSMUSG00000039470	0.3742	8.95E-20
Mns1	ENSMUSG00000032221	0.3732	4.73E-18
Hist1h4f	ENSMUSG00000069274	0.3708	3.89E-08
Fanci	ENSMUSG00000039187	0.3691	7.67E-22
Mms22l	ENSMUSG00000045751	0.3682	1.49E-31
Slc5a3	ENSMUSG00000089774	0.3681	3.75E-35
Rad51ap1	ENSMUSG00000030346	0.3667	1.89E-16
Cenpw	ENSMUSG00000075266	0.3662	1.61E-05
Gas2l3	ENSMUSG00000074802	0.3658	7.41E-35
Fbxo48	ENSMUSG00000044966	0.3655	3.74E-09
Mad2l1	ENSMUSG00000029910	0.3645	3.21E-36
Fam83d	ENSMUSG00000027654	0.3635	6.01E-30
Ercc6l	ENSMUSG00000051220	0.3619	1.99E-11
Ckap2	ENSMUSG00000037725	0.3611	8.99E-25
4632434I11Rik	ENSMUSG00000030641	0.3609	3.95E-34
Hist2h2bb	ENSMUSG00000050936	0.3591	4.44E-15
Rad54b	ENSMUSG00000078773	0.3572	2.51E-21
Cdkn3	ENSMUSG00000037628	0.3566	7.20E-16
Pcsk1	ENSMUSG00000021587	0.3561	2.55E-08
Dbf4	ENSMUSG00000002297	0.3548	1.74E-43
Clspn	ENSMUSG00000042489	0.3534	7.43E-12
Arhgap19	ENSMUSG00000025154	0.3528	8.19E-26
Mcm5	ENSMUSG00000005410	0.3525	7.31E-31
Smc2	ENSMUSG00000028312	0.3522	2.60E-29
Ccnb2	ENSMUSG00000032218	0.3521	4.29E-35
Nr4a2	ENSMUSG00000026826	0.3516	4.53E-36
Rps6ka6	ENSMUSG00000025665	0.3507	6.50E-13
Incenp	ENSMUSG00000024660	0.3505	4.63E-30
Hist1h1b	ENSMUSG00000058773	0.3504	3.76E-30
Dna2	ENSMUSG00000036875	0.3473	1.69E-20
Lig1	ENSMUSG00000056394	0.3468	4.36E-22
Mcm10	ENSMUSG00000026669	0.3462	4.39E-20
Cdca7	ENSMUSG00000055612	0.3459	4.96E-14
Fignl1	ENSMUSG00000035455	0.3447	7.77E-18
Rad54l	ENSMUSG00000028702	0.3442	7.23E-19
Cdca7l	ENSMUSG00000021175	0.3439	3.18E-19
Cldn1	ENSMUSG00000022512	0.3439	9.43E-05

Prc1	ENSMUSG00000038943	0.3420	3.76E-33
Gm8773	ENSMUSG00000073234	0.3420	7.39E-10
Ect2	ENSMUSG00000027699	0.3413	2.37E-36
Entpd1	ENSMUSG00000048120	0.3399	3.28E-07
Slc43a3	ENSMUSG00000027074	0.3372	2.19E-33
Foxm1	ENSMUSG00000001517	0.3366	7.43E-20
Cenpq	ENSMUSG00000023919	0.3346	1.01E-29
Aurka	ENSMUSG00000027496	0.3339	4.44E-31
Racgap1	ENSMUSG00000023015	0.3324	7.18E-32
Kcnh5	ENSMUSG00000034402	0.3316	3.09E-12
Gins1	ENSMUSG00000027454	0.3312	2.63E-17
Plk4	ENSMUSG00000025758	0.3307	4.73E-41
Cenpa	ENSMUSG00000029177	0.3305	2.64E-24
Pole2	ENSMUSG00000020974	0.3292	6.12E-34
Gzmd	ENSMUSG00000059256	0.3285	2.13E-18
Birc5	ENSMUSG00000017716	0.3275	1.64E-18
Mcm6	ENSMUSG00000026355	0.3262	4.36E-39
Mlf1ip	ENSMUSG00000031629	0.3240	8.55E-17
Ndc80	ENSMUSG00000024056	0.3238	5.72E-15
Diap3	ENSMUSG00000022021	0.3225	2.86E-20
Cd34	ENSMUSG00000016494	0.3206	1.57E-17
Cenpf	ENSMUSG00000026605	0.3204	4.46E-37
Fancb	ENSMUSG00000047757	0.3202	4.72E-21
Cenpn	ENSMUSG00000031756	0.3192	1.76E-33
Chaf1b	ENSMUSG00000022945	0.3170	6.82E-24
Mcm3	ENSMUSG00000041859	0.3169	1.45E-25
Prr11	ENSMUSG00000020493	0.3157	2.67E-32
Tyms	ENSMUSG00000025747	0.3155	5.74E-14
Tpx2	ENSMUSG00000027469	0.3144	2.91E-37
Epha1	ENSMUSG00000029859	0.3129	2.41E-19
Fam64a	ENSMUSG00000020808	0.3120	2.09E-14
Pde1a	ENSMUSG00000059173	0.3118	2.10E-28
Tcf19	ENSMUSG00000050410	0.3118	1.69E-16
D2Ertd750e	ENSMUSG00000027331	0.3100	1.27E-33
Cdc20	ENSMUSG00000006398	0.3092	5.71E-16
Cdca2	ENSMUSG00000048922	0.3089	2.12E-24
Brca2	ENSMUSG00000041147	0.3078	1.02E-13
Uhrf1	ENSMUSG00000001228	0.3077	3.41E-14
Sgol2	ENSMUSG00000026039	0.3077	2.65E-27
Mybl1	ENSMUSG00000025912	0.3076	1.02E-38
Tk1	ENSMUSG00000025574	0.3062	6.92E-07
Plk1	ENSMUSG00000030867	0.3059	3.64E-23
Pola1	ENSMUSG00000006678	0.3044	3.87E-30
Ccna2	ENSMUSG00000027715	0.3042	0.00E+00
Hist1h2bb	ENSMUSG00000075031	0.3025	3.58E-15
Cenpi	ENSMUSG00000031262	0.3024	3.81E-35
Gm15697	ENSMUSG00000081670	0.3021	3.63E-05
Ccne2	ENSMUSG00000028212	0.3018	9.52E-34
Rgs4	ENSMUSG00000038530	0.2989	2.42E-14
C330027C09Rik	ENSMUSG00000033031	0.2988	0.00E+00
Kif20a	ENSMUSG00000003779	0.2986	0.00E+00
Cdc25c	ENSMUSG00000044201	0.2983	4.12E-16
Kif22	ENSMUSG00000030677	0.2982	2.00E-22
Ncaph	ENSMUSG00000034906	0.2972	7.40E-40

Kif23	ENSMUSG00000032254	0.2959	0.00E+00
Slc14a1	ENSMUSG00000059336	0.2951	3.58E-13
Mki67	ENSMUSG00000031004	0.2939	5.76E-42
Aspm	ENSMUSG00000033952	0.2925	2.66E-21
Stil	ENSMUSG00000028718	0.2923	3.93E-29
Cdca5	ENSMUSG00000024791	0.2922	1.89E-11
Ccnf	ENSMUSG00000072082	0.2920	2.14E-31
Oip5	ENSMUSG00000072980	0.2904	1.23E-16
Gm12387	ENSMUSG00000084220	0.2895	1.65E-11
Dlgap5	ENSMUSG00000037544	0.2891	1.59E-31
Wdhd1	ENSMUSG00000037572	0.2883	0.00E+00
4930547N16Rik	ENSMUSG00000035365	0.2877	1.49E-24
Spag5	ENSMUSG00000002055	0.2875	5.39E-20
Atad2	ENSMUSG00000022360	0.2875	1.38E-31
Nek2	ENSMUSG00000026622	0.2871	6.63E-20
Bub1b	ENSMUSG00000040084	0.2869	0.00E+00
Brca1	ENSMUSG00000017146	0.2860	1.20E-28
Aurkb	ENSMUSG00000020897	0.2848	5.20E-27
Zwilch	ENSMUSG00000032400	0.2834	2.16E-41
Cdca8	ENSMUSG00000028873	0.2834	6.75E-21
Kntc1	ENSMUSG00000029414	0.2833	0.00E+00
Melk	ENSMUSG00000035683	0.2831	8.14E-24
Mastl	ENSMUSG00000026779	0.2822	1.01E-41
5730590G19Rik	ENSMUSG00000046591	0.2801	1.23E-35
Chek1	ENSMUSG00000032113	0.2772	1.00E-30
Nusap1	ENSMUSG00000027306	0.2755	8.76E-36
Brip1	ENSMUSG00000034329	0.2752	1.35E-22
Fancd2	ENSMUSG00000034023	0.2750	2.66E-22
Top2a	ENSMUSG00000020914	0.2745	0.00E+00
Hist1h2ab	ENSMUSG00000061615	0.2720	1.10E-10
Trip13	ENSMUSG00000021569	0.2715	3.12E-22
Kif11	ENSMUSG00000012443	0.2710	0.00E+00
Sgol1	ENSMUSG00000023940	0.2686	3.42E-30
Apcdd1	ENSMUSG00000071847	0.2684	8.32E-15
Dtl	ENSMUSG00000037474	0.2684	8.25E-33
Scn9a	ENSMUSG00000075316	0.2674	2.06E-11
Spc25	ENSMUSG00000005233	0.2672	1.10E-27
Prim1	ENSMUSG00000025395	0.2659	1.47E-24
Reln	ENSMUSG00000042453	0.2630	0.00E+00
Exo1	ENSMUSG00000039748	0.2602	5.57E-16
Kif18a	ENSMUSG00000027115	0.2592	3.53E-25
Gen1	ENSMUSG00000051235	0.2579	1.16E-29
Hmmr	ENSMUSG00000020330	0.2570	0.00E+00
Shcbp1	ENSMUSG00000022322	0.2556	3.54E-25
Hells	ENSMUSG00000025001	0.2539	7.35E-33
Kif20b	ENSMUSG00000024795	0.2534	9.25E-24
Kif18b	ENSMUSG00000051378	0.2522	3.03E-24
Fam111a	ENSMUSG00000024691	0.2521	6.19E-31
Pole	ENSMUSG00000007080	0.2506	0.00E+00
Slfn9	ENSMUSG00000069793	0.2496	1.55E-13
Kif4	ENSMUSG00000034311	0.2487	1.50E-22
F630043A04Rik	ENSMUSG00000021965	0.2474	2.15E-27
Cenph	ENSMUSG00000045273	0.2472	9.52E-17
Ttk	ENSMUSG00000038379	0.2457	1.89E-26

Cenpe	ENSMUSG00000045328	0.2456	0.00E+00
Nuf2	ENSMUSG00000026683	0.2447	2.79E-32
Ncapg2	ENSMUSG00000042029	0.2435	2.70E-29
Kif15	ENSMUSG00000036768	0.2425	2.15E-29
Casc5	ENSMUSG00000027326	0.2416	4.08E-29
Kif2c	ENSMUSG00000028678	0.2416	2.03E-32
Neil3	ENSMUSG00000039396	0.2394	4.09E-26
Cep55	ENSMUSG00000024989	0.2377	1.66E-27
AC087117.1	ENSMUSG00000091747	0.2373	9.13E-26
Rad51	ENSMUSG00000027323	0.2373	2.29E-20
Cenpk	ENSMUSG00000021714	0.2328	5.40E-25
Ncapg	ENSMUSG00000015880	0.2262	0.00E+00
Pbk	ENSMUSG00000022033	0.2259	1.06E-13
Fbxo5	ENSMUSG00000019773	0.2199	2.15E-13
Bub1	ENSMUSG00000027379	0.2199	7.56E-34
C79407	ENSMUSG00000047534	0.2127	2.93E-35
Esco2	ENSMUSG00000022034	0.1982	1.07E-27
Cxcl12	ENSMUSG00000061353	0.1947	1.30E-30

Chapter 4 - General Discussion

Overview of Findings

As previously discussed in this thesis, the quiescent satellite cell compartment is activated following muscle growth or injury. Once activated, these cells rapidly upregulate the myogenic regulatory factors Myf5 and MyoD, which function as nodal points towards myogenic commitment (Weintraub et al., 1991a). This remains of particular interest as Myf5 expression is the earliest distinguishing factor between satellite stem cells (Pax7+;Myf5-), a population that can undergo asymmetric self-renewal and maintain the satellite cell pool, and committed myogenic satellite cells (Pax7+;Myf5+), which are destined for symmetric expansion as activated myoblasts. In contrast, expression of myogenin and MRF4 are required for the fusion and terminal differentiation of myoblasts, culminating in the generation of the functional unit of multinucleated muscle fibres. These biological events occur following the tightly orchestrated interplay of intrinsic molecular networks and extrinsic signalling pathways.

This body of work has focused on two aspects of satellite cell biology; examining the functional role of Pax7 splice variants (Chapter 2), and characterizing the downstream induction of differentiation by canonical Wnt signalling pathways (Chapter 3) in proliferating satellite cell-derived myoblasts.

While some functional redundancy exists between Pax3 and Pax7, the essential role of Pax7 during adult myogenesis is not compensated by Pax3 expression. More specifically, the ability of Pax7 to bind DNA and recruit the HMT complex establishes transcriptionally active chromatin domains, resulting in activation of target genes (McKinnell et al., 2008). As a result, Pax7 is involved in lineage survival through promoting satellite cell maintenance and expansion (Appendix A). Given its role as a DNA binding protein, we set

out to ascertain the potential role of the four Pax7 splice variants (Pax7a, Pax7b, Pax7c, Pax7d). Notably, these splice variants displayed varying abilities to activate target genes, a feature that was attributed to the GL+/- status within the third α-helix of the carboxyl-terminal paired subdomain. Given the abundance of Pax7d (Q+GL-) transcripts relative to the other splice variants, combined with its ability to preferentially activate myogenic target genes (for example, Myf5, Bmp4, Fgfr2 and Egfr), suggests that this isoform may play a predominant functional role during myogenesis.

Through its ability to bind DNA and recruit the HMT complex, an interesting role of Pax7 as a pioneer transcription factor has recently been described in pituitary cells (Budry et al., 2012). In general, the majority of transcription factors are unable to locate target sequences and bind transcriptionally inactive DNA due to the hindrance of nucleosomes and/or compacted chromatin. Pioneer transcription factors are a subset of factors that are able to access and stably bind their target DNA sequences in inactive heterochromatin preceeding the binding of other necessary transcription factors (Zaret and Carroll, 2011). Our data suggests that this pioneering ability may be limited to the GL- splice variants since it's able to activate Myf5 expression in non-myogenic cells, a unique feature distinguishing Pax7d from the other splice variants. The Forkheadbox transcription factor FoxA was among the first described pioneer factors (Gualdi et al., 1996). As discussed later, this protein belongs to the same family as FoxO1 (FKHR), who are known to translocate with Pax proteins and result in the manifestation of rhabdomyosarcomas (RMS), a soft tissue cancer that remains the most predominant type of malignancy in children. Combined, these observations provide insight into the functional characteristics of Pax7, specifically regarding its ability to bind DNA and activate target gene expression.

While previous studies have examined the ability of Pax proteins to undergo dimerization, a feature previously attributed to the homeodomain, we have demonstrated that this dimer potential is also extended to the Pax7 isoforms. This capacity to form homo- and heterodimers increases the structural organization of the Pax7 protein, and generates additional protein conformations with potentially varying DNA binding specificities. Given the relative abundance of the Pax7d transcript, it remains likely that many dimer complexes are composed of at least one Pax7d protein. In addition, previous studies have observed the interdependence of the Pax3 paired domain and homeodomain for DNA binding (Apuzzo et al., 2004; Fortin et al., 1998; Underhill and Gros, 1997). These findings further suggest that small changes within the paired domain, following alternative splicing events, may modulate the entire Pax protein complex, thus leading to a greater degree of target gene regulation.

In concert with maintaining the satellite cell pool, the ability of these cells to undergo differentiation, following myogenic expansion, remains critical for muscle function and survival. Wnt signalling is involved in the myogenic commitment of adult stem cells following injury, and studies have suggested that canonical Wnt signalling regulates myogenic differentiation through the activation of reserve myoblasts (Polesskaya et al., 2003; Rochat et al., 2004). While Notch signalling is activated and stimulates the proliferation of satellite cells, canonical Wnt/β-Catenin signalling promotes the progression of myogenic commitment and differentiation (Brack et al., 2008). Interestingly, the activation of canonical Wnt signalling induced premature differentiation *in vivo*, and drastically reduced the proliferative capacity of primary myoblasts *in vitro* (Appendix C). Of great interest was the ability of Wnt3a stimulation to activate the myogenin-dependent expression of follistatin. The established role of follistatin in promoting muscle hypertrophy

(Lee and McPherron, 2001), coupled with the characterized role of myogenin expression in promoting cell cycle withdrawal (Liu et al., 2012), led us to further examine the functional role of canonical Wnt stimulation during myogenesis.

The identification of a novel regulatory E-box element upstream of the follistatin promoter suggested a direct mechanistic ability for myogenin to regulate follistatin expression. As discussed in Chapter 3, this element is bound by the Snail repressive transcription factors during proliferative conditions, however, the induction of differentiation results in enhancer switching and the recruitment of myogenin to this regulatory E-box. Strikingly, we observed this switch in proliferating myoblasts following Wnt3a stimulation, in addition to enhanced fusion within differentiation conditions. While not expressed in resting muscles, the regenerative response following injury results in the upregulation of Wnt3a within muscle tissues (Brack et al., 2008). In addition, Wnt3a expression is observed in the dorsal regions of the neural tube during embryonic development and is involved in the induction of somitic myogenesis (Munsterberg et al., 1995). In concert with the regulation by Notch signalling, these results further support the nodal switch between non-canonical Wnt/PCP signalling during the expansion of the satellite stem cell pool, and the canonical Wnt/β-Catenin/MRF signalling during myogenic commitment and differentiation. In addition, these findings further identify the interplay between the molecular regulation by the MRFs and the extrinsic signalling through the canonical Wnt signalling pathway during myogenic differentiation.

Significance

The satellite cell lineage provides a reservoir of lineage committed adult stem cells tasked with maintaining the regenerative potential of skeletal muscle following successive rounds of growth and repair. The satellite cell identity is attributed to the expression of Pax7, as Pax7-null mice are depleted of satellite cells and the capacity for regeneration is severely ablated (Kuang et al., 2006; Seale et al., 2000). While studies have examined alternative cell populations for maintaining adult skeletal muscle, a recent report further confirms that non-myogenic derived cells are not able to replenish the Pax7+ satellite cell pool (Lepper et al., 2011). As a result, further understanding of the specific function of Pax7 within satellite cells, as well as deciphering the commitment to the skeletal muscle lineage, remains of great interest.

Within the satellite cell lineage, this body of work has directly examined the ability of Pax7 to bind DNA, following alternative splicing events within the paired domain. DNA binding of Pax7 to target sequences is facilitated through its recruitment of the HMT complex. The observation that Pax7d retains the greatest transactivation potential provides additional evidence that, while the paired domain cooperatively functions to provide additional target motif binding, the homeodomain is predominantly responsible for DNA binding of Pax7.

In contrast to the Pax7-dependent activation of Myf5 expression and increased proliferation in myoblasts, downstream activation of myogenic differentiation can be modulated by canonical Wnt signalling. While previously shown to enhance differentiation, we mechanistically observed that myogenin-dependent activation of follistatin was sufficient to promote premature differentiation. In the presence of proliferating signals, canonical

Wnt/β-Catenin signalling was sufficient to inhibit cell-cycle progression and induce myoblast differentiation. This was more striking when combined with the observation that repressive Snail proteins prevent premature activation of follistatin expression in proliferating myoblasts, ensuring maintenance of the satellite cell-derived progenitor pool.

Future Directions

The critical importance of Pax7 during adult myogenesis highlights the necessity for obtaining a clearer understanding of its functional role at the molecular level. As a transcription factor, it remains important to examine the ability of Pax7 to bind DNA and elicit a transcriptional response. In contrast to Pax3, the GL splice variant for Pax7 remains functionally important, as our studies have shown the ability of Pax7 splice variants to differentially activate some downstream targets. While Pax7 isoforms exhibit differential abilities to activate Myf5 expression, it remains of interest to examine the composition of endogenous Pax7 protein complexes to identify the functional abundance of Pax7 isoforms at the protein level. While we observed Pax7 isoforms could form homo- and heterodimers *in vitro*, their preferential composition *in vivo* remains elusive. Regardless of their ability to form dimers, it is important to determine if one dimer complex displays favoured DNA binding potential and whether these complex species are equally distributed in quiescent, proliferative and differentiation conditions. Although the relative distribution of Pax7 isoforms remains constant, the abundance of specific dimer combinations has not been assessed. However, current molecular techniques are not able to distinguish two amino acid variations between protein species with high certainty, and these questions will rely on the advent of more advanced protein identification techniques.

Given our identification of target genes that are differentially regulated by Pax7b and Pax7d isoforms, it would be intriguing to examine how Pax7 splice variants bind to regulatory elements upstream of target genes. Recent evidence suggests that Pax7 may bind regulatory enhancer elements distal to the transcriptional start site (TSS) (for example; Myf5 111 kb upstream or Bmp4 116 kb upstream) (Soleimani et al., 2012). In light of these observations, examining these enhancers through chromatin interaction analysis using paired-end tag sequencing (ChIA-PET) (Fullwood et al., 2009; Li et al., 2010), which captures long-range looping events in chromatin, would provide important insight into the transcriptional control of target gene expression. This approach could identify novel Pax7 splice variant binding sites, and provide context to their proximal location relative to the TSS when exerting their transcriptional control. In addition, this data set could be used to complement the recently published Pax7d ChIP-Seq results (Soleimani et al., 2012), and function as a comparative tool for mapping Pax7 isoform DNA binding to known motifs.

As previously discussed, Pax7-null mice are nearly devoid of satellite cells and the regenerative potential is extensively ablated (Seale et al., 2000). However, these mouse models have not addressed whether this ablation is dependent on the loss of all Pax7 splice variants or specifically one isoform (for example, Pax7d), and whether the function of Pax7 is dependent on proper dimer formation. As such, it would be of interest to examine developmental myogenesis and post-natal regeneration following the generation of a Pax7 isoform transgenic mouse line, coupled with the conditional Pax7 knock-out (Lepper et al., 2009). This mouse strain would provide temporal control of Pax7 isoform expression, and allow for comprehensive examination during embryonic development and post-natal

regeneration. In addition, these mice would ascertain whether a single Pax7 splice variant could recapitulate the entire function of Pax7.

In addition to examining the ability of Pax7 to maintain the myogenic identity of satellite cells, it remains of interest to further understand its role in myogenic differentiation. Myostatin has been suggested to negatively regulate myogenesis through dysregulation of Pax7-dependent satellite cell activation and self-renewal (McCroskery et al., 2003; McFarlane et al., 2008). While follistatin is known to inhibit the repressive effects of myostatin, the canonical Wnt-dependent activation of follistatin on the quiescent satellite cell population remains to be investigated. Of particular interest is the response of satellite stem cells to canonical Wnt signals, and whether this would exhaust the satellite cell pool and ablate long-term regenerative potential. This would contribute to a better understanding of potential mechanisms regulating satellite cell aging, where canonical Wnt signalling has resulted in the increase of myogenic-fibrogenic conversion (Brack et al., 2007).

Furthermore, miRNAs are emerging as a new level of post-transcriptional regulators of muscle gene expression during proliferation and differentiation (Chen et al., 2006). Specifically, recent studies have demonstrated the MRFs, including MyoD and myogenin, activate the expression of specific myogenic miRNAs (miR-1, miR-133 and miR-206) (Cao et al., 2006; Chen et al., 2010; Rao et al., 2006), and the loss of myostatin expression correlates with increased expression of these myogenic miRNAs (Rachagani et al., 2010). Given the ability of canonical Wnt signalling to rapidly upregulate myogenin expression, coupled with observations that follistatin expression can negatively regulate myostatin expression, sets the stage for future studies to specifically examine the β-Catenin dependent regulation of miRNAs during myogenic differentiation.

Lastly, it will remain of interest to further characterize the details of Wnt/β-Catenin molecular functions. While β-Catenin is able to complex with MyoD to elicit a transcriptional response independent of TCF/Lef (Kim et al., 2008), other potential TCF/Lef-dependent transcriptional targets following canonical Wnt stimulation warrant further investigation. Recently, the Wnt co-regulator BCL9 was shown to be critical for the nuclear localization of β-Catenin and downstream TCF/Lef-mediated transcription (Brack et al., 2009) during muscle regeneration. Further characterization of these TCF/Lef-dependent targets may provide further insight into the complete function of canonical Wnt signalling during myogenesis. Finally, the observed myogenic-fibrogenic conversion of proliferating satellite cells in response to canonical Wnt signalling can be suppressed by canonical Wnt inhibitors (Brack et al., 2007). Identifying Fzd receptors bound by Wnt3a during myogenic differentiation will provide greater insight to the extrinsic control imparted by canonical Wnt signalling, and provide potential therapeutic targets for sequestering Wnt3a activation.

Biomedical Implications

Exploiting the regenerative potential of adult muscle stem cells has captivated great interest for the therapeutic treatment of degenerative diseases such as muscular dystrophy. Initial studies utilizing myoblast-based treatments have been hindered by poor survival and engraftment of donor cells despite the potential for satellite stem cell transplantation to repopulate the satellite cell compartment (Kuang et al., 2007). Interestingly, muscle residing CD45+/Sca1+ adult stem cells, from Pax7-null muscles, can form myoblasts capable of myogenic differentiation following ectopic Pax7 expression (Seale et al., 2004). These studies illustrate the importance of deciphering Pax7 function during adult myogenesis,

particularly its ability to bind DNA, recruit cofactors and activate target gene expression.

The previously discussed RMS results from the fusion of the potent transactivation domain of FoxO1 with the DNA binding domains of Pax3 or Pax7, leading to the development of soft tissue carcinomas. Recent evidence suggests that these tumors arise from the dysregulation of satellite cells and downstream myogenic progenitors (Doyle et al., 2010; Rubin et al., 2011). Further understanding of the function and role of Pax7 DNA binding will provide greater insight into how their dysregulation leads to the generation and progression of these aggressive childhood tumors.

The importance of the local satellite cell niche becomes apparent as transplantation of myofibre-associated satellite cells into injured muscle has been shown to prevent age-associated muscle atrophy and weakness by increasing muscle mass and force, as well as retention of satellite cell numbers (Hall et al., 2010). Increased canonical Wnt signalling during aging has been demonstrated to alter satellite cell fate by promoting a myogenic-fibrogenic conversion (Brack et al., 2007). Within muscular dystrophies, fibrosis is associated with disease pathology, and the inhibition of canonical Wnt signalling leads to reduced fibrosis (Mann et al., 2011; Trensz et al., 2010). Given these findings, the inhibition of canonical Wnt signals within aged or dystrophic muscle may serve as a potential therapeutic to reduce fibrotic infiltration.

Conclusions

The expression of Pax7 is vital to the function of the satellite cell compartment. Greater understanding of how Pax7 functions, through the generation of splice variants, is important for understanding the molecular control of downstream targets including Myf5

expression. Further, proliferating myoblasts undergo premature differentiation in the presence of canonical Wnt signalling, through upregulating the myogenin-dependent activation of follistatin expression. A clearer understanding of the molecular controls underlying the activation, commitment and differentiation of MRF-dependent myogenesis will provide further insight into the muscle repair process. Ultimately, this knowledge can be translated towards potential stem cell therapies for muscle regeneration and the treatment of degenerative diseases.

REFERENCES

Allouh, M.Z., Yablonka-Reuveni, Z., and Rosser, B.W. (2008). Pax7 reveals a greater frequency and concentration of satellite cells at the ends of growing skeletal muscle fibers. J Histochem Cytochem *56*, 77-87.

Amthor, H., Huang, R., McKinnell, I., Christ, B., Kambadur, R., Sharma, M., and Patel, K. (2002). The regulation and action of myostatin as a negative regulator of muscle development during avian embryogenesis. Dev Biol *251*, 241-257.

Amthor, H., Otto, A., Vulin, A., Rochat, A., Dumonceaux, J., Garcia, L., Mouisel, E., Hourde, C., Macharia, R., Friedrichs, M.*, et al.* (2009). Muscle hypertrophy driven by myostatin blockade does not require stem/precursor-cell activity. Proc Natl Acad Sci U S A *106*, 7479-7484.

Anderson, J.E. (2000). A role for nitric oxide in muscle repair: nitric oxide-mediated activation of muscle satellite cells. Mol Biol Cell *11*, 1859-1874.

Apuzzo, S., Abdelhakim, A., Fortin, A.S., and Gros, P. (2004). Cross-talk between the paired domain and the homeodomain of Pax3: DNA binding by each domain causes a structural change in the other domain, supporting interdependence for DNA Binding. J Biol Chem *279*, 33601-33612.

Armand, O., Boutineau, A.M., Mauger, A., Pautou, M.P., and Kieny, M. (1983). Origin of satellite cells in avian skeletal muscles. Arch Anat Microsc Morphol Exp *72*, 163-181.

Artavanis-Tsakonas, S., Rand, M.D., and Lake, R.J. (1999). Notch signaling: cell fate control and signal integration in development. Science *284*, 770-776.

Barber, T.D., Barber, M.C., Cloutier, T.E., and Friedman, T.B. (1999). PAX3 gene structure, alternative splicing and evolution. Gene *237*, 311-319.

Baroffio, A., Hamann, M., Bernheim, L., Bochaton-Piallat, M.L., Gabbiani, G., and Bader, C.R. (1996). Identification of self-renewing myoblasts in the progeny of single human muscle satellite cells. Differentiation *60*, 47-57.

Barr, F.G., Fitzgerald, J.C., Ginsberg, J.P., Vanella, M.L., Davis, R.J., and Bennicelli, J.L. (1999). Predominant expression of alternative PAX3 and PAX7 forms in myogenic and neural tumor cell lines. Cancer Res *59*, 5443-5448.

Bennicelli, J.L., Edwards, R.H., and Barr, F.G. (1996). Mechanism for transcriptional gain of function resulting from chromosomal translocation in alveolar rhabdomyosarcoma. Proc Natl Acad Sci U S A *93*, 5455-5459.

Berkes, C.A., and Tapscott, S.J. (2005). MyoD and the transcriptional control of myogenesis. Semin Cell Dev Biol *16*, 585-595.

Birrane, G., Soni, A., and Ladias, J.A. (2009). Structural basis for DNA recognition by the human PAX3 homeodomain. Biochemistry *48*, 1148-1155.

Bischoff, R., and Heintz, C. (1994). Enhancement of skeletal muscle regeneration. Dev Dyn *201*, 41-54.

Black, B.L., Martin, J.F., and Olson, E.N. (1995). The mouse MRF4 promoter is trans-activated directly and indirectly by muscle-specific transcription factors. J Biol Chem *270*, 2889-2892.

Bladt, F., Riethmacher, D., Isenmann, S., Aguzzi, A., and Birchmeier, C. (1995). Essential role for the c-met receptor in the migration of myogenic precursor cells into the limb bud. Nature *376*, 768-771.

Bober, E., Franz, T., Arnold, H.H., Gruss, P., and Tremblay, P. (1994). Pax-3 is required for the development of limb muscles: a possible role for the migration of dermomyotomal muscle progenitor cells. Development *120*, 603-612.

Borycki, A.G., Li, J., Jin, F., Emerson, C.P., and Epstein, J.A. (1999). Pax3 functions in cell survival and in pax7 regulation. Development *126*, 1665-1674.

Brack, A.S., Conboy, I.M., Conboy, M.J., Shen, J., and Rando, T.A. (2008). A temporal switch from notch to Wnt signaling in muscle stem cells is necessary for normal adult myogenesis. Cell Stem Cell *2*, 50-59.

Brack, A.S., Conboy, M.J., Roy, S., Lee, M., Kuo, C.J., Keller, C., and Rando, T.A. (2007). Increased Wnt signaling during aging alters muscle stem cell fate and increases fibrosis. Science *317*, 807-810.

Brack, A.S., Murphy-Seiler, F., Hanifi, J., Deka, J., Eyckerman, S., Keller, C., Aguet, M., and Rando, T.A. (2009). BCL9 is an essential component of canonical Wnt signaling that mediates the differentiation of myogenic progenitors during muscle regeneration. Dev Biol *335*, 93-105.

Braun, T., and Arnold, H.H. (1995). Inactivation of Myf-6 and Myf-5 genes in mice leads to alterations in skeletal muscle development. EMBO J *14*, 1176-1186.

Braun, T., Bober, E., Rudnicki, M.A., Jaenisch, R., and Arnold, H.H. (1994). MyoD expression marks the onset of skeletal myogenesis in Myf-5 mutant mice. Development *120*, 3083-3092.

Braun, T., Rudnicki, M.A., Arnold, H.H., and Jaenisch, R. (1992). Targeted inactivation of the muscle regulatory gene Myf-5 results in abnormal rib development and perinatal death. Cell *71*, 369-382.

Braun, T., Winter, B., Bober, E., and Arnold, H.H. (1990). Transcriptional activation domain of the muscle-specific gene-regulatory protein myf5. Nature *346*, 663-665.

Brohmann, H., Jagla, K., and Birchmeier, C. (2000). The role of Lbx1 in migration of muscle precursor cells. Development *127*, 437-445.

Buchberger, A., Ragge, K., and Arnold, H.H. (1994). The myogenin gene is activated during myocyte differentiation by pre-existing, not newly synthesized transcription factor MEF-2. J Biol Chem *269*, 17289-17296.

Buckingham, M., Bajard, L., Chang, T., Daubas, P., Hadchouel, J., Meilhac, S., Montarras, D., Rocancourt, D., and Relaix, F. (2003). The formation of skeletal muscle: from somite to limb. J Anat *202*, 59-68.

Budry, L., Balsalobre, A., Gauthier, Y., Khetchoumian, K., L'Honore, A., Vallette, S., Brue, T., Figarella-Branger, D., Meij, B., and Drouin, J. (2012). The selector gene Pax7 dictates alternate pituitary cell fates through its pioneer action on chromatin remodeling. Genes Dev *26*, 2299-2310.

Calhabeu, F., Hayashi, S., Morgan, J.E., Relaix, F., and Zammit, P.S. (2013). Alveolar rhabdomyosarcoma-associated proteins PAX3/FOXO1A and PAX7/FOXO1A suppress the transcriptional activity of MyoD-target genes in muscle stem cells. Oncogene *32*, 651-662.

Cao, Y., Kumar, R.M., Penn, B.H., Berkes, C.A., Kooperberg, C., Boyer, L.A., Young, R.A., and Tapscott, S.J. (2006). Global and gene-specific analyses show distinct roles for Myod and Myog at a common set of promoters. EMBO J *25*, 502-511.

Chang, T.H., Tsai, M.F., Su, K.Y., Wu, S.G., Huang, C.P., Yu, S.L., Yu, Y.L., Lan, C.C., Yang, C.H., Lin, S.B.*, et al.* (2011). Slug confers resistance to the epidermal growth factor receptor tyrosine kinase inhibitor. Am J Respir Crit Care Med *183*, 1071-1079.

Charge, S.B., and Rudnicki, M.A. (2004). Cellular and molecular regulation of muscle regeneration. Physiol Rev *84*, 209-238.

Chen, J.F., Mandel, E.M., Thomson, J.M., Wu, Q., Callis, T.E., Hammond, S.M., Conlon, F.L., and Wang, D.Z. (2006). The role of microRNA-1 and microRNA-133 in skeletal muscle proliferation and differentiation. Nat Genet *38*, 228-233.

Chen, J.F., Tao, Y., Li, J., Deng, Z., Yan, Z., Xiao, X., and Wang, D.Z. (2010). microRNA-1 and microRNA-206 regulate skeletal muscle satellite cell proliferation and differentiation by repressing Pax7. J Cell Biol *190*, 867-879.

Chen, W., Fu, X., and Sheng, Z. (2002). Review of current progress in the structure and function of Smad proteins. Chin Med J (Engl) *115*, 446-450.

Chi, N., and Epstein, J.A. (2002). Getting your Pax straight: Pax proteins in development and disease. Trends Genet *18*, 41-47.

Christ, B., and Ordahl, C.P. (1995). Early stages of chick somite development. Anat Embryol (Berl) *191*, 381-396.

Christov, C., Chretien, F., Abou-Khalil, R., Bassez, G., Vallet, G., Authier, F.J., Bassaglia, Y., Shinin, V., Tajbakhsh, S., Chazaud, B.*, et al.* (2007). Muscle satellite cells and endothelial cells: close neighbors and privileged partners. Mol Biol Cell *18*, 1397-1409.

Clevers, H. (2006). Wnt/beta-catenin signaling in development and disease. Cell *127*, 469-480.

Collins, C.A., Olsen, I., Zammit, P.S., Heslop, L., Petrie, A., Partridge, T.A., and Morgan, J.E. (2005). Stem cell function, self-renewal, and behavioral heterogeneity of cells from the adult muscle satellite cell niche. Cell *122*, 289-301.

Conboy, I.M., and Rando, T.A. (2002). The regulation of Notch signaling controls satellite cell activation and cell fate determination in postnatal myogenesis. Dev Cell *3*, 397-409.

Cooper, R.N., Tajbakhsh, S., Mouly, V., Cossu, G., Buckingham, M., and Butler-Browne, G.S. (1999). In vivo satellite cell activation via Myf5 and MyoD in regenerating mouse skeletal muscle. J Cell Sci *112 (Pt 17)*, 2895-2901.

Cornelison, D.D., Filla, M.S., Stanley, H.M., Rapraeger, A.C., and Olwin, B.B. (2001). Syndecan-3 and syndecan-4 specifically mark skeletal muscle satellite cells and are implicated in satellite cell maintenance and muscle regeneration. Dev Biol *239*, 79-94.

Cornelison, D.D., and Wold, B.J. (1997). Single-cell analysis of regulatory gene expression in quiescent and activated mouse skeletal muscle satellite cells. Dev Biol *191*, 270-283.

Daston, G., Lamar, E., Olivier, M., and Goulding, M. (1996). Pax-3 is necessary for migration but not differentiation of limb muscle precursors in the mouse. Development *122*, 1017-1027.

Dietrich, S., Abou-Rebyeh, F., Brohmann, H., Bladt, F., Sonnenberg-Riethmacher, E., Yamaai, T., Lumsden, A., Brand-Saberi, B., and Birchmeier, C. (1999). The role of SF/HGF and c-Met in the development of skeletal muscle. Development *126*, 1621-1629.

Doyle, B., Morton, J.P., Delaney, D.W., Ridgway, R.A., Wilkins, J.A., and Sansom, O.J. (2010). p53 mutation and loss have different effects on tumourigenesis in a novel mouse model of pleomorphic rhabdomyosarcoma. J Pathol *222*, 129-137.

Du, S., Lawrence, E.J., Strzelecki, D., Rajput, P., Xia, S.J., Gottesman, D.M., and Barr, F.G. (2005). Co-expression of alternatively spliced forms of PAX3, PAX7, PAX3-FKHR and PAX7-FKHR with distinct DNA binding and transactivation properties in rhabdomyosarcoma. Int J Cancer *115*, 85-92.

Epstein, J.A., Glaser, T., Cai, J., Jepeal, L., Walton, D.S., and Maas, R.L. (1994). Two independent and interactive DNA-binding subdomains of the Pax6 paired domain are regulated by alternative splicing. Genes Dev *8*, 2022-2034.

Epstein, J.A., Shapiro, D.N., Cheng, J., Lam, P.Y., and Maas, R.L. (1996). Pax3 modulates expression of the c-Met receptor during limb muscle development. Proc Natl Acad Sci U S A *93*, 4213-4218.

Feng, X.H., and Derynck, R. (2005). Specificity and versatility in tgf-beta signaling through Smads. Annu Rev Cell Dev Biol *21*, 659-693.

Flanagan-Steet, H., Hannon, K., McAvoy, M.J., Hullinger, R., and Olwin, B.B. (2000). Loss of FGF receptor 1 signaling reduces skeletal muscle mass and disrupts myofiber organization in the developing limb. Dev Biol *218*, 21-37.

Fortin, A.S., Underhill, D.A., and Gros, P. (1998). Helix 2 of the paired domain plays a key role in the regulation of DNA-binding by the Pax-3 homeodomain. Nucleic Acids Res *26*, 4574-4581.

Friedrichs, M., Wirsdoerfer, F., Flohe, S.B., Schneider, S., Wuelling, M., and Vortkamp, A. (2011). BMP signaling balances proliferation and differentiation of muscle satellite cell descendants. BMC Cell Biol *12*, 26.

Fukada, S., Uezumi, A., Ikemoto, M., Masuda, S., Segawa, M., Tanimura, N., Yamamoto, H., Miyagoe-Suzuki, Y., and Takeda, S. (2007). Molecular signature of quiescent satellite cells in adult skeletal muscle. Stem Cells *25*, 2448-2459.

Fullwood, M.J., Wei, C.L., Liu, E.T., and Ruan, Y. (2009). Next-generation DNA sequencing of paired-end tags (PET) for transcriptome and genome analyses. Genome Res *19*, 521-532.

Gehring, W.J., Affolter, M., and Burglin, T. (1994). Homeodomain proteins. Annu Rev Biochem *63*, 487-526.

Gillespie, M.A., Le Grand, F., Scime, A., Kuang, S., von Maltzahn, J., Seale, V., Cuenda, A., Ranish, J.A., and Rudnicki, M.A. (2009). p38-{gamma}-dependent gene silencing restricts entry into the myogenic differentiation program. J Cell Biol *187*, 991-1005.

Giordani, J., Bajard, L., Demignon, J., Daubas, P., Buckingham, M., and Maire, P. (2007). Six proteins regulate the activation of Myf5 expression in embryonic mouse limbs. Proc Natl Acad Sci U S A *104*, 11310-11315.

Glass, D.J. (2005). Skeletal muscle hypertrophy and atrophy signaling pathways. Int J Biochem Cell Biol *37*, 1974-1984.

Gnocchi, V.F., White, R.B., Ono, Y., Ellis, J.A., and Zammit, P.S. (2009). Further characterisation of the molecular signature of quiescent and activated mouse muscle satellite cells. PLoS One *4*, e5205.

Grifone, R., Demignon, J., Giordani, J., Niro, C., Souil, E., Bertin, F., Laclef, C., Xu, P.X., and Maire, P. (2007). Eya1 and Eya2 proteins are required for hypaxial somitic myogenesis in the mouse embryo. Dev Biol *302*, 602-616.

Grifone, R., Demignon, J., Houbron, C., Souil, E., Niro, C., Seller, M.J., Hamard, G., and Maire, P. (2005). Six1 and Six4 homeoproteins are required for Pax3 and Mrf expression during myogenesis in the mouse embryo. Development *132*, 2235-2249.

Gros, J., Manceau, M., Thome, V., and Marcelle, C. (2005). A common somitic origin for embryonic muscle progenitors and satellite cells. Nature *435*, 954-958.

Gross, M.K., Moran-Rivard, L., Velasquez, T., Nakatsu, M.N., Jagla, K., and Goulding, M. (2000). Lbx1 is required for muscle precursor migration along a lateral pathway into the limb. Development *127*, 413-424.

Grumolato, L., Liu, G., Mong, P., Mudbhary, R., Biswas, R., Arroyave, R., Vijayakumar, S., Economides, A.N., and Aaronson, S.A. (2010). Canonical and noncanonical Wnts use a common mechanism to activate completely unrelated coreceptors. Genes Dev *24*, 2517-2530.

Gualdi, R., Bossard, P., Zheng, M., Hamada, Y., Coleman, J.R., and Zaret, K.S. (1996). Hepatic specification of the gut endoderm in vitro: cell signaling and transcriptional control. Genes Dev *10*, 1670-1682.

Hall, J.K., Banks, G.B., Chamberlain, J.S., and Olwin, B.B. (2010). Prevention of muscle aging by myofiber-associated satellite cell transplantation. Sci Transl Med *2*, 57ra83.

Hasty, P., Bradley, A., Morris, J.H., Edmondson, D.G., Venuti, J.M., Olson, E.N., and Klein, W.H. (1993). Muscle deficiency and neonatal death in mice with a targeted mutation in the myogenin gene. Nature *364*, 501-506.

Hemmati-Brivanlou, A., Kelly, O.G., and Melton, D.A. (1994). Follistatin, an antagonist of activin, is expressed in the Spemann organizer and displays direct neuralizing activity. Cell *77*, 283-295.

Hollway, G., and Currie, P. (2005). Vertebrate myotome development. Birth Defects Res C Embryo Today *75*, 172-179.

Horst, D., Ustanina, S., Sergi, C., Mikuz, G., Juergens, H., Braun, T., and Vorobyov, E. (2006). Comparative expression analysis of Pax3 and Pax7 during mouse myogenesis. Int J Dev Biol *50*, 47-54.

Hu, J.S., Olson, E.N., and Kingston, R.E. (1992). HEB, a helix-loop-helix protein related to E2A and ITF2 that can modulate the DNA-binding ability of myogenic regulatory factors. Mol Cell Biol *12*, 1031-1042.

Iemura, S., Yamamoto, T.S., Takagi, C., Uchiyama, H., Natsume, T., Shimasaki, S., Sugino, H., and Ueno, N. (1998). Direct binding of follistatin to a complex of bone-morphogenetic protein and its receptor inhibits ventral and epidermal cell fates in early Xenopus embryo. Proc Natl Acad Sci U S A *95*, 9337-9342.

Jen, Y., Weintraub, H., and Benezra, R. (1992). Overexpression of Id protein inhibits the muscle differentiation program: in vivo association of Id with E2A proteins. Genes Dev *6*, 1466-1479.

Jennische, E., Ekberg, S., and Matejka, G.L. (1993). Expression of hepatocyte growth factor in growing and regenerating rat skeletal muscle. Am J Physiol *265*, C122-128.

Jones, N.C., Tyner, K.J., Nibarger, L., Stanley, H.M., Cornelison, D.D., Fedorov, Y.V., and Olwin, B.B. (2005). The p38alpha/beta MAPK functions as a molecular switch to activate the quiescent satellite cell. J Cell Biol *169*, 105-116.

Jun, S., and Desplan, C. (1996). Cooperative interactions between paired domain and homeodomain. Development *122*, 2639-2650.

Kablar, B., Krastel, K., Ying, C., Asakura, A., Tapscott, S.J., and Rudnicki, M.A. (1997). MyoD and Myf-5 differentially regulate the development of limb versus trunk skeletal muscle. Development *124*, 4729-4738.

Kassar-Duchossoy, L., Gayraud-Morel, B., Gomes, D., Rocancourt, D., Buckingham, M., Shinin, V., and Tajbakhsh, S. (2004). Mrf4 determines skeletal muscle identity in Myf5:Myod double-mutant mice. Nature *431*, 466-471.

Kaufman, M.H. (1992). The Atlas of Mouse Development. Academic Press *4*.

Kawabe, Y., Wang, Y.X., McKinnell, I.W., Bedford, M.T., and Rudnicki, M.A. (2012). Carm1 regulates Pax7 transcriptional activity through MLL1/2 recruitment during asymmetric satellite stem cell divisions. Cell Stem Cell *11*, 333-345.

Kelly, A.M. (1978). Perisynaptic satellite cells in the developing and mature rat soleus muscle. Anat Rec *190*, 891-903.

Kim, C.H., Neiswender, H., Baik, E.J., Xiong, W.C., and Mei, L. (2008). Beta-catenin interacts with MyoD and regulates its transcription activity. Mol Cell Biol *28*, 2941-2951.

Kitzmann, M., Carnac, G., Vandromme, M., Primig, M., Lamb, N.J., and Fernandez, A. (1998). The muscle regulatory factors MyoD and myf-5 undergo distinct cell cycle-specific expression in muscle cells. J Cell Biol *142*, 1447-1459.

Kuang, S., Charge, S.B., Seale, P., Huh, M., and Rudnicki, M.A. (2006). Distinct roles for Pax7 and Pax3 in adult regenerative myogenesis. J Cell Biol *172*, 103-113.

Kuang, S., Kuroda, K., Le Grand, F., and Rudnicki, M.A. (2007). Asymmetric self-renewal and commitment of satellite stem cells in muscle. Cell *129*, 999-1010.

Langley, B., Thomas, M., Bishop, A., Sharma, M., Gilmour, S., and Kambadur, R. (2002). Myostatin inhibits myoblast differentiation by down-regulating MyoD expression. J Biol Chem *277*, 49831-49840.

Le Grand, F., Jones, A.E., Seale, V., Scime, A., and Rudnicki, M.A. (2009). Wnt7a activates the planar cell polarity pathway to drive the symmetric expansion of satellite stem cells. Cell Stem Cell *4*, 535-547.

Lee, S.-J., and McPherron, A.C. (2001). Regulation of myostatin activity and muscle growth. Proceedings of the National Academy of Sciences *98*, 9306-9311.

Lee, S.J. (2007). Quadrupling muscle mass in mice by targeting TGF-beta signaling pathways. PLoS One *2*, e789.

Lee, S.J., Lee, Y.S., Zimmers, T.A., Soleimani, A., Matzuk, M.M., Tsuchida, K., Cohn, R.D., and Barton, E.R. (2010). Regulation of muscle mass by follistatin and activins. Mol Endocrinol *24*, 1998-2008.

Lee, S.J., Reed, L.A., Davies, M.V., Girgenrath, S., Goad, M.E., Tomkinson, K.N., Wright, J.F., Barker, C., Ehrmantraut, G., Holmstrom, J.*, et al.* (2005). Regulation of muscle growth by multiple ligands signaling through activin type II receptors. Proc Natl Acad Sci U S A *102*, 18117-18122.

Lepper, C., Conway, S.J., and Fan, C.M. (2009). Adult satellite cells and embryonic muscle progenitors have distinct genetic requirements. Nature *460*, 627-631.

Lepper, C., and Fan, C.M. (2010). Inducible lineage tracing of Pax7-descendant cells reveals embryonic origin of adult satellite cells. Genesis *48*, 424-436.

Lepper, C., Partridge, T.A., and Fan, C.M. (2011). An absolute requirement for Pax7-positive satellite cells in acute injury-induced skeletal muscle regeneration. Development *138*, 3639-3646.

Leroy, P., and Mostov, K.E. (2007). Slug is required for cell survival during partial epithelial-mesenchymal transition of HGF-induced tubulogenesis. Mol Biol Cell *18*, 1943-1952.

Li, G., Fullwood, M.J., Xu, H., Mulawadi, F.H., Velkov, S., Vega, V., Ariyaratne, P.N., Mohamed, Y.B., Ooi, H.S., Tennakoon, C.*, et al.* (2010). ChIA-PET tool for comprehensive chromatin interaction analysis with paired-end tag sequencing. Genome Biol *11*, R22.

Liu, Q.C., Zha, X.H., Faralli, H., Yin, H., Louis-Jeune, C., Perdiguero, E., Pranckeviciene, E., Munoz-Canoves, P., Rudnicki, M.A., Brand, M.*, et al.* (2012). Comparative expression profiling identifies differential roles for Myogenin and p38alpha MAPK signaling in myogenesis. J Mol Cell Biol *4*, 386-397.

Logan, C.Y., and Nusse, R. (2004). The Wnt signaling pathway in development and disease. Annu Rev Cell Dev Biol *20*, 781-810.

MacDonald, B.T., Tamai, K., and He, X. (2009). Wnt/beta-catenin signaling: components, mechanisms, and diseases. Dev Cell *17*, 9-26.

Mann, C.J., Perdiguero, E., Kharraz, Y., Aguilar, S., Pessina, P., Serrano, A.L., and Munoz-Canoves, P. (2011). Aberrant repair and fibrosis development in skeletal muscle. Skelet Muscle *1*, 21.

Maroto, M., Reshef, R., Munsterberg, A.E., Koester, S., Goulding, M., and Lassar, A.B. (1997). Ectopic Pax-3 activates MyoD and Myf-5 expression in embryonic mesoderm and neural tissue. Cell *89*, 139-148.

Mauro, A. (1961). Satellite cell of skeletal muscle fibers. J Biophys Biochem Cytol *9*, 493-495.

McCroskery, S., Thomas, M., Maxwell, L., Sharma, M., and Kambadur, R. (2003). Myostatin negatively regulates satellite cell activation and self-renewal. J Cell Biol *162*, 1135-1147.

McCroskery, S., Thomas, M., Platt, L., Hennebry, A., Nishimura, T., McLeay, L., Sharma, M., and Kambadur, R. (2005). Improved muscle healing through enhanced regeneration and reduced fibrosis in myostatin-null mice. J Cell Sci *118*, 3531-3541.

McFarlane, C., Hennebry, A., Thomas, M., Plummer, E., Ling, N., Sharma, M., and Kambadur, R. (2008). Myostatin signals through Pax7 to regulate satellite cell self-renewal. Exp Cell Res *314*, 317-329.

McKinnell, I.W., Ishibashi, J., Le Grand, F., Punch, V.G., Addicks, G.C., Greenblatt, J.F., Dilworth, F.J., and Rudnicki, M.A. (2008). Pax7 activates myogenic genes by recruitment of a histone methyltransferase complex. Nat Cell Biol *10*, 77-84.

McPherron, A.C., Lawler, A.M., and Lee, S.J. (1997). Regulation of skeletal muscle mass in mice by a new TGF-beta superfamily member. Nature *387*, 83-90.

Megeney, L.A., Kablar, B., Garrett, K., Anderson, J.E., and Rudnicki, M.A. (1996). MyoD is required for myogenic stem cell function in adult skeletal muscle. Genes Dev *10*, 1173-1183.

Mennerich, D., Schafer, K., and Braun, T. (1998). Pax-3 is necessary but not sufficient for lbx1 expression in myogenic precursor cells of the limb. Mech Dev *73*, 147-158.

Miskiewicz, P., Morrissey, D., Lan, Y., Raj, L., Kessler, S., Fujioka, M., Goto, T., and Weir, M. (1996). Both the paired domain and homeodomain are required for in vivo function of Drosophila Paired. Development *122*, 2709-2718.

Molkentin, J.D., and Olson, E.N. (1996). Combinatorial control of muscle development by basic helix-loop-helix and MADS-box transcription factors. Proc Natl Acad Sci U S A *93*, 9366-9373.

Munsterberg, A.E., Kitajewski, J., Bumcrot, D.A., McMahon, A.P., and Lassar, A.B. (1995). Combinatorial signaling by Sonic hedgehog and Wnt family members induces myogenic bHLH gene expression in the somite. Genes Dev *9*, 2911-2922.

Murre, C., McCaw, P.S., Vaessin, H., Caudy, M., Jan, L.Y., Jan, Y.N., Cabrera, C.V., Buskin, J.N., Hauschka, S.D., Lassar, A.B.*, et al.* (1989). Interactions between heterologous helix-loop-helix proteins generate complexes that bind specifically to a common DNA sequence. Cell *58*, 537-544.

Nabeshima, Y., Hanaoka, K., Hayasaka, M., Esumi, E., Li, S., and Nonaka, I. (1993). Myogenin gene disruption results in perinatal lethality because of severe muscle defect. Nature *364*, 532-535.

Nakamura, T., Takio, K., Eto, Y., Shibai, H., Titani, K., and Sugino, H. (1990). Activin-binding protein from rat ovary is follistatin. Science *247*, 836-838.

Nusse, R. (2012). Wnt signaling. Cold Spring Harb Perspect Biol *4*.

Olguin, H.C., and Olwin, B.B. (2004). Pax-7 up-regulation inhibits myogenesis and cell cycle progression in satellite cells: a potential mechanism for self-renewal. Dev Biol *275*, 375-388.

Olguin, H.C., Patzlaff, N.E., and Olwin, B.B. (2011). Pax7-FKHR transcriptional activity is enhanced by transcriptionally repressed MyoD. J Cell Biochem *112*, 1410-1417.

Ono, Y., Calhabeu, F., Morgan, J.E., Katagiri, T., Amthor, H., and Zammit, P.S. (2011). BMP signalling permits population expansion by preventing premature myogenic differentiation in muscle satellite cells. Cell Death Differ *18*, 222-234.

Otto, A., Schmidt, C., Luke, G., Allen, S., Valasek, P., Muntoni, F., Lawrence-Watt, D., and Patel, K. (2008). Canonical Wnt signalling induces satellite-cell proliferation during adult skeletal muscle regeneration. J Cell Sci *121*, 2939-2950.

Pani, L., Horal, M., and Loeken, M.R. (2002). Rescue of neural tube defects in Pax-3-deficient embryos by p53 loss of function: implications for Pax-3- dependent development and tumorigenesis. Genes Dev *16*, 676-680.

Parker, M.H., Seale, P., and Rudnicki, M.A. (2003). Looking back to the embryo: defining transcriptional networks in adult myogenesis. Nat Rev Genet *4*, 497-507.

Patapoutian, A., Yoon, J.K., Miner, J.H., Wang, S., Stark, K., and Wold, B. (1995). Disruption of the mouse MRF4 gene identifies multiple waves of myogenesis in the myotome. Development *121*, 3347-3358.

Polesskaya, A., Seale, P., and Rudnicki, M.A. (2003). Wnt signaling induces the myogenic specification of resident CD45+ adult stem cells during muscle regeneration. Cell *113*, 841-852.

Pritchard, C., Grosveld, G., and Hollenbach, A.D. (2003). Alternative splicing of Pax3 produces a transcriptionally inactive protein. Gene *305*, 61-69.

Puschel, A.W., Gruss, P., and Westerfield, M. (1992). Sequence and expression pattern of pax-6 are highly conserved between zebrafish and mice. Development *114*, 643-651.

Rachagani, S., Cheng, Y., and Reecy, J.M. (2010). Myostatin genotype regulates muscle-specific miRNA expression in mouse pectoralis muscle. BMC Res Notes *3*, 297.

Rao, P.K., Kumar, R.M., Farkhondeh, M., Baskerville, S., and Lodish, H.F. (2006). Myogenic factors that regulate expression of muscle-specific microRNAs. Proc Natl Acad Sci U S A *103*, 8721-8726.

Rawls, A., Valdez, M.R., Zhang, W., Richardson, J., Klein, W.H., and Olson, E.N. (1998). Overlapping functions of the myogenic bHLH genes MRF4 and MyoD revealed in double mutant mice. Development *125*, 2349-2358.

Relaix, F., Montarras, D., Zaffran, S., Gayraud-Morel, B., Rocancourt, D., Tajbakhsh, S., Mansouri, A., Cumano, A., and Buckingham, M. (2006). Pax3 and Pax7 have distinct and overlapping functions in adult muscle progenitor cells. J Cell Biol *172*, 91-102.

Relaix, F., Rocancourt, D., Mansouri, A., and Buckingham, M. (2004). Divergent functions of murine Pax3 and Pax7 in limb muscle development. Genes Dev *18*, 1088-1105.

Relaix, F., Rocancourt, D., Mansouri, A., and Buckingham, M. (2005). A Pax3/Pax7-dependent population of skeletal muscle progenitor cells. Nature *435*, 948-953.

Rochat, A., Fernandez, A., Vandromme, M., Moles, J.P., Bouschet, T., Carnac, G., and Lamb, N.J. (2004). Insulin and wnt1 pathways cooperate to induce reserve cell activation in differentiation and myotube hypertrophy. Mol Biol Cell *15*, 4544-4555.

Rubin, B.P., Nishijo, K., Chen, H.I., Yi, X., Schuetze, D.P., Pal, R., Prajapati, S.I., Abraham, J., Arenkiel, B.R., Chen, Q.R*., et al.* (2011). Evidence for an unanticipated relationship between undifferentiated pleomorphic sarcoma and embryonal rhabdomyosarcoma. Cancer Cell *19*, 177-191.

Rudnicki, M.A., Braun, T., Hinuma, S., and Jaenisch, R. (1992). Inactivation of MyoD in mice leads to up-regulation of the myogenic HLH gene Myf-5 and results in apparently normal muscle development. Cell *71*, 383-390.

Rudnicki, M.A., and Jaenisch, R. (1995). The MyoD family of transcription factors and skeletal myogenesis. Bioessays *17*, 203-209.

Rudnicki, M.A., Schnegelsberg, P.N., Stead, R.H., Braun, T., Arnold, H.H., and Jaenisch, R. (1993). MyoD or Myf-5 is required for the formation of skeletal muscle. Cell *75*, 1351-1359.

Ruvinsky, I., Katz, M., Dreazen, A., Gielchinsky, Y., Saada, A., Freedman, N., Mishani, E., Zimmerman, G., Kasir, J., and Meyuhas, O. (2009). Mice deficient in ribosomal protein S6 phosphorylation suffer from muscle weakness that reflects a growth defect and energy deficit. PLoS One *4*, e5618.

Sabourin, L.A., Girgis-Gabardo, A., Seale, P., Asakura, A., and Rudnicki, M.A. (1999). Reduced differentiation potential of primary MyoD-/- myogenic cells derived from adult skeletal muscle. J Cell Biol *144*, 631-643.

Sambasivan, R., Yao, R., Kissenpfennig, A., Van Wittenberghe, L., Paldi, A., Gayraud-Morel, B., Guenou, H., Malissen, B., Tajbakhsh, S., and Galy, A. (2011). Pax7-expressing satellite cells are indispensable for adult skeletal muscle regeneration. Development *138*, 3647-3656.

Saneyoshi, T., Kume, S., Amasaki, Y., and Mikoshiba, K. (2002). The Wnt/calcium pathway activates NF-AT and promotes ventral cell fate in Xenopus embryos. Nature *417*, 295-299.

Schienda, J., Engleka, K.A., Jun, S., Hansen, M.S., Epstein, J.A., Tabin, C.J., Kunkel, L.M., and Kardon, G. (2006). Somitic origin of limb muscle satellite and side population cells. Proc Natl Acad Sci U S A *103*, 945-950.

Schultz, E. (1976). Fine structure of satellite cells in growing skeletal muscle. Am J Anat *147*, 49-70.

Seale, P., Ishibashi, J., Scime, A., and Rudnicki, M.A. (2004). Pax7 is necessary and sufficient for the myogenic specification of CD45+:Sca1+ stem cells from injured muscle. PLoS Biol *2*, E130.

Seale, P., Sabourin, L.A., Girgis-Gabardo, A., Mansouri, A., Gruss, P., and Rudnicki, M.A. (2000). Pax7 is required for the specification of myogenic satellite cells. Cell *102*, 777-786.

Simons, M., and Mlodzik, M. (2008). Planar cell polarity signaling: from fly development to human disease. Annu Rev Genet *42*, 517-540.

Smith, C.K., 2nd, Janney, M.J., and Allen, R.E. (1994). Temporal expression of myogenic regulatory genes during activation, proliferation, and differentiation of rat skeletal muscle satellite cells. J Cell Physiol *159*, 379-385.

Soleimani, V.D., Punch, V.G., Kawabe, Y., Jones, A.E., Palidwor, G.A., Porter, C.J., Cross, J.W., Carvajal, J.J., Kockx, C.E., van, I.W.F*., et al.* (2012). Transcriptional dominance of Pax7 in adult myogenesis is due to high-affinity recognition of homeodomain motifs. Dev Cell *22*, 1208-1220.

Spitz, F., Demignon, J., Porteu, A., Kahn, A., Concordet, J.P., Daegelen, D., and Maire, P. (1998). Expression of myogenin during embryogenesis is controlled by Six/sine oculis homeoproteins through a conserved MEF3 binding site. Proc Natl Acad Sci U S A *95*, 14220-14225.

Tajbakhsh, S., Rocancourt, D., and Buckingham, M. (1996). Muscle progenitor cells failing to respond to positional cues adopt non-myogenic fates in myf-5 null mice. Nature *384*, 266-270.

Tajbakhsh, S., Rocancourt, D., Cossu, G., and Buckingham, M. (1997). Redefining the genetic hierarchies controlling skeletal myogenesis: Pax-3 and Myf-5 act upstream of MyoD. Cell *89*, 127-138.

Tatsumi, R., Anderson, J.E., Nevoret, C.J., Halevy, O., and Allen, R.E. (1998). HGF/SF is present in normal adult skeletal muscle and is capable of activating satellite cells. Dev Biol *194*, 114-128.

Tatsumi, R., Hattori, A., Ikeuchi, Y., Anderson, J.E., and Allen, R.E. (2002). Release of hepatocyte growth factor from mechanically stretched skeletal muscle satellite cells and role of pH and nitric oxide. Mol Biol Cell *13*, 2909-2918.

Tiffin, N., Williams, R.D., Shipley, J., and Pritchard-Jones, K. (2003). PAX7 expression in embryonal rhabdomyosarcoma suggests an origin in muscle satellite cells. Br J Cancer *89*, 327-332.

Tremblay, P., Dietrich, S., Mericskay, M., Schubert, F.R., Li, Z., and Paulin, D. (1998). A crucial role for Pax3 in the development of the hypaxial musculature and the long-range migration of muscle precursors. Dev Biol *203*, 49-61.

Trensz, F., Haroun, S., Cloutier, A., Richter, M.V., and Grenier, G. (2010). A muscle resident cell population promotes fibrosis in hindlimb skeletal muscles of mdx mice through the Wnt canonical pathway. Am J Physiol Cell Physiol *299*, C939-947.

Underhill, D.A., and Gros, P. (1997). The paired-domain regulates DNA binding by the homeodomain within the intact Pax-3 protein. J Biol Chem *272*, 14175-14182.

Vasyutina, E., Stebler, J., Brand-Saberi, B., Schulz, S., Raz, E., and Birchmeier, C. (2005). CXCR4 and Gab1 cooperate to control the development of migrating muscle progenitor cells. Genes Dev *19*, 2187-2198.

Vogan, K.J., Underhill, D.A., and Gros, P. (1996). An alternative splicing event in the Pax-3 paired domain identifies the linker region as a key determinant of paired domain DNA-binding activity. Mol Cell Biol *16*, 6677-6686.

von Maltzahn, J., Chang, N.C., Bentzinger, C.F., and Rudnicki, M.A. (2012). Wnt signaling in myogenesis. Trends Cell Biol *22*, 602-609.

Vorobyov, E., and Horst, J. (2004). Expression of two protein isoforms of PAX7 is controlled by competing cleavage-polyadenylation and splicing. Gene *342*, 107-112.

Wang, Q., Fang, W.H., Krupinski, J., Kumar, S., Slevin, M., and Kumar, P. (2008). Pax genes in embryogenesis and oncogenesis. J Cell Mol Med *12*, 2281-2294.

Weintraub, H., Davis, R., Tapscott, S., Thayer, M., Krause, M., Benezra, R., Blackwell, T.K., Turner, D., Rupp, R., Hollenberg, S.*, et al.* (1991a). The myoD gene family: nodal point during specification of the muscle cell lineage. Science *251*, 761-766.

Weintraub, H., Dwarki, V.J., Verma, I., Davis, R., Hollenberg, S., Snider, L., Lassar, A., and Tapscott, S.J. (1991b). Muscle-specific transcriptional activation by MyoD. Genes Dev *5*, 1377-1386.

Wexler, L.H., and Helman, L.J. (1994). Pediatric soft tissue sarcomas. CA: A Cancer Journal for Clinicians *44*, 211-247.

Williams, B.A., and Ordahl, C.P. (1997). Emergence of determined myotome precursor cells in the somite. Development *124*, 4983-4997.

Winbanks, C.E., Weeks, K.L., Thomson, R.E., Sepulveda, P.V., Beyer, C., Qian, H., Chen, J.L., Allen, J.M., Lancaster, G.I., Febbraio, M.A.*, et al.* (2012). Follistatin-mediated skeletal muscle hypertrophy is regulated by Smad3 and mTOR independently of myostatin. The Journal of Cell Biology *197*, 997-1008.

Wozniak, A.C., and Anderson, J.E. (2007). Nitric oxide-dependence of satellite stem cell activation and quiescence on normal skeletal muscle fibers. Dev Dyn *236*, 240-250.

Wu, Z., Woodring, P.J., Bhakta, K.S., Tamura, K., Wen, F., Feramisco, J.R., Karin, M., Wang, J.Y., and Puri, P.L. (2000). p38 and extracellular signal-regulated kinases regulate the myogenic program at multiple steps. Mol Cell Biol *20*, 3951-3964.

Xu, H.E., Rould, M.A., Xu, W., Epstein, J.A., Maas, R.L., and Pabo, C.O. (1999). Crystal structure of the human Pax6 paired domain-DNA complex reveals specific roles for the linker region and carboxy-terminal subdomain in DNA binding. Genes Dev *13*, 1263-1275.

Yablonka-Reuveni, Z., Seger, R., and Rivera, A.J. (1999). Fibroblast growth factor promotes recruitment of skeletal muscle satellite cells in young and old rats. J Histochem Cytochem *47*, 23-42.

Yoshida, N., Yoshida, S., Koishi, K., Masuda, K., and Nabeshima, Y. (1998). Cell heterogeneity upon myogenic differentiation: down-regulation of MyoD and Myf-5 generates 'reserve cells'. J Cell Sci *111 (Pt 6)*, 769-779.

Yu, M., Smolen, G.A., Zhang, J., Wittner, B., Schott, B.J., Brachtel, E., Ramaswamy, S., Maheswaran, S., and Haber, D.A. (2009). A developmentally regulated inducer of EMT, LBX1, contributes to breast cancer progression. Genes Dev *23*, 1737-1742.

Yusuf, F., Rehimi, R., Morosan-Puopolo, G., Dai, F., Zhang, X., and Brand-Saberi, B. (2006). Inhibitors of CXCR4 affect the migration and fate of CXCR4+ progenitors in the developing limb of chick embryos. Dev Dyn *235*, 3007-3015.

Zammit, P.S., Golding, J.P., Nagata, Y., Hudon, V., Partridge, T.A., and Beauchamp, J.R. (2004). Muscle satellite cells adopt divergent fates: a mechanism for self-renewal? J Cell Biol *166*, 347-357.

Zammit, P.S., Relaix, F., Nagata, Y., Ruiz, A.P., Collins, C.A., Partridge, T.A., and Beauchamp, J.R. (2006). Pax7 and myogenic progression in skeletal muscle satellite cells. J Cell Sci *119*, 1824-1832.

Zaret, K.S., and Carroll, J.S. (2011). Pioneer transcription factors: establishing competence for gene expression. Genes Dev *25*, 2227-2241.

Zetser, A., Gredinger, E., and Bengal, E. (1999). p38 mitogen-activated protein kinase pathway promotes skeletal muscle differentiation. Participation of the Mef2c transcription factor. J Biol Chem *274*, 5193-5200.

Zhang, W., Behringer, R.R., and Olson, E.N. (1995). Inactivation of the myogenic bHLH gene MRF4 results in up-regulation of myogenin and rib anomalies. Genes Dev *9*, 1388-1399.

Ziman, M.R., and Kay, P.H. (1998). Differential expression of four alternate Pax7 paired box transcripts is influenced by organ- and strain-specific factors in adult mice. Gene *217*, 77-81.

Appendix A - Pax7 is Critical for the Normal Function of Satellite Cells in Adult Skeletal Muscle

Pax7 is Critical for the Normal Function of Satellite Cells in Adult Skeletal Muscle

Julia von Maltzahn[1,2], Andrew E. Jones[1,2], Robin J. Parks[1] and Michael A. Rudnicki[1,2,3]

1. Sprott Centre for Stem Cell ResearchOttawa Hospital Research InstituteOttawa, OntarioCanada 2. Department of Cellular and Molecular MedicineFaculty of MedicineUniversity of OttawaOttawa, OntarioCanada 3. Corresponding author:Regenerative Medicine ProgramOttawa Hospital Research Institute501 Smyth RoadOttawa, OntarioCanada, K1H 8L6Tel: 613-739-6740Fax: 613-737-8803Email: mrudnicki@ohri.ca

Submitted to Proceedings of the National Academy of Sciences of the United States of America

Extensive analyses of mice carrying null mutations in Pax7 have confirmed the progressive loss of the satellite cell lineage in skeletal muscle, resulting in severe muscle atrophy and death. A recent study using floxed alleles and tamoxifen-induced inactivation concluded that after three weeks of age, Pax7 was entirely dispensable for satellite cell function. Here, we demonstrate that Pax7 is an absolute requirement for satellite cell function in adult skeletal muscle. Following Pax7 deletion, satellite cells and myoblasts exhibit cell-cycle arrest and dysregulation of myogenic regulatory factors. Maintenance of Pax7 deletion through continuous tamoxifen administration prevented regrowth of Pax7-expressing satellite cells and a profound muscle regeneration deficit that resembles the phenotype of skeletal muscle following genetically engineered ablation of satellite cells. Therefore, we conclude that Pax7 is essential for regulating the expansion and differentiation of satellite cells during both neonatal and adult myogenesis.

CreERT2 | Pax7 | regeneration | satellite cells | skeletal muscle

Introduction

Skeletal muscle exhibits a remarkable ability to regenerate, a process that has been demonstrated to be dependent on satellite cells (1-5). In resting muscle, satellite cells remain quiescent whereas in response to growth or trauma, satellite cells become activated, enter the cell cycle, and give rise to proliferating myogenic precursor cells that either differentiate by fusing with existing myofibers or forming new myofibers (6, 7). This process is highly regulated by growth factors and the composition of the niche, and by expression of key transcriptional regulators such as Pax7 and myogenic regulatory factors (MRFs), which control specification and differentiation analogously to embryonic development (6, 8-10).

Satellite cells uniformly express the transcription factor Pax7, and extensive analysis of *Pax7*$^{-/-}$ mice has thoroughly documented the progressive loss of the satellite cell lineage in multiple muscle groups likely due to a failure to proliferate together with precocious differentiation (1, 5, 11, 12). *Pax7*$^{-/-}$ muscles are reduced in size, the myofibers contain approximately 50% the normal number of nuclei, and fiber diameters are significantly reduced. The mice exhibit poor survivability and typically die within the first three weeks of life.

Consistent with a central role for Pax7 in satellite cell function, siRNA-mediated knockdown of *Pax7* in any age of cultured myoblasts or satellite cells, results in growth arrest and loss of Myf5 expression (13, 14). Indeed, Pax7 has been shown to inhibit differentiation by inhibiting MyoD-dependent activation of myogenin (15, 16). Recently, ChIP-seq analysis indicates that Pax7 binds to distinct DNA motifs to activate genes involved in specifying myogenic identity, promoting proliferation and inhibiting differentiation (17). Together, these data support an essential role for Pax7 in regulating the myogenic potential and function of satellite cells. By contrast to these findings, a provocative study by Lepper *et al*., (2009) suggested that Pax7 was entirely dispensable in adult life. Tamoxifen-induced Pax7-deletion in satellite cells after three weeks of age (P21) was reported to not lead to any deficiency in muscle regeneration or satellite cell number (18). In this report, we demonstrate that Pax7 expression is an absolute prerequisite for the normal function of satellite cells during regenerative myogenesis at any age.

Results

Pax7 Deficiency Results in Cell-Cycle Arrest and Precocious Differentiation

To investigate the growth and differentiation of Pax7-deficient primary myoblasts, we employed adenovirus expressing Cre recombinase (Ad-Cre) to efficiently delete Pax7 in primary myoblasts derived from 6-week old *Pax7*$^{fl/fl}$ mice. Primary myoblasts (*Pax7*$^{fl/fl}$) infected with Ad-Cre clearly showed a complete loss of Pax7 expression in 100% of the cells (Fig. 1A and 1B). Strikingly, Pax7 deletion resulted in an immediate and complete growth arrest, with no appreciable proliferation after 6d in culture (Fig. 1C). By contrast, primary myoblasts infected with a control adenovirus (Ad-GFP) underwent a 50-fold expansion during the same time period (Fig. 1C). We also noted that infection with Ad-Cre also did not have a discernable effect on the proliferation of wild type primary myoblasts.

We have previously documented that Myf5 is a direct target gene of Pax7, and that Myf5 transcription varies directly with Pax7 levels (13, 17). Primary myoblasts where *Pax7* was deleted with Ad-Cre exhibited an almost 75% reduction in the levels of *Myf5* mRNA, a 25% reduction in *MyoD* expression, and no change in *myogenin* expression levels (Fig. S1A). Notably, Pax7-deficient myoblasts plated at high density were nevertheless able to undergo normal differentiation, as evidenced by the diameter and fusion index of the myotubes (Fig. S1B-D).

Knock down of Pax7 prevents the activation of Myf5 following an asymmetric satellite stem cell division on cultured myofibers from adult skeletal muscle (14). Therefore, we investigated the ability of Pax7-deficient satellite cells on cultured myofibers to undergo proliferation and differentiation. Following siRNA mediated knock down of *Pax7*, the numbers of satellite cells were decreased 2.4-fold after 72h of culture (Fig. 1E, n=4, $p<0.001$; *Pax7* siRNA knockdown efficiency: 90%±15%, n=4). Furthermore numbers of multi-cell clusters were reduced 3.5-fold (Fig. 1F, n=4, $p<0.01$), while numbers of single satellite cells were increased 3-fold (Fig. 1G, n=4, $p<0.01$). We also observed a 2.6-fold increase in the numbers of satellite cells

Reserved for Publication Footnotes

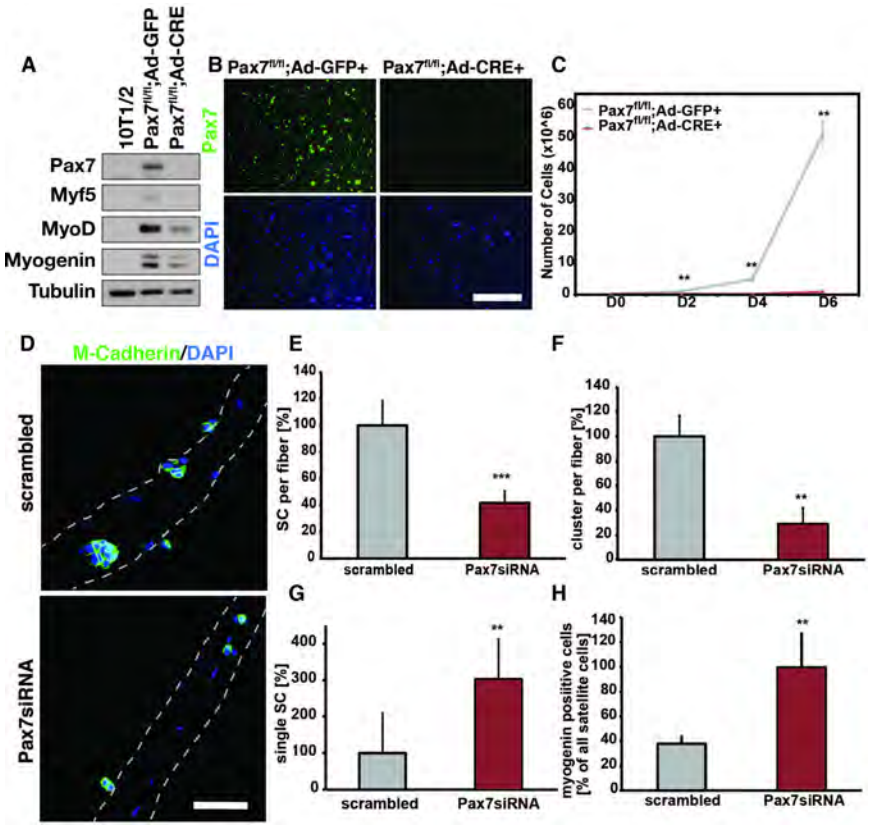

Fig. 1. Pax7 deletion results in cell-cycle arrest and precocious differentiation. (*A*) Infection of *Pax7*$^{fl/fl}$myoblasts with an adenovirus encoding the Cre gene leads to depletion of Pax7 expression and loss of Myf5 protein expression. (*B*) Infection of *Pax7*$^{fl/fl}$myoblasts with an adenovirus encoding the Cre gene leads to depletion of Pax7 expression, Pax7 immunostaining is depicted in green, nuclei are counterstained with DAPI. Scale bar: 100μm. (*C*) Ad-Cre mediated *Pax7* deletion results in growth arrest in primary myoblasts, relative to control (Ad-GFP) myoblasts. (*D*) siRNA mediated depletion of *Pax7* expression in satellite cells leads to reduced numbers of satellite cells (marked by M-Cadherin staining in green) after 72h of culture. Nuclei are counterstained with DAPI, scale bar: 100um. (*E*) Following depletion of *Pax7* in satellite cells on single myofibers the number of satellite cells per fiber is significantly reduced, n=4, ***p<0.001. (*F*) Numbers of clusters (three or more satellite cells on a fiber attached to each other) are reduced following treatment with *Pax7* siRNA compared to scrambled control, n=4, ***p<0.01. (*G*) Increase in the number of single satellite cells on myofibers following 72h in culture and treatment with Pax7siRNA, n=4, ***p<0.01. (*H*) Numbers of myogenin positive satellite cells increase after 72h in culture following depletion of Pax7 expression with *Pax7* siRNA, n=4, ***p<0.01.

expressing myogenin suggesting precocious differentiation (Fig. 1H, n=4, p<0.01). Similar results were obtained by comparing single myofiber cultures from tamoxifen induced *Pax7*$^{fl/CreERT2}$ and *Pax7*$^{fl/+}$ mice (Fig. S2). Therefore, we conclude that satellite cells and primary myoblasts lacking Pax7 undergo cell cycle arrest and precocious differentiation.

Inactivation of Pax7 in Adult Satellite Cells Markedly Impairs Muscle Regeneration

By employing the same alleles generated by Lepper *et al.*, (2009), we next set out to examine the adult phenotype of Pax7-deficient satellite cells. *Pax7*$^{fl/CreERT2}$ and *Pax7*$^{fl/+}$ mice were injected four times intraperitonally (IP) with tamoxifen between P40 and P44 to induce the excision of exon 2, partially encoding the paired domain, and generate an out-of-frame mutant *Pax7* transcript in satellite cells (Fig. 2A). One week later, muscle regeneration was induced by injection of cardiotoxin (CTX) into the *tibialis anterior* (TA) muscle in the hind limb. The TA muscles in control *Pax7*$^{fl/+}$ mice were efficiently regenerated 21d after acute injury (Fig. 2A). Notably, regenerated muscle in *Pax7*$^{fl/CreERT2}$ mice following tamoxifen IP-injection exhibited evidence of accumulation of cells in interstitial spaces and ectopic adipogenesis (Fig. 2B) at 21d following CTX injection.

This partial phenotype led us to hypothesize that tamoxifen injection was not 100% effective in deleting the floxed *Pax7* allele in satellite cells. To address this possibility, mice that were IP-injected with tamoxifen were additionally maintained on chow containing tamoxifen throughout the experimental time course (Fig. 2A). Importantly, control *Pax7*$^{fl/+}$ mice subjected to continuous tamoxifen treatment, exhibited efficient regeneration of the *tibialis anterior* (TA) muscle 21d after acute injury as evidenced by centrally located nuclei and no appreciable deposition of fibrotic tissue, adipose tissue or deposition of calcium (Fig. 2B-E, Fig. S3). By contrast, the TA muscles of *Pax7*$^{fl/CreERT2}$ mice continuously treated with tamoxifen exhibited a severe regeneration deficit characterized by smaller numbers of regenerating fibers, extensive deposition of adipose tissue, fibrotic tissue and calcium deposits (Fig. S2B-E and S3, Tables S1 and S2).

To quantitatively evaluate muscle regeneration in *Pax7*$^{fl/+}$ versus *Pax7*$^{fl/CreERT2}$ mice, we examined histological sections of TA muscles at 10d after acute injury through CTX injection in mice where CreERT2 activity was maintained with tamoxifen-containing chow. In comparison with mice treated only by tamoxifen IP-injection, muscle regeneration was dramatically impaired in *Pax7*$^{fl/CreERT2}$ mice continuously treated with tamoxifen (Fig. 3A). We observed a 2.1-fold reduction in the number of regenerated myofibers (Fig. 3B and 3D) together with a marked increase in the numbers of interstitial cells relative to *Pax7*$^{fl/+}$ TA muscle (Fig. 3A and 3G). Moreover, myofibers were 1.8-fold smaller as measured by the minimal fiber feret and the overall numbers of myonuclei were reduced 3.3-fold (Fig. 3C and S4E).

Consistent with a significant delay in regeneration, immunostaining for developmental myosin heavy chain (devMHC) revealed a 7.5-fold increase in the numbers of immature myofibers (Fig. S4A and S4B), and a 1.8-fold increase in the numbers of myogenin expressing cells (Fig. S4C and S4D). Furthermore, we observed a 6.7-fold increase in the numbers of MyoD negative smooth muscle actin (SMA) positive cells (Fig. 3E and 3F), indicative of myofibroblasts. Therefore, we conclude that maintenance of CreERT2 activity by continuous exposure to tamoxifen results in a dramatic enhancement of a muscle regeneration deficit due to a loss of satellite cell proliferative capacity.

Continuous Tamoxifen Treatment Prevents Grow-Back of Pax7-Expressing Satellite Cells

One explanation for the apparently normal regeneration following IP-injection of tamoxifen (18), is that satellite cells that

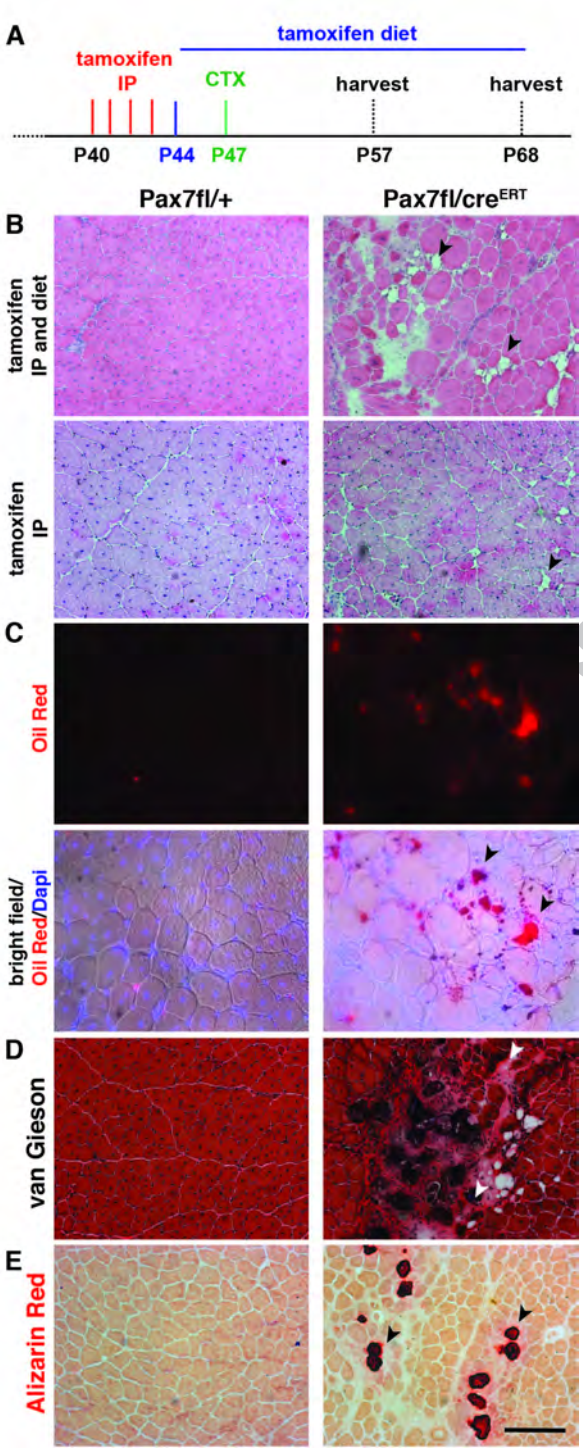

Fig. 2. Inactivation of Pax7 in adult satellite cells markedly impairs muscle regeneration. (*A*) Schematic showing the experimental regime used in this study. (*B*) H&E staining of *tibialis anterior* muscle 21d after acute injury induced by CTX injection. Arrowheads point to fat depositions. (*C*) Oil Red staining showing lipid deposits (in red, marked by arrowheads) in $Pax7^{fl/CreERT2}$ mice maintained on tamoxifen diet. (*D*) van Gieson staining demonstrating increased connective tissue deposition (bright red, marked by arrowheads) in $Pax7^{fl/CreERT2}$ mice maintained on tamoxifen diet. (*E*) Alizarin Red staining marking calcium deposition (in red, marked arrowheads) in $Pax7^{fl/CreERT2}$ mice maintained on tamoxifen diet. Scale bar: 100μm.

escape tamoxifen-induced deletion of the floxed *Pax7* allele are capable of repopulating a regenerating muscle to mediate a partial regeneration phenotype. To test this hypothesis, we enumerated the numbers of Pax7-expressing satellite cells in $Pax7^{fl/CreERT2}$ mice that had received continuous tamoxifen treatment (see Fig. 2A) in the injured TA muscle relative to the uninjured contralateral TA muscle or mice that had only received IP injections of tamoxifen (Fig. 4). The uninjured muscle exhibited efficient excision of *Pax7* in satellite cells with an over 80% reduction in the numbers of Pax7-expressing satellite cells (Fig. 4A-D). Strikingly, in mice that only received tamoxifen through IP injections, the number of residual Pax7-expressing satellite cells increased over 10-fold following acute injury (Fig. 4A,C). By contrast, continuous exposure to tamoxifen completely suppressed the regrowth of Pax7-expressing satellite cells (Fig. 4B, D). Taken together, these results underscore the need to perform control experiments when using conditional alleles in conditions where a small subpopulation that escapes deletion can repopulate the tissue due to a tremendous growth advantage.

Discussion

In adult muscle, satellite cells express Pax7, a paired-box transcription factor, and remain quiescent under normal physiological conditions. Satellite cells are readily responsive to molecular triggers from exercise, injuries or disease, and have a remarkable ability to self-renew, expand, proliferate as myoblasts, or undergo myogenic differentiation to fuse and restore damaged muscle. Since the discovery of satellite cells, extensive evidence from multiple laboratories has accumulated to demonstrate that they are the primary contributors to postnatal growth, maintenance, and repair of skeletal muscle (6, 19).

Many studies have demonstrated that Pax7 plays a critical role in regulating the function of satellite cells. We and others have performed extensive analyses of $Pax7^{-/-}$ mice and have thoroughly documented the progressive loss of the satellite cell lineage in all muscle groups (1, 5, 11, 12). By contrast, the study by Lepper et al., (2009) suggested that Pax7 was entirely dispensable for normal satellite cell function after a critical juvenile period.

Our experiments demonstrate that deletion of *Pax7* in adult satellite cells results in markedly impaired regeneration as evidenced by extensive deposition of fibrotic and adipose tissue and reduced formation of myofibers. Notably, this prominent regeneration deficit was only observed when $Pax7^{fl/CreERT2}$ mice were continuously treated with tamoxifen after receiving IP injections of tamoxifen (Fig. 2-4). Indeed, the regeneration phenotype in our experiments is highly similar to that observed following genetically engineered ablation of satellite cells in adult muscle (2, 3).

Our observations indicate that the observed difference in the severity of the regeneration phenotype is attributable to the regrowth of the small population of Pax7-expressing satellite cells when mice are not continuously treated with tamoxifen (Fig. 4). This argument is strongly supported by our observation that deletion of Pax7 in primary myoblasts and satellite cells results in growth arrest and down-regulation of the myogenic regulatory factors (Fig. 1). Our data strongly supports the interpretation that the limited regeneration that occurs in adult muscle in the absence of Pax7 is mediated by the precocious differentiation of committed satellite cells without their normal proliferation. Thus, Pax7-deficient satellite cells are unable to self-renew leading to their ultimate loss.

An interesting question is what is the fate of satellite stem cells that have yet to activate myogenic factor transcription. Satellite stem cells give rise to committed satellite myogenic cells through asymmetric cell divisions (20). Satellite stem cells express Pax7 but do not transcribe *Myf5*. Following an asymmetric cell division, Carm1-mediated arginine methylation of residues in the N-Terminus of Pax7 allows the binding MLL1/2 and the activation the Myf5 transcription in the daughter satellite myogenic cell

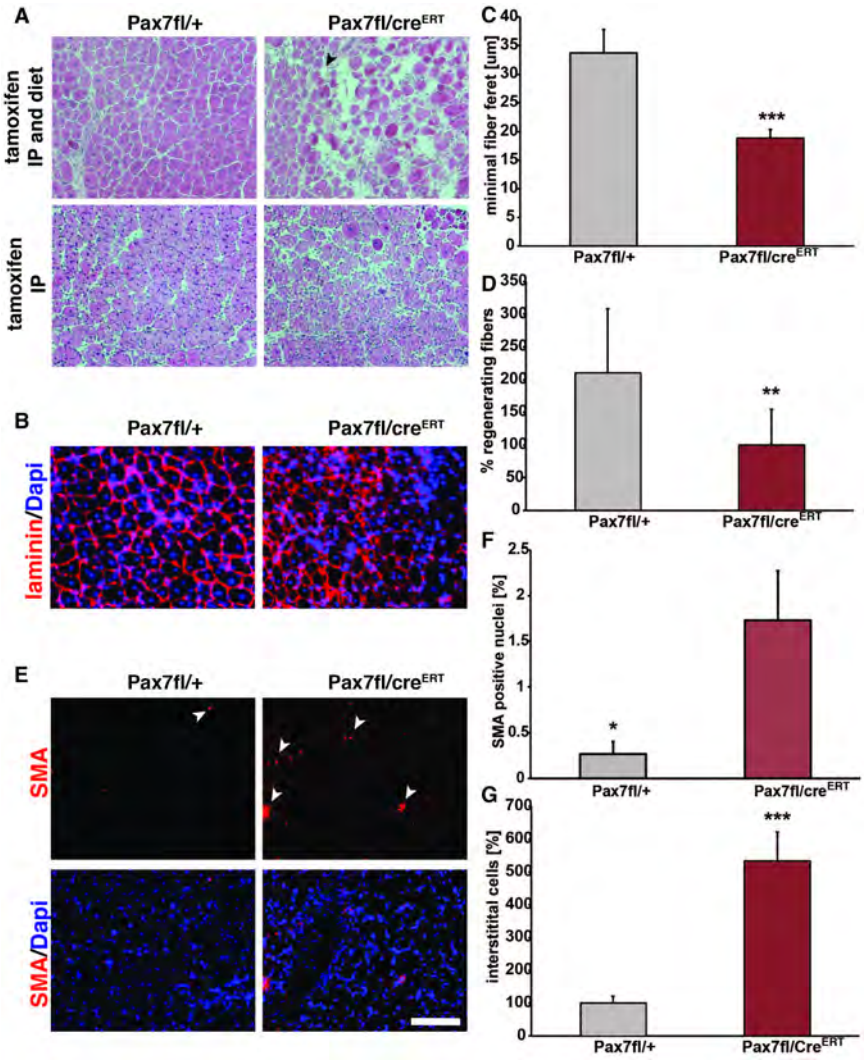

Fig. 3. Significantly impaired muscle regeneration with continuous tamoxifen treatment. (*A*) HE staining 10d after acute injury reveals markedly impaired regeneration following continuous tamoxifen treatment. Scale bar: 100µm. (*B*) Immunostaining for laminin (in red) showing decreased numbers of fibers and also reduced fiber feret. Nuclei are counterstained with DAPI (in blue). Scale bar: 100µm. (*C*) Quantification of the minimal fiber feret of muscles at 10d after acute injury, n= 6, ***p<0.001. (*D*) Quantification of the amount of regenerating fibers at 10d after CTX injury, n=6, p<0.01. (*E*) Immunostaining for smooth muscle actin (SMA, in red) demonstrating increased numbers SMA positive nuclei in *Pax7*$^{fl/CreERT2}$ animals compared to *Pax7*$^{fl/+}$ animals at 10d after acute injury. Nuclei are counterstained with DAPI (in blue). Scale bar: 100µm. (*F*) Quantification of SMA positive nuclei relative to the total number of nuclei, n=6, *p<0.05. (*G*) Quantification of the numbers of interstitital cells, n=4, ***p<0.001.

(14). We have recently demonstrated that satellite stem cells are multipotent stem cells capable of myogenic and brown adipogenic commitment (21). Thus it is interesting to speculate that in the absence of Pax7, lineage switching to alternative fates would also contribute to the loss of the satellite cell pool.

In this manuscript, we report using the same *Pax7* alleles that were used by Lepper et al., 2009, that continuous tamoxifen treatment results in a pronounced muscle regeneration deficit. Moreover, primary myoblasts in culture and satellite cells in myofiber culture exhibit cell-cycle arrest following *Pax7* deletion. Our observations indicate that Pax7-deficient progenitors are incapable of expansion *in vivo* and undergo precocious differentiation. Therefore, we conclude that Pax7 is absolutely required for the normal function of satellite cells in regenerative myogenesis in both neonatal and adult skeletal muscle.

Material and Methods

Mouse Procedures and Tissue Culture

All animal procedures conform with the Canadian Council on Animal Care's Guide to the Care and Use of Experimental Animals, the Animals for Research Act, and were approved by the Animal Care Committee at University of Ottawa. For the study we used female *Pax7*$^{fl/CreERT2}$ or *Pax7*$^{fl/+}$ mice (18) that were kindly provided by Dr. Chen-Ming Fan. Adult mice were injected intraperitoneally with tamoxifen (10mg/ml in corn oil) and kept on tamoxifen containing standard chow (1mg tamoxifen per day/20g body weight). The TA muscle was injured by injection of 50µl cardiotoxin (Sigma, 10µM). Single myofibers were isolated from the *extensor digitorum longus* (EDL) muscle and cultured as described previously (8). Primary myoblasts were derived from lower hind limb skeletal muscle of 6 week old mice as described previously (22). For adenoviral infections, primary myoblasts were seeded and infected the following day with Ad-Cre or Ad-GFP at 5 multiplicity of infection (MOI) for 1h using established techniques (23).

Immunostaining, Protein and RNA Analyses

Western blot analyses, immunofluorescence analyses, RNA purification and quantitative RT-PCR were carried out as previously described (24). Antibodies used in the study were used as follows: Laminin (Sigma, 1:1000), Pax7 (Developmental Studies Hybridoma Bank, undiluted), Myogenin (Sigma, 1:200), Tubulin (Sigma, 1:5000), developmental Myosin (Leica, 1:50), Perilipin (Sigma, 1:200), smooth muscle actin (Sigma, 1:200), M-Cadherin (Millipore, 1:500), Myosin heavy chain (Developmental Hybridoma Bank, undiluted).

Statistical Analyses

Three or more replicates were analyzed for each experiment presented. Data are shown as standard error of the mean (Microsoft Excel), statistical significance was assessed by a Student's

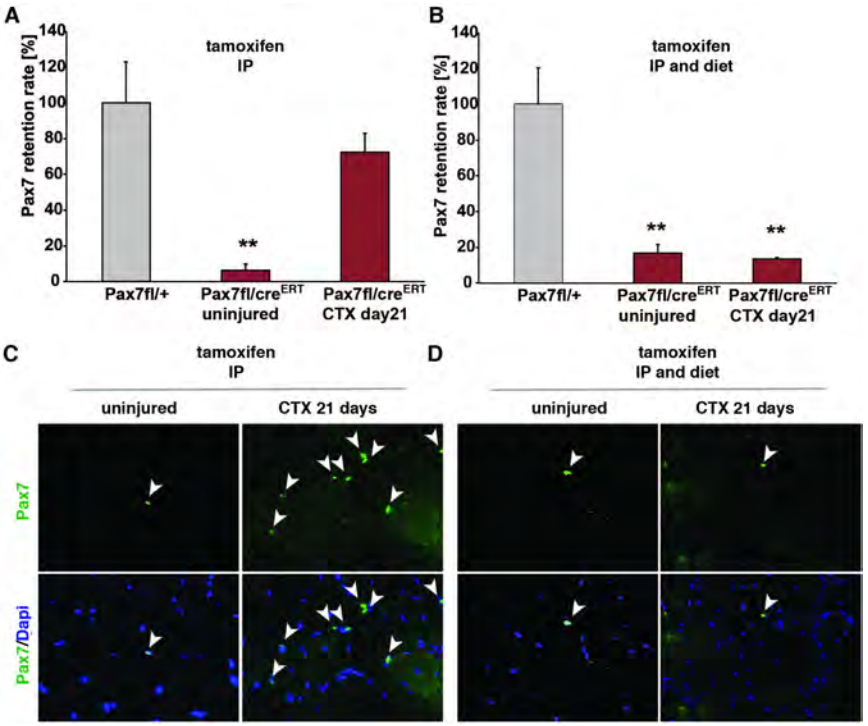

Fig. 4. Continuous tamoxifen treatment prevents grow-back of residual Pax7-expressing satellite cells. (*A*) Quantification of Pax7 expressing nuclei in *Pax7*$^{fl/CreERT2}$ mice induced with tamoxifen before and after acute injury. (*B*) Quantification of Pax7 expressing nuclei in *Pax7*$^{fl/CreERT2}$ mice with continuous tamoxifen application before and after acute injury. (*C*) Pax7 expression is lost after tamoxifen induced excision in *Pax7*$^{fl/CreERT2}$ mice (intraperitoneal injection) but reoccurs after acute injury, Pax7 immunostaining is shown in green, nuclei are counterstained with DAPI (in blue). (*D*) Pax7 deletion is only maintained when tamoxifen is continuously administered during regeneration of CTX injured muscles, Pax7 immunostaining is shown in green, nuclei are counterstained with DAPI (in blue). Scale bar: 50µm.

t-test (Microsoft Excel). Differences were considered significant with a p value <0.05.

Acknowledgements.

We thank Jennifer Ritchie and David Wilson for expert technical assistance. This work was supported by grants from the Canadian Institutes of Health Research, National Institutes of Health, the Muscular Dystrophy Association, and the Canada Research Chair Program. M.A.R. holds the Canada Research Chair in Molecular Genetics. **Author contributions** J.V.M., A.E.J. and M.A.R. planned the experimental design, analyzed the data, and wrote the paper. J.V.M. and A.E.J. conducted the experiments. R.J.P. provided the adenovirus used in the study.

1. Relaix F, *et al.* (2006) Pax3 and Pax7 have distinct and overlapping functions in adult muscle progenitor cells. *The Journal of cell biology* 172(1):91-102.
2. Lepper C, Partridge TA, & Fan CM (2011) An absolute requirement for Pax7-positive satellite cells in acute injury-induced skeletal muscle regeneration. *Development* 138(17):3639-3646.
3. Sambasivan R, *et al.* (2011) Pax7-expressing satellite cells are indispensable for adult skeletal muscle regeneration. *Development* 138(17):3647-3656.
4. Seale P, Ishibashi J, Scime A, & Rudnicki MA (2004) Pax7 Is Necessary and Sufficient for the Myogenic Specification of CD45(+):Sca1(+) Stem Cells from Injured Muscle. *PLoS Biol* 2(5):E130.
5. Oustanina S, Hause G, & Braun T (2004) Pax7 directs postnatal renewal and propagation of myogenic satellite cells but not their specification. *The EMBO journal* 23(16):3430-3439.
6. Yin H, Price F, & Rudnicki MA (2013) Satellite cells and the muscle stem cell niche. *Physiol Rev* 93(1):23-67.
7. von Maltzahn J, Chang NC, Bentzinger CF, & Rudnicki MA (2012) Wnt signaling in myogenesis. *Trends in cell biology* 22(11):602-609.
8. Bentzinger CF, *et al.* (2013) Fibronectin regulates wnt7a signaling and satellite cell expansion. *Cell Stem Cell* 12(1):75-87.
9. Bentzinger CF, Wang YX, & Rudnicki MA (2012) Building muscle: molecular regulation of myogenesis. *Cold Spring Harbor perspectives in biology* 4(2).
10. Bentzinger CF, Wang YX, von Maltzahn J, & Rudnicki MA (2012) The emerging biology of muscle stem cells: Implications for cell-based therapies. *BioEssays : news and reviews in molecular, cellular and developmental biology*.
11. Seale P, *et al.* (2000) Pax7 is required for the specification of myogenic satellite cells. *Cell* 102(6):777-786.
12. Kuang S, Charge SB, Seale P, Huh M, & Rudnicki MA (2006) Distinct roles for Pax7 and Pax3 in adult regenerative myogenesis. *The Journal of cell biology* 172(1):103-113.
13. McKinnell IW, *et al.* (2008) Pax7 activates myogenic genes by recruitment of a histone methyltransferase complex. *Nature cell biology* 10(1):77-84.
14. Kawabe Y, Wang YX, McKinnell IW, Bedford MT, & Rudnicki MA (2012) Carm1 regulates Pax7 transcriptional activity through MLL1/2 recruitment during asymmetric satellite stem cell divisions. *Cell stem cell* 11(3):333-345.
15. Olguin HC & Olwin BB (2004) Pax-7 up-regulation inhibits myogenesis and cell cycle progression in satellite cells: a potential mechanism for self-renewal. *Dev Biol* 275(2):375-388.
16. Olguin HC, Yang Z, Tapscott SJ, & Olwin BB (2007) Reciprocal inhibition between Pax7 and muscle regulatory factors modulates myogenic cell fate determination. *J Cell Biol* 177(5):769-779.
17. Soleimani VD, *et al.* (2012) Transcriptional dominance of Pax7 in adult myogenesis is due to high-affinity recognition of homeodomain motifs. *Developmental cell* 22(6):1208-1220.
18. Lepper C, Conway SJ, & Fan CM (2009) Adult satellite cells and embryonic muscle progenitors have distinct genetic requirements. *Nature* 460(7255):627-631.
19. Charge SB & Rudnicki MA (2004) Cellular and molecular regulation of muscle regeneration. *Physiol Rev* 84(1):209-238.
20. Kuang S, Kuroda K, Le Grand F, & Rudnicki MA (2007) Asymmetric self-renewal and commitment of satellite stem cells in muscle. *Cell* 129(5):999-1010.
21. Yin H, *et al.* (2013) MicroRNA-133 Controls Brown Adipose Determination in Skeletal Muscle Satellite Cells by Targeting Prdm16. *Cell Metab* in press.
22. Seale P, Ishibashi J, Holterman C, & Rudnicki MA (2004) Muscle satellite cell-specific genes identified by genetic profiling of MyoD-deficient myogenic cell. *Dev Biol* 275(2):287-300.
23. Huh MS, Parker MH, Scime A, Parks R, & Rudnicki MA (2004) Rb is required for progression through myogenic differentiation but not maintenance of terminal differentiation. *J Cell Biol* 166(6):865-876.
24. von Maltzahn J, Bentzinger CF, & Rudnicki MA (2012) Wnt7a-Fzd7 signalling directly activates the Akt/mTOR anabolic growth pathway in skeletal muscle. *Nature cell biology* 14(2):186-191.

Supplemental Material

Table S1: Continuous tamoxifen treatment leads to strongly impaired regeneration in *Pax7*$^{fl/CreERT2}$ mice 21 days after acute injury.

Animal ID	genotype	CTX damage*
364	Pax7fl/+	+/++
366	Pax7fl/+	+
370	Pax7fl/+	+/++
372	Pax7fl/+	+
981	Pax7fl/+	+
988	Pax7fl/+	+
989	Pax7fl/+	+
982	Pax7fl/cre	+++
983	Pax7fl/cre	+++
984	Pax7fl/cre	+++
985	Pax7fl/cre	+
987	Pax7fl/cre	++
989	Pax7fl/cre	++
990	Pax7fl/cre	+
365	Pax7fl/cre	++
367	Pax7fl/cre	++
369	Pax7fl/cre	+++
371	Pax7fl/cre	+++

*regenerating fibers, no fat: +; regenerating fibers, few fat depositions: ++; regenerating fibers, extensive fat deposition, fibrosis: +++.

Table S2: **Deletion of Pax7 expression leads to impairment of muscle regeneration 21 days after acute injury**

Animal ID	Genotype	CTX damage*
486	Pax7fl/+	+
490	Pax7fl/+	+/++
491	Pax7fl/+	+
487	Pax7fl/cre	++
488	Pax7fl/cre	++
489	Pax7fl/cre	++

* regenerating fibers, no fat: +; regenerating fibers, few fat depositions: ++; regenerating fibers, extensive fat deposition, fibrosis: +++.

Supplemental figure legends

Fig. S1. Pax7 is not required for the differentiation of primary myoblasts. (*A*) qPCR analysis confirms loss of Pax7 expression and dysregulation of Myf5 and MyoD following infection of *Pax7*$^{fl/fl}$ myoblasts with an adenovirus encoding the Cre gene. Data are presented as the mean + SEM, normalized to GAPDH and shown relative to Ad-GFP infected control myoblasts. (*B*) No differences in myotube diameter were observed following infection of *Pax7*$^{fl/fl}$ myoblasts with an adenovirus encoding the Cre gene compared to *Pax7*$^{fl/fl}$ myoblasts infected with an adenovirus encoding the GFP gene, n=3. (*C*) Primary myoblasts depleted for Pax7 expression differentiate normally, myosin heavy chain in green, nuclei are counterstained with DAPI (in blue), scale bar: 100um. (*D*) no differences in the fusion index (nuclei per myotube) were observed after depletion of Pax7 expression and consecutive differentiaton, n=3, cells were differentiated at similar confluencies.

Fig. S2. Pax7 is required for primary myoblasts proliferation. (*A*) Numbers of satellite cells on single myofibers are significantly decreased when satellite cells do not express Pax7 following tamoxifen induced induction of the CreERT in *Pax7*$^{fl/CreERT2}$ mice, n=2, $p<0.05$, 72h culture. (*B*) Reduced numbers of satellite cell clusters on EDL fibers of *Pax7*$^{fl/CreERT2}$ mice , n=2, $p<0.05$, 72h culture. (*C*) increase in the numbers of single satellite cells on single fibers from *Pax7*$^{fl/CreERT2}$ mice, n=2, $p<0.01$, 72h culture. (*D*) increase in the percentage of myogenin positive satellite cells on single fibers from *Pax7*$^{fl/CreERT2}$ mice, n=2, $p<0.05$, 72h culture.

Fig. S3. Maintenance of CreERT2 activity with continuous tamoxifen treatment leads to increased adipogenesis in *Pax7*$^{fl/CreERT2}$ mice. Immunostaining for perilipin (in green) demonstrates increased adipogenesis in *Pax7*$^{fl/CreERT2}$ mice, laminin staining in red, nuclei are counterstained with DAPI (in blue), scale bar: 100μm.

Fig. S4. Impairment of muscle regeneration following deletion of Pax7 in satellite cells. (*A*) Deletion of Pax7 in adult satellite cells results in delayed regeneration marked by expression of developmental myosin (in green) at day 10 after acute injury. Laminin staining in red, nuclei are counterstained with DAPI (in blue). Scale bar: 100μm. (*B*) Quantification of developmental myosin heavy chain fibers at day 10 after CTX injury, n=6, $p<0.001$. (*C*) Immunostaining for myogenin (in green demonstrating increased numbers of myogenin positive nuclei in *Pax7*$^{fl/CreERT2}$ animals compared to *Pax7*$^{fl/+}$ animals at 10 d after acute injury. Nuclei are counterstained with DAPI (in blue). Scale bar: 100μm. (*D*) Quantification of myogenin positive nuclei relative to the total number of nuclei, n=6, $^{**}p<0.01$. (*E*) Quantification of the number of myonuclei, n=4, $p<0.05$.

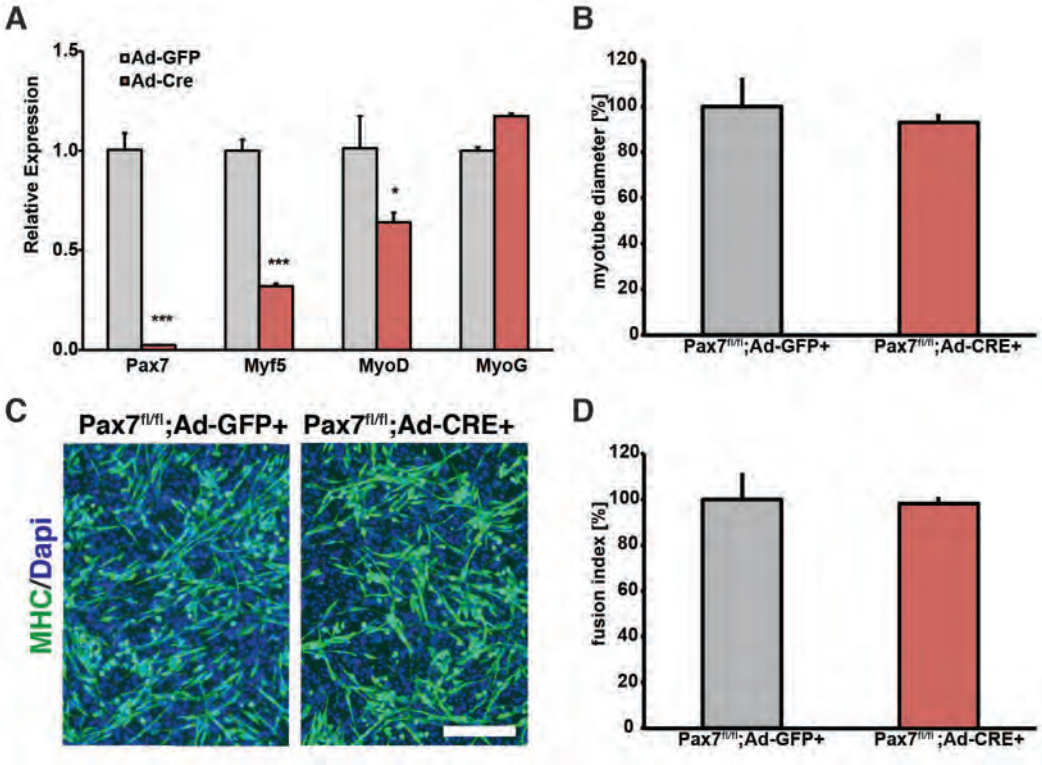
A
Ad-GFP
Ad-Cre
Relative Expression
1.5
1.0
0.5
0.0
***
***
*
Pax7
Myf5
MyoD
MyoG
B
myotube diameter [%]
120
100
80
60
40
20
0
Pax7fl/fl;Ad-GFP+
Pax7fl/fl;Ad-CRE+
C
Pax7fl/fl;Ad-GFP+
Pax7fl/fl;Ad-CRE+
MHC/Dapi
D
fusion index [%]
120
100
80
60
40
20
0
Pax7fl/fl;Ad-GFP+
Pax7fl/fl;Ad-CRE+

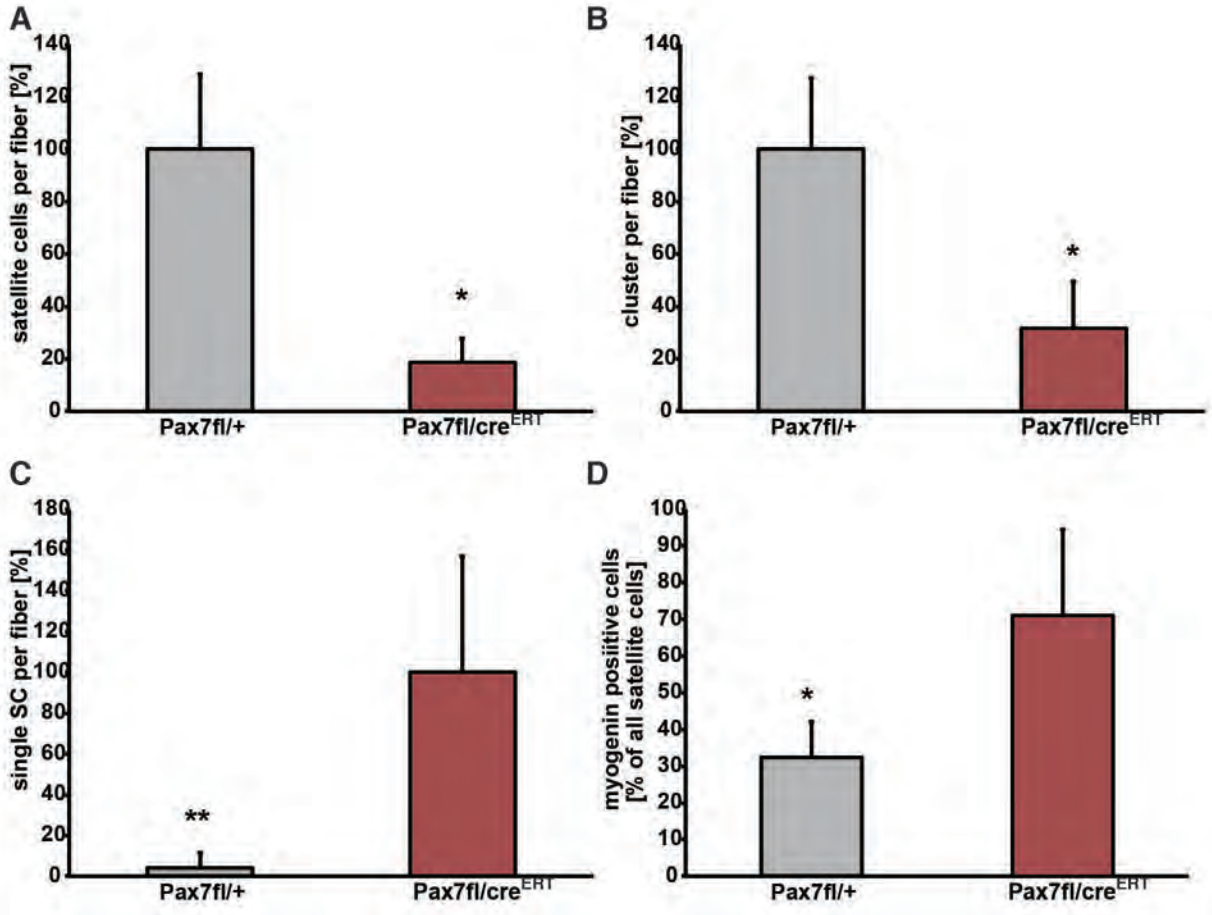
A
satellite cells per fiber [%]
140
120
100
80
60
40
20
0
*
Pax7fl/+
Pax7fl/creERT
B
cluster per fiber [%]
140
120
100
80
60
40
20
0
*
Pax7fl/+
Pax7fl/creERT
C
single SC per fiber [%]
180
160
140
120
100
80
60
40
20
0
**
Pax7fl/+
Pax7fl/creERT
D
myogenin posiitive cells
[% of all satellite cells]
100
90
80
70
60
50
40
30
20
10
0
*
Pax7fl/+
Pax7fl/creERT

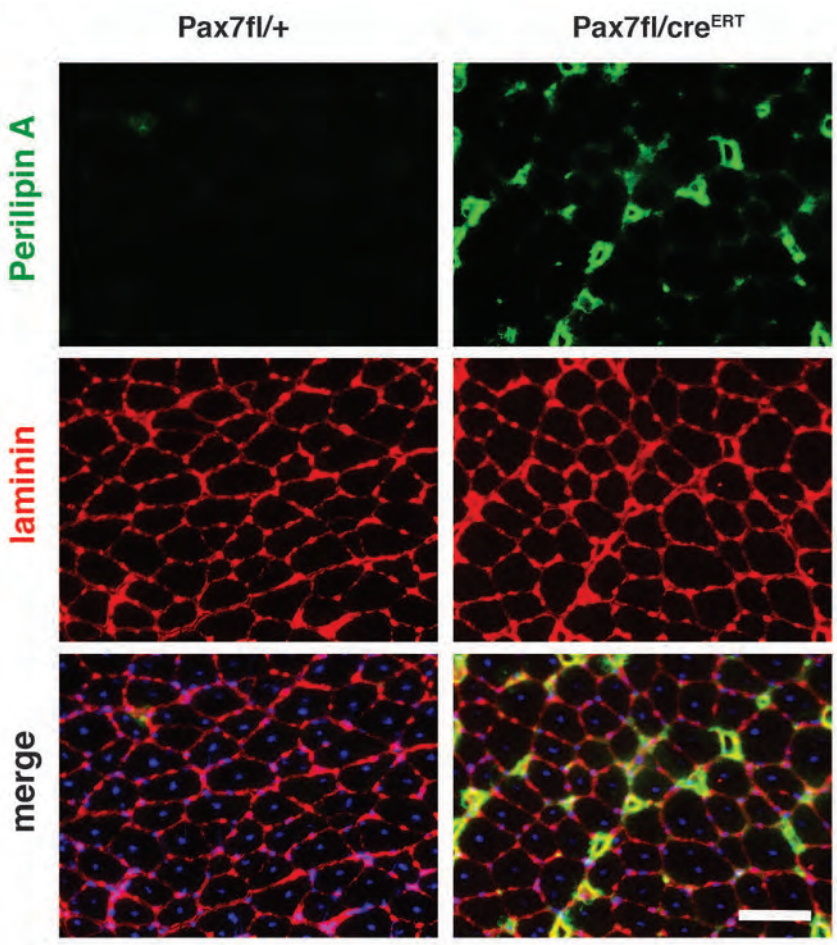
Pax7fl/+
Pax7fl/creERT
Perilipin A
laminin
merge

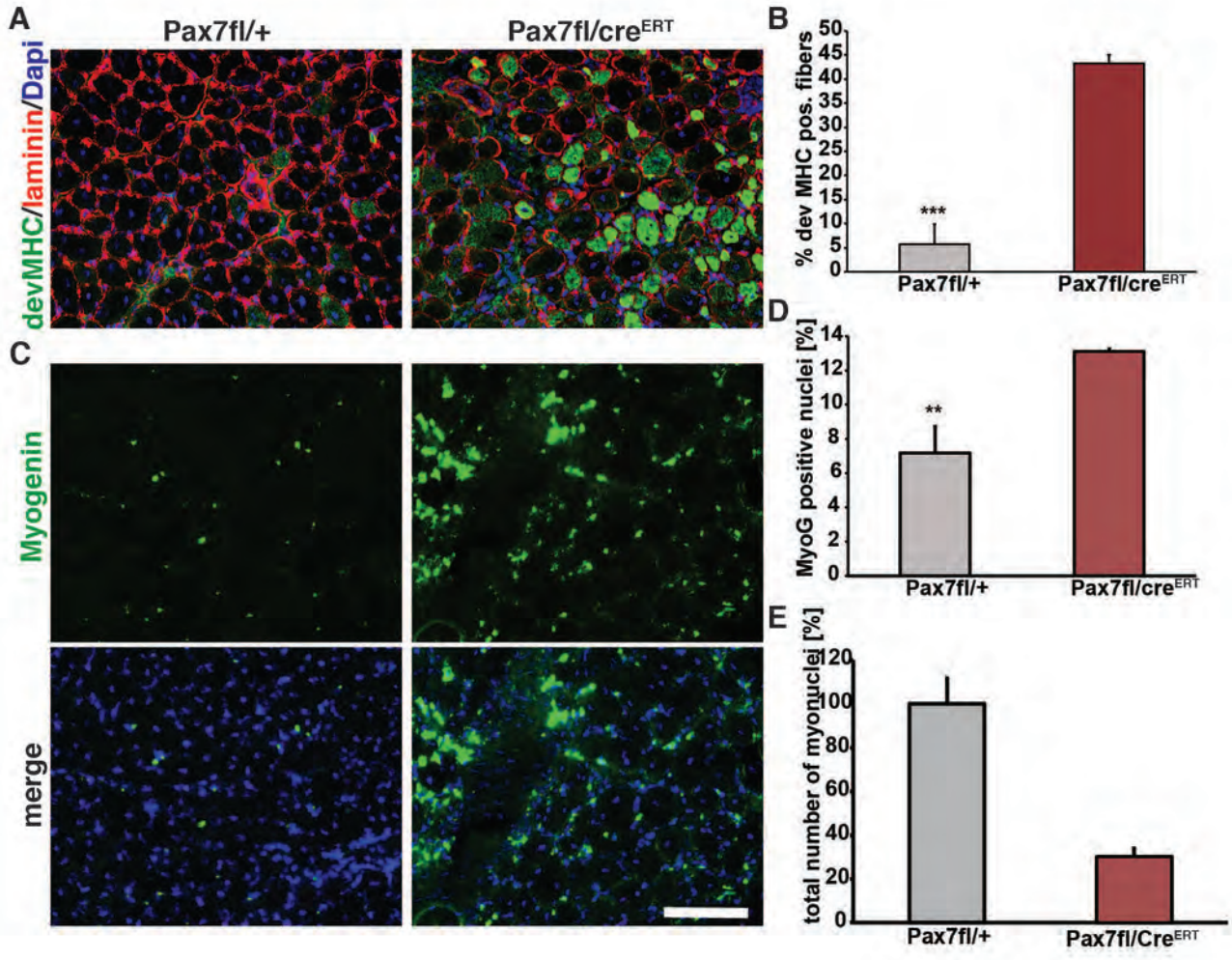
A
Pax7fl/+
Pax7fl/creERT
devMHC/laminin/Dapi
C
Myogenin
merge
B
% dev MHC pos. fibers
50
45
40
35
30
25
20
15
10
5
0
***
Pax7fl/+
Pax7fl/creERT
D
MyoG positive nuclei [%]
14
12
10
8
6
4
2
0
**
Pax7fl/+
Pax7fl/creERT
E
total number of myonuclei [%]
120
100
80
60
40
20
0
Pax7fl/+
Pax7fl/CreERT

Appendix B - Transcriptional Dominance of Pax7 in Adult Myogenesis Is Due to High-Affinity Recognition of Homeodomain Motifs

Developmental Cell
Article

Transcriptional Dominance of Pax7 in Adult Myogenesis Is Due to High-Affinity Recognition of Homeodomain Motifs

Vahab D. Soleimani,[1,2,5] Vincent G. Punch,[1,2,5] Yoh-ichi Kawabe,[1,2] Andrew E. Jones,[1,2] Gareth A. Palidwor,[1] Christopher J. Porter,[1] Joe W. Cross,[3] Jaime J. Carvajal,[3] Christel E.M. Kockx,[4] Wilfred F.J. van IJcken,[4] Theodore J. Perkins,[1,2] Peter W.J. Rigby,[3] Frank Grosveld,[4] and Michael A. Rudnicki[1,2,*]
[1]Sprott Centre for Stem Cell Research, Ottawa Hospital Research Institute, Ottawa, ON K1H 8L6, Canada
[2]Department of Medicine, University of Ottawa, Ottawa, ON K1H 8M5, Canada
[3]Section of Gene Function and Regulation, The Institute of Cancer Research, London SW3 6JB, United Kingdom
[4]Erasmus University and Medical Center & Center for Biomedical Genetics, 3000 CA Rotterdam, The Netherlands
[5]These authors contributed equally to this work
*Correspondence: mrudnicki@ohri.ca
DOI 10.1016/j.devcel.2012.03.014

SUMMARY

Pax3 and Pax7 regulate stem cell function in skeletal myogenesis. However, molecular insight into their distinct roles has remained elusive. Using gene expression data combined with genome-wide binding-site analysis, we show that both Pax3 and Pax7 bind identical DNA motifs and jointly activate a large panel of genes involved in muscle stem cell function. Surprisingly, in adult myoblasts Pax3 binds a subset (6.4%) of Pax7 targets. Despite a significant overlap in their transcriptional network, Pax7 regulates distinct panels of genes involved in the promotion of proliferation and inhibition of myogenic differentiation. We show that Pax7 has a higher binding affinity to the homeodomain-binding motif relative to Pax3, suggesting that intrinsic differences in DNA binding contribute to the observed functional difference between Pax3 and Pax7 binding in myogenesis. Together, our data demonstrate distinct attributes of Pax7 function and provide mechanistic insight into the nonredundancy of Pax3 and Pax7 in muscle development.

INTRODUCTION

The maintenance and repair of adult muscle tissue is directed by satellite cells. Quiescent satellite cells are activated by exercise or injury and enter the cell cycle to produce progeny myogenic precursor cells that undergo multiple rounds of division before entering terminal differentiation and fusing to multinucleated myofibers (Chargé and Rudnicki, 2004). Moreover, satellite cells exist as a heterogeneous population based on *Myf5* expression, a feature that divides the satellite cell pool into a subpopulation of self-renewing stem cells (*Myf5*$^{-}$) and committed progenitors (*Myf5*$^{+}$) (Kuang et al., 2007).

Satellite cells express the paired box transcription factors Pax3 and Pax7, which lie genetically upstream of the myogenic regulatory factors (MRFs) MyoD and Myf5 (Buckingham and Relaix, 2007). Pax7 is uniformly expressed at high levels in satellite cells and plays a critical role in regulating their function. By contrast, equivalent level of Pax3 is expressed in satellite cells in a subset of muscles such as diaphragm, but satellite cells in most muscle groups express very low levels (Kassar-Duchossoy et al., 2005). Extensive analyses of *Pax7*$^{-/-}$ mice have confirmed the progressive loss of the satellite cell lineage in multiple muscle groups (Kuang et al., 2006; Oustanina et al., 2004; Relaix et al., 2006; Seale et al., 2000). Small numbers of Pax7-deficient cells do survive in the satellite cell position but these cells are progressively lost, likely due to survival deficits or precocious differentiation. *Pax7*$^{-/-}$ muscles are reduced in size, the fibers contain approximately 50% the normal number of nuclei, and fiber diameters are significantly reduced (Kuang et al., 2006). Notably, Pax7 dependency in satellite cells has been suggested to be limited to a critical juvenile period when satellite cells are transitioning to a quiescent state (Lepper et al., 2009).

Our current understanding is that Pax3 and Pax7 play some overlapping but mostly nonredundant roles in the specification and progression of the adult satellite cell lineage. During early myogenesis, Pax3 and Pax7 expression defines a population of embryonic progenitors that have been suggested to later give rise to satellite cells. In the absence of both Pax3/7, these progenitors undergo apoptosis, or adopt alternative nonmyogenic cell fates (Kassar-Duchossoy et al., 2005; Relaix et al., 2005). However, Pax3 expression does not rescue the loss of Pax7 in adult satellite cells. For example, while Pax3-expressing cells are found in the limb muscles of *Pax7*$^{-/-}$ mice and express MyoD, these cells are progressively lost, display poor myogenic potential, and are located in the interstitial space rather than the satellite cell niche (Kuang et al., 2006; Relaix et al., 2006). Notably, satellite cells in the diaphragm express high levels of Pax3, but nonetheless, in *Pax7*$^{-/-}$ mice are similarly lost leading to progressive muscle wasting in the same manner as other muscle groups (Seale et al., 2000). Together, these data underscore the nonredundant functions of Pax3 and Pax7 in the myogenic program.

The transcriptional network that controls satellite cell lineage progression is similar to that deployed during embryonic myogenesis. During development, Pax3 has been shown to be

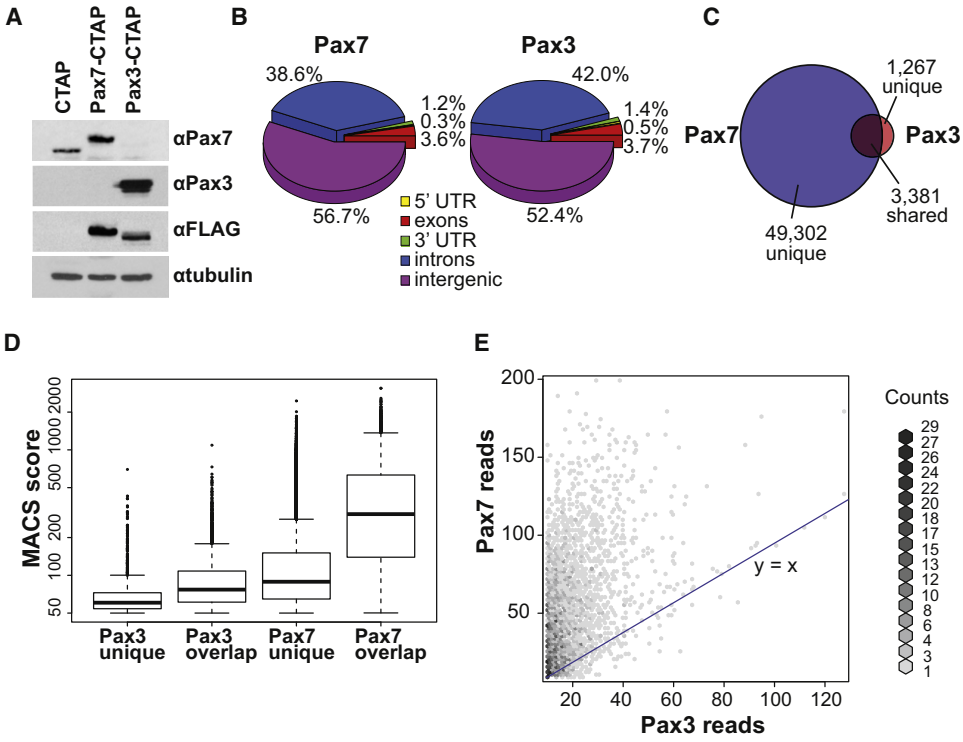

Figure 1. Pax3 Binds a Subset of Pax7 Binding Sites

(A) Overexpression of Pax7- and Pax3-CTAP in primary myoblasts reveals a reduction in endogenous levels of Pax7. Pax3 is not expressed in control cells. Also see Figure S1 for a quantitative estimate of proviral versus endogenous Pax7 protein measured as number of molecules per cell.

(B) Analysis of peak locations relative to gene start sites indicates Pax3 and Pax7 binding is predominantly in intergenic or intronic regions.

(C) Overlap of Pax3 and Pax7 peak data reveals that Pax3 binds only 6.4% of Pax7 sites.

(D) Comparison of peaks subsets for Pax3 and Pax7 indicates a stronger binding of Pax7 to DNA in adult skeletal muscle cells as shown by the MACS (Zhang et al., 2008) scores, calculated as $-10 \times \log_{10}$ (p value of the peaks).

(E) Plot of Pax3 versus Pax7 reads in common peaks shows that Pax7 peaks have generally higher sequence reads than Pax3 counterparts. Counts in the legend indicate number of peaks.

See also Figure S1 and Tables S1 and S2.

involved in the delamination and migration of embryonic myoblasts toward developing limb buds (Bober et al., 1994). Pax3 can also directly activate Myf5 and MyoD in the embryo, thereby initiating myogenic differentiation (Punch et al., 2009). Embryonic progenitors that give rise to satellite cells are characterized by Pax3/Pax7 expression and the lack of expression of other myogenic regulatory factors (MRFs: Myf5, MyoD, Mrf4, and Myogenin). Pax3/7$^+$ cells enter the myogenic program by upregulation of Myf5/MyoD, or give rise to satellite cells during late fetal myogenesis without upregulating MRFs. Pax3/7$^+$MRF$^-$ progenitors are first found to align with nascent myotubes at E15.5, then become satellite cells by taking a sublaminar position (Relaix et al., 2005). Intriguingly, Pax3/7$^+$MRF$^-$ progenitors rapidly upregulate Myf5 and downregulate Pax3 expression upon arrival at the nascent muscle groups (Kassar-Duchossoy et al., 2005). Lineage tracing suggests that Pax3$^+$ cells contribute to embryonic myoblasts and the endothelial lineage whereas Pax7$^+$ cells contribute to fetal myoblasts supporting the notion that these represent distinct myogenic lineages (Hutcheson et al., 2009). Thus, satellite stem cells (Pax7$^+$/Myf5$^-$) in adult muscle may be a lineage continuum of the embryonic Pax3/7$^+$MRF$^-$ progenitors (Kuang et al., 2007).

Pax3 and Pax7 have overlapping but largely nonredundant roles in the myogenic developmental program. An outstanding question is which target genes mediate the distinct function of Pax7 in adult satellite cells? Given the 86% sequence similarity between Pax3 and Pax7 proteins, an even intriguing question is which attributes of Pax7 specify those distinct biological functions. Here, we tackled these key questions using genomic approaches. Our experiments have provided a mechanistic understanding of transcription activities of Pax7 and Pax3 in adult satellite cells.

RESULTS

Genome-wide Binding of Pax3 and Pax7 in Adult Skeletal Muscle

To facilitate comparative analysis between Pax3 and Pax7, we produced stable cell lines with similar expression level of Pax3-TAP and Pax7-TAP (Figure 1A). Importantly, this approach facilitated our analysis as endogenous Pax7 was completely repressed by proviral expression of either Pax3-TAP or Pax7-TAP, and thus not involved in the dimerization of Pax complexes. We estimated proviral expression levels against wild-type

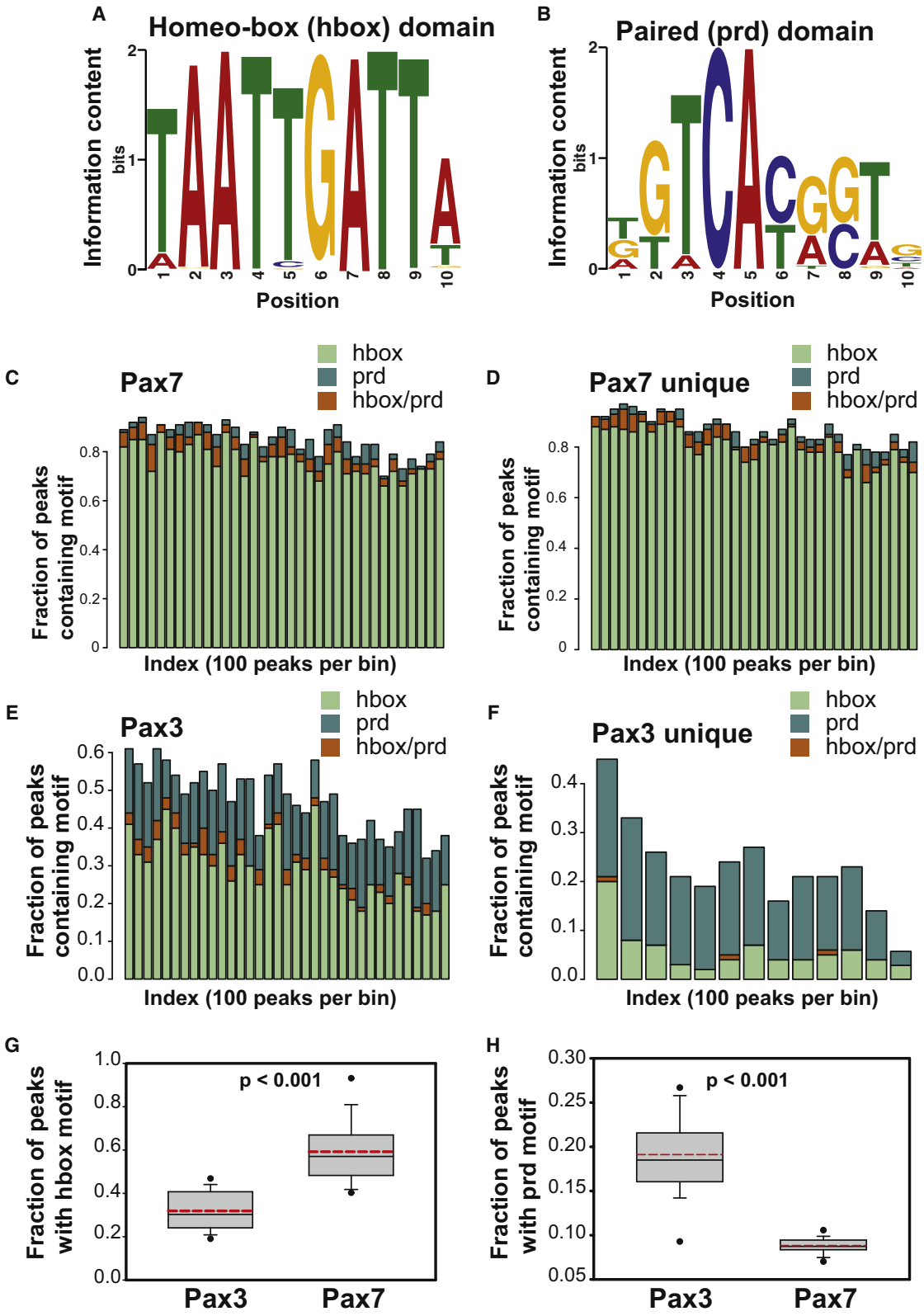

Figure 2. Differential Binding of Pax7 and Pax3 to Homeobox and Paired Motifs

(A and B) Pax7 and Pax3 binding sites obtained from ChTAP-seq are enriched for homeobox (hbox) and paired (prd) motifs. Consensus sequence of hbox and prd motif obtained from MEME (Bailey et al., 2009) analysis of the top 500 Pax3/Pax7 peaks, ranked based on MACS (Zhang et al., 2008) scores. MEME search was restricted to a 50 bp window around peak summit. See Figure S2 for a description of ChTAP and validation of a subset of targets.

myoblasts by fluorescent activated cell sorting coupled with quantitative western blot analysis. Proviral Pax7 was expressed at 6×10^5 molecules per cell compared to 2.75×10^4 endogenous Pax7 molecules per cell (Figure S1 available online).

The use of ChTAP allowed us to perform ChIP using two sequential immunoprecipitation steps under identical conditions by using same affinity reagents in experiments and control reactions, therefore reducing the likelihood of false positives (Figure S2; Supplemental Experimental Procedures). This approach allowed us to conduct a direct comparison between Pax3 and Pax7.

Ultra high-throughput sequencing of ChTAP fragments on a GAIIx sequencer (Illumina) (see Supplemental Experimental Procedures) yielded 11.4 million uniquely mapped reads for Pax7, 12.4 million reads for Pax3, and 8.5 million reads for the control sample (The ELAND output of Pax3 and Pax7 ChIP-seq data are available in GEO as the series GSE25064 containing TAP-tagged Pax7, TAP-tagged Pax3, and control samples; GSM615619, GSM615620, and GSM615621, respectively). To identify genome-wide Pax3 and Pax7 binding sites, reads from Pax3 or Pax7 together with the corresponding control reads were analyzed using Model-based Analysis for ChIP-Seq (MACS v 1.3) (Zhang et al., 2008). Binding sites (peaks) were identified by comparing Pax3 and Pax7 read densities against the TAP background (control).

ChIP-PCR established the veracity of binding site identification in 100% of the sites tested (Figure S2).

We have previously shown that the presence of C-terminal TAP tag does not interfere with Pax7 function (McKinnell et al., 2008). Similarly, we found that the C-terminal TAP tagged Pax3 fully retains its function (Figure S3).

The vast majority of Pax3 and Pax7 binding sites were located within intergenic or intronic regions away from the transcription start sites (TSS) (Figure 1B; Figure S4). Few binding sites were observed within 5′ or 3′ untranslated regions. The majority of Pax3 binding sites were found to overlap Pax7 binding sites (Figure 1C). Surprisingly, while more than 52,683 genomic loci were enriched for Pax7 binding only 4,648 sites were similarly enriched for Pax3 (Figure 1C). This striking difference in binding was observed despite each transcription factor having a comparable numbers of reads and equivalent expression levels (Figures 1A and 1D).

Although the majority of Pax3 binding sites overlap with Pax7 binding sites, a significant 1,267 binding sites were uniquely occupied by Pax3 and not by Pax7 (Figure 1C). Analysis revealed that Pax3/Pax7 common peaks set had the highest quality score compared to the other peak sets (Figure 1D). Analysis of read distribution within the common peak set showed a modest correlation between Pax3 and Pax7. However, these peaks were more enriched for Pax7 reads than Pax3 (Figure 1E). Taken together, these finding suggest that Pax7 has more extensive genome coverage in adult myoblasts than Pax3. However, Pax3 binds a substantial set of targets not bound by Pax7. Thus, these data argue that Pax3 and Pax7 binding dynamics are markedly different in primary adult myoblasts.

Pax3 and Pax7 Bind to Identical DNA Motifs

To determine the consensus-binding motif of Pax3 and Pax7, we ran MEME (Bailey et al., 2009) on the highest scoring Pax3 and Pax7 unique peaks (Figures 1C and 1D), restricting our search to the 50 bp region around the peak summit. Peaks that spanned more than 800 bp were excluded from all downstream analysis as these were thought less likely to be the result of a single binding site. The MEME search of Pax7 peaks found the homeobox-binding (hbox) motif (Figure 2A) in 409 out of the top 500 peaks. The search of Pax3 peaks identified a paired (prd) motif (Figure 2B) in 131 out of 499 peaks.

We then used the position weight matrix (PWM) of these motifs to search a 200 bp region surrounding the summit of all Pax3, Pax7, Pax3 unique and Pax7 unique peaks using FIMO (Grant et al., 2011). Globally, we found that both Pax7 and Pax3 peaks were highly enriched for hbox motifs (Figures 2C–2E). On average more than 60% of all Pax7 and 30% of all Pax3 peaks contained hbox motif (Figures 2C–2E). Interestingly, both Pax3 peaks and Pax3 unique peaks were more enriched for the prd motif than the Pax7 peaks (Figures 2D and 2F).

To test the statistical significance for differential enrichment of Pax3 and Pax7 peaks for prd versus hbox motifs, we ranked Pax3 and Pax7 peaks into percentile and determined mean number of hbox and prd motifs within each group. The Wilcoxon rank-sum test showed that the differential enrichment of Pax3 and Pax7 for prd and hbox motif, respectively, is statistically significant (p value < 0.001) (Figures 2G and 2H). This finding suggests that while both Pax3 and Pax7 recognize the same DNA motif, there is a differential preference for prd versus hbox between the two transcription factors.

To test the biological significance of Pax3 and Pax7 bias toward prd and hbox motifs, we performed electromobility shift assay (EMSA) using short oligonucleotides derived from a common Pax3/Pax7 binding site (Myf5 ECR111, Supplemental Experimental Procedures and described below) that contains both hbox and prd motifs (Figure 3). EMSA confirmed the differential binding bias for hbox versus paired-domain motifs between Pax7 and Pax3 respectively (Figures 3A and 3B).

(C) Pax7 peaks were ranked based on MACS scores. Peaks were binned into groups of 100. A single bar represents each bin. The fraction of peaks containing prd, hbox or both prd/hbox was determined by FIMO (Grant et al., 2011) using the PWM obtained from MEME suite above from the scan of 200 bp around the peak summit.

(D) Similar analysis of Pax7 unique peaks also showed that hbox motif is highly enriched in this peak subset.

(E and F) The relative distribution of prd and hbox motifs in Pax3 and Pax3 unique peaks. Pax3 peaks have a higher proportion of prd to hbox compared to Pax7.

(G) Box plots visualizing fraction of peaks containing hbox motif for Pax3 and Pax7 total peaks. Peaks were ranked based on MACS scores and binned into 100-peak groups. The fraction of peaks within each 100-peak group containing the hbox motif was calculated based on the FIMO analysis as describe earlier. Data were transformed into percentiles. Wilcoxon rank-sum test shows that the mean fraction peaks containing hbox motif is significantly higher in Pax7 data set compared to Pax3. Dashed red line represents the mean; solid black line inside the box represent median. Lower and upper solid circles represent the 5th and the 95th percentiles, respectively.

(H) Similar analysis as in (G) showing that the fraction of Pax3 peaks containing prd motif is significantly higher than those of Pax7.

See also Figure S2.

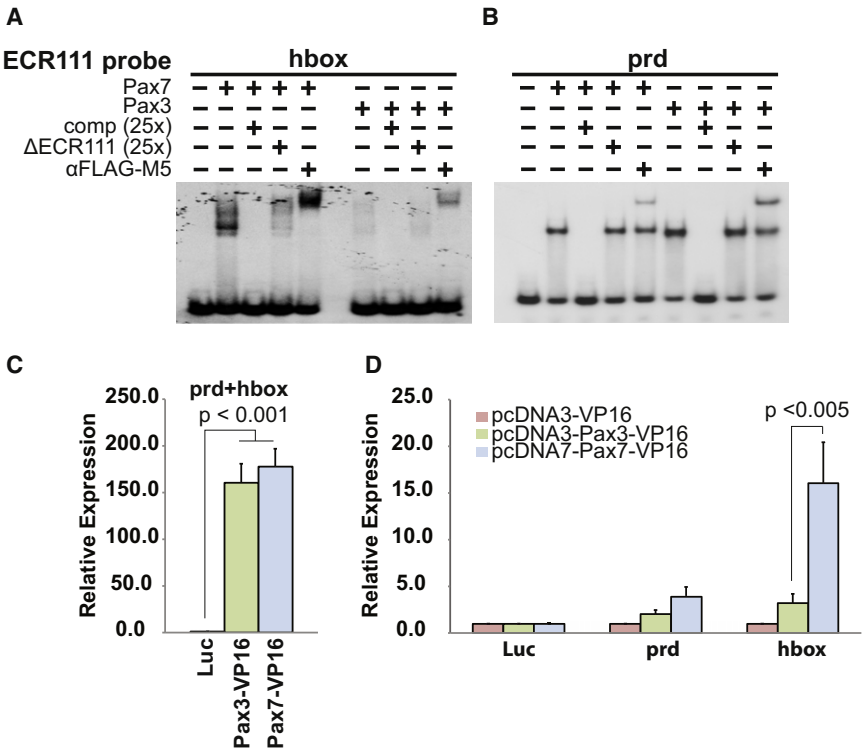

Figure 3. Pax7 Dominantly Binds Homeobox Motif

(A and B) EMSA showing Pax3 and Pax7 binding to hbox and prd motif taken from Myf5 ECR111 locus. Pax7 shows higher affinity to hbox motif than Pax3 (A). On the other hand both Pax3 and Pax7 show equal affinity for prd motif. Also see Figure S3 and Supplemental Experimental Procedures.

(C) Three copies of ECR111 were directionally cloned into a pGL4.10 reporter vector driven by a *Myf5* minimal promoter (Summerbell et al., 2000). 10T1/2 fibroblasts were cotransfected with Pax3- and Pax7-VP16 fusion constructs consisting of Pax3 or Pax7 fused in-frame with a VP16 transcriptional activation domain (Lin et al., 1991) at the C terminus. Expression of *luciferase* was measured and normalized to *renilla* expression. Relative luciferase activity was normalized against a control (VP16) reporter construct. Both Pax3- and Pax7-VP16 drove luciferase expression to high levels, demonstrating that ECR111 has enhancer activity and suggests that a combination of paired and homeodomain motifs produce synergistic effects on enhancer activity.

(D) Luciferase reporter assay showing transcriptional output of Pax3- and Pax7-VP16 on prd and hbox motifs. Three copies of the prd or hbox of ECR111 were concatamerized and cloned into pGL4.10 luciferase construct as described. Pax7-VP16 produced a significant increase in luciferase expression relative to controls and Pax3-VP16. Error bars represent SD.

See also Figure S3.

Pax3 weakly shifted the hbox probe, whereas equivalent amounts of Pax7 protein resulted in a robust shift (Figure 3A). Two species of shifted probe were identified, likely representing monomer and dimer binding consistent with a previous report suggesting that homeobox repeats facilitate dimerization (Birrane et al., 2009).

To further document the differential affinities of Pax3 versus Pax7 for paired-and homeodomain motifs, we performed luciferase reporter assays on a set of reporter plasmids containing different permutations of the Myf5 −111 kb binding site (ECR111). Reporter constructs were engineered that contained either three copies of the paired-domain sequence (*prd*), three copies of the homeodomain sequence (*hbox*), or three copies of the full binding site (*prd* + *hbox*) (Supplemental Experimental Procedures).

Reporter plasmids were cotransfected with plasmids expressing Pax3-VP16, Pax7-VP16, or empty vector, into 10T1/2 fibroblasts. Both Pax3- and Pax7-VP16 were able to induce the expression of luciferase reporter gene when prd and hbox were juxtaposed (Figure 3C). However only Pax7 significantly induced the expression of reporter gene from the hbox motif alone (Figure 3D), and both Pax3- and Pax7-VP16 were weak inducers from prd motif alone (Figure 3D). Pax3- and Pax7-VP16 showed comparable effect on induction of reporter gene expression from the juxtaposed prd and hbox motifs (Figure 3C). Notably, the presence of prd and hbox domain has a synergistic effect on gene expression.

The unique ability of Pax7 to induce expression from the hbox motif in addition to prd/hbox is consistent with the enrichment of Pax7 binding to hbox motifs in the genome-wide binding data (Figure 2). Therefore, high affinity of Pax7 for hbox motif (Figure 3A) and the higher fraction of Pax7 peaks containing this motif (Figures 2C and 2D) is consistent with the notion that Pax7 binding to hbox motifs has a biologically important role in adult myogenesis. Conversely, lower affinity of Pax3 for the hbox motif (Figure 3A) combined with the lower fraction of Pax3 peaks containing this motif (Figures 2E–2H) suggests that the two Pax proteins have markedly different DNA-binding dynamics.

Pax7 Acts over Long Ranges to Regulate the Adult Myogenic Program

Investigation of Pax3 and Pax7 genome-wide binding data suggests that they both can regulate their targets from a wide range of distances to the TSS (Figure 1B; Figure S4). To investigate the functional significance of genes associated with Pax3 and Pax7 peaks, we used Genomic Regions Enrichment of Annotation Tools (GREAT) (McLean et al., 2010) to perform association analysis. We used the basal regulatory domain of between −5 kb and + 1 kb of the TSS and extending to 500 kb in both upstream and down stream directions to obtain gene ontologies that were significantly associated with Pax3 and Pax7 binding sites.

We observed significant enrichment of Gene Ontology terms such as regulation of myoblast proliferation, hepatocyte growth factor receptor signaling, regulation of mitosis, regulation of glucagon secretion and apical junction assembly among other, associated with Pax7 or Pax3 peaks (Tables S1 and S2). Interestingly, peaks that were uniquely present in the Pax3 and absent

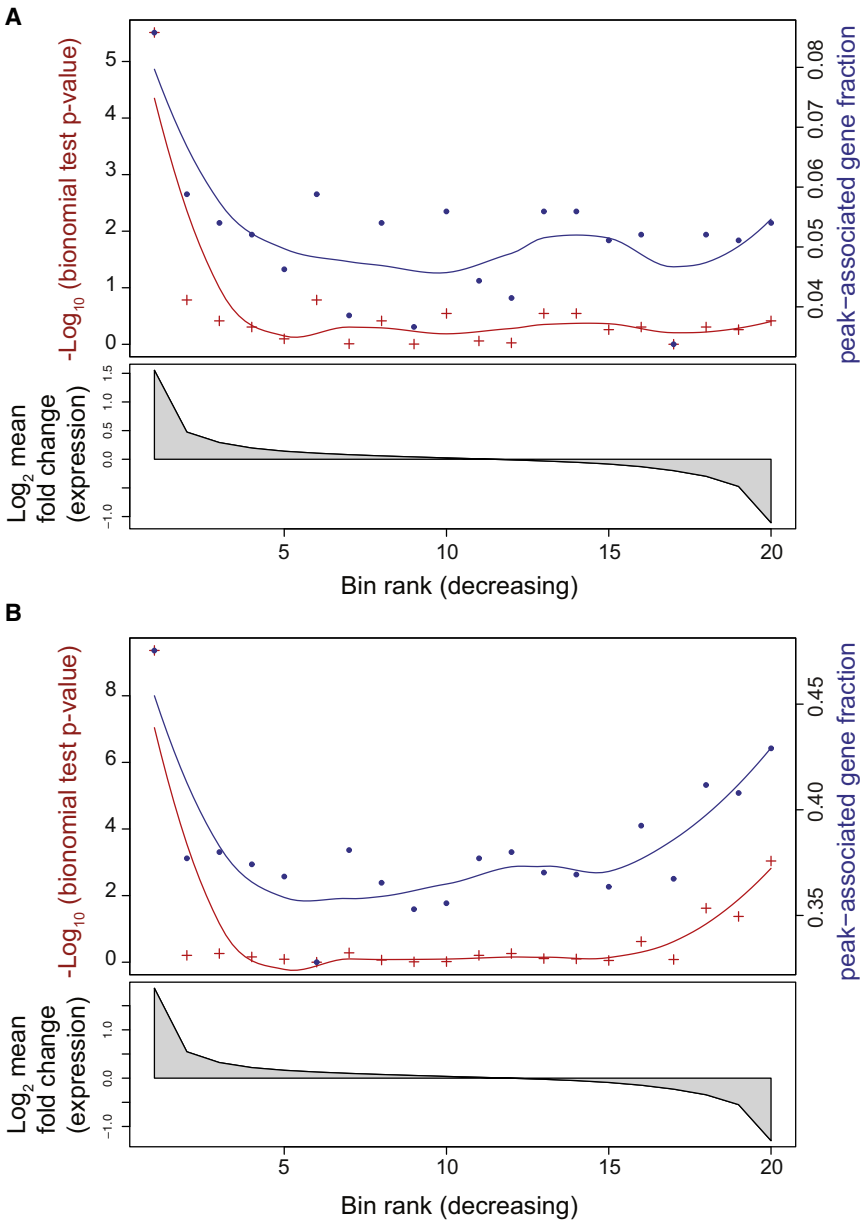

Figure 4. Pax3 and Pax7 Binding Sites Are Associated with Their Target Genes

(A) Gene expression values from Pax3 overexpressing cells were ranked based on SAM fold change and binned into 20 groups. See Figure S4 for significant target genes. Peaks located between −30 and + 5 kb from the TSS were assigned to those genes. The significance of peak to gene association for each bin was analyzed by one-sided binomial test against the global peak to gene fraction (red shows binomial test p values, blue shows peak associated gene fractions for each bin). The lines are LOESS fits of the data to help visualize the trend. Lower graph shows ranked gene expression values.

(B) Similar analysis as above for the association of peaks to genes for Pax7 data set. Input gene expression is from Pax7 overexpressing primary myoblasts and genome-wide Pax7 binding sites. The association analysis was restricted to binding sites within −30 and + 5 kb of the TSS, excluding binding sites that were further away from TSS. See Figure S4 for the distribution of Pax3 and Pax7 binding sites with respect to TSS.

See also Tables S3, S4, S5, and S6.

from the Pax7 data set showed significant enrichment for ontology terms such as skeletal muscle morphogenesis, neural tube formation and epithelial tube formation among others (data not shown). This finding suggests that Pax3 peaks that are not present in the Pax7 data set may represent a set of Pax3 targets involved in embryonic myogenesis.

To assess the relationship between genome-wide binding data and gene expression, we performed microarray analysis on Pax3- and Pax7-CTAP overexpressing skeletal myoblasts. We used significance analysis of microarray (SAM) with a raw p value < 0.01 and a fold change ≥2.0 (positive or negative) to derive the list of genes that were differentially regulated. Consistent with our observation on genome-wide binding data, Pax7 overexpression resulted in differential regulation of a larger set of genes than Pax3 overexpression (Figure S4).

A set of 840 genes was significantly regulated by both Pax7 and Pax3, while 128 genes were significantly regulated by Pax3 only, and a larger set of 439 genes was regulated by Pax7 only (Figure S4). Many genes associated with growth and proliferation, such as *Fgfr2*, *Egfr*, *BMP4*, etc., were significantly upregulated by both Pax3 and Pax7 (Table S3). Differentiation-specific genes, such as *Myh1*, *Myh3*, *Myh8*, *Mef2c*, *Myog*, *Ttn*, etc., were significantly repressed by both Pax3 and Pax7 (Table S3).

Gene ontology analysis showed that both Pax3 and Pax7 regulated genes are involved in cell growth, proliferation, signaling, adhesion, etc. (Tables S4 and S5). However, Pax7 induced the expression of many genes involved in growth and proliferation of muscle cells and repressed a large set of genes involved in muscle cell differentiation. The latter gene sets are not significantly regulated by Pax3 (Table S6).

Based on a statistical analysis of peak association with significantly regulated gene expression (data not shown), we chose a 35 kb window (−30 kb to +5 kb) around the TSS. To determine the significance of association between Pax3 and Pax7 binding and expression of target genes, we grouped genes into 20 bins ranked by their expression fold change. A binomial test on the number of genes with associated peaks in each bin versus the proportion of all genes with associated peaks showed that genes that are up- or downregulated in Pax7 overexpressing cells and genes that are upregulated in Pax3 overexpressing cells have significantly more associated peaks than would be expected at random or nonregulated genes (Figure 4).

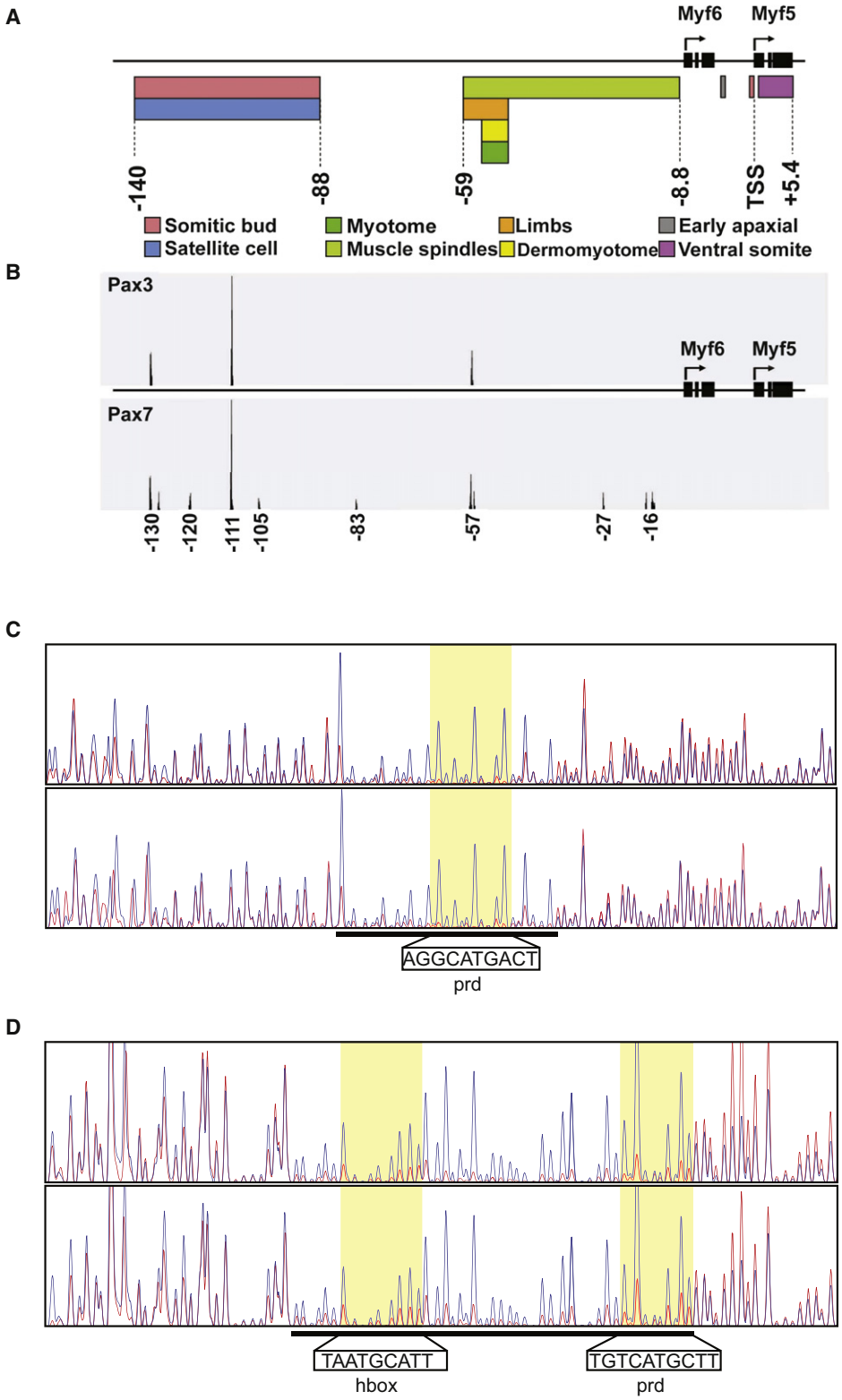

Figure 5. Myf5 –111 kb Is a Common Evolutionarily Conserved Target of Pax3/7

(A) Schematic of the regulatory regions for *Myf5* depicting the multitude of enhancer elements that direct Myf5 expression at different times and at different anatomical locations.

(B) Pax3 binding sites are found at −129, −111, and −57.5 kb, as determined by ChIP-Seq analysis primary myoblasts stably expressing Pax3. The regulatory element at −57.5 kb directs *Myf5* expression in somites, trunk, and limb muscles (Bajard et al., 2006). Pax7 binding sites are also present on Myf5/6 regulatory

We performed similar analysis using Gene Set Enrichment Analysis (GSEA) (Broad Institute, v 2.07) (Subramanian et al., 2005) and observed comparable results (data not shown). Taken together, these analyses suggest that overall transcriptional activity of Pax3 and Pax7 can be predicted from their binding patterns. Moreover, despite a significant amount of functional overlap between the two Pax genes in skeletal muscle cells Pax7 plays a more dominant role in adult skeletal myogenesis.

Distinct Roles for Pax3 and Pax7 in Adult Myogenesis

Pax3 has been documented to target several enhancers that are activated during embryonic myogenesis. We examined Pax7 and Pax3 binding to these regions to elucidate whether the adult myogenic program is simply a continuation of the embryonic myogenic program. Surprisingly, we did not find extensive Pax3 binding to known targets. For example, no Pax3 peak was identified at the paired motif-containing +22 kb enhancer downstream from Fgfr4, which is bound by Pax3 during embryonic limb development (Bajard et al., 2006; Lagha et al., 2008). However, this element is strongly bound by Pax7 (Figure S5).

Dmrt2, a known Pax3 target is involved in somite maturation and is regulated by Pax3 via a conserved element located 18 kb upstream of the TSS (Sato et al., 2010). However, our data show that in adult myoblasts this element is strongly bound by Pax7 but not Pax3 (Figure S5). Another Pax3-regulated gene, Spry1 (Lagha et al., 2008) has a Pax7 binding site but no Pax3 binding at a conserved element located +12 kb downstream of the TSS (Figure S5).

Binding sites uniquely recognized by Pax7 were also found near key myogenic genes. For example, two prominent Pax7 binding sites were found in conserved intergenic regions upstream of MyoD. These sites were also not bound by Pax3 (Figure S5). In other instances we observed that Pax7 binding sites were frequently adjacent to Pax3 target genes. For example, prominent binding sites were observed in the promoter of *Lbx1*, and within and downstream of *Itm2a* (Figure S5).

Consistent with previous findings, common Pax3/7 binding sites were observed within or near known target genes, including *Myf5* (Bajard et al., 2006), *C-met* (Epstein et al., 1996), and *Cdh11* (McKinnell et al., 2008) (Figure S5). Other Pax3/7 sites were observed adjacent to genes linked to muscle-related processes like myogenic inhibition (such as *Mdfic*; Ma et al., 2003) and myogenic signaling (*Stat1*; Sun et al., 2007) (Figure S5; data not shown). Although *Myf5* showed Pax3/7 binding at its −57 kb limb enhancer (Bajard et al., 2006), we noted a larger peak located at −111 kb from the *Myf5* TSS in both Pax3 and Pax7 data sets (Figure 5B). These observations suggest that in adult cells Pax7 binds strongly to many sites occupied by Pax3 in the embryo. Taken together, these data support the notion that adult and embryonic programs represent discrete myogenic programs.

Our experiments reveal that Pax7 plays an extensive role in adult myogenesis by activating multiple programs to promote myoblast growth and inhibit differentiation. Pax7 also activates components of multiple signaling pathways that have been implicated in adult myogenesis.

Pax7 Activates Myf5 in Satellite Cells via ECR111 Element

Myf5 is a direct Pax3/7 target gene that is transcriptionally poised in quiescent satellite stem cells. Myf5 is induced through asymmetric satellite stem cell division and is rapidly upregulated during activation of satellite myogenic cells (Kuang et al., 2007; Le Grand et al., 2009; McKinnell et al., 2008). Pax7 is a potent positive regulator of Myf5 in cultured myogenic cells. BAC transgenes carrying 195 kb upstream of the Myf5 transcriptional start site are sufficient to recapitulate the expression pattern of Myf5 and Myf6 in the embryo (Carvajal et al., 2001), and in the adult (Zammit et al., 2004). The −140 to −88 kb interval is necessary for the expression of Myf5 in quiescent satellite cells, while the element directing Myf5 expression in proliferating myogenic cells is located between −59 and +40.6 kb (Zammit et al., 2004) (summarized in Figure 5).

Analysis of Pax3 and Pax7 ChIP-Seq data identified a number of binding sites across the *Myf5* regulatory region (Figures 5A–5C). Both Pax3 and Pax7 bound sites are located at conserved loci at −57.5, −111, and −129 kb (relative to the Myf5 TSS). Within the 52 kb upstream interval (−140 to −88 kb), harboring the satellite cell enhancer we identified four evolutionary conserved regions (ECRs) (Figure 5B), among them ECR111 (Ribas et al., 2011) is conserved in all vertebrates. We confirmed the precise binding of Pax3/7 to the −57 kb enhancer (Figure 5C) and the ECR111 by DNaseI foot printing (Figure 5D) and Supplemental Experimental Procedures.

We examined Myf5 expression in vivo using a *Myf5-nLacZ* BAC carrying 195 kb of upstream sequence (Figures 6A–6H; Figure S6; Supplemental Experimental Procedures). Transgenic mice harboring a deletion of the ECR111 sequence from the BAC transgene (Ribas et al., 2011) abolished the expression of *Myf5-nLacZ* from adult quiescent satellite cells, but not muscle spindles (Figure 6; Figure S6). These results indicate that ECR111 is required for the expression of Myf5 in satellite cells but is not required for its expression in muscle spindles. Interestingly, activated satellite cell derived myogenic cells from cultured EDL single fibers expressed *Myf5-nLacZ* in the absence of ECR111 (data not shown). Therefore, we conclude that the ECR111 is a bona fide Pax7-dependent enhancer, which is required for Myf5 expression in adult quiescent satellite cells.

region and are found within the satellite cell region as well as regions directing expression in limbs and muscle spindles. Pax7 commonly binds all Pax3 sites; however, the peak at −111 kb is the most enriched. Also see Figure S5 for binding of Pax3 and Pax7 of a representative set of known targets.

(C) Chromatogram of *Myf5* −57 kb probe incubated with Pax3 or Pax7 (red) or BSA (blue) and digested with DNaseI. The 29-bp footprint (black bar) is identical between Pax3 and Pax7, centered on a paired domain motif.

(D) Chromatogram of *Myf5* −111 kb probe. Identical protected regions (black bar) were observed in the presence of Pax3 or Pax7. The footprint spans a region containing a putative paired domain and a separate homeodomain motif (Wilson et al., 1993). The distance between each motif and the length of the footprint implies that multiple Pax7 molecules may simultaneously bind.

See also Figure S5.

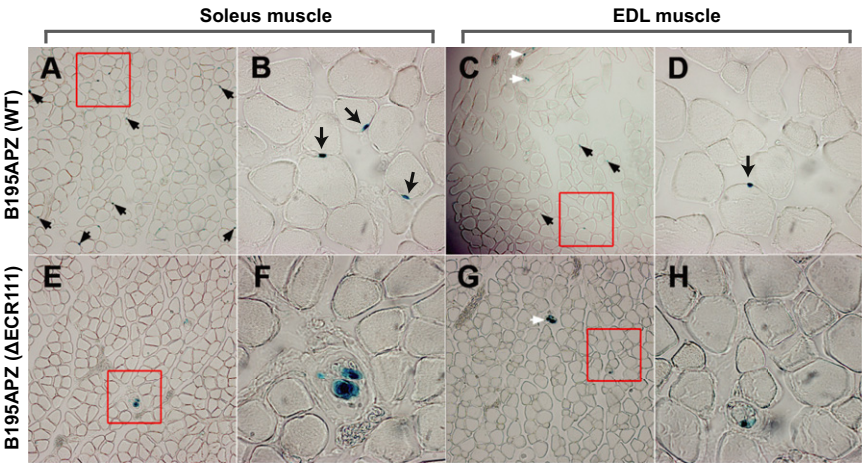

Figure 6. ECR111 Is an Enhancer Element Required for Myf5 Expression in Quiescent Satellite Cells

Cryosections of adult Soleus (A, B, E, and F) and EDL (C, D, G, and H) muscles from B195APZWT. (A–D) and B195APZΔ111 (E–H) transgenic lines show that in the absence of the ECR111 enhancer harboring the Pax7 binding site, expression in the satellite cells is abolished. Note that in transgenic animals carrying the deleted BAC construct expression in muscle spindle cells, under the transcriptional control of a separate enhancer, is not affected.

Red boxes in (A), (C), (E), and (G) indicate the zoomed regions shown in (B), (D), (F), and (H), respectively. Additional satellite and muscle spindle cells not included within the close-up figures are also indicated (black and white arrows, respectively).

See Figure S6.

DISCUSSION

In the hierarchy of the myogenic transcriptional network, Pax3 and Pax7 lie upstream of the basic helix-loop-helix (bHLH) transcription factors Myf5 and MyoD. Together, these transcription factors regulate satellite cell commitment to the myogenic lineage and self-renewal through a spatial-temporal network regulated by various signaling pathways. Deciphering the precise underlying molecular mechanisms that regulate this network is fundamentally important in understanding muscle development and diseases. Pax3/7 expressing cells that originate from somites give rise to the satellite cells of postnatal muscle (Buckingham and Relaix, 2007).

Gene replacement studies have demonstrated temporal and functional overlap of Pax3 and Pax7 in both embryonic and adult tissue. However, both factors have critical nonredundant roles in embryonic and adult muscle development. Pax7 can competently replace Pax3 in neural crest cells, dorsal neural tube, and trunk muscles, but cannot compensate for Pax3 function in the delamination and migration of limb muscle progenitor cells (Relaix et al., 2004). Conversely, Pax7 alone is essential for satellite cells up to a critical postnatal period (Kuang et al., 2007; Lepper et al., 2009; Oustanina et al., 2004; Relaix et al., 2006; Seale et al., 2000).

To mechanistically investigate the functional differences between Pax3 and Pax7 in skeletal myogenesis, we combined global gene expression profiling with genome-wide binding site analysis of these two closely related transcription factors in satellite cell-derived myoblasts. Our analyses of genome-wide binding site and gene expression data point to a more dominant role for Pax7 in adult skeletal muscle cells. Surprisingly, we found that Pax7 binds to many more sites (Figure 1) than the number of genes it regulates (Figure S4). This discrepancy between binding and expression data can be partially explained by the occurrence of multiple binding sites on the same gene. For example, analysis of Pax7-regulated genes revealed that on average there were three binding sites within 35 kb of the TSS of these genes. However, a large fraction of the remaining binding sites were dispersed throughout the genome. The functional relevance of these binding sites is unknown.

Analysis of peak to gene association revealed that both Pax3 and Pax7 regulated genes are significantly enriched for Pax3 and Pax7 peaks compared to nonregulated genes (Figure 4). Association studies between binding sites and nearby genes using GREAT (McLean et al., 2010) revealed that Pax7 binding sites are highly associated with genes involved in growth, myoblast proliferation and muscle cell differentiation (Table S1). This finding is consistent with the expression data in which Pax7 upregulates a significant set of genes that are involved in cellular growth, adhesion, and signaling pathways (Table S3). On the other hand, Pax7 also represses numerous genes that are involved in terminal differentiation (Table S3). Global analysis of peak to gene association showed that both up- and downregulated genes are significantly enriched for Pax7 binding sites (Figure 4). This raises the question of whether Pax7 can act as a repressor. Previous studies have indicated that Pax7 appears exclusively associated with active chromatin (McKinnell et al., 2008). Therefore, it is interesting to speculate that Pax7 binding to differentiation-specific genes functions to maintain these genes transcriptionally poised during progenitor proliferation.

Strikingly, our data show that despite recognizing the same binding motifs, Pax3 and Pax7 have significant differential affinities for paired versus hbox motifs (Figures 2 and 3). Pax7 strongly binds to hbox motifs (Figure 3A) and potently induces transcription of a reporter gene from this motif (Figure 3D), while Pax3 has low affinity for hbox motifs (Figure 3A) and a correspondingly lower transcriptional output on the same motif relative to Pax7 (Figure 3D). On the other hand, when prd and hbox are juxtaposed, both Pax3 and Pax7 have a similar effect on the transcription of a reporter gene (Figure 3C). This finding is consistent with the distribution of prd and hbox motifs in the full set of Pax3 and Pax7 binding sites (Figure 2). The observed differences between Pax3 and Pax7 affinities for prd and hbox motifs is surprising given the degree of protein sequence similarity between the two transcription factors in their paired and homeodomains.

Our data demonstrate that these intrinsic differences in DNA binding between Pax3 and Pax7 drive differential activation from promoters containing specific paired and hbox configurations. Work in *Drosophila* suggests that Pax proteins recognize

target genes through various combinations of DNA-binding domains. Synergistic binding of paired- and homeodomains is required for the expression of *even-skipped* (Jun and Desplan, 1996); similarly, we observed synergistic activation of the ECR111 element in *Myf5* when both domains were juxtaposed (Figure 3C). Our data suggest that the distinguishing feature of Pax7 and Pax3 in adult skeletal muscles is that Pax7 can activate target gene expression from combined prd/hbox or hbox motifs alone, while Pax3 is ineffective in inducing transcription from only hbox motifs. We hypothesize that the observed transcriptional dominance of Pax7 over Pax3 is largely due to the greater affinity of Pax7 for hbox elements relative to Pax3.

Additional mechanisms may differentially influence the DNA binding affinity of Pax3 and Pax7. We observed several cases where embryonic Pax3 binding sites are poorly associated with Pax3 in adult cells, but robustly bound by Pax7 as indicated previously. DNA binding by Pax3 may require the presence of specific coactivators or posttranslational modifications. It has been suggested that Pax3 activity is dependent on phosphorylation, as Pax3 transcriptional activity is blocked by kinase inhibition (Amstutz et al., 2008; Miller et al., 2008). Pax3 is phosphorylated at Ser205, proximal to the octapeptide domain. Mutation of this site not only abolishes phosphorylation, but also disrupts dimerization of Pax3 proteins. Homeodomain-binding motifs are thought to facilitate dimerization through inverted repeats of "TAAT" and we see a substantial difference in affinity between Pax3 and Pax7 binding to hbox motifs. Pax3 has been shown to cooperate with Sox10 to synergistically activate target gene expression (Mascarenhas et al., 2010).

Epigenetic modifications may also play a role in directing availability of binding sites to Pax3 or Pax7. For example, RARγ/RXRα heterodimers competently bind and induce retinoic acid response elements (RAREs) regulating Hoxa1 and Cyp26a1 in F9 teratocarcinoma stem cells, but not in Balb/c 3T3 fibroblasts (Kashyap and Gudas, 2010). This is attributed to retinoic acid-induced reduction of polycomb protein Suz12 and associated H3K27 trimethylation of Hoxa1 and Cyp26a1 RAREs. To what extent each of these factors contribute to the overall transcriptional network of Pax3 and Pax7 during myogenesis remains largely unknown.

Our experiments indicate that in adult myoblasts, Pax7 regulates many more genes than Pax3. We propose that many Pax7-only binding sites are regulatory elements for genes essential to the normal function of adult myogenic cells while their low affinity to Pax3 explains the inability of Pax3 to compensate for Pax7 in *Pax7*$^{-/-}$ muscles such as in the diaphragm. Ultimately, the distinct characteristics of Pax3 and Pax7 binding provide a framework for understanding the differences in transcriptional network organization between embryonic and adult myogenesis. Both factors may be sufficient to initiate myogenic programs, but different developmental contexts may utilize alternative networks to fulfill other essential roles.

Consistent with the dominant role of Pax7 DNA binding, our gene expression data show a panel of 439 genes that are significantly regulated by Pax7 but not Pax3. These genes are involved in diverse biological functions such as growth, signaling, cell adhesion, and muscle cell differentiation (Table S6). For example, Pax7's ability to induce Rspo1 and BMP4 among others (Table S3) suggests a mechanism by which Pax7 functions in the expansion of satellite cell population. Rspo1, a known Wnt/ β-catenin activator is known to regulate Myf5 expression in myoblasts (Han et al., 2011). We observed a Pax7 peak located at +12 kb of the TSS of Rspo1. BMP4 is characterized in its ability to block the differentiation of myogenic cells (Dahlqvist et al., 2003). We observed a Pax7 peak on a highly conserved element at −28.7 kb of BMP4. Additionally Pax7 overexpression resulted in the repression of many muscle differentiation genes (Tables S3 and S6).

Myf5 is activated by Pax3 or Pax7 in both embryonic and skeletal muscle, and it has been shown that adult Myf5 enhancers operate independently of one another (Carvajal et al., 2008; Zammit et al., 2004). Embryonic regulation of Myf5 can occur through the −57.5 kb enhancer, whereas deletions within *Myf5-LacZ* BACs show the −140 to −88 kb region is critical for the expression of Myf5 in quiescent satellite cells. Our data confirm that ECR111 is a Pax7-dependent enhancer that is evolutionarily conserved and directs Myf5 expression in quiescent satellite cells (Figure 6; Figure S6). The continued expression of *Myf5-nLacZ* in the ECR111 mutant in muscle spindles reinforces the idea that separate genetic elements control Myf5 expression between quiescent satellite cells and muscle spindles.

We have mapped Pax3 and Pax7 binding sites and identified common and discrete target genes. Our experiments have demonstrated that the disparate affinities of Pax3 and Pax7 for paired- versus homeomotif provide a mechanistic explanation for the distinct role played by Pax7 in adult myogenesis. Importantly, the ability of Pax7 to specify myogenic identity while stimulating growth and inhibiting differentiation points to a central role in the regulation of myogenic progression of the adult satellite cell lineage. This work has facilitated the identification of gene interactions and represents an important step toward comprehensively defining the myogenic regulatory transcriptional network. Understanding the myogenic transcriptional network will have important implications for elucidating the molecular control of the myogenic developmental program, and for the genetic modulation of stem cells for use in the amelioration of muscle disease.

EXPERIMENTAL PROCEDURES

Chromatin Tandem Affinity Purification

Subconfluent myoblasts stably expressing a C terminus TAP-tagged Pax3 or Pax7 were crosslinked with 1% formaldehyde in 1 × PBS. Cells were harvested by scraping and the cell pellet was dissolved in ChIP lysis buffer (Supplemental Experimental Procedures). Chromatin was purified using two sequential immunoprecipitation steps. The first immunoprecipitation was done using anti-3×FLAG antibody conjugated to agarose beads (Sigma Aldrich) using 20 mg of cell lysate as input for 2 hr at 4°C. Beads containing antigen/antibody complex were washed three times with 10 mM Tris-HCl (pH 8.0); 100 mM NaCl; 0.1% Triton X-100 containing protease inhibitors. Protein complex was eluted from M2-conjugated agarose beads using proteolytic cleavage with Tobacco Etch Virus (TEV) protease (Invitrogen) together with competition with 3×FLAG peptide (Sigma Aldrich) at 4°C overnight. Two additional rounds of elution with 3×FLAG peptides were done using 200 μg/ml of 3×FLAG peptide in TBS (50 mM Tris-HCl [pH 7.4]; 150 mM NaCl). The eluted product was used as input for the second affinity pull down using His-Select nickel beads (Sigma-Aldrich) for three hours at 4°C following manufacture's recommendations. Beads were washed three times with wash buffer (20 mM Tris-HCl [pH 7.4]; 150 mM NaCl; 5 mM

imidazole). Final DNA/protein complex was eluted by 400 mM imidazole at room temperature. Reverse crosslinking and phenol/chloroform extraction of chromatin were done as described previously (Gillespie et al., 2009). ChIP with Pax7-FLAG, EGFP, and puro cell lines were fixed in 1% formaldehyde solution and immunoprecipitated with M2-agarose (Sigma-Aldrich). Washing and DNA elution were performed according to the ChIP Assay Kit (Upstate). Enrichment of particular loci within ChIP DNA pools was determined by quantitative real-time PCR.

Gene Expression Analysis

Total RNA was isolated from mouse skeletal muscle cells in triplicate by the RNeasy kit (QIAGEN) and hybridized to Affymetrix Mouse Gene Array ST 1.0 chips and scanned using a GeneChip Scanner 30007G. Raw expression data were assembled using the Affymetrix GeneChip Command Console v1.1. SAM was used to derive differentially expressed genes. See Supplemental Experimental Procedures for more details.

Peak Calling

Peaks in the mapped Pax7 and Pax3 sequences were identified using MACS v1.3 (Zhang et al., 2008) using an empty TAP vector ChIP-seq as control. The following parameters: *mfold* = 16, *bw* = 150, p value cutoff of 10^{-5} were used in the peak calling procedure. Peaks greater than 800 bp in width were excluded from further analysis, based on the size of excised ChIP fragments used for Solexa sequencing.

Motif Analysis

MEME (Bailey et al., 2009) was used to identify overrepresented motifs in Pax3 and Pax7 peak set subsets, restricting the search to 50 bp around the peak summit. Peaks were filtered by width, MACS score ($-10 \times \log_{10}$ [p value]) and repeat content to select regions most likely to reflect specific high-affinity binding events, and least likely to identify spurious motifs within repetitive sequences. Peaks greater than 800 bp in length were excluded from the analysis. See Supplemental Experimental Procedures for more details.

Affymetrix MoGene ST 1.0 Analysis and Annotations

Nine microarrays were used in the analysis. See Supplemental Experimental Procedures for GEO accession numbers. Transcript cluster identifiers (TCID) of the Affymetrix MoGene 1.0 ST chipsets were RMA normalization (Irizarry et al., 2003) using the xps in Bioconductor (Gentleman et al., 2004) R package with the Affymetrix provided MoGene-1_0-st-v1.r4 chip layout and scheme files. The RMA normalized results were $\log_2$ transformed and analyzed using the SAM (Tusher et al., 2001) method as implemented in the Bioconductor siggenes package. The resulting SAM fold changes and raw p values were integrated into a single table by common TCID and annotated with gene associations based on probe to gene mappings downloaded from Ensembl v64 BioMart. TCIDs mapping to zero or more than one gene were excluded from the analysis. Gene properties were downloaded from Ensembl v64 BioMart and counts of MACS peaks identified peak positions falling within the chosen gene association window (−30 to +5 kb around the TSS) were provided for each gene.

See Supplemental Experimental Procedures for a more extensive description of procedures and computational methods.

Electromobility Shift Assay

Baculovirus-purified Pax3-FLAG, Pax3-CTAP, or Pax7-FLAG was incubated with 1.25 ng (ATP γ-^{32}P-labeled) DNA probe and nonspecific carrier (poly dI-dC) in a binding buffer containing 75 mM NaCl, 1 mM EDTA, 1 mM DTT, 10 mM Tris (pH 7.5), 6% glycerol, and 0.25% BSA at room temperature for 20 min (Supplemental Experimental Procedures). Cold probe (25×) was used for competitive binding assays. Supershifts were carried out with the addition of 1 μg M2- or M5-FLAG antibody (Sigma-Aldrich). Reactions were analyzed on a 5% nondenaturing polyacrylamide gel (0.5 × TBE), dried onto 3 mm Whatman paper, and exposed to BioMax MS X-ray film (Kodak).

Luciferase Reporter Assay

ECR111 reporter vectors were constructed as follows. For the paired domain (PD) and homeodomain (HD) reporters, three copies of 30 bp sequences covering the prd and hbox motifs were directionally concatamerized and cloned upstream of a minimal Myf5 promoter driving the *luc* gene of pGL4.10 (Promega). A 70 bp sequence covering the entire −111 kb region, including both the prd and hbox regions was also concatamerized and cloned as above to generate the PDHD reporter. Reporter vectors were cotransfected with a *renilla* vector standard and either empty vector (VP16), VP16-Pax7 or VP16-Pax3 for 24 hr into C3H10T1/2 fibroblasts (also see Supplemental Experimental Procedures). Luciferase assays were carried out using the Dual-Reporter Luciferase Assay System (Promega) and analyzed on a Lumistar Optima (BMG Labtech) fluorescent plate reader.

DNase I Footprinting

Baculoviral purified Pax7 or Pax3 protein or equivalent amount of BSA (NEB) was equilibrated for 10 min at room temperature in the following buffer: 150 mM KCl, 5 mM $MgCl^2$, 0.1 mM EDTA, 8% glycerol, 30 mM Tris-Cl (pH 8.0), 1 mM DTT along with 1 μg of poly dI-dC (Sigma). DNA probes were made from ECR57 and ECR111 of the Myf5 locus (Supplemental Experimental Procedures). One hundred fifty micrograms of each probe was then added for 20 min at room temperature (also see Supplemental Experimental Procedures). Probes were then digested with 7.5×10^{-3} units of DNase I (Worthington Biochemicals) for 15 min at room temperature. DNA was purified using MinElute enzymatic reaction cleanup (QIAGEN). Control digestions were performed on an IgH probe. Digested DNA was added to HiDi formamide (Applied Biosystems) and 0.1 μl GeneScan 500 LIZ size standards (Applied Biosystems). Mixtures were then heat denatured for 5 min at 95°C, immediately cooled on ice, and analyzed with a 3730 DNA Analyzer (ABI) running a G5 dye set (see Supplemental Experimental Procedures for more details).

Statistical Analysis

Gene expression values from Pax3 and Pax7 overexpressing myoblasts were each ranked based on SAM fold change and binned into 20 groups. For each bin, we performed a one-tailed binomial test of the proportion of peak-associated genes in that bin versus all genes. We tested the hypothesis that the binned genes are more likely to be associated with peaks. The graphs in Figure 4 show the base 10 logarithms of the binomial test p values.

SUPPLEMENTAL INFORMATION

Supplemental Information includes six figures, six tables, and Supplemental Experimental Procedures and can be found with this article online at doi:10.1016/j.devcel.2012.03.014.

ACKNOWLEDGMENTS

We thank Dr. Ricardo Ribas for providing the B195APZ BAC constructs. We thank Dr. Hang Yin at the Ottawa Hospital Research Institute (OHRI) for his valuable comments and suggestion on the manuscript. M.A.R. holds the Canada Research Chair in Molecular Genetics and is an International Research Scholar of the Howard Hughes Medical Institute. This work was supported by grants from the National Institutes of Health, the Howard Hughes Medical Institute, the Canadian Institutes of Health Research, and the Canada Research Chair Program to M.A.R., by EuTRACC, a European Commission 6th Framework grant to F.G., and by the Institute of Cancer Research, a Medical Research Council Programme Grant, and MYORES, a European Commission 6th Framework grant to J.J.C. and P.W.J.R.

Received: December 29, 2010
Revised: January 20, 2012
Accepted: March 28, 2012
Published online: May 17, 2012

REFERENCES

Amstutz, R., Wachtel, M., Troxler, H., Kleinert, P., Ebauer, M., Haneke, T., Oehler-Jänne, C., Fabbro, D., Niggli, F.K., and Schäfer, B.W. (2008). Phosphorylation regulates transcriptional activity of PAX3/FKHR and reveals novel therapeutic possibilities. Cancer Res. *68*, 3767–3776.

Bailey, T.L., Boden, M., Buske, F.A., Frith, M., Grant, C.E., Clementi, L., Ren, J., Li, W.W., and Noble, W.S. (2009). MEME SUITE: tools for motif discovery and searching. Nucleic Acids Res. *37* (Web Server issue), W202-8.

Bajard, L., Relaix, F., Lagha, M., Rocancourt, D., Daubas, P., and Buckingham, M.E. (2006). A novel genetic hierarchy functions during hypaxial myogenesis: Pax3 directly activates Myf5 in muscle progenitor cells in the limb. Genes Dev. *20*, 2450–2464.

Birrane, G., Soni, A., and Ladias, J.A. (2009). Structural basis for DNA recognition by the human PAX3 homeodomain. Biochemistry *48*, 1148–1155.

Bober, E., Franz, T., Arnold, H.H., Gruss, P., and Tremblay, P. (1994). Pax-3 is required for the development of limb muscles: a possible role for the migration of dermomyotomal muscle progenitor cells. Development *120*, 603–612.

Buckingham, M., and Relaix, F. (2007). The role of Pax genes in the development of tissues and organs: Pax3 and Pax7 regulate muscle progenitor cell functions. Annu. Rev. Cell Dev. Biol. *23*, 645–673.

Carvajal, J.J., Cox, D., Summerbell, D., and Rigby, P.W. (2001). A BAC transgenic analysis of the Mrf4/Myf5 locus reveals interdigitated elements that control activation and maintenance of gene expression during muscle development. Development *128*, 1857–1868.

Carvajal, J.J., Keith, A., and Rigby, P.W. (2008). Global transcriptional regulation of the locus encoding the skeletal muscle determination genes Mrf4 and Myf5. Genes Dev. *22*, 265–276.

Chargé, S.B., and Rudnicki, M.A. (2004). Cellular and molecular regulation of muscle regeneration. Physiol. Rev. *84*, 209–238.

Dahlqvist, C., Blokzijl, A., Chapman, G., Falk, A., Dannaeus, K., Ibâñez, C.F., and Lendahl, U. (2003). Functional Notch signaling is required for BMP4-induced inhibition of myogenic differentiation. Development *130*, 6089–6099.

Epstein, J.A., Shapiro, D.N., Cheng, J., Lam, P.Y., and Maas, R.L. (1996). Pax3 modulates expression of the c-Met receptor during limb muscle development. Proc. Natl. Acad. Sci. USA *93*, 4213–4218.

Gentleman, R.C., Carey, V.J., Bates, D.M., Bolstad, B., Dettling, M., Dudoit, S., Ellis, B., Gautier, L., Ge, Y., Gentry, J., et al. (2004). Bioconductor: open software development for computational biology and bioinformatics. Genome Biol. *5*, R80.

Gillespie, M.A., Le Grand, F., Scimè, A., Kuang, S., von Maltzahn, J., Seale, V., Cuenda, A., Ranish, J.A., and Rudnicki, M.A. (2009). p38-gamma-dependent gene silencing restricts entry into the myogenic differentiation program. J. Cell Biol. *187*, 991–1005.

Grant, C.E., Bailey, T.L., and Noble, W.S. (2011). FIMO: scanning for occurrences of a given motif. Bioinformatics *27*, 1017–1018.

Han, X.H., Jin, Y.R., Seto, M., and Yoon, J.K. (2011). A WNT/beta-catenin signaling activator, R-spondin, plays positive regulatory roles during skeletal myogenesis. J. Biol. Chem. *286*, 10649–10659.

Hutcheson, D.A., Zhao, J., Merrell, A., Haldar, M., and Kardon, G. (2009). Embryonic and fetal limb myogenic cells are derived from developmentally distinct progenitors and have different requirements for beta-catenin. Genes Dev. *23*, 997–1013.

Irizarry, R.A., Hobbs, B., Collin, F., Beazer-Barclay, Y.D., Antonellis, K.J., Scherf, U., and Speed, T.P. (2003). Exploration, normalization, and summaries of high density oligonucleotide array probe level data. Biostatistics *4*, 249–264.

Jun, S., and Desplan, C. (1996). Cooperative interactions between paired domain and homeodomain. Development *122*, 2639–2650.

Kashyap, V., and Gudas, L.J. (2010). Epigenetic regulatory mechanisms distinguish retinoic acid-mediated transcriptional responses in stem cells and fibroblasts. J. Biol. Chem. *285*, 14534–14548.

Kassar-Duchossoy, L., Giacone, E., Gayraud-Morel, B., Jory, A., Gomès, D., and Tajbakhsh, S. (2005). Pax3/Pax7 mark a novel population of primitive myogenic cells during development. Genes Dev. *19*, 1426–1431.

Kuang, S., Chargé, S.B., Seale, P., Huh, M., and Rudnicki, M.A. (2006). Distinct roles for Pax7 and Pax3 in adult regenerative myogenesis. J. Cell Biol. *172*, 103–113.

Kuang, S., Kuroda, K., Le Grand, F., and Rudnicki, M.A. (2007). Asymmetric self-renewal and commitment of satellite stem cells in muscle. Cell *129*, 999–1010.

Lagha, M., Kormish, J.D., Rocancourt, D., Manceau, M., Epstein, J.A., Zaret, K.S., Relaix, F., and Buckingham, M.E. (2008). Pax3 regulation of FGF signaling affects the progression of embryonic progenitor cells into the myogenic program. Genes Dev. *22*, 1828–1837.

Le Grand, F., Jones, A.E., Seale, V., Scimè, A., and Rudnicki, M.A. (2009). Wnt7a activates the planar cell polarity pathway to drive the symmetric expansion of satellite stem cells. Cell Stem Cell *4*, 535–547.

Lepper, C., Conway, S.J., and Fan, C.M. (2009). Adult satellite cells and embryonic muscle progenitors have distinct genetic requirements. Nature *460*, 627–631.

Lin, H., Yutzey, K.E., and Konieczny, S.F. (1991). Muscle-specific expression of the troponin I gene requires interactions between helix-loop-helix muscle regulatory factors and ubiquitous transcription factors. Mol. Cell. Biol. *11*, 267–280.

Ma, X.Y., Wang, H., Ding, B., Zhong, H., Ghosh, S., and Lengyel, P. (2003). The interferon-inducible p202a protein modulates NF-kappaB activity by inhibiting the binding to DNA of p50/p65 heterodimers and p65 homodimers while enhancing the binding of p50 homodimers. J. Biol. Chem. *278*, 23008–23019.

Mascarenhas, J.B., Littlejohn, E.L., Wolsky, R.J., Young, K.P., Nelson, M., Salgia, R., and Lang, D. (2010). PAX3 and SOX10 activate MET receptor expression in melanoma. Pigment Cell Melanoma Res. *23*, 225–237.

McKinnell, I.W., Ishibashi, J., Le Grand, F., Punch, V.G., Addicks, G.C., Greenblatt, J.F., Dilworth, F.J., and Rudnicki, M.A. (2008). Pax7 activates myogenic genes by recruitment of a histone methyltransferase complex. Nat. Cell Biol. *10*, 77–84.

McLean, C.Y., Bristor, D., Hiller, M., Clarke, S.L., Schaar, B.T., Lowe, C.B., Wenger, A.M., and Bejerano, G. (2010). GREAT improves functional interpretation of cis-regulatory regions. Nat. Biotechnol. *28*, 495–501.

Miller, P.J., Dietz, K.N., and Hollenbach, A.D. (2008). Identification of serine 205 as a site of phosphorylation on Pax3 in proliferating but not differentiating primary myoblasts. Protein Sci. *17*, 1979–1986.

Oustanina, S., Hause, G., and Braun, T. (2004). Pax7 directs postnatal renewal and propagation of myogenic satellite cells but not their specification. EMBO J. *23*, 3430–3439.

Punch, V.G., Jones, A.E., and Rudnicki, M.A. (2009). Transcriptional networks that regulate muscle stem cell function. Wiley Interdiscip Rev Syst Biol Med *1*, 128–140.

Relaix, F., Rocancourt, D., Mansouri, A., and Buckingham, M. (2004). Divergent functions of murine Pax3 and Pax7 in limb muscle development. Genes Dev. *18*, 1088–1105.

Relaix, F., Rocancourt, D., Mansouri, A., and Buckingham, M. (2005). A Pax3/Pax7-dependent population of skeletal muscle progenitor cells. Nature *435*, 948–953.

Relaix, F., Montarras, D., Zaffran, S., Gayraud-Morel, B., Rocancourt, D., Tajbakhsh, S., Mansouri, A., Cumano, A., and Buckingham, M. (2006). Pax3 and Pax7 have distinct and overlapping functions in adult muscle progenitor cells. J. Cell Biol. *172*, 91–102.

Ribas, R., Moncaut, N., Siligan, C., Taylor, K., Cross, J.W., Rigby, P.W., and Carvajal, J.J. (2011). Members of the TEAD family of transcription factors regulate the expression of Myf5 in ventral somitic compartments. Dev. Biol. *355*, 372–380.

Sato, T., Rocancourt, D., Marques, L., Thorsteinsdóttir, S., and Buckingham, M. (2010). A Pax3/Dmrt2/Myf5 regulatory cascade functions at the onset of myogenesis. PLoS Genet. *6*, e1000897.

Seale, P., Sabourin, L.A., Girgis-Gabardo, A., Mansouri, A., Gruss, P., and Rudnicki, M.A. (2000). Pax7 is required for the specification of myogenic satellite cells. Cell *102*, 777–786.

Subramanian, A., Tamayo, P., Mootha, V.K., Mukherjee, S., Ebert, B.L., Gillette, M.A., Paulovich, A., Pomeroy, S.L., Golub, T.R., Lander, E.S., and Mesirov, J.P. (2005). Gene set enrichment analysis: a knowledge-based approach for interpreting genome-wide expression profiles. Proc. Natl. Acad. Sci. USA *102*, 15545–15550.

Summerbell, D., Ashby, P.R., Coutelle, O., Cox, D., Yee, S., and Rigby, P.W. (2000). The expression of Myf5 in the developing mouse embryo is controlled by discrete and dispersed enhancers specific for particular populations of skeletal muscle precursors. Development *127*, 3745–3757.

Sun, H., Li, L., Vercherat, C., Gulbagci, N.T., Acharjee, S., Li, J., Chung, T.K., Thin, T.H., and Taneja, R. (2007). Stra13 regulates satellite cell activation by antagonizing Notch signaling. J. Cell Biol. *177*, 647–657.

Tusher, V.G., Tibshirani, R., and Chu, G. (2001). Significance analysis of microarrays applied to the ionizing radiation response. Proc. Natl. Acad. Sci. USA *98*, 5116–5121.

Wilson, D., Sheng, G., Lecuit, T., Dostatni, N., and Desplan, C. (1993). Cooperative dimerization of paired class homeo domains on DNA. Genes Dev. *7*, 2120–2134.

Zammit, P.S., Golding, J.P., Nagata, Y., Hudon, V., Partridge, T.A., and Beauchamp, J.R. (2004). Muscle satellite cells adopt divergent fates: a mechanism for self-renewal? J. Cell Biol. *166*, 347–357.

Zhang, Y., Liu, T., Meyer, C.A., Eeckhoute, J., Johnson, D.S., Bernstein, B.E., Nusbaum, C., Myers, R.M., Brown, M., Li, W., and Liu, X.S. (2008). Model-based analysis of ChIP-Seq (MACS). Genome Biol. *9*, R137.

Appendix C - Wnt7a Activates the Planar Cell Polarity Pathway to Drive the Symmetric Expansion of Satellite Stem Cells

Cell Stem Cell
Article

Wnt7a Activates the Planar Cell Polarity Pathway to Drive the Symmetric Expansion of Satellite Stem Cells

Fabien Le Grand,[1,2,3] Andrew E. Jones,[1,2] Vanessa Seale,[1] Anthony Scimè,[1,2] and Michael A. Rudnicki[1,2,*]
[1]Sprott Center for Stem Cell Research, Ottawa Hospital Research Institute, Regenerative Medicine Program, 501 Smyth Road, Ottawa, ON K1H 8L6, Canada
[2]Department of Medicine, University of Ottawa, 451 Smyth Road, Ottawa, ON K1H 8M5, Canada
[3]Present address: Institut Cochin, INSERM U567, Université Paris Descartes, Paris 75014, France
*Correspondence: mrudnicki@ohri.ca
DOI 10.1016/j.stem.2009.03.013

SUMMARY

Satellite cells in skeletal muscle are a heterogeneous population of stem cells and committed progenitors. We found that quiescent satellite stem cells expressed the Wnt receptor Fzd7 and that its candidate ligand Wnt7a was upregulated during regeneration. Wnt7a markedly stimulated the symmetric expansion of satellite stem cells but did not affect the growth or differentiation of myoblasts. Silencing of Fzd7 abrogated Wnt7a binding and stimulation of stem cell expansion. Wnt7a signaling induced the polarized distribution of the planar cell polarity effector Vangl2. Silencing of Vangl2 inhibited Wnt7a action on satellite stem cell expansion. Wnt7a overexpression enhanced muscle regeneration and increased both satellite cell numbers and the proportion of satellite stem cells. Muscle lacking Wnt7a exhibited a marked decrease in satellite cell number following regeneration. Therefore, Wnt7a signaling through the planar cell polarity pathway controls the homeostatic level of satellite stem cells and hence regulates the regenerative potential of muscle.

INTRODUCTION

Satellite cells in adult skeletal muscle are located in small depressions between the sarcolemma of their host myofibers and the basal lamina. Upon damage, such as physical trauma, repeated exercise, or in disease, satellite cells become activated, proliferate, and give rise to a population of myogenic precursors cells (myoblasts) expressing the myogenic regulatory factors (MRFs) MyoD and Myf5. In the course of the regeneration process, myoblasts undergo multiple rounds of division before committing to terminal differentiation, fusing with the host fibers or generating new myofibers to reconstruct damaged tissue (Charge and Rudnicki, 2004).

During skeletal muscle regeneration, the satellite cell population is maintained by a stem cell subpopulation, thus allowing tissue homeostasis and multiple rounds of regeneration during the life span of an individual (Kuang et al., 2008). Transplantation experiments of either intact myofibers with their associated satellite cells (Collins et al., 2005), or FACS-sorted satellite cells (Kuang et al., 2007; Montarras et al., 2005), or individual cells (Sacco et al., 2008) demonstrated that a subpopulation of quiescent satellite cells are capable of both extensive contribution to muscle regeneration and self-renewal by giving rise to new satellite cells within the transplanted host muscle.

Recent findings from our laboratory using Cre/*loxP* lineage-tracing identified a subpopulation of satellite cells that have never expressed Myf5 and function as a stem cell reservoir (Kuang et al., 2007). Satellite stem cells ($Pax7^+/Myf5^-$) represent about 10% of the adult satellite cell pool and give rise to daughter satellite myogenic cells ($Pax7^+/Myf5^+$) through asymmetric apical-basal cell divisions. Transplantation of both $Myf5^-$ and $Myf5^+$ FACS-sorted satellite cells demonstrated that satellite stem cells are capable of repopulating the adult satellite cell niche as well as self-renewal (Kuang et al., 2007). Nevertheless, our knowledge of the molecular networks regulating satellite stem cell fate decisions has remained unclear.

The paired-box transcription factor Pax7 plays a central regulatory role in satellite cell function and survival (Kuang et al., 2006; Seale et al., 2000). The satellite cell population in Pax7-deficient mice is progressively lost, and the residual cells in the satellite niche are unable to sustain efficient skeletal muscle regeneration (Kuang et al., 2006; Oustanina et al., 2004). Recent work has revealed that Pax7 recruits the Ash2L-Wdr5-MML2 histone methyltransferase complex to target genes such as *Myf5* leading to histone 3 K4 trimethylation and subsequent gene activation (McKinnell et al., 2008). However, the signaling pathways and molecular mechanisms that regulate the activity of Pax7 in satellite stem cells are undefined.

Wnt signaling plays a key role in regulating developmental programs through embryonic development and in regulating stem cell function in adult tissues (Clevers, 2006). Wnts have been demonstrated to be necessary for embryonic myogenic induction in the paraxial mesoderm (Borello et al., 2006; Chen et al., 2005; Tajbakhsh et al., 1998) as well in the control of differentiation during muscle fiber development (Anakwe et al., 2003). Recently, the Wnt planar cell polarity (PCP) pathway has been implicated in regulating the orientation of myocyte growth in the developing myotome (Gros et al., 2009). In the adult, Wnt signaling is necessary for the myogenic commitment of adult stem cells in muscle tissue following acute

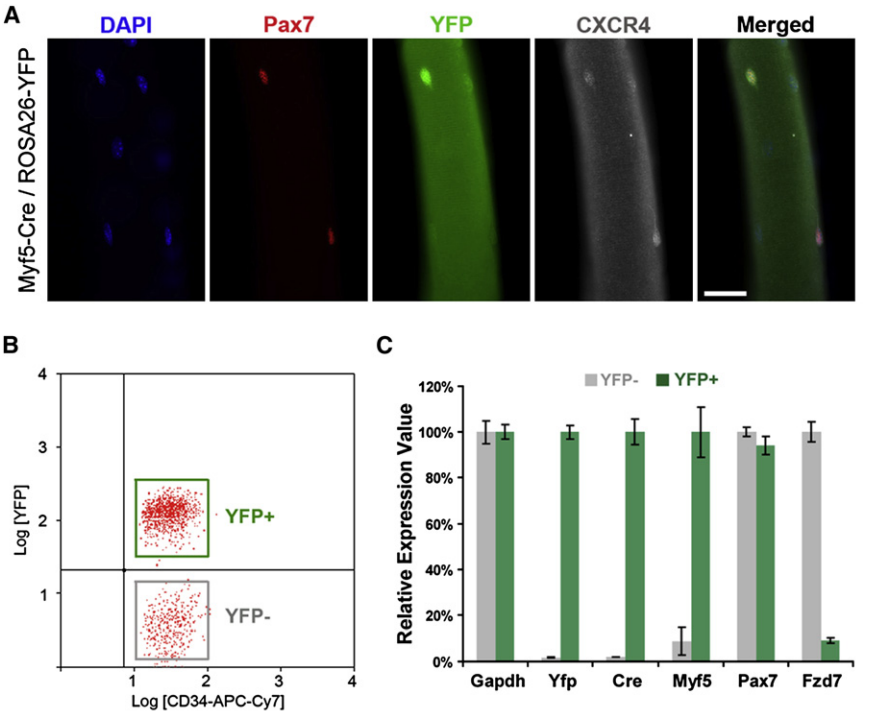

Figure 1. Satellite Stem Cells Express the Wnt Receptor Frizzled7

(A) Single myofibers isolated from *Myf5-Cre/ROSA26-YFP* mice. Ninety percent of Pax7$^+$ cells expressed YFP, and 10% of Pax7$^+$ cells were YFP$^-$. Satellite cells uniformly expressed the stem cell marker CXCR4.

(B) Gated satellite cells (α7-integrin$^+$, CD34$^+$, CD45$^-$, CD31$^-$, CD11b$^-$, Sca1$^-$) extracted from resting limb skeletal muscle were separated on the basis of *Myf5-Cre*-activated YFP fluorescence.

(C) Real-time PCR analysis of sorted cells showing the absence of *Myf5* and *YFP* transcripts as well as the expression of *Fzd7* transcripts in YFP$^-$-sorted cells (n = 3).

(D) Fzd7 was expressed specifically in quiescent Pax7$^+$/YFP$^-$ satellite stem cells (left), but not in Pax7$^+$/YFP$^+$ satellite myogenic cells (right) in freshly isolated *Myf5-Cre/ROSA26-YFP* myofibers.

(E) Proliferating satellite cells and myogenic precursor cells express Fzd7. Regenerating EDL myofibers were isolated 4 days after TA muscle injury. Both Pax7$^+$/Myf5$^-$ (left) and Pax7$^+$/Myf5$^+$ (right) dividing satellite cells expressed Fzd7.

Scale bars are 10 μm. Errors bars represent SEM.

damage (Polesskaya et al., 2003; Torrente et al., 2004). Other studies suggest that the canonical Wnt/β-catenin signaling regulates myogenic differentiation through activation and recruitment of reserve myoblasts (Rochat et al., 2004). In addition, the Wnt/β-catenin signaling in satellite cells within adult muscle appears to control myogenic lineage progression by limiting Notch signaling and thus promoting differentiation (Brack et al., 2008).

In this study, we undertook a molecular characterization of satellite stem cells using a subtractive hybridization approach to identify uniquely expressed genes. We found that the Wnt receptor Fzd7 was markedly upregulated in quiescent satellite stem cells, suggesting a role for noncanonical Wnt signaling. Investigation of this hypothesis revealed that Wnt7a is expressed during muscle regeneration and acts through its receptor Fzd7 and Vangl2, a component of the PCP pathway, to induce symmetric satellite stem cell expansion and dramatically enhance muscle regeneration. Together these results reveal a role for the PCP pathway in regulating the homeostatic maintenance of the stem cell compartment during adult skeletal muscle regeneration.

RESULTS

Frizzled7 Is Highly Expressed in Quiescent Satellite Stem Cells

Satellite cells are a heterogeneous population composed of stem cells and committed progenitors. All satellite cells express Pax7 and markers such as CXCR4; however, a subset of about 10% of cells have never expressed Myf5 during their developmental history (Figure 1A). As previously demonstrated, Pax7$^+$/Myf5$^-$ satellite cells represent a stem cell population within the satellite cell niche (Kuang et al., 2007).

Toward performing gene expression analysis of quiescent satellite stem cells, we first improved our previously described methodology for satellite cell isolation by fluorescence-activated cell sorting (FACS) as described in the Experimental Procedures. FACS-purified cells (CD34$^+$, α7-integrin$^+$, CD31$^-$, CD45$^-$, CD11b$^-$, Sca1$^-$) (see Figure S1A available online), were >95% satellite cells, as determined by Pax7 and Syndecan-4 (Syn4) expression (Figure S1B), and exhibited robust growth and differentiation potential in vitro (Figure S1C).

FACS-purified satellite cells were further separated on the basis of Myf5-conditional YFP fluorescence (Figure 1B). In vitro-cultured YFP$^-$ satellite cells gave rise to proliferating cells

expressing Pax7, but not YFP or Myf5 protein, when maintained at low density (Figure S2), thus validating that YFP$^-$ cells do not and have not expressed Myf5. Real-time PCR analysis of freshly sorted cells confirmed Pax7 expression (Figure 1C) as well as several other satellite cell markers, such as cMet, Syn4, Caveolin1, and α7-integrin (data not shown) in isolated YFP$^+$ and YFP$^-$ satellite cells. In addition, YFP and Myf5 transcripts were detected in YFP$^+$ satellite cells, while virtually no YFP and Myf5 expression (not significantly different from RT$^-$ controls) was detected in YFP$^-$ satellite cells (Figure 1C).

To gain insight into the molecular mechanisms responsible for regulating satellite stem cell function, suppressive subtractive hybridization (SSH) of cDNAs (Diatchenko et al., 1997) was employed to identify genes expressed specifically in quiescent Pax7$^+$/Myf5$^-$ satellite stem cells. Notably, one of the differentially expressed clones encoded a fragment from within the Frizzled7 (Fzd7) mRNA. Fzd7 is a G protein-coupled transmembrane Wnt receptor that belongs to a protein family encoded by multiple genes (Egger-Adam and Katanaev, 2008). Real-time PCR analysis confirmed that Fzd7 transcripts were abundantly expressed in YFP$^-$ satellite cells and only marginally detected in YFP$^+$ satellite cells (Figure 1C).

To confirm the differential expression suggested by real-time PCR, we examined Fzd7 protein expression on myofibers fixed immediately following isolation from extensor digitorum longus (EDL) muscles. Immunohistological analysis revealed that 12% ± 3% of Pax7$^+$ satellite cells expressed readily detectable levels of Fzd7 (n = 3 mice, >150 cells/mouse). Analysis of myofibers isolated from *Myf5-Cre/ROSA26-YFP* EDL muscles demonstrated that Fzd7 was specifically upregulated in satellite stem cells (Pax7$^+$/Myf5$^-$) that do not contain detectable levels of YFP (Figure 1D).

However, culture of fibers in suspension for 2 days resulted in upregulation of Fzd7 in virtually all satellite cells (99%, n = 3 mice, ≥100 cells per mouse) (Figure S3). Furthermore, examination of regenerating myofibers from EDL muscle following cardiotoxin (CTX)-induced damage of the tibialis anterior (TA) muscle (Kuang et al., 2007) revealed Fzd7 expression on doublets of Pax7$^+$/Myf5$^-$ and Pax7$^+$/Myf5$^+$ cells (Figure 1E).

Taken together, these results demonstrate that, in resting muscle, the Wnt receptor Fzd7 is specifically expressed in quiescent satellite stem cells. However, Fzd7 is also upregulated in proliferating satellite cells and myoblasts.

Wnt Expression during Muscle Regeneration

Coexpression of Fzd7 and Wnt7a during embryonic myogenesis suggests that Wnt7a is a candidate ligand for Fzd7 (Cossu and Borello, 1999). Moreover, Wnt7a has been implicated as a major regulator of embryonic and adult myogenesis (Chen et al., 2005; Polesskaya et al., 2003; Tajbakhsh et al., 1998). We therefore employed real-time PCR array analysis of freeze-injured TA muscle to document Wnt expression during regenerative myogenesis. We chose freeze injury of muscle because of the significantly reduced inflammatory response relative to other methods such as CTX injection. Changes in gene expression were analyzed at 3 days postinjury, during the acute phase of regeneration, where most of the Pax7$^+$ cells are proliferating, and at 6 days postinjury, when satellite cells have returned to a quiescent sublaminar position (Figure 2A).

At 3 days postinjury, we detected significant increases (as compared to contralateral leg, n = 3 mice, $p < 0.05$) in 31 transcripts including those for multiple Wnts (*Wnt-1*, *-2*, *-5b*, *-8b*, *-10a*, *-16a*), Frizzled receptors, and sFRP inhibitors (Figure S4). Notably, at 6 days postinjury, we detected a significant increase (n = 3 mice, $p < 0.05$) in the transcript levels for *Wnt7a* and *Wnt10a* (Figure 2B). *Wnt3a* levels were below the limit of detection in our analyses at both 3 and 6 days of regeneration (Table S1). Therefore, *Wnt7a* mRNA was markedly upregulated at the time when satellite stem cells replenish the resident satellite cell pool.

To confirm Wnt7a upregulation during muscle regeneration in another muscle injury model, we performed immunohistochemical analysis of Wnt7a protein expression on cryosections of CTX-injured TA (fixed 4 days postinjury) and the contralateral resting TA. In undamaged muscle, Wnt7a was not expressed at detectable levels (Figure 2E, left). By contrast, Wnt7a was strongly upregulated in regenerating fibers (of smaller size than the intact fibers and containing myogenin$^+$ nuclei) and was not expressed by CD144$^+$ endothelial cells (Figure 2E, right).

To determine whether Wnt7a is a ligand for Fzd7, cultured satellite cell-derived myoblasts were incubated with recombinant human Wnt7a protein for 30 min, washed, fixed, and immunostained with anti-Wnt7a antibody. Cells incubated with BSA did not show membrane staining for Wnt7a protein. By contrast, cells incubated with Wnt7a protein exhibited immunostaining on the membrane (Figure 2C). Importantly, transfection of Fzd7 siRNA abrogated binding of Wnt7a (Figure 2C). Fzd7 silencing was effective, specific, and did not significantly alter the other Frizzled transcripts expressed in myoblasts (Figure S6A). Taken together, these data provide compelling evidence that Fzd7 is the receptor for Wnt7a in myogenic cells.

Wnt7a has been described as either a canonical (Hirabayashi et al., 2004) or a noncanonical Wnt (Kengaku et al., 1998), depending on cell type and receptor context. To evaluate the possible function of Wnt7a as a canonical Wnt, we stimulated satellite cell-derived myoblasts with Wnt7a and Wnt3a proteins for 24 hr. Wnt3a activates the canonical Wnt pathway in myogenic cells (Brack et al., 2008), and in our experiment, Wnt3a stimulation resulted in increased expression of β-catenin/TCF target genes—for example, a 5-fold and 50-fold increase of *Tcf7* and *Axin2* mRNAs, respectively, (n = 5, $p \leq 0.001$). By contrast, Wnt7a stimulation did not result in any significant change in *Tcf7* and *Axin2* levels, which were similar to BSA-treated samples (Figure 2D). In addition, Wnt3a, but not Wnt7a, stimulation robustly induced the stabilization and nuclear localization of activated β-catenin (Figure S5), and Wnt3a, but not Wnt7a, robustly activated the β-catenin luciferase reporter TOP-Flash in transient transfection experiments (data not shown).

Taken together, these results indicate that Wnt7a is markedly upregulated by newly formed myofibers during regenerative myogenesis, binds to the Fzd7 receptor at the surface of myogenic cells, and does not utilize the canonical Wnt/β-catenin signaling pathway.

Symmetry of Satellite Stem Cell Divisions Is Regulated by Wnt7a-Frizzled7

The expression of Fzd7 specifically in quiescent satellite stem cells and the marked upregulation in Wnt7a during muscle

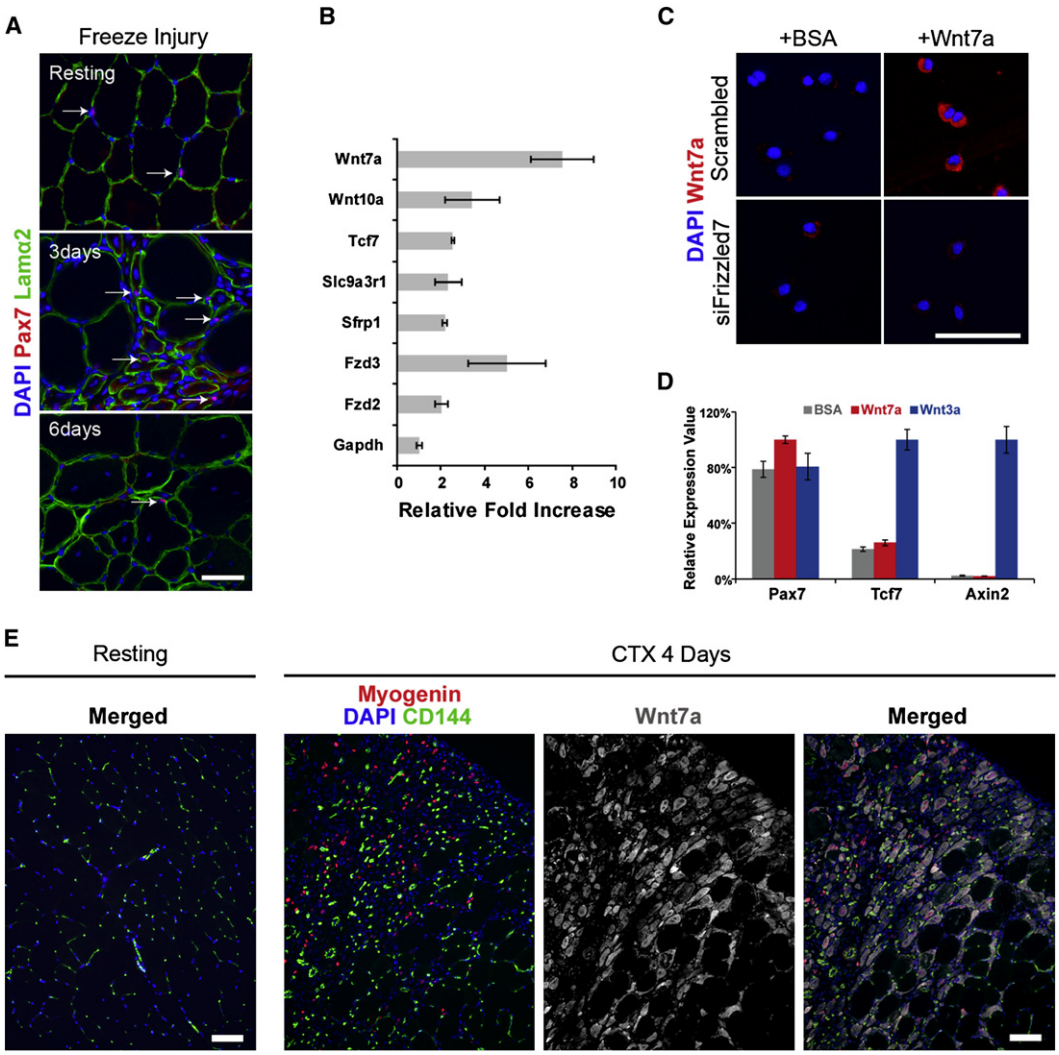

Figure 2. Wnt7a Is Highly Upregulated during Muscle Regeneration

(A) Cryosections of resting (top) and freeze-injured TA muscles analyzed at 3 (middle) and 6 (bottom) days following injury. The basal lamina of myofibers is revealed by laminin α2 chain staining, and satellite cell nuclei were visualized by Pax7 staining.

(B) Real-time PCR array analysis of regenerating TA muscle 6 days following freeze injury revealed upregulation of *Wnt7a* mRNA at the time that satellite cells return to quiescence (n = 3).

(C) Recombinant Wnt7a protein binds Fzd7 at the surface of myogenic cells, and this binding is abolished after knockdown of Fzd7.

(D) Wnt3a, but not Wnt7a, activates β-catenin/TCF target genes. Shown is real-time PCR analysis of cultured myogenic cells after stimulation with BSA (control) and recombinant Wnt proteins. Only Wnt3a induced the transcription of the β-catenin/TCF target genes *Tcf7* and *Axin2* (n = 5).

(E) Wnt7a protein is expressed by regenerating myofibers, and not by vascular endothelial cells. Shown are cryosections of 4-day CTX-induced regenerating (left) and resting contralateral (right) TA muscles. Sections were examined for the expression of myogenin (differentiating myogenic cells), CD144 (endothelial cells), and Wnt7a proteins.

Scale bars are 25 μm. Errors bars represent SEM.

regeneration suggested that Wnt7a-Fzd7 signaling is involved in regulating muscle stem cell function. In addition, Wnt7a had no effect on the growth or differentiation of cultured primary myoblasts in vitro (Figure S8). Therefore, to investigate the role of Wnt7a-Fzd7 signaling in satellite cells, we examined the ability of recombinant Wnt7a to alter the ratio between asymmetric and symmetric cell divisions of satellite stem cells in vitro. Myofibers were isolated from *Myf5-Cre/ROSA26-YFP* EDL muscle and cultured under nonadherent conditions. In our culture system, quiescent satellite cells become activated immediately following myofiber isolation. Satellite cells leave their niche, migrate across the basal lamina, and undergo their first cell division in a synchronous fashion. Thus, we visualized the outcome of the first division by fixing and staining the myofibers after 42 hr of culture. Importantly, live imaging analysis confirms that satellite cells do not move on myofibers before dividing and that scored cell doublets are of clonal origin (Kuang et al., 2007).

Satellite stem cells (YFP^-) underwent either a symmetrical cell division to give rise to two YFP^- daughter cells, or an asymmetric cell division to give rise to one YFP^- stem cell and one YFP^+

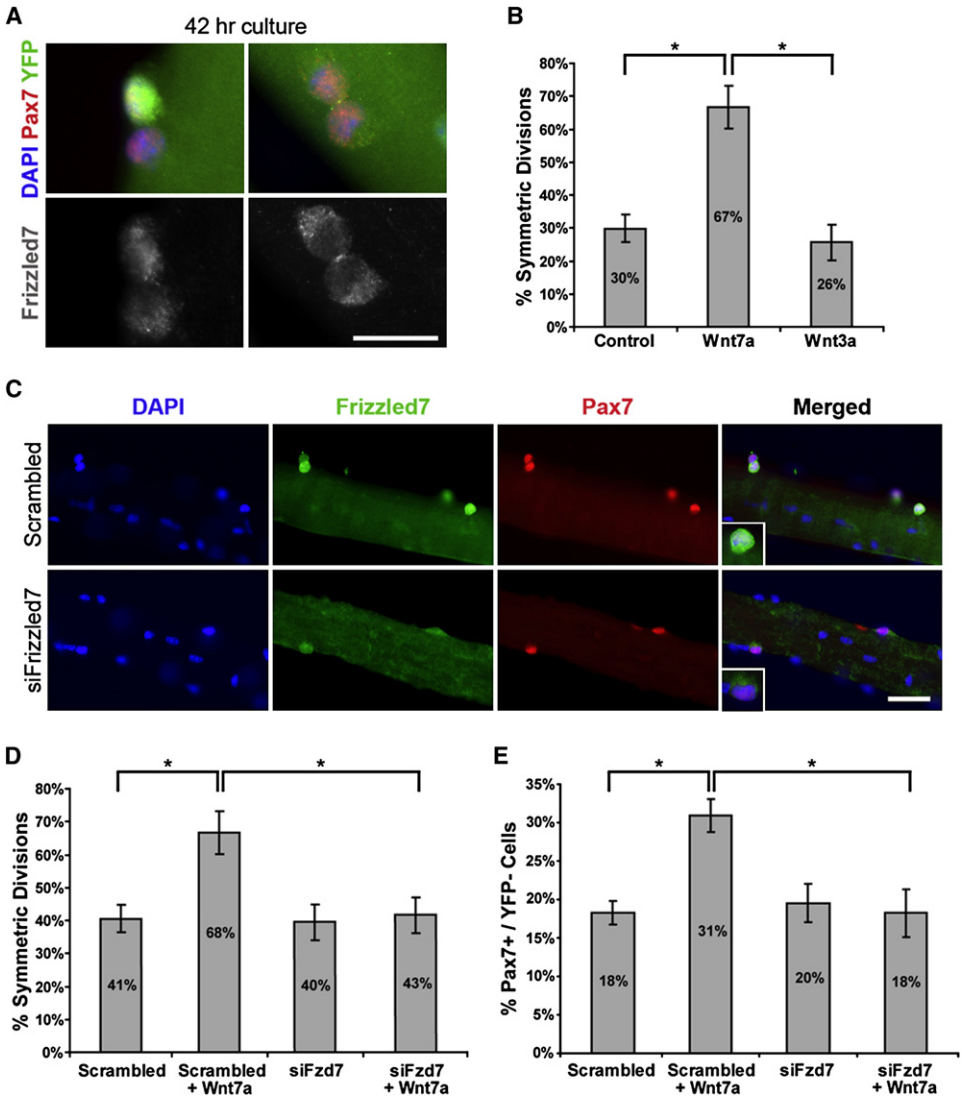

Figure 3. Wnt7a-Frizzled7 Signaling Drives Satellite Stem Cell Expansion

(A) First division of Pax7$^+$/YFP$^-$ satellite stem cells, 42 hr after isolation of EDL single myofibers from *Myf5-Cre/ROSA26-YFP* mice, cultured in floating conditions. Satellite stem cells either give rise to one YFP$^-$ stem cell and one YFP$^+$ committed cell, via asymmetric cell division (left), or alternatively give rise to two YFP$^-$ daughter cells by symmetric cell division (right).

(B) Wnt7a, but not Wnt3a, stimulation markedly increased the proportion of symmetric cell divisions resulting in satellite stem cell expansion (n = 3, *p = 0.009).

(C) Activated satellite cells on cultured myofibers at 42 hr after isolation do not express Fzd7 (bottom) after knockdown of Fzd7 with siRNA, as compared to cells in nonsilencing conditions (top).

(D) The Wnt7a-induced increase in the rate of symmetric satellite stem cell divisions was abrogated following silencing of Fzd7 on myofibers after 42 hr of culture (n = 3, *p < 0.02).

(E) The increase in satellite stem cell numbers induced by Wnt7a was blocked by silencing of Fzd7 on myofibers after 52 hr of culture (n = 3, *p < 0.03).

Scale bars are 10 μm. Errors bars represent SEM.

committed precursor (Figure 3A). When stimulated with Wnt7a, we observed a dramatic increase in the proportion of symmetric cell divisions from 30% to 67% (n = 3, n ≥ 152 pairs, p = 0.009). By contrast, Wnt3a treatment did not induce any significantly change (Figure 3B). Therefore, Wnt7a stimulated an increase in symmetric satellite stem cell divisions.

Our experimental analysis suggested that Wnt7a specifically binds the Fzd7 receptor (Figures 2C and 2D). Therefore, to determine whether the induction of symmetric stem cell divisions by Wnt7a required the presence of Fzd7, we performed Fzd7 knockdown experiments on isolated myofibers. Immunostaining of treated fibers demonstrated extensive silencing of Fzd7 expression after 42 hr (Figure 2C). Importantly, siRNA-induced knockdown of Fzd7 resulted in a complete abrogation of the ability of Wnt7a to induce symmetric satellite stem cell divisions (n = 3, ≥ 123 pairs, p ≤ 0.02). By contrast, scrambled siRNA treatment did not significantly affect this activity of Wnt7a (Figure 3D). Consistent with these results, the proportion of

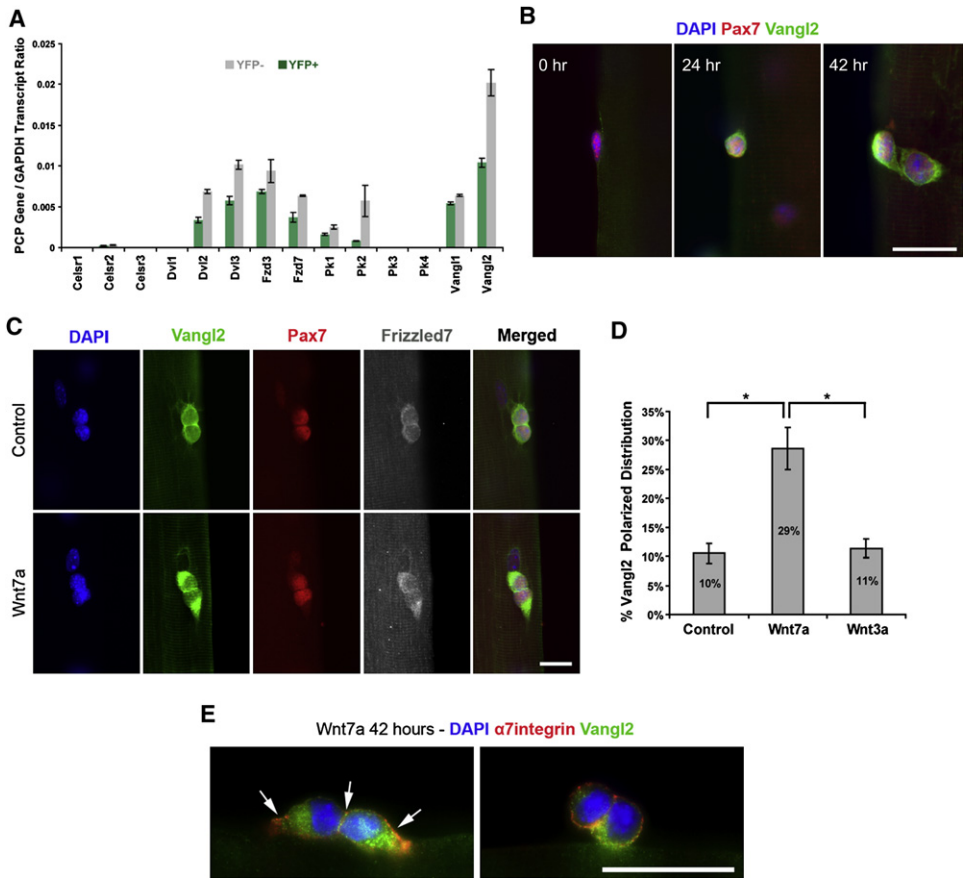

Figure 4. PCP Components Are Expressed by Myogenic Cells

(A) Quantitative real-time PCR analysis indicated expression of PCP core component transcripts by YFP$^+$ and YFP$^-$ satellite cell-derived myoblasts (n = 3).

(B) Immunostaining indicated that Vangl2 is upregulated during activation of Pax7$^+$ satellite cells by 24 hr on cultured myofibers.

(C) Wnt7a induces polarized Vangl2 cellular localization on opposite poles of dividing Pax7$^+$ satellite cells on cultured myofibers. EDL myofibers were cultured in control medium or medium supplemented with Wnt7a and fixed 42 hr after isolation.

(D) Effects of Wnt treatment on Vangl2 polarization during initial division. Wnt7a signaling, but not Wnt3a, induces polarized localization of Vangl2 and Fzd7 during satellite cell division (n = 3, *p = 0.006).

(E) Wnt7a-treated myofibers were immunolocalized for Vangl2 and the membrane marker α7-integrin. Vangl2 is polarized and colocalizes to the membrane in planar-dividing satellite cells (arrows). Note the polarized and upregulated expression of α7-integrin, which facilitates adhesion to the basal lamina of both daughter cells.

Scale bars are 10 μm. Errors bars represent SEM.

satellite stem cells (Pax7$^+$/YFP$^-$) after the second division (50 hr) was significantly increased by 13% after Wnt7a treatment (n = 3, $\geq$ 1203 cells, $p \leq 0.03$), resulting in an increase in the number of stem cells per fiber (Figure 3E, Figure S6B). Similarly, Fzd7 silencing efficiently blocked the effect of Wnt7a stimulation. We observed that the total number of Pax7$^+$ cells per fiber remained constant between each condition, confirming that Wnt7a does not effect cell proliferation or differentiation (Figure S6C).

These results demonstrate that Wnt7a signals via Fzd7 to stimulate symmetric satellite stem cell division and thus drive the expansion of the satellite stem cell pool.

Role for the PCP Component Vangl2 in Satellite Stem Cell Self-Renewal

Our analysis indicated that Wnt7a does not activate the canonical Wnt/β-catenin signaling pathway (Figure 2D, Figure S4) and that Wnt7a signals through the Fzd7 receptor to drive satellite stem cell symmetric divisions (Figures 2C, 3B, and 3D). In *Xenopus laevis*, xFzd7 is considered a component of the PCP signaling pathway involved in gastrulation (Goto et al., 2005). Therefore, we hypothesized that Wnt7a acts through Fzd7 to activate the PCP pathway and drive satellite stem cell expansion.

To investigate if Wnt7a activates the PCP pathway, we first analyzed the relative transcript levels of a set of core PCP components (Seifert and Mlodzik, 2007) in myogenic cells. Interestingly, myoblasts expressed significant levels of *Dvl-2* and *-3*, *Fzd-3* and *-7*, *Pk-1* and *-2*, and *Vangl-1* and *-2* and low levels of *Celsr2*. Other PCP component genes tested were called absent with cutoff values over 30 cycles (Figure 4A). In addition, cultured satellite stem cells (YFP$^-$) expressed significantly higher levels of all PCP components (n = 3, $p < 0.05$), with a marked upregulation of *Vangl2*, consistent with a role for PCP signaling in regulating satellite stem cell function.

Vangl2 is a crucial regulator of PCP and noncanonical Wnt signaling in *Drosophila* and vertebrates (Torban et al., 2004). In cells with active PCP signaling, Vangl2 protein is distributed at the poles at either end of the axis of polarization, and this distribution is lost in PCP mutants (Montcouquiol et al., 2006). Vangl2 protein was not detected in quiescent satellite cells on isolated myofibers but was upregulated in activated satellite cells as they entered the cell cycle by 24 hr in culture. After 48 hr, all $Pax7^+$-activated satellite cells were also positive for Vangl2 (100%, n = 3 mice, $\geq$100 cells per mouse) (Figure 4B). We also confirmed the expression in satellite cells of Prickle1 and Celsr2 proteins that interact with Vangl2 in vivo (data not shown).

Importantly, in the presence of Wnt7a, a significant proportion of dividing doublets of satellite cells on cultured myofibers (29% ± 4%, n = 3, $\geq$240 pairs, $p \leq 0.006$) exhibited polarized localization of Vangl2 on opposite poles of the daughter cells (Figures 4C and 4D). By contrast, following BSA (control) or Wnt3a treatment, Vangl2 protein was uniformly dispersed in satellite cell doublets (90% ± 2% and 89% ± 2%, respectively) (Figures 4C and 4D). Moreover, double staining with anti-Vangl2 and anti-α7-integrin antibodies revealed that Wnt7a appeared to induce enhanced membrane localization of Vangl2 and polarized distribution α7-integrin. This redistribution did not occur in untreated cells or in cells undergoing apical-basal cell divisions (Figure 4E). Taken together, these observations strongly support the assertion that Wnt7a induces a redistribution of the polarity effector Vangl2 and α7-integrin and that the upregulated expression of α7-integrin at the poles of daughter cells allows them to remain adherent with the basal lamina and to remain in the stem cell niche.

To investigate the role of Vangl2 in satellite stem cell function, we performed siRNA silencing of Vangl2 on single *Myf5-Cre/ROSA26-YFP* myofibers stimulated with Wnt7a. Myofibers were first stained with Pax7 and Syn4 antibodies to allow visualization of the plane of satellite cell division relative to the fiber, and cell divisions scored as either planar or apical-basal (Figure 5A). At 42 hr after the first cell division, Wnt7a stimulation induced planar divisions and accordingly resulted in a 12% decrease in apical-basal cell divisions. By contrast, Vangl2 silencing increased the proportion of apical-basal cell divisions by 15%, (n = 3, $\geq$154 pairs, $p \leq 0.02$) (Figure 5B). Myofibers from the same experiments were also stained with Pax7 and YFP antibodies and the percentage of symmetric cell divisions scored. We observed a close inverse correlation between the proportions of apical-basal versus symmetric cell divisions. Wnt7a stimulation increased the proportion of symmetric cell divisions, whereas Vangl2 knockdown markedly impaired the ability of Wnt7a to stimulate symmetric cell divisions (n = 3, $\geq$65 pairs, $p \leq 0.02$) (Figure 5C).

To analyze the role of Vangl2 in satellite cell proliferation and myogenic potential, we cultured fibers for 50 hr and assessed Vangl2 silencing by immunostaining (Figure 5D). At this point, Vangl2 knockdown continued to increase the rate of apical-basal cell divisions (n = 5, $\geq$150 pairs, p = 0.001) (Figure 5E) while depleting the population of satellite stem cells (n = 3, $\geq$330 cells, p = 0.03) (Figure 5F). This resulted in a marked diminution in the total number of satellite cells per fibers (n = 5, $\geq$500 cells, p = 0.001) (Figure 5G). At 3 days after knockdown of Vangl2 (Figure 5H), we observed a doubling in the number of cells expressing myogenin, an early marker for differentiation (n = 4, $\geq$550 cells, $p = 10^{-5}$) (Figure 5I) along with a loss of half the cells on fibers (n = 4, $\geq$550 cells, p = 0.001) (Figure 5J). Vangl2 silencing on satellite cell-derived myoblasts resulted in reduced levels of Pax7 and Myf5 transcripts, along with increased levels of myogenin (n = 4, $p \leq 0.05$) (Figure 5K). Together, these data suggest that Vangl2 is required for self-renewal of both satellite stem cells and the generation of transient-amplifying myoblasts.

These data demonstrate that Wnt7a signaling through Fzd7 requires Vangl2 to induce symmetric expansion of the satellite stem cell pool. Wnt7a also induces polarized distribution of Vangl2 protein at the opposite poles of cells undergoing a symmetric planar cell division. Hence, Wnt7a utilizes the PCP pathway to control the orientation of satellite cell division and their fate within the niche.

Wnt7a Enhances Muscle Regeneration by Expanding the Stem Cell Pool

To investigate the role of the Wnt7a-Fzd7-Vangl2 pathway in muscle regeneration in vivo, we overexpressed Wnt7a by electroporation of a CMV-Wnt7a expression plasmid into TA muscles of 3-month-old mice. Histological analysis of muscles electroporated with CMV-*lacZ* plasmid revealed that the majority (>80%) of the myofibers expressed the β-galactosidase (Figure S7A) and that we did not detect any regeneration deficit following electroporation of control plasmid (Figure S7B). In addition, immunostaining revealed that myofibers electroporated with CMV-Wnt7a plasmid secreted readily detectable levels of Wnt7a protein (Figure S7C).

Notably, TA muscles electroporated with CMV-Wnt7a exhibited an 18% ± 4% (p = 0.009, n = 8) increase in mass after 3 weeks. Examination of serial sections of electroporated muscles revealed an increase in the overall size of the muscle as well as a significant increase in caliber size and numbers of fibers throughout the body of the muscle (Figure 6). By contrast, overexpression of Wnt3a resulted in a larger increase in the number of myofibers, but these exhibited a dramatic reduction in cross-sectional area, resulting in reduced regeneration efficiency (Figure 6). We did not observe an effect of Wnt7a overexpression on other cell types in muscle tissue. However, overexpression of Wnt3a resulted in abnormal matrix deposition, suggesting an enhancement of proliferation of fibroblastic/smooth muscle progenitors resulting in increased fibrosis (Figure 6B). Taken together, our results indicate that overexpression of Wnt7a markedly enhances muscle regeneration, as evidenced by the presence of increased numbers of larger fibers and the significantly increased mass of muscle.

As previously noted, Wnt7a treatment did not alter the growth or differentiation of activated satellite cells or primary myoblasts in vitro (Figures S6C, S8A, S8C, and S8D). In addition, Wnt7a did not induce the expression of MyoD or of Wnt/β-catenin target genes in differentiated myocytes (Figures S8B and S8E). However, our in vitro experiments established that Wnt7a-Fzd7-Vangl2 signaling stimulated the symmetrical expansion of satellite stem cells, which would then give rise to transient amplifying progenitors that undergo normal proliferation and differentiation. To assess whether Wnt7a similarly stimulates the expansion of satellite stem cells in vivo, we enumerated the numbers of satellite cells and satellite stem cells in regenerated muscle following electroporation of CMV-Wnt7a.

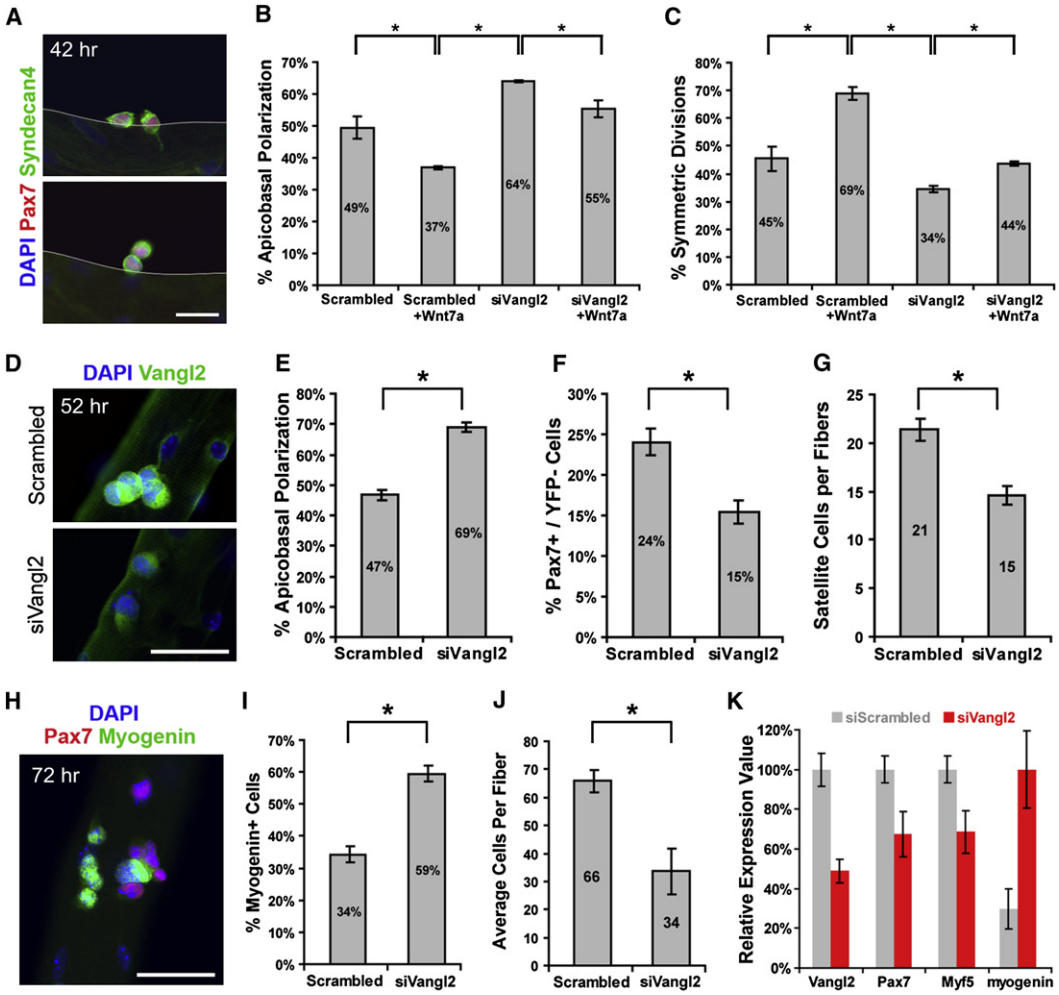

Figure 5. Vangl2 Is Required for Symmetric Expansion of Satellite Stem Cells

EDL single myofibers from *Myf5-Cre/ROSA26-YFP* mice were cultured in floating conditions and subjected to either nonsilencing or Vangl2 siRNA transfection.

(A) Orientation of $Pax7^+$/Syndecan-4^+ satellite cell first cell division at 42 hr. Divisions were scored either as planar (top) or apical-basal (bottom). Note, in myofiber culture, satellite cells translocate to the outside surface of the basal lamina (white line), and apical-basal cell divisions are directed into the media.

(B) Wnt7a induces a significant decrease in the proportion of apical-basal cell divisions after 42 hr of culture, supporting its function in stimulating stem cell expansion. Knockdown of Vangl2 inhibits the ability of Wnt7a to stimulate planar cell divisions (n = 3, *$p < 0.02$).

(C) The Wnt7a-induced increase in symmetric satellite stem cell divisions was abrogated following silencing of Vangl2 on myofibers after 42 hr of culture (n = 3, *$p < 0.02$).

(D) Activated satellite cells on myofibers knocked down for Vangl2 after 52 hr of culture do not express Vangl2 (bottom) as compared to cells in nonsilencing conditions (top).

(E) Knockdown of Vangl2 increased the rate of apical-basal divisions (n = 5, *p = 0.001).

(F) Knockdown of Vangl2 decreased the proportion of $Pax7^+/YFP^-$ stem cells (n = 3, *p = 0.03).

(G) Knockdown of Vangl2 decreased the number of cells per fibers (n = 5, *p = 0.001).

(H and I) Silencing of Vangl2 increased the proportion of differentiating $myogenin^+/Pax7^-$ cells myofibers after 3 days of culture (n = 4, *$p = 10^{-5}$).

(J) Silencing of Vangl2 depleted the satellite cells pool (n = 4, *p = 0.001).

(K) Vangl2 silencing promotes myogenic differentiation as revealed by real-time PCR analysis of gene expression in satellite cell-derived myoblasts (n = 4).

Scale bars are 10 μm. Errors bars represent SEM.

Overexpression of Wnt7a resulted in about a 2-fold increase in the number of $Pax7^+$ satellite cells per myofiber on sections at 3 weeks after electroporation (p = 0.03, n = 4). By contrast, overexpression of Wnt3a did not alter the number of satellite cells (Figures 7A and 7B). To enumerate the proportion of satellite stem cells, FACS-isolated satellite cells were isolated from *Myf5-Cre/ROSA26-YFP* TA muscle at 3 weeks following electroporation, cultured for 24 hr, then immunostained for Pax7 and YFP (Figure 7C). Consistent with our observations that Wnt7a induces symmetrical satellite stem cell divisions in vitro, we observed that overexpression of Wnt7a in regenerating muscle in about a 63% increase (n = 5, p = 0.0001) in the proportion of $Pax7^+/YFP^-$ satellite stem cells (Figures 7C and 7D). Therefore, these data indicate that, similarly, Wnt7a acts on the satellite stem cell compartment in vitro and in vivo.

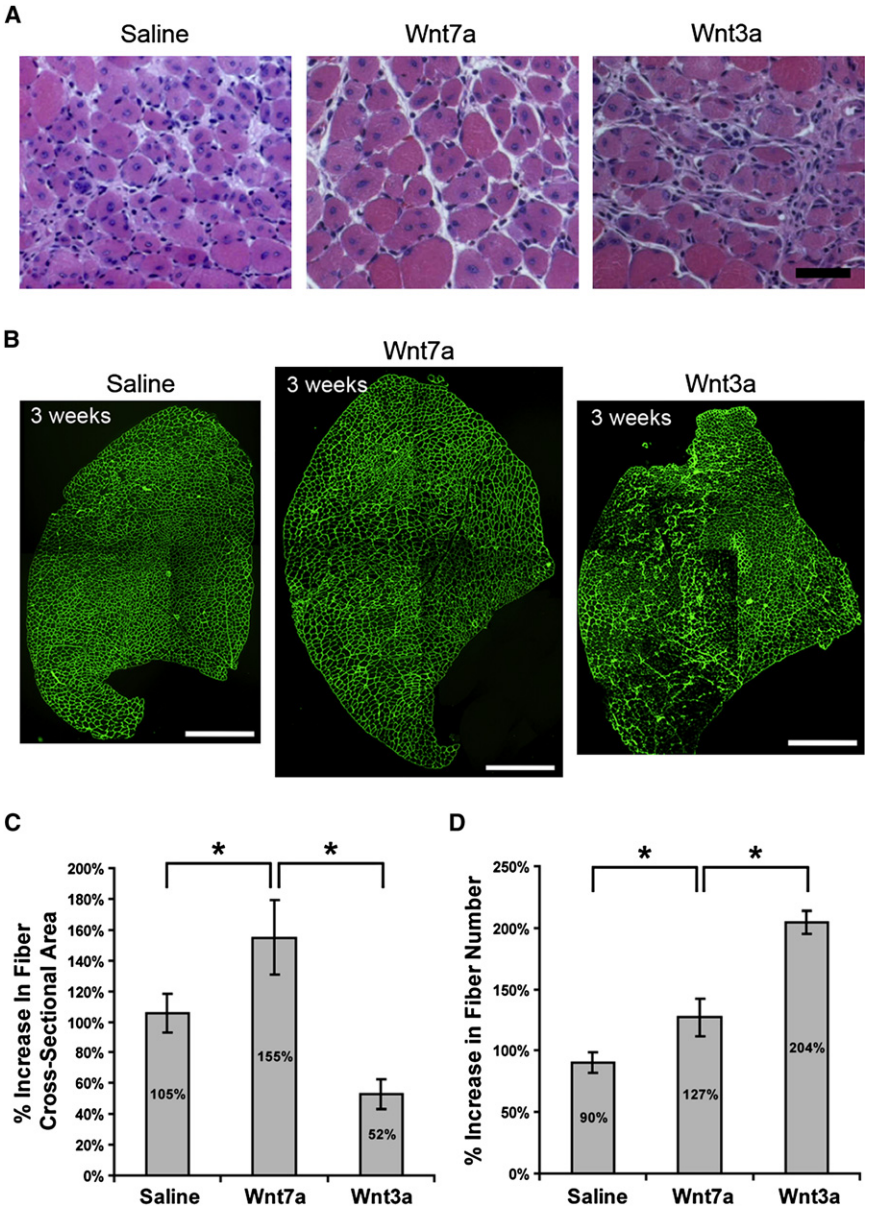

Figure 6. Ectopic Wnt7a Enhances Muscle Regeneration

(A) Representative histology of regenerated TA muscles of 3-month-old mice, 8 days following electrotransfer-induced injury. Regenerated myofibers show centrally located nuclei. Scale bar is 25 μm.

(B) Representative cryosections of TA muscles 3 weeks following electroporation with CMV-Wnt7a plasmid exhibit accelerated regeneration as evidenced by increased mass, and number and caliber of fibers. Electroporation with CMV-Wnt3a resulted in malformed muscle with abnormal accumulation of matrix. The basal lamina of myofibers was detected by laminin α2 chain immunostaining. Scale bars are 200 μm.

(C) Quantification of muscle fiber caliber in TA muscles electroporated with either saline or a Wnt7a/Wnt3a expression plasmids, as compared to contralateral leg, 3 weeks after electroporation ($n = 4$, $^*p \leq 0.008$). Wnt7a and Wnt3a have divergent effects on myofiber caliber.

(D) Quantification of muscle fiber number in TA muscles electroporated with either saline or a Wnt7a/Wnt3a expression plasmid, as compared to contralateral leg, 3 weeks after electroporation ($n = 4$, $^*p \leq 0.03$).

Errors bars represent SEM.

To investigate satellite stem cell function in the absence of Wnt7a, we analyzed the regeneration phenotype of 3-month-old *Wnt7a*$^{-/-}$ null mice (Miller and Sassoon, 1998). Quantification of Pax7-expressing satellite cells on freshly isolated myofibers from EDL muscle demonstrated that *Wnt7a*$^{-/-}$ null mice exhibit about an 18% decrease in number of satellite cells per fiber ($p = 0.03$, $n = 4$) (Figure 7E). Three weeks following a freeze-crush injury, the regenerated *Wnt7a*$^{-/-}$ TA muscles appeared grossly normal (Figure 7F). Importantly, examination of sections of regenerated *Wnt7a*$^{-/-}$ TA muscles revealed a significant 36% decrease in the numbers of satellite cells ($p = 0.03$, $n = 3$) (Figure 7G). This result strongly supports the notion that Wnt7a plays an important role in regulating satellite stem cell function.

Overexpression of Wnt7a in muscle drives expansion of the satellite stem cell pool, and conversely, the satellite cell compartment becomes depleted in the absence of Wnt7a. Together, our data demonstrate a role for Wnt7a signaling via the PCP pathway to stimulate satellite stem cell symmetrical cell division to drive expansion. Therefore, Wnt7a regulates the homeostatic levels of the satellite stem cell compartment and thus regulates the efficiency of regenerative myogenesis in adult skeletal muscle.

DISCUSSION

We undertook a gene expression analysis of satellite stem cells toward identifying signaling pathways that regulate their function. Satellite stem cells represent a small subpopulation of satellite cells that are capable of self-renewal and long-term reconstitution of the satellite cell niche following transplantation (Kuang et al., 2007). Our experiments identified the noncanonical Wnt receptor Fzd7 as being specifically expressed in quiescent satellite cells (Figure 1). Wnt7a was examined as a candidate receptor for Fzd7 because of its expression and role during embryonic and adult myogenesis (Chen et al., 2005; Cossu and Borello, 1999; Polesskaya et al., 2003; Tajbakhsh et al., 1998). We found by real-time PCR and immunohistochemistry that Wnt7a was markedly upregulated in newly formed myofibers during regenerative myogenesis (Figures 2B, 2E) and that the Fzd7 receptor is necessary for Wnt7a binding at the surface of myogenic cells (Figure 2C).

Satellite stem cells undergo apical-basal asymmetric cell divisions to give rise to committed myogenic cells that express

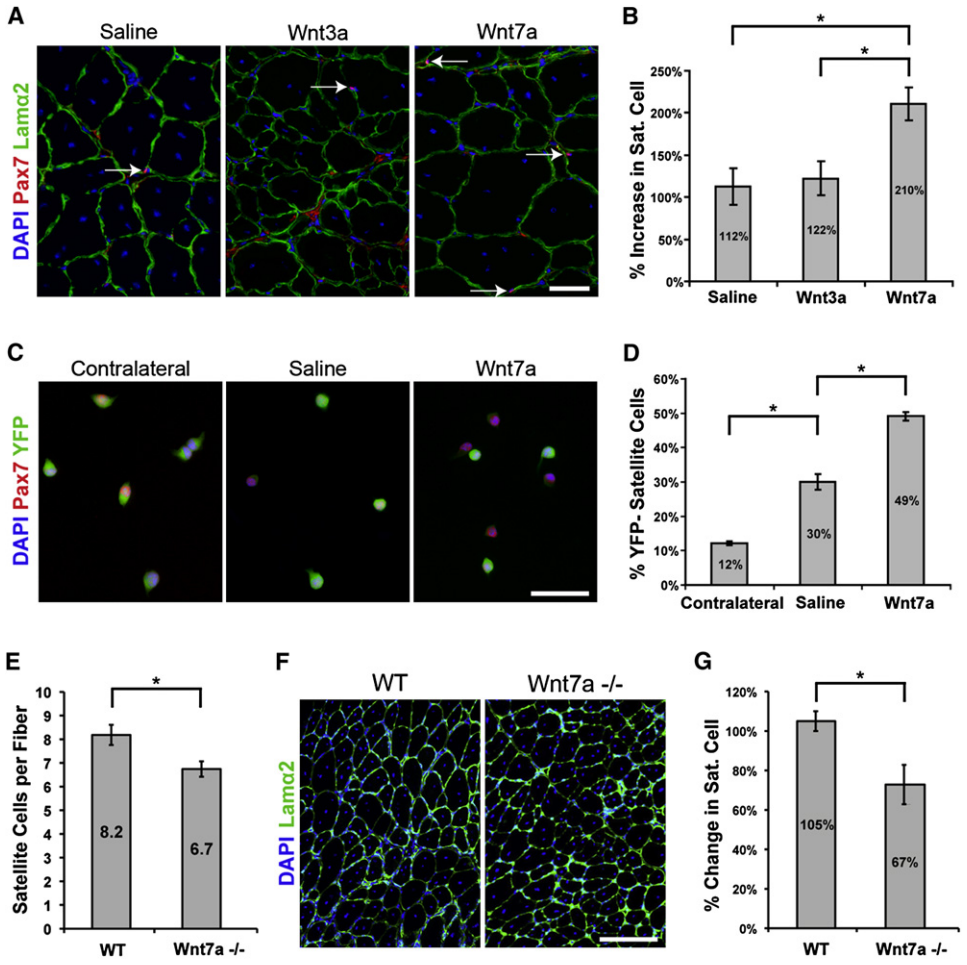

Figure 7. Wnt7a Drives Satellite Stem Cell Expansion In Vivo

(A) TA muscles of 3-month-old mice were electroporated with either saline or a Wnt7a/Wnt3a expression plasmid and dissected after 3 weeks. Sublaminar $Pax7^+$ satellite cells were scored on cryosections of electroporated muscles. Note the increased numbers of $Pax7^+$ satellite cells (arrows) following electroporation with CMV-Wnt7a plasmid. Scale bar is 25 μm.

(B) The satellite cell population was increased by 2-fold following electroporation of CMV-Wnt7a plasmid (n = 4, *$p \leq 0.03$) as compared to saline- or Wnt3a-electroporated samples.

(C) Satellite cells were FACS sorted from electroporated *Myf5-Cre/ROSA26-YFP* TA muscles, 3 weeks after electroporation, and plated in culture for 24 hr, fixed, and stained for Pax7 and YFP. Scale bar is 10 μm.

(D) The proportion of $Pax7^+/YFP^-$ satellite stem cells was significantly increased following overexpression of Wnt7a in electroporated TA muscles (n = 5, *$p \leq 0.0001$).

(E) *Wnt7a*$^{-/-}$ myofibers showed that a reduced population of Pax7+ satellite cells on myofibers was isolated from EDL muscle. (n = 4, *p = 0.03).

(F) Cryosections of freeze-injured TA muscles of 3-month-old *Wnt7a*$^{-/-}$ null mice and their littermate controls analyzed at 3 weeks following injury. No significant difference in terms of structure or cross-sectional area was observed in the regenerated muscle. Scale bar is 20 μm (n = 3).

(G) Decreased numbers of satellite cells were observed in regenerated *Wnt7a*$^{-/-}$ TA muscles normalized to the number of myofibers in cross-sectional area and to the contralateral leg (n = 3, *p = 0.03).

Errors bars represent SEM.

Myf5, and to maintain their population through self-renewal. Alternatively, satellite stem cells can undergo planar symmetric cell divisions to drive expansion of their population (Kuang et al., 2007). Importantly, we found that recombinant Wnt7a protein dramatically stimulated the symmetric expansion of satellite stem cells and that this expansion required Fzd7 and Vangl2 (Figures 3 and 5), both components of the PCP signaling pathway. Moreover, Wnt7a induced polarized localization of Vangl2 at opposite poles in pairs of dividing cells (Figure 4) in a manner consistent with Wnt7a activating PCP signaling. Overexpression of Wnt7a during muscle regeneration resulted in an impressive enhancement of the regeneration process, generating more fibers of bigger caliber, independent of an effect on myoblast proliferation or differentiation (Figure 6). Importantly, Wnt7a overexpression resulted in a large expansion of the satellite stem cell population, and Wnt7a loss resulted in impaired maintenance of the satellite cell compartment (Figure 7). These results provide important new insights into the

molecular regulation of satellite cell self-renewal and implicate the Wnt noncanonical PCP pathway in the regulation of adult stem cell function.

The Wnt-PCP pathway plays a role in patterning by instituting polarity of cells within a tissue, such as with the organized orientation of epithelial cells in *Drosophila* (Zallen, 2007). In vertebrates, PCP signaling, and particularly its effecter Vangl2 (also known as Strabismus), is required for the polarization of stereociliary bundles in the cochlea (Montcouquiol et al., 2003), for convergent extension (CE) movements regulating gastrulation and neurulation (Torban et al., 2004), for neural tube closure (Torban et al., 2008), and in regulating myocyte orientation in the developing myotome (Gros et al., 2009). During zebrafish neurulation, loss of Vangl2 abrogates polarization of neural keel cells by preventing reintercalation of daughter cells into the neuroepithelium, resulting in ectopic neural progenitor accumulation (Ciruna et al., 2006).

We propose that the symmetric expansion of satellite stem cells results from a PCP-mediated orientation of the axis of stem cell division. Since PCP is a positional signal relying on the redistribution of effectors proteins, polarization of PCP core molecules on opposite poles of the daughter cells allows both cells to maintain contact with the basal lamina and thus preserve their orientation relative to the niche (Figure 4 and Figure S9). Notably, Wnt7a induced polarized distribution of Vangl2 and α7-integrin (Figure 4E). The upregulated and polarized localization of α7-integrin allows both daughter cells to remain attached to the basal lamina. By contrast, α7-integrin expression is reduced and evenly distributed in apical-basal-oriented cell divisions. Daughter cells that are "pushed" toward the sarcolemma, thus losing contact with the basal lamina, activate Myf5 transcription and commit to a progenitor state (Kuang et al., 2007). Therefore, these data suggest that the PCP pathway intersects with the mechanisms that control apical-basal cell divisions and commitment and function through a mechanism that promotes adhesion to the basal lamina.

Our experiments suggest that polarized distribution of Vangl2 protein at the poles of a couplet of daughter cells allows both cells to remain attached to the basal lamina and therefore maintain a stem cell state, resulting in expansion of the stem cell population. Subsequent cell divisions will generate larger numbers of committed daughter cells through apical-basal asymmetric divisions that will undergo normal expansion and differentiation (Figure 6). We previously noted that the proportion of $Pax7^{+}$/$Myf5^{-}$ satellite stem cells increased from 10% to about 30% at 3 weeks following injury (Kuang et al., 2007) and that overexpression of Wnt7a further increased the level to 50% (Figures 7C and 7D). By contrast, satellite cell numbers decreased by 36% in Wnt7a-deficient muscle following injury and regeneration Figure 7G). These data strongly support both the model through which Wnt7a regulates the homeostatic maintenance of the satellite stem cell pool by modulating the increase in satellite stem cell expansion during regenerative myogenesis, and that basal levels of PCP signaling are insufficient to maintain the satellite cell pool at normal levels.

In the fly, it has been demonstrated that, in parallel to the frizzled-induced PCP signaling, Strabismus collaborates with Flamingo to mediate planar cell orientation. A secondary PCP mechanism is regulated by the protocadherins Fat and Dachsous independently of the core effectors Frizzled and Strabismus (Zallen, 2007). In our in vitro single myofiber system, the basal rate of symmetric divisions was not perturbed by the loss of Fzd7. By contrast, silencing of Vangl2 not only abrogated Wnt7a stimulation of symmetric expansion but also reduced the basal state of symmetric stem cell division. Therefore, it is likely that other PCP mechanisms, dependent on Vangl2 or on the protocadherins, mediate basal PCP signaling independent of Wnt binding.

It is possible that basal levels of PCP signaling are activated through other effectors. One such candidate is Syn4, a cell surface heparan sulfate proteoglycan expressed by quiescent satellite cells and their activated progeny (Cornelison et al., 2001). Satellite cells in mice deficient for *Syn4* are compromised in activation, proliferation, and differentiation in vitro, and they fail to reconstitute damaged muscle in vivo (Cornelison et al., 2004). Importantly, during *Xenopus* embryogenesis, xSyn4 interacts directly with xFzd7 and xDsh to activate noncanonical Wnt ignaling to regulate convergent and extension (CE) movements (Munoz et al., 2006). In addition, Syn4 and noncanonical Wnt signaling regulates the directional migration of neural crest cells (Matthews et al., 2008). Therefore, Syn4 and Fzd7 appear to cooperate to activate noncanonical Wnt signaling through the PCP pathway. Consistent with this hypothesis, we found that Syn4 expression was severely perturbed in satellite cells following Vangl2 silencing on myofibers (data not shown). Thus, the inability of satellite cells from $Syn4^{-/-}$ mice to regenerate muscle may be a consequence of a defect in PCP signaling.

Canonical Wnt signaling plays a well-documented role in regulating myogenic growth and differentiation. Recently, the temporal balance between proliferation and differentiation of satellite cells in adult muscle was demonstrated to be regulated by crosstalk between Notch and Wnt/β-catenin signaling pathways (Brack et al., 2008). Activation of the Wnt/β-catenin signaling pathway inhibits Notch-mediated maintenance of the undifferentiated state and thus facilitates differentiation. Our experiments indicate that activation of Wnt/β-catenin signaling using Wnt3a did not interfere with satellite stem cell choice between commitment and symmetric expansion (Figures 3B and 4D). Nevertheless, overexpression of Wnt3a in vivo appeared to impair regeneration possibly by promoting premature differentiation and the formation of myofibers of reduced size (Figure 6). Indeed, Wnt3a stimulation of satellite cells on single myofibers drove their differentiation, as evidenced by significant increase in the number of $Pax7^{-}$/$MyoD^{+}$ cells (data not shown). However, we were unable to detect Wnt3a expression in undamaged or regenerating skeletal muscle by real-time PCR. Potentially other upregulated Wnts, such as Wnt10a (Figure 2B, Figure S4), may function to activate the Wnt/β-catenin signaling pathway in myogenic cells. Furthermore, we observed a large upregulation of the Wnt inhibitors sFRPs during the early stages of the regenerative process. Perhaps this represents a physiological feedback system that inhibits canonical Wnt signaling, allowing the proliferation of myogenic progenitors. Thus, as hypothesized by Brack et al. (2008), inhibition of Wnt/β-catenin signaling would act to promote muscle regeneration.

In *Xenopus* embryos, the Vangl2 homolog Strabismus inhibits Wnt/β-catenin-activated transcription by competing for

Disheveled (Park and Moon, 2002). Thus, PCP signaling may also act to keep satellite stem cells in an uncommitted state by antagonizing canonical Wnt/β-catenin signaling. In *Drosophila* eye development, Frizzled/PCP signaling induces cell-fate specification of the R3/R4 photoreceptors through regulation of Notch activation in R4 (del Alamo and Mlodzik, 2006). This raises the possibility that crosstalk between Frizzled/PCP and Notch pathways, as well as Wnt/β-catenin pathways, acts to coordinate satellite stem cell choice between self-renewal/commitment and expansion.

Molecular characterization of satellite stem cells is providing important insights into the molecular mechanisms regulating their function. Our identification of a role for the Wnt7a/Fzd7/Vangl2 signal transduction cascade reveals an unanticipated role for the PCP pathway in regulating the symmetric expansion of satellite stem cells. This finding represents a significant advance in our understanding of satellite cell biology and muscle regeneration. Future experiments will investigate the utility of modulating the PCP pathway to augment muscle regeneration toward ameliorating the loss of muscle function in neuromuscular disease.

EXPERIMENTAL PROCEDURES

Mice and Animal Care

Adult (8–12 weeks of age) *Myf5-Cre/ROSA26-YFP* mice were obtained by crossing the knockin *Myf5-Cre* (Tallquist et al., 2000) heterozygous mice with *ROSA26-YFP* (Srinivas et al., 2001) homozygous reporter mice. *ROSA26-YFP* mice were used as wild-type controls. Wnt7a null mice and their littermate controls were obtained by crossing heterozygous *Wnt7a*$^{+/-}$ mice. All mice were maintained inside a barrier facility, and experiments were performed following the University of Ottawa regulations for animal care and handling.

Cell Sorting

Mononucleated muscle-derived cells were isolated from hindlimb muscles and staining was performed as previously described (Ishibashi et al., 2005; Kuang et al., 2007). Cells were separated on a MoFlo cytometer (DakoCytomation) equipped with three lasers. Dead cells and debris were excluded by Hoescht staining and by gating on forward and side scatter profiles (Figure S1).

Myofiber Isolation, Culture, and Immunohistochemistry

Single myofibers were isolated from the EDL muscles as previously described (Charge et al., 2002). Isolated myofibers were cultured in suspension in 6-well plates coated with horse serum to prevent fiber attachment (Kuang et al., 2006). Fibers were incubated in plating medium consisting of 15% FBS (Hyclone) and 1% chick embryo extract (CEE, Accurate Chemicals) in DMEM containing 2% L-glutamine, 4,5% glucose, and 110 mg/ml sodium pyruvate. For myoblast culture, satellite cells were sorted and plated on collagen-coated dishes in Ham's F10 medium supplemented with 20% FBS and 5 ng/ml of basic FGF (Invitrogen). For Wnt stimulation, recombinant Wnt7a or Wnt3a proteins were added in the plating medium (25 ng/ml, R&D Systems). For in vivo activation of satellite cells, regeneration was induced by CTX injection in the TA muscle, and 4 days later, individual myofibers were isolated from the neighboring EDL muscle. Immunochemical labeling of cryosections, myofibers, and cells were performed as previously reported (Kuang et al., 2006). The primary antibodies used are listed in Table S2.

siRNA Knockdown

For EDL myofibers, transfections were carried at 4 and 24 hr postdissection in plating medium using Lipofectamine 2000 reagent (Invitrogen) as per manufacturer's instructions. Fibers were refed in fresh media on the next mornings and fixed after 42–72 hr of culture. For satellite cell-derived myoblasts, cells were refed 3 hr prior to transfection, and transfections were carried in growth medium. Cells were washed and refed with Ham's Complete media 6 hr following transfections. RNA was harvested 48 hr following transfection. siRNA duplexes were from Ambion siFzd7 (ID s66314) and siVangl2 (ID s96802) and used at the final concentration of 10 nM each. Transfection efficiency was monitored using Cy3-labeled siRNA. Knockdown efficiency was assessed by real-time PCR (Figures S6A and S5K).

Real-Time PCR

RNA was isolated using the RNEasy kits (QIAGEN) and subjected to on-column DNase digestion as per the manufacturer's instructions. cDNA synthesis was performed using the Superscript III reverse transcriptase and random hexamer primers (Invitrogen). Real-time PCR was carried out as previously described (Ishibashi et al., 2005). Transcript levels were normalized to GAPDH transcript levels. Relative fold change in expression was calculated using the ΔΔCT method (CT values <30). For relative transcript quantification, each cDNA sample was run on a five-point standard curve so as to assure a PCR efficiency of $\geq$95%. Wnt signaling pathway PCR arrays were purchased from Superarray Bioscience Corporation (PAMM-043), and analysis was performed as per the manufacturer's instructions. See Table S3 for primer sequences.

Statistical Analysis

A minimum of three and up to five replicates were done for the experiments presented. Data are presented as standard error of the mean. Results were assessed for statistical significance using Student's t test (Microsoft Excel), and differences were considered statistically significant at the $p < 0.05$ level.

SUPPLEMENTAL DATA

Supplemental Data include Supplemental Experimental Procedures, nine figures, and three tables and can be found with this article online at http://www.cell.com/cell-stem-cell/supplemental/S1934-5909(09)00148-9.

ACKNOWLEDGMENTS

We thank Shihuan Kuang, Feodor Price, Iain McKinnell, Mark Gillespie, and Jeffrey Dilworth for helpful discussions throughout the study and Caroline Vergette and Paul Oleynick for cell sorting. We thank Drs. P. Soriano for the *Myf5-Cre* mice, F. Costantini for the *ROSA-YFP* mice, and Alysia vandenBerg and David Sassoon for the *Wnt7a*$^{-/-}$ mice. M.A.R. holds the Canada Research Chair in Molecular Genetics and is an International Research Scholar of the Howard Hughes Medical Institute (HHMI). This work was supported by grants to M.A.R. from the Canadian Institutes of Health Research, Muscular Dystrophy Association, the National Institutes of Health, HHMI, the Canadian Stem Cell Network, and the Canada Research Chair Program. The authors declare no conflict of interest.

Received: October 20, 2008
Revised: February 12, 2009
Accepted: March 19, 2009
Published: June 4, 2009

REFERENCES

Anakwe, K., Robson, L., Hadley, J., Buxton, P., Church, V., Allen, S., Hartmann, C., Harfe, B., Nohno, T., Brown, A.M., et al. (2003). Wnt signalling regulates myogenic differentiation in the developing avian wing. Development *130*, 3503–3514.

Borello, U., Berarducci, B., Murphy, P., Bajard, L., Buffa, V., Piccolo, S., Buckingham, M., and Cossu, G. (2006). The Wnt/beta-catenin pathway regulates Gli-mediated Myf5 expression during somitogenesis. Development *133*, 3723–3732.

Brack, A.S., Conboy, I.M., Conboy, M.J., Shen, J., and Rando, T.A. (2008). A temporal switch from notch to Wnt signaling in muscle stem cells is necessary for normal adult myogenesis. Cell Stem Cell *2*, 50–59.

Charge, S.B., and Rudnicki, M.A. (2004). Cellular and molecular regulation of muscle regeneration. Physiol. Rev. *84*, 209–238.

Charge, S.B., Brack, A.S., and Hughes, S.M. (2002). Aging-related satellite cell differentiation defect occurs prematurely after Ski-induced muscle hypertrophy. Am. J. Physiol. Cell Physiol. *283*, C1228–C1241.

Chen, A.E., Ginty, D.D., and Fan, C.M. (2005). Protein kinase A signalling via CREB controls myogenesis induced by Wnt proteins. Nature *433*, 317–322.

Ciruna, B., Jenny, A., Lee, D., Mlodzik, M., and Schier, A.F. (2006). Planar cell polarity signalling couples cell division and morphogenesis during neurulation. Nature *439*, 220–224.

Clevers, H. (2006). Wnt/β-catenin signaling in development and disease. Cell *127*, 469–480.

Collins, C.A., Olsen, I., Zammit, P.S., Heslop, L., Petrie, A., Partridge, T.A., and Morgan, J.E. (2005). Stem cell function, self-renewal, and behavioral heterogeneity of cells from the adult muscle satellite cell niche. Cell *122*, 289–301.

Cornelison, D.D., Filla, M.S., Stanley, H.M., Rapraeger, A.C., and Olwin, B.B. (2001). Syndecan-3 and syndecan-4 specifically mark skeletal muscle satellite cells and are implicated in satellite cell maintenance and muscle regeneration. Dev. Biol. *239*, 79–94.

Cornelison, D.D., Wilcox-Adelman, S.A., Goetinck, P.F., Rauvala, H., Rapraeger, A.C., and Olwin, B.B. (2004). Essential and separable roles for Syndecan-3 and Syndecan-4 in skeletal muscle development and regeneration. Genes Dev. *18*, 2231–2236.

Cossu, G., and Borello, U. (1999). Wnt signaling and the activation of myogenesis in mammals. EMBO J. *18*, 6867–6872.

del Alamo, D., and Mlodzik, M. (2006). Frizzled/PCP-dependent asymmetric neuralized expression determines R3/R4 fates in the *Drosophila* eye. Dev. Cell *11*, 887–894.

Diatchenko, L., Lau, Y., Campbell, A., Chenchik, A., Moqadam, F., Huang, B., Lukyanov, S., Lukyanov, K., Gurskaya, N., Sverdlov, E., et al. (1997). Suppression subtractive hybridization: a method for generating differentially regulated or tissue-specific cDNA probes and libraries. Proc. Natl. Acad. Sci. USA *93*, 6025–6030.

Egger-Adam, D., and Katanaev, V.L. (2008). Trimeric G protein-dependent signaling by Frizzled receptors in animal development. Front. Biosci. *13*, 4740–4755.

Goto, T., Davidson, L., Asashima, M., and Keller, R. (2005). Planar cell polarity genes regulate polarized extracellular matrix deposition during frog gastrulation. Curr. Biol. *15*, 787–793.

Gros, J., Serralbo, O., and Marcelle, C. (2009). WNT11 acts as a directional cue to organize the elongation of early muscle fibres. Nature *457*, 589–593.

Hirabayashi, Y., Itoh, Y., Tabata, H., Nakajima, K., Akiyama, T., Masuyama, N., and Gotoh, Y. (2004). The Wnt/beta-catenin pathway directs neuronal differentiation of cortical neural precursor cells. Development *131*, 2791–2801.

Ishibashi, J., Perry, R.L., Asakura, A., and Rudnicki, M.A. (2005). MyoD induces myogenic differentiation through cooperation of its NH2- and COOH-terminal regions. J. Cell Biol. *171*, 471–482.

Kengaku, M., Capdevila, J., Rodriguez-Esteban, C., De La Pena, J., Johnson, R.L., Belmonte, J.C., and Tabin, C.J. (1998). Distinct WNT pathways regulating AER formation and dorsoventral polarity in the chick limb bud. Science *280*, 1274–1277.

Kuang, S., Charge, S.B., Seale, P., Huh, M., and Rudnicki, M.A. (2006). Distinct roles for Pax7 and Pax3 in adult regenerative myogenesis. J. Cell Biol. *172*, 103–113.

Kuang, S., Kuroda, K., Le Grand, F., and Rudnicki, M.A. (2007). Asymmetric self-renewal and commitment of satellite stem cells in muscle. Cell *129*, 999–1010.

Kuang, S., Gillespie, M.A., and Rudnicki, M.A. (2008). Niche regulation of muscle satellite cell self-renewal and differentiation. Cell Stem Cell *2*, 22–31.

Matthews, H.K., Marchant, L., Carmona-Fontaine, C., Kuriyama, S., Larraín, J., Holt, M.R., Parsons, M., and Mayor, R. (2008). Directional migration of neural crest cells in vivo is regulated by Syndecan-4/Rac1 and non-canonical Wnt signaling/RhoA. Development *135*, 1771–1780.

McKinnell, I.W., Ishibashi, J., Le Grand, F., Punch, V.G., Addicks, G.C., Greenblatt, J.F., Dilworth, F.J., and Rudnicki, M.A. (2008). Pax7 activates myogenic genes by recruitment of a histone methyltransferase complex. Nat. Cell Biol. *10*, 77–84.

Miller, C., and Sassoon, D.A. (1998). Wnt-7a maintains appropriate uterine patterning during the development of the mouse female reproductive tract. Development *125*, 3201–3211.

Montarras, D., Morgan, J., Collins, C., Relaix, F., Zaffran, S., Cumano, A., Partridge, T., and Buckingham, M. (2005). Direct isolation of satellite cells for skeletal muscle regeneration. Science *309*, 2064–2067.

Montcouquiol, M., Rachel, R.A., Lanford, P.J., Copeland, N.G., Jenkins, N.A., and Kelley, M.W. (2003). Identification of Vangl2 and Scrb1 as planar polarity genes in mammals. Nature *423*, 173–177.

Montcouquiol, M., Sans, N., Huss, D., Kach, J., Dickman, J.D., Forge, A., Rachel, R.A., Copeland, N.G., Jenkins, N.A., Bogani, D., et al. (2006). Asymmetric localization of Vangl2 and Fz3 indicate novel mechanisms for planar cell polarity in mammals. J. Neurosci. *26*, 5265–5275.

Munoz, R., Moreno, M., Oliva, C., Orbenes, C., and Larrain, J. (2006). Syndecan-4 regulates non-canonical Wnt signalling and is essential for convergent and extension movements in Xenopus embryos. Nat. Cell Biol. *8*, 492–500.

Oustanina, S., Hause, G., and Braun, T. (2004). Pax7 directs postnatal renewal and propagation of myogenic satellite cells but not their specification. EMBO J. *23*, 3430–3439.

Park, M., and Moon, R.T. (2002). The planar cell-polarity gene stbm regulates cell behaviour and cell fate in vertebrate embryos. Nat. Cell Biol. *4*, 20–25.

Polesskaya, A., Seale, P., and Rudnicki, M.A. (2003). Wnt signaling induces the myogenic specification of resident CD45+ adult stem cells during muscle regeneration. Cell *113*, 841–852.

Rochat, A., Fernandez, A., Vandromme, M., Moles, J.P., Bouschet, T., Carnac, G., and Lamb, N.J. (2004). Insulin and wnt1 pathways cooperate to induce reserve cell activation in differentiation and myotube hypertrophy. Mol. Biol. Cell *15*, 4544–4555.

Sacco, A., Doyonnas, R., Kraft, P., Vitorovic, S., and Blau, H.M. (2008). Self-renewal and expansion of single transplanted muscle stem cells. Nature *456*, 502–506.

Seale, P., Sabourin, L.A., Girgis-Gabardo, A., Mansouri, A., Gruss, P., and Rudnicki, M.A. (2000). Pax7 is required for the specification of myogenic satellite cells. Cell *102*, 777–786.

Seifert, J.R., and Mlodzik, M. (2007). Frizzled/PCP signalling: a conserved mechanism regulating cell polarity and directed motility. Nat. Rev. Genet. *8*, 126–138.

Srinivas, S., Watanabe, T., Lin, C.S., William, C.M., Tanabe, Y., Jessell, T.M., and Costantini, F. (2001). Cre reporter strains produced by targeted insertion of EYFP and ECFP into the ROSA26 locus. BMC Dev. Biol. *1*, 4. 10.1186/1471-213X-1-4.

Tajbakhsh, S., Borello, U., Vivarelli, E., Kelly, R., Papkoff, J., Duprez, D., Buckingham, M., and Cossu, G. (1998). Differential activation of Myf5 and MyoD by different Wnts in explants of mouse paraxial mesoderm and the later activation of myogenesis in the absence of Myf5. Development *125*, 4155–4162.

Tallquist, M.D., Weismann, K.E., Hellstrom, M., and Soriano, P. (2000). Early myotome specification regulates PDGFA expression and axial skeleton development. Development *127*, 5059–5070.

Torban, E., Kor, C., and Gros, P. (2004). Van Gogh-like2 (Strabismus) and its role in planar cell polarity and convergent extension in vertebrates. Trends Genet. *20*, 570–577.

Torban, E., Patenaude, A.M., Leclerc, S., Rakowiecki, S., Gauthier, S., Andelfinger, G., Epstein, D.J., and Gros, P. (2008). Genetic interaction between members of the Vangl family causes neural tube defects in mice. Proc. Natl. Acad. Sci. USA *105*, 3449–3454.

Torrente, Y., Belicchi, M., Sampaolesi, M., Pisati, F., Meregalli, M., D'Antona, G., Tonlorenzi, R., Porretti, L., Gavina, M., Mamchaoui, K., et al. (2004). Human circulating AC133(+) stem cells restore dystrophin expression and ameliorate function in dystrophic skeletal muscle. J. Clin. Invest. *114*, 182–195.

Zallen, J.A. (2007). Planar polarity and tissue morphogenesis. Cell *129*, 1051–1063.

Cell Stem Cell, Volume *4*

Supplemental Data

Wnt7a Activates the Planar Cell

Polarity Pathway to Drive the Symmetric

Expansion of Satellite Stem Cells

**Fabien Le Grand, Andrew E. Jones, Vanessa Seale,
Anthony Scimè, and Michael A. Rudnicki**

SUPPLEMENTAL EXPERIMENTAL PROCEDURES

Muscle Injury

For freeze-induced muscle regeneration, skin and fascia of anesthetized mice were opened and the TA muscles were subjected to three consecutive cycles of freezing–thawing by applying a liquid nitrogen-cooled metallic rod, and the wound closed by suture. For CTX-induced muscle regeneration, 25ul of diluted cardiotoxin were directly injected into the TA muscle without opening of the skin.

In vivo Electroporation

40 µg of plasmid DNA in 0.9 % NaCl or 0.9 % NaCl (saline) was injected directly into the left TA muscle of anesthetized mice, that had been exposed by an incision through the skin. Immediately after injection, electric stimulation was applied directly to the TA by a pulse generator (ECM 830, BTX) of 100-150 volts for 6 pulses, with a fixed duration of 20 ms and an interval of 200 ms using 5 mm needle electrodes (BTX). Experimental and contralateral TA muscles were isolated and embedded in OCT-15% Sucrose (Tissue-Tek) and frozen with isopentane cooled by cold nitrogen.

Histology and Quantification

Transverse sections (8 µm) of experimental and contralateral muscles were cut with a cryostat (Leica CM1850). The entire TA muscles were sectioned, in order to compare experimental and contralateral muscles at the same level on serial sections (around 400 sections were obtained from each TA muscle). For LacZ reaction, cryosections were fixed with 0.1% gluteraldehyde and exposed to X-gal solution. For H&E and immonostaining, sections were fixed with 4% paraformaldehyde. For enumeration of fibers, pictures of laminin-stained cryosections were assembled and counted on Adobe Photoshop CS2. Quantification of myofibers caliber was performed with ImageJ. The satellite cell enumeration was performed on Photoshop, on pictures of Pax7 and Laminin co-immunostained cryosections taken in regenerated areas where all the fibers had centrally located nuclei. “Satellite Cell Content” represents the number of sub-laminar Pax7+ve satellite cells normalized per fiber number, and to the contralateral leg.

Subtractive Hybridization

RNA samples (10ng) from sorted YFP+ and YFP- satellite cells were amplified using the Super-SMART cDNA amplification kit (Clontech) following the protocols provided. 2ug of representative cDNA from each sample were used to generate a subtractive library with the PCR-Select kit (Clontech) as per manufacturer' instructions. The amplified cDNA from sorted YFP^- was used as "tester" and the amplified cDNA from sorted YFP^+ was used as "driver". SSH products were cloned in pCR®2.1vector using a TA cloning Kit (Invitrogen) and 200 clones from the SSH library were sequenced with nested primers using the ABI 3730 DNA Analyzers (Applied Biosystems), according to the manufacturers' protocols and manuals.

SUPPLEMENTAL FIGURES

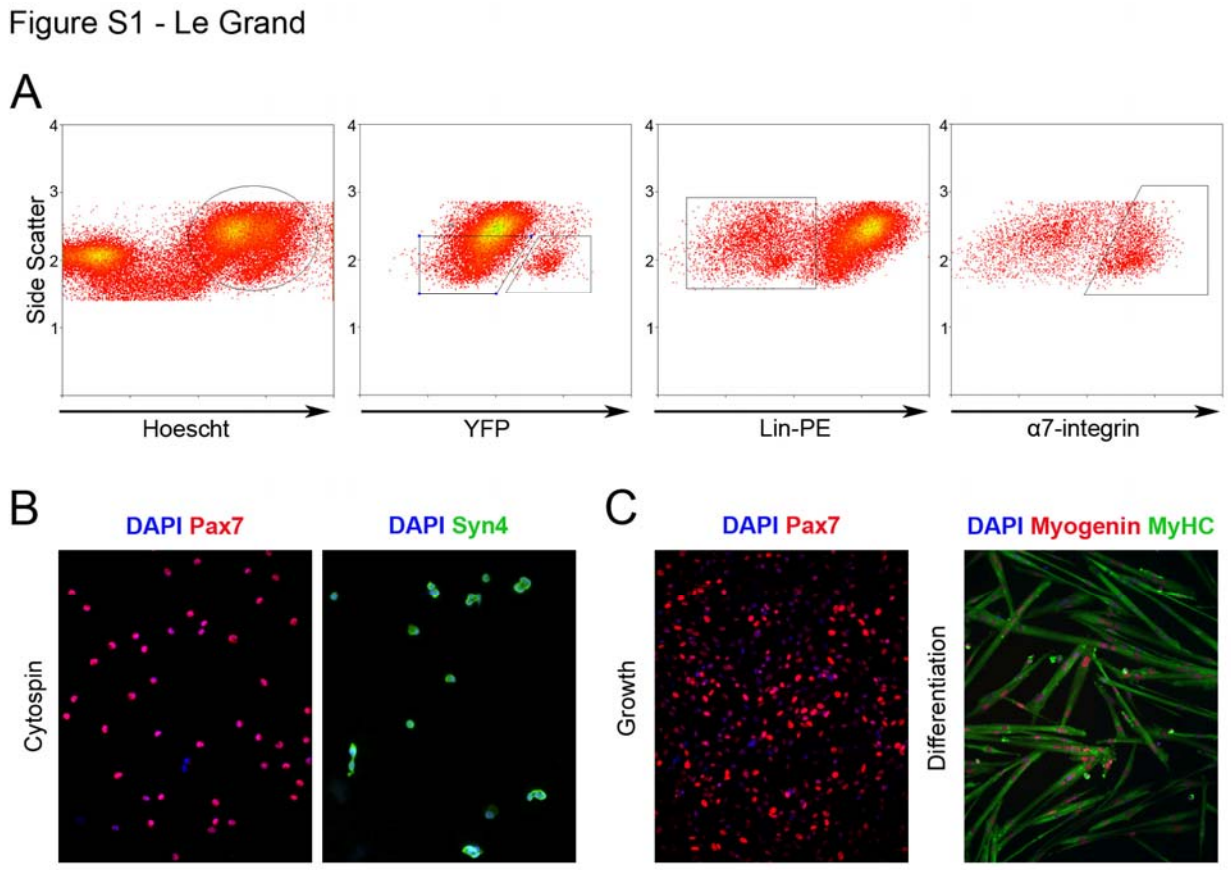

Figure S1. FACS purification of muscle satellite cells.
(A) FACS profiles for selection of live satellite cells from fore- and hindlimb skeletal muscles. Cells were positively selected for CD34 (APC-Cy7) and α7-Integrin (APC) and negatively selected for CD11b CD31, CD45 and Sca1 (all in PE). $Myf5^{+}$ and $Myf5^{-}$ satellite cells were then separated on the basis of YFP fluorescence.
(B) Cytospin of freshly isolated {$CD34^{+}$, α7-$Integrin^{+}$, Lin^{-}} satellite cells. Sorted cells express the satellite cell markers Pax7 (left) and Syndecan4 (right).
(C) In vitro development of sorted {$CD34^{+}$, α7-$Integrin^{+}$, Lin^{-}} satellite cells. After one week in culture, 98% of sorted cells express Pax7 (unequal levels of Pax7 staining account for differences in individual myoblasts cell cycle). After 4 days in differentiation medium, sorted cells form multinucleated myotubes expressing Myogenin and myosin heavy chains.

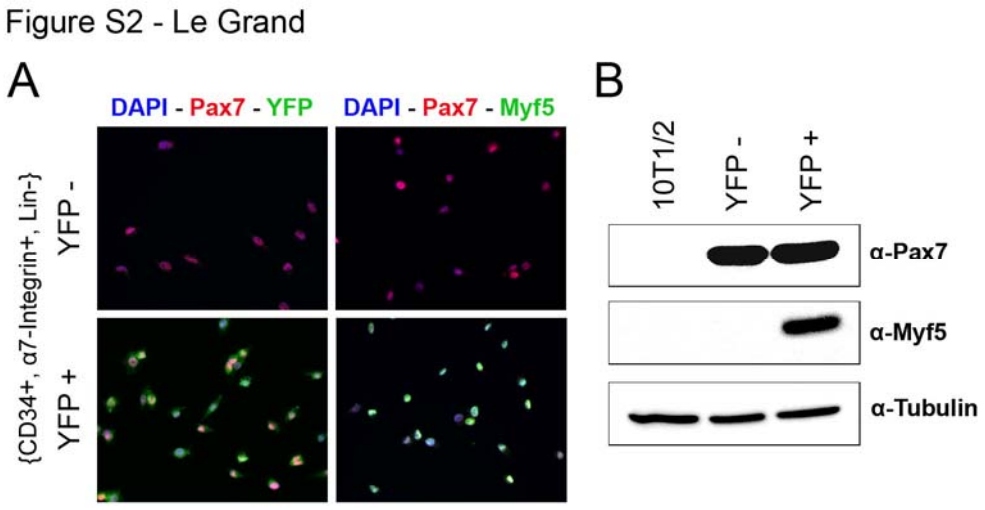

Figure S2. YFP$^-$ satellite cell-derived myoblasts do not express Myf5 protein.
FACS-sorted YFP$^+$ and YFP$^-$ satellite cells were cultured in high mitogenic medium for 2 weeks. Cells were maintained at less than 10% confluence to avoid myogenic commitment of YFP$^-$ cells. Cycling YFP$^+$ myoblasts express high levels of Myf5 protein while YFP$^-$ myoblasts do not exhibit any detectable Myf5 protein expression, as revealed by immunostaining (A) and western (B) analysis. 10T1/2 cells were used as a negative non-myogenic control (n=3).

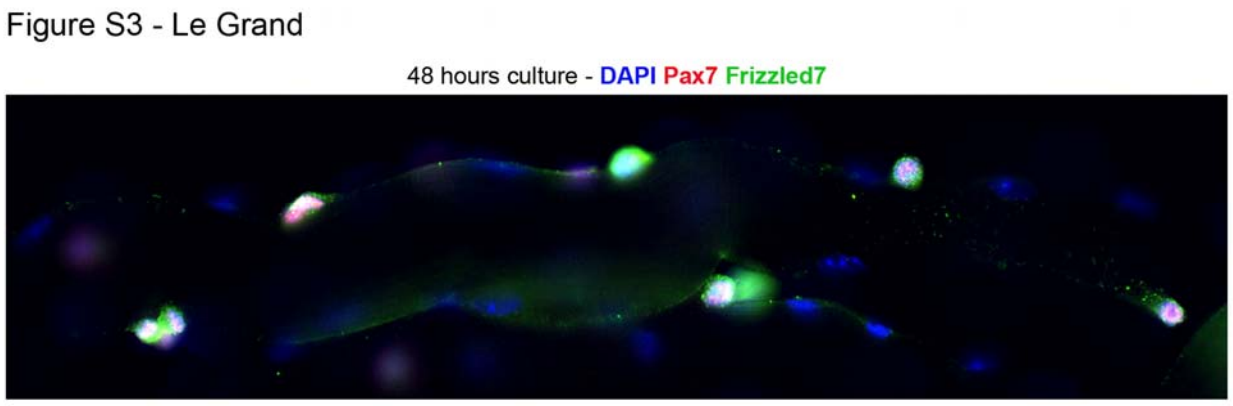

Figure S3. Frizzled7 is expressed by all the activated satellite cells *in vitro*.
EDL single myofibers were cultured in floating conditions for 48 hours. All the Pax7+ve cells at the surface of the fibers were also positive for Frizzled7 staining.

Figure S4 - Le Grand

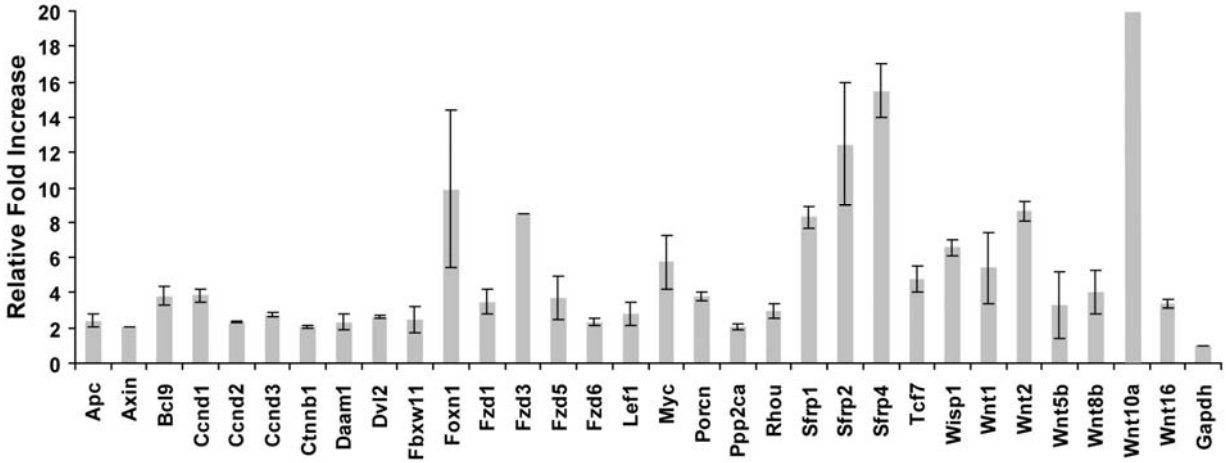

Figure S4. Wnt array Real-Time PCR analysis of 3-days regenerating freeze-injured TA muscles.
Significant changes were observed in 31 transcripts expression levels (with cut-off values as Ct<31), as compared to contralateral TA and normalized to GAPDH transcripts levels (n=3). Wnt10a transcripts were over-expressed more than 40-fold as compared to contralateral. Errors bars represent SEM.

Figure S5 - Le Grand

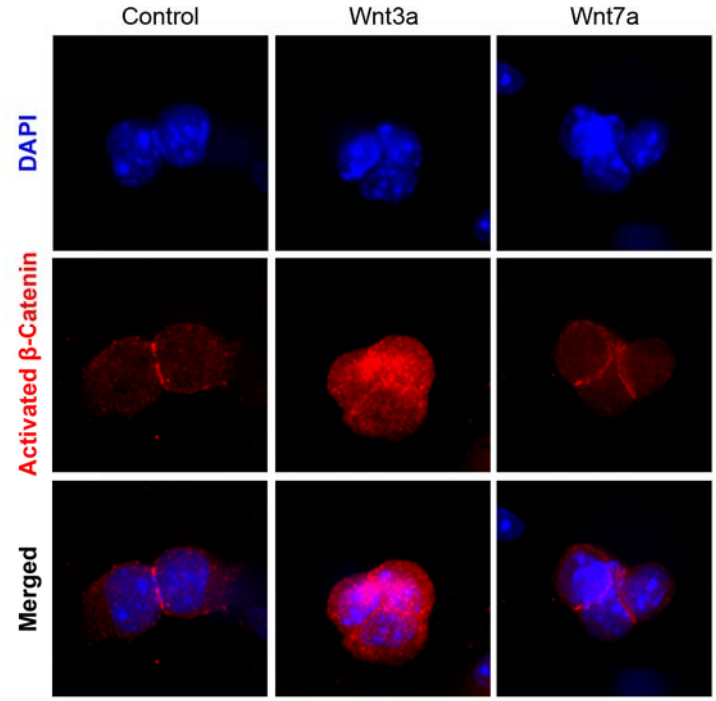

Figure S5. Wnt7a do not induce stabilization and nuclear localization of ß-Catenin in activated muscle satellite cells.
Single EDL myofibers were cultured in suspension for 2 days, in control medium or with medium supplemented with Wnt3a or Wnt7a. Myofibers were stained with an antibody recognizing the active form of ß-Catenin. Wnt3a treatment causes ß-Catenin stabilization and translocation into satellite cells' nucleus. Wnt7a do not activate Wnt canonical signaling in dividing satellite cells.

Figure S6 - Le Grand

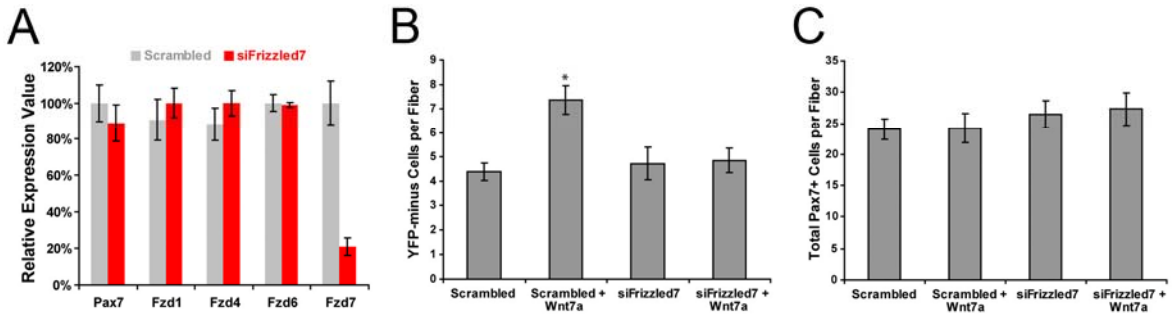

Figure S6. Wnt7a increase satellite stem cell self-renewal while not modifying satellite cells' proliferation kinetics.

(A) Real-time PCR analysis of Frizzled transcripts in cultured myogenic cells in control (non-silencing) and *Fzd7*-silencing conditions. Fzd7 transcription was reduced by 80% (n=3, p=0.01, n=3). Knock-down of *Fzd7* is specific and does not effect the expression of other Frizzled transcripts expressed in myogenic cells.

(B) EDL single myofibers from *Myf5-Cre/ROSA26-YFP* mice were cultured in floating conditions for 52 hours. The Wnt7a-induced increase in satellite stem cell number was abrogated following silencing of Fzd7 on myofibers (n=3, *p<0.03).

(C) Wnt7a treatment did not have an impact on the total number of Pax7+ cells per myofibers (n=3). Errors bars represent SEM.

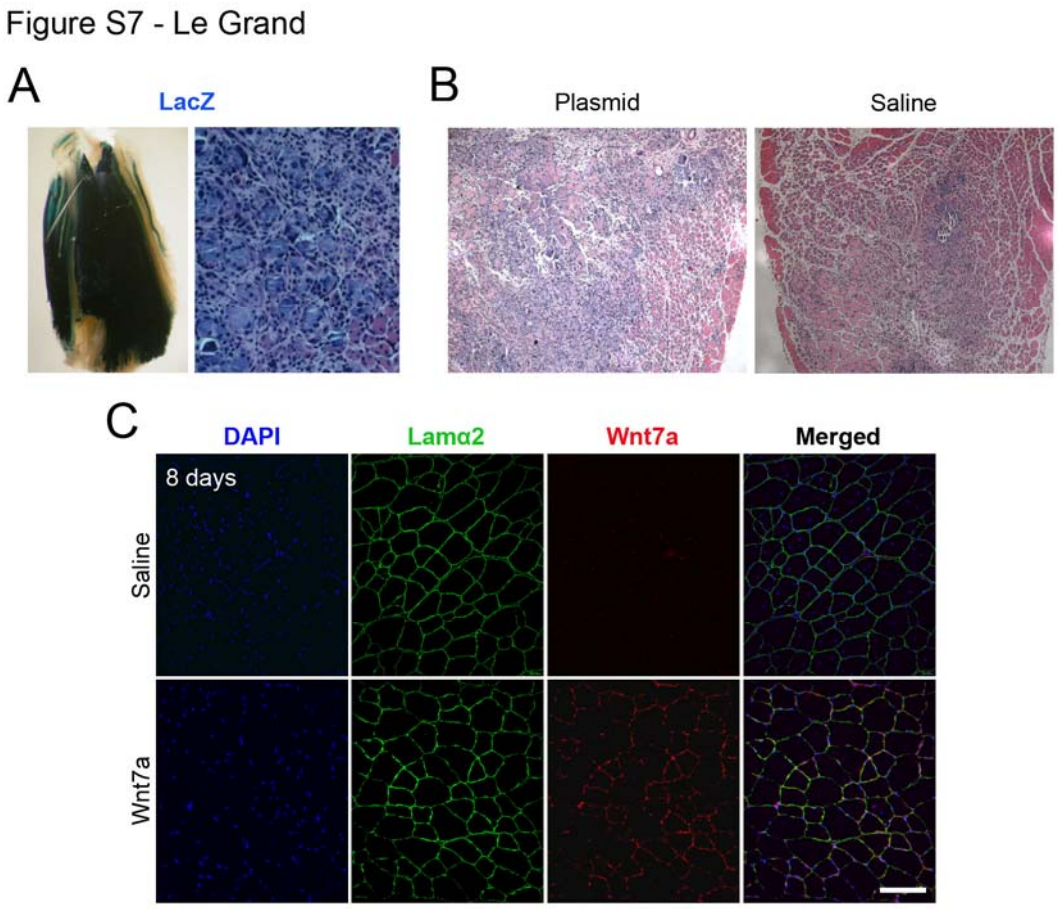

Figure S7 Efficient electroporation of plasmids in the adult TA muscle.
(A) The vast majority of the TA myofibers were transfected with a CMV-LacZ expression plasmid. X-Gal staining revealing ß-galactosidase activity in whole-mount view (left), and histology on cryosections (right).
(B) Representative histology of transfected muscle 1 week after electroporation. Electroporation with a control plasmid (left) did not yield any significant differences in the regeneration process, as compared to a saline electroporation (right).
(C) Ectopic expression of Wnt7a by majority of the fibers 8 days after electroporation of TA muscle with a CMV-Wnt7a expression plasmid. Immunohistochemistry of cryosections stained with specific antibodies reactive with a2-laminin and Wnt7a.

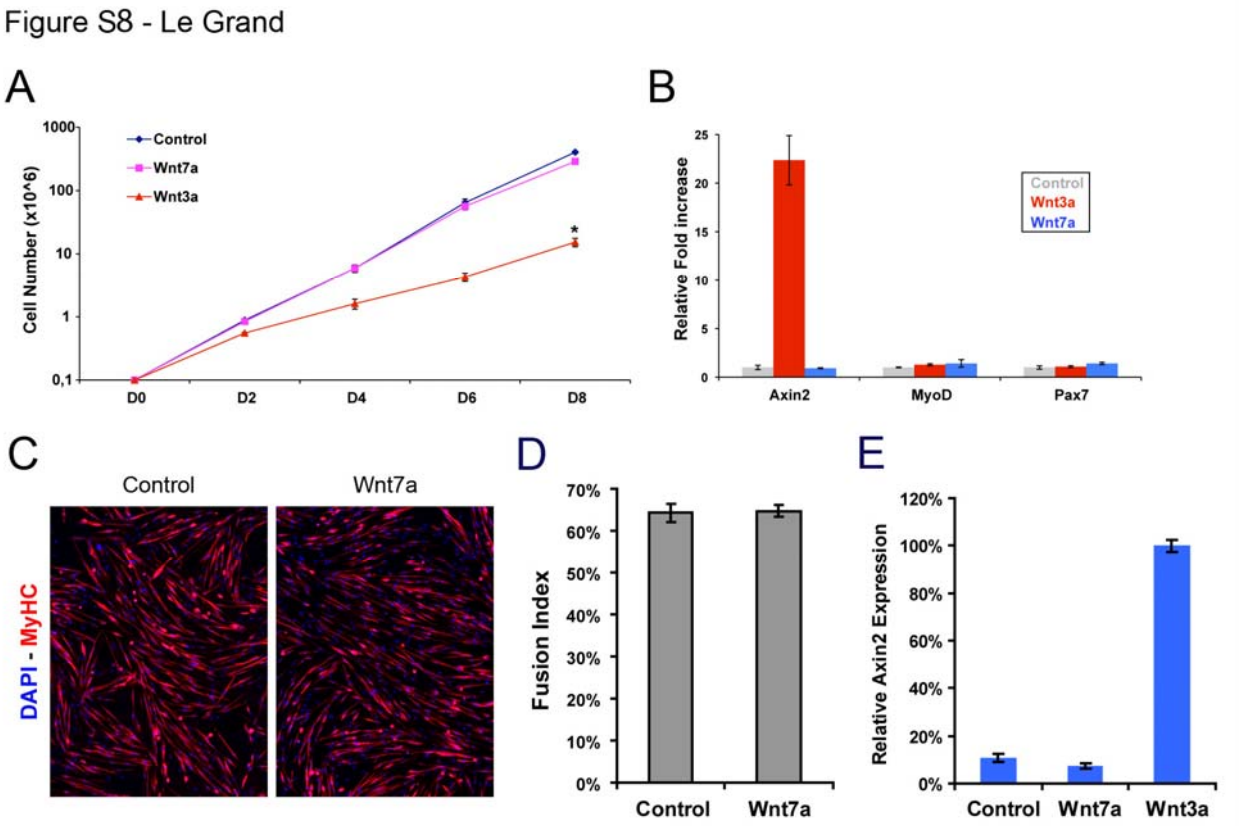

Figure S8. Wnt7a do not have an effect on myogenic proliferation nor differentiation.
(A) Satellite cell-derived myoblasts were grown *in vitro* in control or Wnt-supplemented growth media. Wnt7a treatment did not alter the kinetics of committed myogenic progenitors. Wnt3a treatment resulted in a reduced cell proliferation (n=3, p=0,01).
(B) Satellite cell-derived myoblasts cultured in differentiation media for 24 hours were treated for 24 hours with either Wnt3a or Wnt7a recombinant proteins. Wnt treatment did not activate MyoD or Pax7 transcription (n=5). Wnt3a treatment activated *Axin2* transcription.
(C) Satellite cell-derived myoblasts were grown to 60% confluence and shifted to control differentiation media or in differentiation medium supplemented with Wnt7a for 4 days. Differentiated cells were immunostained for myosin heavy chains. No differences in morphology or size of the differentiated myotubes were observed between control and Wnt7a-treated cultures.
(D) Fusion index quantification did not show any significant differences between control and Wnt7a-treated cultures (n=3).
(E) Myoblasts cultured in differentiation media for 24 hours were treated for 6 hours with either Wnt3a or Wnt7a recombinant proteins. Wnt3a, but not Wnt7a, activated the transcription of Wnt-ß-Catenin target genes such as Axin2 (10-fold increase, n=3).
Errors bars represent SEM.

Figure S9 - Le Grand

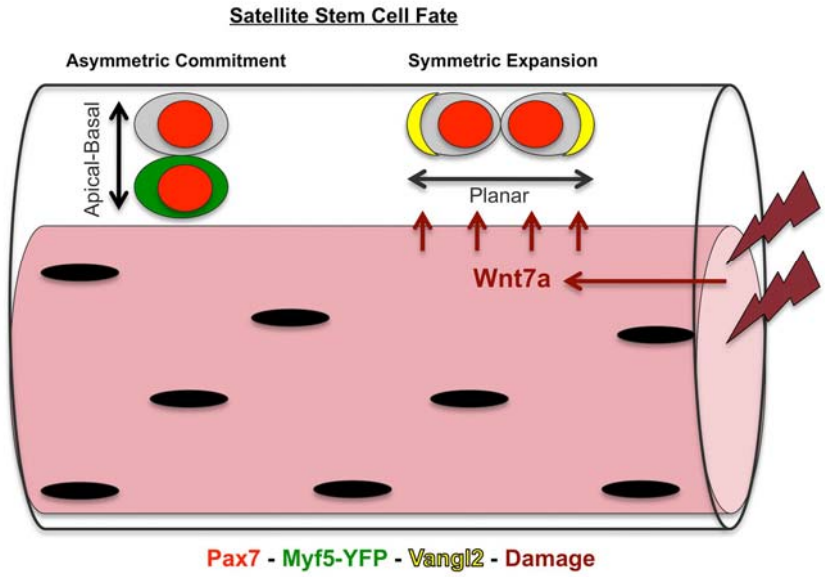

Figure S9. A model for stem cell fate within the satellite cell niche.